Western Australian School of Mines

Department of Mining Engineering & Metallurgical Engineering

# Effect of Electrostatic Fields on Mass Transfer in Solvent Extraction

Simon Assmann

This thesis is presented for the Degree of

Doctor of Philosophy

of

Curtin University

December 2014

# DECLARATION

To the best of my knowledge and belief this thesis contains no material previously published by any other person except where due acknowledgment has been made.

This thesis contains no material which has been accepted for the award of any other degree or diploma in any university.

_____

Simon Assmann

December 2014

# ABSTRACT

Solvent extraction (SX) is essential in process metallurgy as it can be used to purify a wide variety of metals from solutions of various concentrations, range of pH and levels of impurity. It is also the only commercially proven separation technique that can be used to purify chemically similar metals. Thus, its use in hydrometallurgy has been increasing and expanding, and this trend is set to continue given the increasing need to purify highly contaminated leach solutions generated from low grade and complex ores. The current SX technology, however, has inherent limitations in terms of achievable extraction efficiencies. These are largely owing to the use of mechanical agitation, as control of droplet size and droplet motion is poor and limited.

A promising alternative is the use of electrostatic fields in contacting the aqueous and organic phases to facilitate mass transfer and hence called electrostatic solvent extraction (ESX). It is a particularly attractive alternative because, theoretically, it could circumvent the limitations associated with mechanical agitation while retaining the inherent strengths of SX. The efforts to develop the technique have already yielded significant advancements including the achievement of a volumetric throughput that is comparable to that of a conventional pulse column and the purification of various feed solutions. In spite of this, however, a commercial application is yet to be achieved, which may be attributed to the still scarce technical data particularly in regards to the effect of electrostatic fields on mass transfer under experimental conditions that are relevant to hydrometallurgical SX as well as several inconsistencies in available data. To assist in addressing this gap, the present study was aimed at determining how electrostatic fields (1) influence interfacial phenomena and mass transfer across an aqueous-organic interface, and (2) effect and affect droplet dispersion, droplet agitation in the resulting dispersions and mass transfer within the dispersions.

To achieve these aims, two experimental techniques were used: a modified Lewis cell to pursue the first objective, and a droplet column to pursue the second objective. The extraction of Co(II) by Cyanex® 272 was used as the test system to generate data that are relevant to this ESX application. The types of electrostatic fields used were direct current (DC), pulsed direct current (PDC), and alternating current (AC).

The investigation of the effect of electrostatic fields on interfacial phenomena and mass transfer across an aqueous-organic interface revealed that:

- The mass transfer of Co(II) across the organic diffusion region is enhanced by electrostatic fields with fixed polarity (DC and PDC), but not by fields with alternating polarity (AC), indicating that the process is influenced by electrostatic attraction between the extracted species and the applied field.
- Electrostatic fields have no effect on the mass transfer of Co(II) across the aqueous diffusion region, as no field could be sustained in this region owing to the high conductivity and thus, the fast dissipation of charges. Electrostatic fields also have no effect on the rate of the chemical reaction between Co(II) and Cyanex® 272 at the aqueous-organic interface.

The investigation of the effect of electrostatic fields on droplet dispersion, droplet agitation in the resulting dispersion and mass transfer within the dispersion revealed that:

- All types of electrostatic fields—positive and negative DC, positive and negative PDC and AC—can be used to disperse aqueous feed in the organic phase. The size of the droplets decreases with increases in field strength but AC fields provide the finest droplets with the narrowest size distribution at far lower field strengths with the highest degree of insulation. The dispersion occurred through two previously known mechanisms but three previously unknown mechanisms were also observed.
- Transient fields (AC and PDC) induce a proportion of droplets to oscillate while steady fields (DC) induce a proportion of droplets to elongate only. Both are manifestations of orientational polarisation and thus, the proportion of droplets and amplitude of oscillation or elongation increases with increases in the field strength.
- All field types induced the majority of the droplets to move horizontally in a zigzagging fashion and the speed increased with increases in field strength. Under the influence of DC and PDC fields, droplets change direction only on contact with an electrode while those under AC fields change direction in synchrony with the frequency of the field. Under PDC fields, droplets stagger in synchrony with the pulse frequency. These are a manifestation of interfacial polarisation.

- As predicted, based on the systematic characterisation of field effects on the droplet dispersion and agitation, the mass transfer of Co(II) increases with increases in the field strength and decreases in the frequency, which equates to increases in both the interfacial area and droplet agitation.

Therefore, the most suitable electrostatic field conditions for ESX are high strength and low frequency AC fields as these provide the largest interfacial area and most intense agitation at the lowest field strengths with highest degree of insulation.

# ACKNOWLEDGEMENTS


- My supervisor, Dr. Don Ibana, for his continuous support throughout this work, including many helpful discussions on various aspects of the work, his encouragement and positive attitude when setbacks were encountered, and for developing my professional writing skills.

- My co-supervisor, Dr. Christopher McRae, for constructing the high voltage power supplies used in this work, for his assistance in developing the laboratory apparatuses used in this work, and for many helpful technical discussions.

- The Australian Postgraduate Award (APA), Curtin Research Scholarship (CRS), Parker Centre CRC for Integrated Hydrometallurgy Solutions, and the Minerals and Energy Research Institute of Western Australia (MERIWA) for my scholarships.

- Dr. Marc Steffens for sharing his technical knowledge and experience on the topic, and for his advice on several aspects of this work.

- Amy Lu for assisting with the commissioning of the modified Lewis cell used in this work, as well as helping to carry out preliminary experiments with this apparatus.

- Peter Haig of Shell Chemicals Australia for supplying the ShellSol® 2046 used in this work, and Shane Wigget of Cytec Australia for supplying the Cyanex® 272 used in this work.

- My late father for encouraging me to pursue postgraduate research, and my family and friends for their continuous support and encouragement throughout this work.

# TABLE OF CONTENTS

# LIST OF FIGURES

# LIST OF TABLES

# Chapter 1

# GENERAL INTRODUCTION

## 1.1. HYDROMETALLURGICAL SOLVENT EXTRACTION

Solvent extraction (SX) is a separation and concentration technique that allows the selective transfer of a desired chemical species between two immiscible liquids, which are commonly referred to as the aqueous and organic phases. Hydrometallurgical SX applications involve the reaction of target metal ions (M) in an aqueous pregnant liquor stream (PLS) with an extractant (E) in an organic solvent to form an extracted species (ME) that is stable in the organic phase (Equation 1).

$$M_{(aq)} + E_{(org)} \rightleftharpoons ME_{(org)} \qquad \text{(Equation 1)}$$

After intimately contacting the two phases to effect the reaction, the solvent, which is loaded with the target metal ions, and the barren PLS, which contains only impurity ions, are separated. The loaded solvent is then contacted with a fresh aqueous 'stripping' solution to transfer the metal ions back into an aqueous phase that is suitable for further refining processes to produce a final metal product.

Commercial application of hydrometallurgical SX has increased and expanded since its inception in the 1950s to process uranium. It is now used to process a wide range of metals including copper, nickel and cobalt, the rare earth metals, and zinc among many others (Ritcey 2006a). The growth of SX may be attributed to its unique advantages including it being the only commercially proven technique that allows complete separation of chemically similar metals such as nickel and cobalt, and the rare earth metals. It is also effective in the purification of metal ions from highly contaminated PLSs such as those generated from complex and low grade ores using vigorous leaching conditions. The application of SX on the latter is particularly significant given continuing increase in the demand for metals while the reserves of high grade ores are fast depleting and thus, the increasing need to exploit these complex and low grade ores.

In spite of the numerous advantages of the technique, the viability of any commercial SX operation is largely dependent on the mass transfer rate of metal ions between the aqueous and organic phases which, in turn, is dependent on the technique of contacting the phases.

## 1.2. CURRENT SX TECHNOLOGY

A mixer-settler is the most commonly used contactor in commercial hydrometallurgical SX applications. A mixer-settler (Figure 1.1) consists of a mechanically agitated mixing tank, in which one phase is dispersed into the other to intimately contact the two phases, and a settling tank, in which the phases disengage.

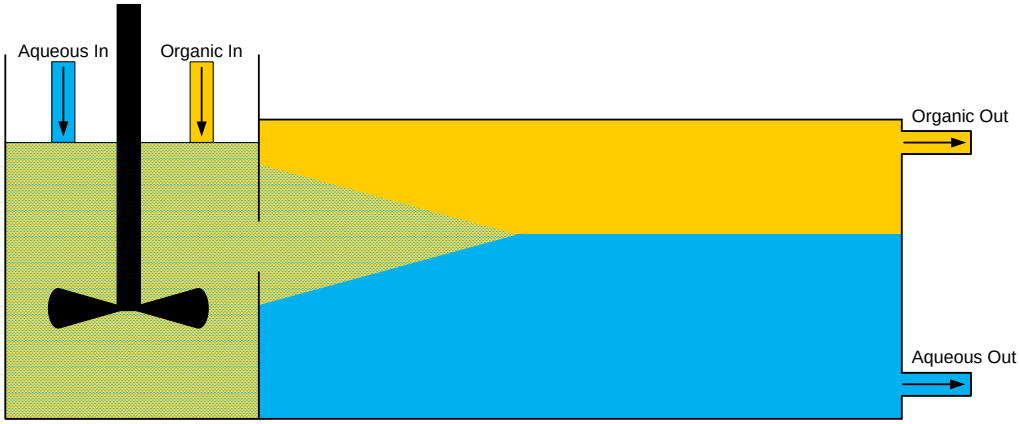


Figure 1.1 Diagram of a mixer-settler

Numerous operational limitations of mixer-settlers have been identified, most of which are at least partly due to the use of mechanical agitation. This includes a wide droplet size distribution, which is undesirable because large droplets have a small specific interfacial area and very small droplets exhibit slow motion. Both of these lead to poor mass transfer. In addition, the latter requires significantly longer disengagement time to avoid entrainment in the opposite phase (Ritcey 2002). Mechanical agitation promotes high shear mixing favouring third phase formation and, eventually, crud, which can significantly impede contactor operation (Ritcey 1980). Mechanical agitators have poor energy efficiency, and therefore high power consumption, because energy is applied to the bulk of the continuous phase and they only provide adequate mixing near the agitator. As a result of their inefficiency, often many mixer-settler units are required in series, which leads to requirements for a large solvent inventory and a large plant footprint. Mixer-settlers also exhibit high solvent losses owing to misting in the mixer, and evaporation in both the mixer and settler.

The pulse column is the other main contactor that has been used in commercial hydrometallurgical SX applications. A pulse column (Figure 1.2) is a vertical column that contains perforated plates and is equipped with a pulsing device, which is typically a diaphragm pulse pump. The organic phase, which has lower density, enters at the bottom of the column, the aqueous phase enters at the top, and the phases flow counter-current through the column owing to the difference in their density. The

pulsing action induces turbulence and mixing within the column to intimately contact the two phases.

Development of pulse columns has circumvented some of the disadvantages of the mixer-settler, but many limitations inherent to mechanical agitation remain. Pulse columns require smaller solvent inventory, minimise solvent losses, and reduce the plant footprint requirement. This contactor, however, is not suitable for SX systems with slow kinetics since prohibitively tall columns would be required to provide sufficient residence time for mass transfer. Significantly, pulse columns retain many of the inherent limitations of mechanical agitation which result in poor mass transfer, including a wide droplet size distribution, and decreasing motion with droplet size. Clearly, the two requirements for efficient mass transfer, which are high interfacial area and fast dispersed phase motion, are mutually exclusive in mechanically agitated contactors.

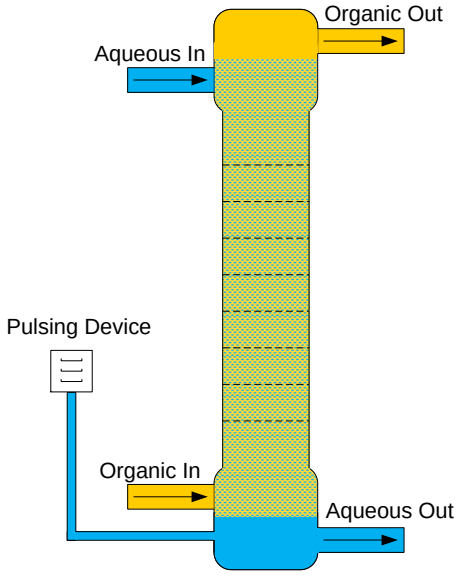


Figure 1.2 Diagram of a pulse column

Other contactors that have been used in commercial hydrometallurgical SX applications include centrifugal contactors, in-line mixers and various column designs. They however have not received as much attention as mixer-settlers and pulse columns.

After more than half a century of efforts to optimise mass transfer in mechanically agitated contactors, it is reasonable to suggest that significant improvement is unlikely unless an altogether new agitation technique is used. The use of electrostatic fields is a promising alternative.

## 1.3. ELECTROSTATIC SOLVENT EXTRACTION

Electrostatic solvent extraction (ESX) is a modification of SX. The main difference is that ESX utilises electrostatic fields, rather than mechanical agitation, to intimately contact the aqueous and organic phases. The technique is based on the principle that when a droplet of a conductive liquid, such as a PLS, that is suspended in a relatively non-conductive liquid, such as an organic solvent, is subjected to a high strength electrostatic field, the conductive liquid is dispersed into smaller droplets.

In theory, ESX promises to overcome several of the inherent limitations of mechanical agitation. For example, the use of electrostatic fields has been shown to be more energy efficient leading to lower power consumption (Scott, DePaoli and Sisson 1994), provide low shear mixing (Scott and Wham 1989), and may also be used to enhance phase disengagement (Bailes & Larkai 1981; Bailes 1992).

Theoretically, one of the main advantages of ESX is enhanced mass transfer, which accordingly occurs as a result of several fundamental effects of electrostatic fields. Firstly, electrostatic fields may induce phenomena that promote mass transfer at droplet interfaces. Secondly, electrostatically induced dispersion may allow greater control of droplet size distributions by altering the properties of the field. Thirdly, electrostatic fields may induce vigorous motion of droplets of all sizes as they pass through the continuous phase in response to gravity and thus, effect an electrostatically induced droplet agitation. It therefore appears that interfacial phenomena, droplet dispersion, and droplet agitation are the main factors that influence mass transfer in ESX.

Recent studies carried out at Curtin University's Western Australian School of Mines (Heckley 2002, Collard 2011, Steffens 2011), have been directed toward developing an application of ESX for hydrometallurgical systems. These studies have already yielded significant advancements including the achievement of a volumetric throughput that is comparable to that of a conventional pulse column at pilot-plant scale, as well as the purification of feed solutions generated from the leaching of nickel laterite ores. Despite their promising results, however, a commercial ESX application is yet to be developed. This may be attributed to the still scarce technical data particularly in regards to the effect of electrostatic fields on mass transfer under experimental conditions that are relevant to hydrometallurgical SX, as well as several inconsistencies in the scientific literature and thus, a lack of fundamental understanding of the main factors that influence mass transfer in ESX.

## 1.4. AIMS OF THE PRESENT STUDY

The aim of the present study is to further the understanding of the main factors that influence mass transfer in ESX. Specifically, this study aims to:

- review the current understanding of the effect of electrostatic fields on mass transfer in SX,
- develop laboratory equipment to allow investigation of the main factors that influence mass transfer in ESX,
- determine how electrostatic fields influence the interfacial phenomena and the mass transfer across the aqueous-organic interface under conditions that are relevant to hydrometallurgical SX,
- determine how the properties of electrostatic fields effect and affect the droplet dispersion, the droplet agitation in the resulting dispersions and the mass transfer within the dispersions, and
- determine the most suitable electrostatic field conditions for practical applications of ESX.

## 1.5. SCOPE AND LIMITATIONS OF THE PRESENT STUDY

The scope of the present study is to further the knowledge on electrostatically induced interfacial phenomena, droplet dispersion, and droplet agitation, and to determine the effect of these factors on mass transfer.

The extraction of Co(II) with Cyanex® 272 was used as the test system to assist the efforts to develop an ESX application for the purification of nickel and cobalt from nickel laterite leach solutions. In addition, the distinctive colours of the aqueous and organic phases in this system facilitated the use of the analytical techniques that were required for parts of this study.

Given that this work was fundamental in nature, synthetic solutions were used to minimise the effect of extraneous factors that could influence the results. Since ESX is based on the principle of droplets of a conductive liquid, which are suspended in a relatively non-conductive liquid, the investigation of droplet dispersion and agitation was limited to an organic-continuous system.

The study was also limited to investigating the effect of the properties of electrostatic fields on mass transfer on the test system. Other variables, such as the physical properties of the solutions, may also be relevant but including them would have made the scope too large for the given period to complete the study.

## 1.6. CHAPTER SUMMARY

In summary, the use of hydrometallurgical SX for the processing of metals has been increasing and expanding, but after more than 50 years of commercial application it is clear that the technique has some limitations that are inherent to the use of mechanical agitation. These limitations adversely affect the mass transfer rate of species between the aqueous and organic phases.

Clearly, the use of electrostatic fields is a promising alternative to mechanical agitation. ESX has a number of theoretical advantages, including enhanced mass transfer. In spite of its advantages, no commercial application of ESX has been developed, which may be partly attributed to a lack of fundamental understanding of the main factors that influence mass transfer in ESX. The aim of the present study is to address this gap in the knowledge.

# Chapter 2

# REVIEW OF STUDIES ON THE EFFECT OF ELECTROSTATIC FIELDS ON MASS TRANSFER IN SOLVENT EXTRACTION

## 2.1. INTRODUCTION

This chapter contains a review of previous investigations on the effect of electrostatic fields on mass transfer in solvent extraction (SX). This is preceded by a brief overview of mass transfer in SX to provide a context and focus.

The application of electrostatic fields across a liquid-liquid interface has been proposed to induce phenomena that influence interfacial processes, including (1) the Marangoni effect and Marangoni-type turbulence, (2) movement of electric charges in the organic phase (3) electromigration of species in the aqueous phase and (4) orientation of species in the organic phase. It has also been proposed that, in organic-continuous systems, electrostatic fields induce droplet dispersion and can influence several forms of droplet agitation, including (1) droplet oscillation, (2) droplet speed and (3) droplet zigzagging.

In theory, all of these effects of electrostatic fields influence mass transfer, but little work has been done on this topic, particularly in regards to hydrometallurgical SX systems, and therefore, there is currently insufficient understanding of how to exploit electrostatic fields to enhance mass transfer. As a first step to address this gap in the knowledge, the current understanding of the effect of electrostatic fields on mass transfer was reviewed. Previous studies were grouped into the effects of electrostatic fields on (1) interfacial phenomena, (2) droplet dispersion and (3) droplet agitation.

An experimental investigation on the effect of electrostatic fields on mass transfer is also required to address the gaps in the knowledge and therefore, the relevant experimental techniques were also reviewed. Given that no standard technique exists for investigating the effect of electrostatic fields on mass transfer, this review was focused on conventional techniques for measuring mass transfer in solvent extraction. The review includes the significant modifications that have been reported to improve the techniques, as well as previous attempts to adapt the techniques to investigate the effect of electrostatic fields.

## 2.2. OVERVIEW OF MASS TRANSFER IN SOLVENT EXTRACTION

The transfer of masses between two immiscible liquids may be described by the extended two-film theory. The original two-film theory, which was proposed by Whitman (1923), postulates that the mass transfer rate of solutes is controlled by the rate of diffusion through two diffusion regions that exist on either side of a liquid-gas interface. Lewis (1954) extended this theory to mass transfer of solutes across a liquid-liquid interface. Application of the two-film theory to immiscible phases in solvent extraction (SX) is illustrated in Figure 2.1. The thickness of the diffusion regions, δ, is dependent on the hydrodynamics within the apparatus that is being used to carry out mass transfer. Increases in the stirring of the bulk phases causes decreases in the thickness of the diffusion regions until a minimum practical thickness of $10^{-3}$ – $10^{-4}$ cm (Danesi 2004) is reached.

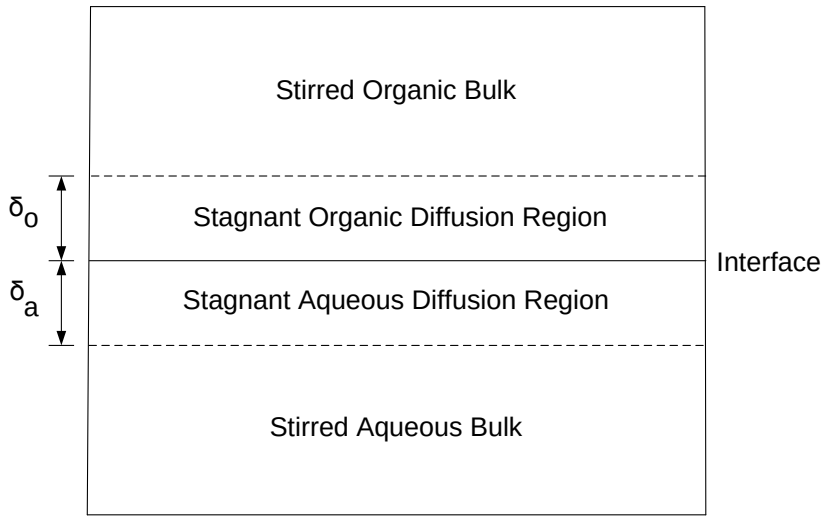


Figure 2.1 Diagram of the interfacial region at a liquid-liquid interface according to the extended two-film theory

The theory is based on the assumptions that the only concentration gradient exists in the diffusion regions, and that equilibrium exists at the interface. Therefore, the concentrations of species at the interface are dependent on the equilibrium relationship. The theoretical concentration profile according to the two-film theory is shown in Figure 2.2.

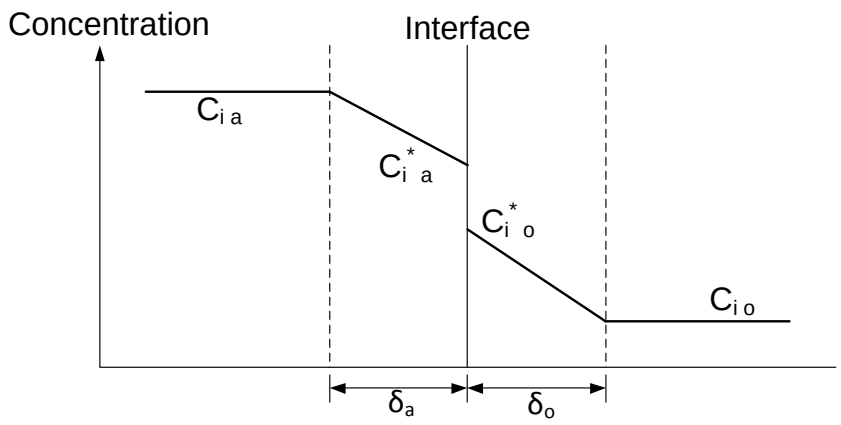


Figure 2.2 Theoretical concentration profile for the transfer of species from the aqueous phase to the organic phase

Mass transfer may also be described by other theories, including the boundary layer theory, surface renewal theory and penetration theory. Each of these involves different assumptions about the nature of mass transfer and therefore each is only applicable for certain scenarios. Nevertheless, measures of mass transfer may be calculated using the general equation shown in Equation 2, which is derived from Fick's law of steady-state diffusion.

$$J_i = k_i(C_i - C_i^*) \qquad \text{(Equation 2)}$$

where: $J$ is the mass transfer flux, $k$ is the mass transfer coefficient, $C_i$ is the concentration of the species of interest at a given time, and $C^*_i$ is the concentration of the species of interest at equilibrium.

Measures of mass transfer reported in scientific literature are expressed as either the mass transfer rate, which is the ratio of the change in concentration of the species of interest to the change in time; the mass transfer coefficient, which is the ratio of the mass transfer flux to the concentration driving force; or the mass transfer flux.

Mass transfer between two immiscible liquids may be described as either non-reactive mass transfer or reactive mass transfer, depending on whether the system involves a chemical reaction. In non-reactive systems, the overall rate of mass transfer depends only on the rate of physical transport of the species through the diffusion regions. In reactive systems, however, the overall rate of mass transfer may be controlled by either the rates of the chemical reactions or physical transport or both depending on the relative rates of these processes. If the speed of the chemical reactions is fast in comparison with the rate of diffusion, the system is referred to as diffusion-controlled. If, however, the chemical reactions are much slower than transport processes, the

system is referred to as kinetic-controlled. If the rate of transport through the diffusion regions is comparable to the speed of the chemical reaction, the system is referred to as mixed control (Danesi, Chiarizia & Coleman 1980). The rate-controlling process in reactive mass transfer systems is dependent on the nature of the reactants as well as the hydrodynamics within the apparatus that is being used to carry out mass transfer. The majority of hydrometallurgical SX systems are reactive mass transfer systems.

It follows that the rate of mass transfer in SX may be changed by altering the processes at a liquid-liquid interface. The rate of mass transfer in a diffusion-controlled system may be increased by enhancing the transport of reactants toward the interface, or by enhancing the transport of products away from the interface. The rate of mass transfer in a kinetic-controlled system may be increased by enhancing the speed of the chemical reaction. In the present study, a phenomenon that can alter these interfacial processes, whether naturally occurring or induced by an external means, will be referred to as an interfacial phenomenon. Researchers have proposed that application of electrostatic fields across a liquid-liquid interface may induce phenomena that influence interfacial processes and thus, alter mass transfer rates.

In the case of mass transfer between droplets and a continuous phase, the rate of mass transfer is also influenced by the droplet's interfacial area and internal circulation. A greater interfacial area, which can be achieved by decreasing the droplet size, is favourable for mass transfer as it creates more sites for mass transfer to occur. Greater internal circulation, which is a form of agitation that can occur within moving droplets (Figure 2.3), is favourable for mass transfer as it decreases the thickness of the diffusion regions.

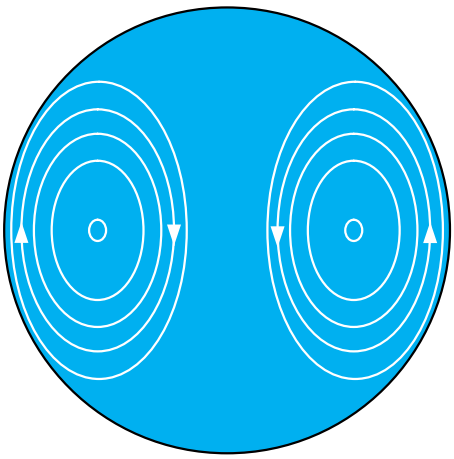

Figure 2.3 Diagram of internal circulation that can occur within moving droplets

It follows that the ideal conditions to maximise the mass transfer rate are to generate droplets that have (1) a large interfacial area, and (2) intense internal circulation. These conditions, however, are mutually exclusive using the current SX technology because decreases in droplet size leads to decreases in internal droplet motion in mechanically agitated contactors (Ritcey 2006b). Researchers have suggested that application of electrostatic fields to an organic-continuous system may generate droplets with large interfacial area and induce intense droplet agitation and thus, increase mass transfer rates.

## 2.3. EFFECT OF ELECTROSTATIC FIELDS ON INTERFACIAL PHENOMENA

### 2.3.1. The Marangoni Effect

It is well known that when two liquids with different surface tensions are in contact with each other, the liquid with higher surface tension has a stronger pull for the liquid with lower surface tension, leading to a movement of liquid toward the region of higher surface tension. This phenomenon was first reported by Marangoni (1871), and has since been referred to as Marangoni effect to honour its discoverer. A familiar example of this phenomenon is the so-called "tears of wine", which occurs owing to the difference in surface tensions of ethanol and water. In the case of immiscible liquids that are in contact with each other and are not at equilibrium, the Marangoni effect can cause turbulence and thus, induce intense mixing, at the liquid-liquid interface.

Qualitative investigation of the Marangoni effect was the focus of early work on the topic. In some cases, such as the "tears of wine", the Marangoni effect can be observed by the naked eye. When this is not the case, however, flow visualisation techniques such as the schlieren technique are used. This technique detects changes in the refractive index of liquids, and produces a magnified image of these changes. An example of an image generated by the schlieren technique is shown in Figure 2.4.

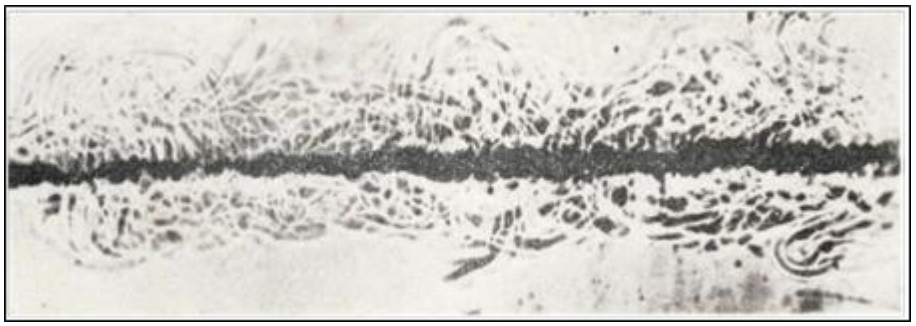

Figure 2.4 Schlieren image showing turbulence near the interface of carbon tetrachloride and water (Maroudas & Sawistowski 1964)

In the case of immiscible liquids, local gradients in the interfacial tension promote the Marangoni effect. Sternling and Scriven (1959) carried out mathematical modelling and postulated that interfacial turbulence is promoted by (1) larger differences in the kinematic viscosity and solute diffusivity between the two phases, (2) solute transfer out of the phase with higher viscosity and lower solute diffusivity, (3) steep concentration gradients near the interface, (4) larger interfacial area, and (5) the absence of surface-active agents. Later investigations have found, however, that experimental results are consistent with these postulates for only some chemical systems. In addition, the intensity of interfacial turbulence varies significantly between chemical systems (Austin, Ying & Sawistowski 1966). Evidently, the occurrence and intensity of the Marangoni effect are difficult to predict from theory.

One focus of research on the Marangoni effect has been directed towards understanding how it affects the mass transfer of solutes between two immiscible liquids. As may be expected, the Marangoni effect leads to higher mass transfer rates compared with diffusion alone but the actual enhancement varies significantly between chemical systems. This may be attributed partly to the differences in the rate-controlling processes, and partly to other contributing factors such as the experimental variables mentioned previously. It is difficult to quantify the effect of this naturally occurring phenomenon on mass transfer rates because it cannot be isolated from other phenomena that may be deliberately induced to increase mass transfer rates. Nonetheless, the presence of Marangoni effect is clearly an advantage if the aim is to enhance mass transfer rates.

It is for this reason that, in the present study, it is of particular interest to determine whether and, if so, how electrostatic fields influence the Marangoni effect and thus, affect mass transfer rates. Although only a few studies on this topic have been reported, the results indicate that subjecting a liquid-liquid interface to an electrostatic field can

alter, either enhance or depress, the intensity of naturally occurring Marangoni effect, or induce Marangoni-type turbulence. The focus of research on this topic has been on the latter. The occurrence and intensity of Marangoni-type turbulence cannot be predicted from theory, which is similar to the naturally occurring phenomenon. Studies on this topic are grouped into the effect of electrostatic fields on (1) non-reactive mass transfer systems and (2) reactive mass transfer systems.

#### *2.3.1.1. Non-Reactive Mass Transfer Systems*

Electrostatic fields can enhance or depress the intensity of naturally occurring Marangoni effect, as well as induce Marangoni-type turbulence in non-reactive mass transfer systems. The occurrence and intensity of interfacial turbulence is influenced by several properties of the electrostatic field, such as the applied voltage (Austin, Banczyk & Sawistowski 1971; Hund & Lancelot 1986; Gneist & Bart 2003), electrode polarity (Iyer & Sawistowski 1974), and the type of electrostatic field (Gneist & Bart 2003) as well as several properties of the two phases, such as the differences between the kinematic viscosity (Gneist & Bart 2003) and the dielectric constants. The effect of electrostatic fields on mass transfer rates, however, cannot be attributed to only interfacial turbulence.

The applied voltage of an electrostatic field is a major factor that influences Marangoni-type turbulence. In some systems, increases in the applied voltage do not have a uniform effect on mass transfer rates. In their pioneering work, Austin, Banczyk and Sawistowski (1971) used a laminar flow apparatus to study the effect of direct current (DC) fields on the transfer of water into four different organic liquids that had been shown previously (Austin, Ying & Sawistowski 1966) to not exhibit naturally occurring Marangoni effect. Qualitative evidence indicates that Marangoni-type turbulence was induced in the presence of a field (Figure 2.5). Increases in the applied voltage led to increases in the intensification of the interfacial turbulence in several systems. Consistent with these observations, increases in the applied voltage from 0 – 2.25 kV led to increases in the mass transfer coefficient of water by up to 1000% (Figure 2.6). A similar observation of increases in applied voltage leading to increases in Marangoni-type turbulence was also reported by Hund and Lancelot (1986) for the transfer of acetic acid from water into an organic phase containing tri-butyl-phosphate and dodecane, and by Gneist and Bart (2003) for the transfer of acetone from water into toluene.

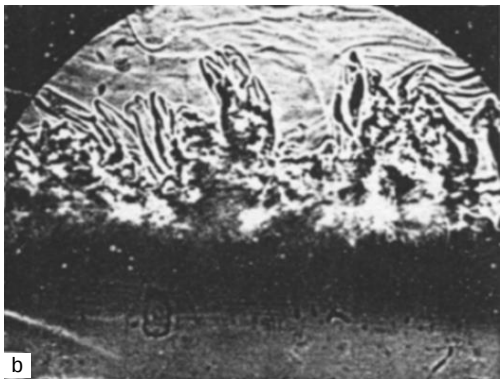


Figure 2.5 Schlieren photographs showing turbulence at the interface of cyclohexanol and water (Austin, Banczyk & Sawistowski 1971)

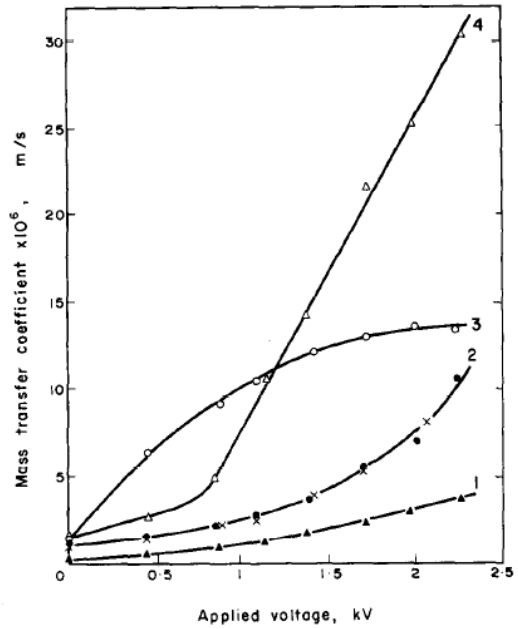


Figure 2.6 Effect of applied voltage on the mass transfer coefficient of water into several organic liquids (Curve 1 - cyclohexanol, Curve 2 - isobutanol, Curve 3 - aniline, Curve 4 - ethyl acetate) (Austin, Banczyk & Sawistowski 1971)

Austin, Banczyk and Sawistowski (1971) proposed that the application of electrostatic fields creates local variations in the density of electric charges at an interface, which causes a corresponding gradient in the interfacial tension and thus promotes Marangoni-type turbulence. Clearly, electrostatic fields induced Marangoni-type turbulence in these immiscible liquids, and increases in the applied voltage led to increases in the intensity of the turbulence.

It is interesting to note, however, the rather disparate curves in Figure 2.6. There is no clear pattern for the effect of applied voltage on the mass transfer coefficient of water into the organic liquids that were investigated in this work. The authors made no attempt to explain these data. Closer examination of the physical properties of the liquids used in this study reveals that decreases in the differences between the kinematic

viscosities of the phases led to increases in the maximum mass transfer coefficient. The kinematic viscosity is the ratio of the dynamic viscosity to the density. In addition, increases in the differences between the dielectric constants of the phases led to increases in the maximum mass transfer coefficient. The dielectric constant is the ratio of the electric displacement to the electric field strength when an external field is applied. The relevant physical properties for these solutions were obtained from Lide (2002) and Ullmann's Encyclopedia of Industrial Chemistry (2012) and are summarised in Table 2.1.

Table 2.1 Physical properties of selected solutions used by Austin, Banczyk and Sawistowski (1971)

| **Physical Property at 20 °C** | Ethyl acetate | Aniline | Isobutanol | Cyclohexanol | Water |
|---|---|---|---|---|---|
| **Density (g/cm$^3$)** | 0.900 | 1.02 | 0.802 | 0.962 | 1.00 |
| **Viscosity (mPa s)** | 0.42 | 3.85 | 3.95 | 57.5 | 0.89 |
| **Kinematic Viscosity (cSt)** | 0.47 | 3.76 | 4.93 | 59.7 | 0.89 |
| **Dielectric Constant** | 6.08 | 7.06 | 18.8 | 16.40 | 80.1 |

One relationship that may be inferred from the data of Austin, Banczyk and Sawistowski (1971) is that decreases in the differences between the kinematic viscosities of the phases leads to greater Marangoni-type turbulence. It is interesting to note that this relationship, shown in Table 2.2, is the opposite of that which has been proposed for naturally occurring Marangoni effect. It is likely that increases in the viscosity of the organic phase would dampen Marangoni-type turbulence and thus lead to less increase of mass transfer rates. The findings of Gneist and Bart (2003) are also consistent with these data. They reported that, under comparable DC field conditions, interfacial turbulence was less pronounced for the transfer of 1-propanol from water into isotridecanol, which has a substantially higher viscosity, than for the transfer of acetone from water into toluene.

Table 2.2 Effect of the viscosity of the phases on the maximum mass transfer coefficient for the systems investigated by Austin, Banczyk and Sawistowski (1971)

| **Organic Phase** | Cyclohexanol | Isobutanol | Aniline | Ethyl Acetate |
|---|---|---|---|---|
| **System number on Figure 2.6** | 1 | 2 | 3 | 4 |
| **Difference between the kinematic viscosity of the phases (cSt)** | 58.86 | 4.04 | 2.87 | 0.42 |
| **Maximum mass transfer coefficient (x $10^{-6}$ m/s)** | 3.5 | 11.0 | 13.5 | 31.0 |

Another relationship that can be inferred from the data of Austin, Banczyk and Sawistowski (1971) is that increasing differences in the dielectric constants of the two phases that are in contact leads to greater interfacial turbulence. This is evident in the effect of the dielectric constant on the maximum mass transfer coefficient (Figure 2.7). Predictions of the effect of dielectric constant on Marangoni-type turbulence in a later modelling study by Mohan, Padmanabhan and Chandrasekharan (1983) is consistent with these data.

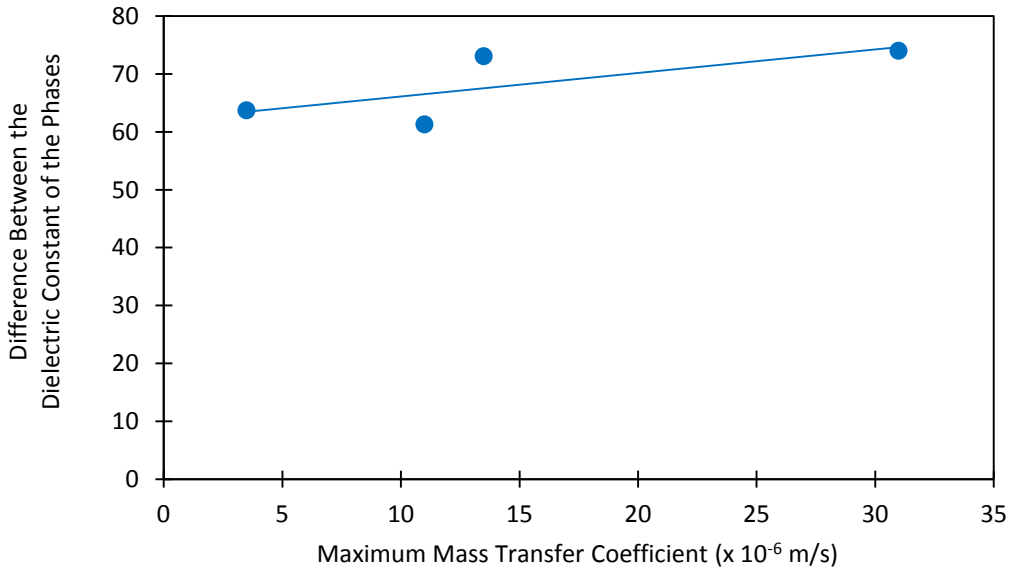


Figure 2.7 Effect of the dielectric constant of the phases on the maximum mass transfer coefficient for the systems investigated by Austin, Banczyk and Sawistowski (1971)

The electrode polarity of electrostatic fields is another factor that can influence Marangoni-type turbulence. In a later publication by the same research group, Iyer and Sawistowski (1974) found that the magnitude of interfacial turbulence in some systems was unaffected by the polarity, while others such as isobutanol/water exhibited more intense turbulence with positive polarity, and others such as n-butyl acetate/water were more affected by negative polarity. These authors stated that their data were insufficient to predict the effect of electrode polarity on Marangoni-type turbulence.

The type of electrostatic field also appears to influence Marangoni-type turbulence. This was shown by Gneist and Bart (2003), who compared the effect of DC and alternating current (AC) fields on the interface of single stationary aqueous droplets that were immersed in a continuous organic phase. The droplets were held from a charged capillary that was mounted vertically above a grounded electrode. In the absence of an applied field, interfacial turbulence was initially observed, but the intensity declined

gradually and led to the formation of what the authors referred to as a diffusion layer around the droplet, which hindered mass transfer. Application of a DC field (2 kV) enhanced Marangoni-type turbulence at the interface and, in contrast to that in the absence of a field, did not form a diffusion layer. On the other hand, application of an AC field (2 kV, 30 kHz) suppressed interfacial turbulence and enhanced the rate of formation of a diffusion layer. These authors concluded that a DC field increased the mass transfer rate owing to ion-drag phenomena, while an AC field decreased the mass transfer rate compared with that in the absence of a field. It should be noted, however, that while a number of studies have reported consistent trends in regards to the effect of DC fields on Marangoni-type turbulence, no other study has been reported on the effect of AC fields.

In spite of the effects of Marangoni-type turbulence on mass transfer that have been discussed, this is not the only interfacial phenomenon induced by electrostatic fields. Sawistowski and co-workers (1971, 1974) proposed that the increases in mass transfer rates in their work could not be completely attributed to interfacial turbulence. This is supported by the work of Glitzenstein, Tamir and Oren (1995), who reported that interfacial turbulence was not responsible for an enhancement in the transfer of acetic acid from kerosene into water in the presence of DC fields.

#### *2.3.1.2. Reactive Mass Transfer Systems*

Electrostatic fields can induce Marangoni-type turbulence in reactive mass transfer systems. The occurrence and intensity of interfacial turbulence are influenced by several properties of the electrostatic field, such as the applied voltage and electrode polarity (Hund & Lancelot 1986), as well as properties of the phases, such as the number of charge carriers in the organic phase (Kuipa & Hughes 1999). Interfacial turbulence may also be influenced by the type of chemical reaction in reactive mass transfer systems (Hund & Lancelot 1986). The effect of electrostatic fields on mass transfer rates, however, cannot be completely attributed to interfacial turbulence only. It should be noted however that these findings are based on only two studies on interfacial turbulence in reactive mass transfer systems that have been reported.

The effect of electrostatic fields on Marangoni-type turbulence for reactive mass transfer systems is influenced by the applied voltage and electrode polarity. Hund and Lancelot (1986) reported that increases in the applied voltage led to increases in interfacial turbulence for the ion exchange system. These authors also found that the

intensity of the turbulence was greater with a positive polarity in the same system. The effect of applied voltage and the non-uniform effect of the electrode polarity on interfacial turbulence are similar to those for non-reactive mass transfer systems.

The number of charge carriers in the organic phase appears to influence Marangoni-type turbulence. Kuipa and Hughes (1999) suggested that increasing the number of charge carriers in the organic phase favours a steeper gradient in the density of electrostatic charges at the interface and thus promotes favourable conditions for Marangoni-type turbulence. As evidence, they pointed to the data from experiments using a rotating diffusion cell, which show that DC fields only influenced the extraction flux of Cu(II) with bis(2-ethylhexyl)phosphoric acid (D2EHPA) and 5-nonylsalicylaldoxime (P50) when octanol was added to the diluent that initially consisted of only heptane. The addition of octanol also caused a dramatic increase in the current in the organic phase, which is further evidence consistent with the authors' hypothesis.

The effect of electrostatic fields on Marangoni-type turbulence may be influenced by the type of chemical reaction in a reactive mass transfer system. Using a modified Lewis cell, Hund and Lancelot (1986) compared the effect of DC fields on mass transfer in the stripping of rare earth species from an unspecified loaded solvent with nitric acid, which they indicated was an ion exchange reaction and the extraction of Cu(II) with LIX 65N, which is a chelation reaction. The authors reported that they observed some Marangoni-type turbulence in the ion exchange system, but none in the chelation system. Their data showed that electrostatic fields increased the mass transfer rate in the ion exchange system, which they attributed partly to the interfacial turbulence.

Marangoni-type turbulence is not the only interfacial phenomenon that causes increased mass transfer rates in the presence of electrostatic fields. Hund and Lancelot (1986) reported that the mass transfer rate increased in the chelation system, even though no Marangoni-type turbulence was observed in this system. Clearly, Marangoni-type turbulence is not the only interfacial phenomenon induced by electrostatic fields. This finding is similar to that for non-reactive mass transfer systems.

### 2.3.2. Movement of Electric Charge in the Organic Phase

Movement of electric charge refers to electrostatically induced movement of electrons within an organic phase between a charged electrode and a discontinuity of electrical properties, such as a liquid-liquid interface. Several investigators have observed turbulence in the organic phase in the presence of electrostatic fields and all of these

investigators have speculated that this is owing to field-induced movement of electric charges in this phase. This phenomenon increases mass transfer rates, but its intensity is influenced by several properties of the electrostatic field, such as the applied voltage (Austin, Banczyk & Sawistowski 1971) and electrode polarity (Iyer & Sawistowski 1974), as well as properties of the phases, such as the dielectric constant (Glitzenstein, Tamir & Oren 1995) and the number of charge carriers.

The effect of electrostatic fields on the movement of electric charges in the organic phase is influenced by the applied voltage and electrode polarity. Austin, Banczyk and Sawistowski (1971) reported that increases in the applied voltage caused increases in the intensity of turbulence in the organic phase for several non-reactive mass transfer systems. In a later study by the same research group, Iyer and Sawistowski (1974) found that the polarity of the charged electrode in a DC field did not have a uniform effect on turbulence in the organic phase. That is, the intensity of turbulence in the organic phase was dependent on the polarity of the charged electrode for some systems, but this observation was not uniform for all systems that were investigated. Sawistowski and co-workers (1971, 1974) concluded that the movement of electric charge in the organic phase is a distinct phenomenon that contributes to increases in the rates of mass transfer.

The movement of electric charge is also dependent on the dielectric constant of the phases. Glitzenstein, Tamir and Oren (1995) suggested that this phenomenon only occurs in the organic phase owing to its relatively low dielectric constant. These authors investigated the effect of DC fields on the transfer of acetic acid from kerosene into water. Their experimental method involved adding alumina powder (60 nm Ø) into the organic phase to act as a tracer and thus, allowed observation of liquid motion in this phase. They reported that an applied field caused the tracer, which had concentrated at the interface in the absence of a field, to move between the interface and the electrode in the organic phase (Figure 2.8).

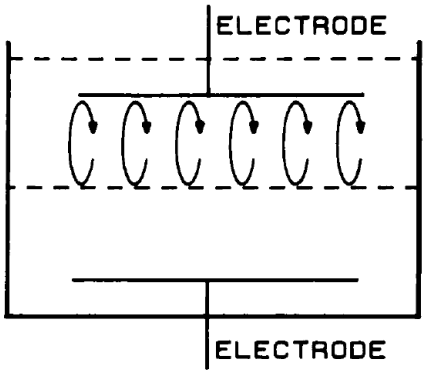


Figure 2.8 Liquid motion induced by an applied field at a water-kerosene interface (Glitzenstein, Tamir & Oren 1995)

This (Glitzenstein, Tamir & Oren 1995) is the only study that has attempted to explain how this phenomenon induces turbulence in the organic phase, which leads to increases in mass transfer rates. These investigators proposed that the liquid motion was responsible for a 150% increase in the mass transfer coefficient of acetic acid in their experiments. They speculated that the liquid motion may be caused by field-induced polarization of the kerosene molecules, and the subsequent interaction of these molecules with the partly dissociated acetic acid molecules. This, however, is difficult to imagine given that the dissociation of acetic acid would be negligible in an organic solvent such as kerosene.

It may also be postulated, however, given the information presented by Glitzenstein, Tamir and Oren (1995), that the movement of electric charges is dependent on the number of charge carriers in the organic phase. These investigators found that the liquid motion induced by the applied field only occurred when the organic phase contained acetic acid. Clearly, the addition of acetic acid increases the number of charge carriers in the organic phase because acetic acid is a polar molecule when dissolved in kerosene. The permanent dipoles of acetic acid would provide more pathways for the movement of electric charge through the organic phase in the presence of an applied field.

### 2.3.3. Electromigration of Species in the Aqueous Phase

Electromigration refers to the movement of charged species in the aqueous phase due to attraction or repulsion between the species and a charged electrode (Martin et al. 1983; Wildberger & Bart 2002). That is, if the species has the opposite charge to an electrode, the species will be attracted toward the electrode. On the other hand, if the species has the same charge as an electrode, the species will be repelled away from the electrode. In theory, electromigration can therefore increase or decrease the mass

transfer rate of charged species by altering their rate of movement toward a liquid-liquid interface, but this is dependent on the electrode configuration of the experimental apparatus. Researchers have proposed that if the upper electrode in a modified Lewis cell is positively charged, as shown in Figure 2.9, the electromigration phenomenon would cause negatively charged species in the aqueous phase to be attracted toward the interface. On the other hand, positively charged species would be repelled away from the interface.

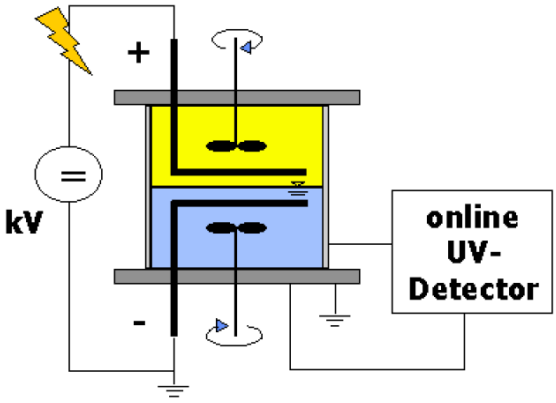


Figure 2.9 Modified Lewis cell with a positively charged upper electrode immersed in the organic phase and an earthed lower electrode immersed in the aqueous phase (Wildberger & Bart 2002)

The effect of electromigration on mass transfer rates was first reported by Martin et al. (1983). These authors investigated the effect of DC fields on the extraction of Cu(II) with LIX 65N (Equation 3) using a modified Lewis cell with electrodes placed on either side of the interface similar to that in Figure 2.9. They compared Cu(II) extraction in the absence of an applied field with that with an applied voltage of +10 kV and -10 kV. Their results indicate that, relative to without an applied field, the rate of transfer of Cu(II) increases in the presence of an applied field with both positive and negative electrode polarities (Figure 2.10). The authors proposed that the increased rate of mass transfer may be partly attributed to the electromigration of species toward the interface. This explanation, however, is inconsistent with the electromigration phenomenon. The authors could not explain why both positive and negative electrode polarities resulted in increased mass transfer rates. They stated that further work was being carried out, but no further work has been reported.

$$Cu^{2+}_{(aq)} + 2RH_{(org)} \leftrightarrow CuR_{2(org)} + 2H^{+}_{(aq)} \qquad \text{(Equation 3)}$$

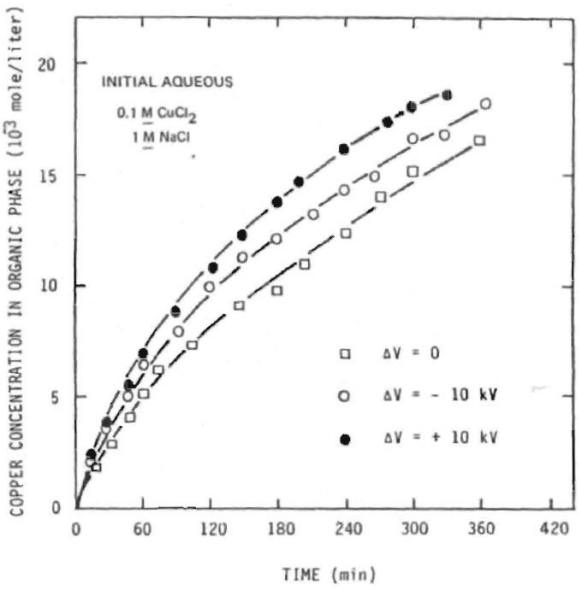


Figure 2.10 The effect of applied fields on the transfer of Cu(II) into the organic phase (Martin et al. 1983)

Consistent with the electromigration phenomenon were the findings of a later study by Wildberger and Bart (2002). These authors investigated the effect of DC fields on mass transfer in the reactive extraction of p-toluenesulfonic acid (HA) with tri-n-octylamine (TOA) (Equation 4) using a modified Lewis cell. They stated that the experimental conditions were such that the system was kinetic-controlled, and they proposed that any effect on mass transfer could only be attributed to migration induced by the applied field rather than by diffusion. They found that increases in the applied voltage resulted in increases in the mass transfer rate. The authors attributed this to the attraction of HA anions in the lower phase to the positively charged electrode in the upper phase, and thus, the enhanced migration of HA anions toward the interface.

$$HA_{(aq)} + TOA_{(org)} \leftrightarrow TOAHA_{(org)} \qquad \text{(Equation 4)}$$

These researchers also observed that the extraction of Zn(II) with D2EHPA (Equation 5) was consistent with the electromigration phenomenon. Their results indicated that increases in the applied voltage resulted in decreases in the mass transfer rate of Zn(II). The authors attributed this to the repulsion of the Zn(II) cations in the lower phase by the positively charged upper electrode, and thus, the reduced migration of Zn(II) toward the interface.

$$Zn^{2+}_{(aq)} + 2RH_{(org)} \leftrightarrow ZnR_{2(org)} + 2H^{+}_{(aq)} \qquad \text{(Equation 5)}$$

Quite clearly, these two studies reported contrasting results. On the one hand, Martin et al. (1983) found that both positive and negative electrode polarities caused increases in

the mass transfer rate of positively charged species relative to that without an applied field. On the other hand, Wildberger and Bart (2002) found that a positive electrode polarity caused an increase in the mass transfer rate of negatively charged species and a decrease in the mass transfer rate of positively charged species.

### 2.3.4. Orientation of Species in the Organic Phase

Orientation refers to a field-induced orientation of species in the organic phase, such as extractant molecules, at a liquid-liquid interface in a way that is favourable for a chemical reaction to occur. An applied field causes molecular dipoles in a polar dielectric liquid to align in the direction of the field (Inculet 1973). Although the diluents in SX are largely non-polar, it is reasonable to suggest that the polar extractant molecules within the diluent may be aligned in response to an applied field.

The influence of the orientation of extractant molecules on mass transfer across a liquid-liquid interface was proposed by Hund and Lancelot (1986). They investigated the effect of a DC field on the extraction of Cu(II) with LIX 65N using the modified Lewis cell shown in Figure 2.11. They found that, relative to without an applied field, a negative electrode polarity increased the rate of extraction, whereas a positive polarity decreased the rate of extraction. They attributed these results to the favourable orientation of the LIX 65N molecules under the influence of a negative voltage, and unfavourable orientation with a positive voltage.

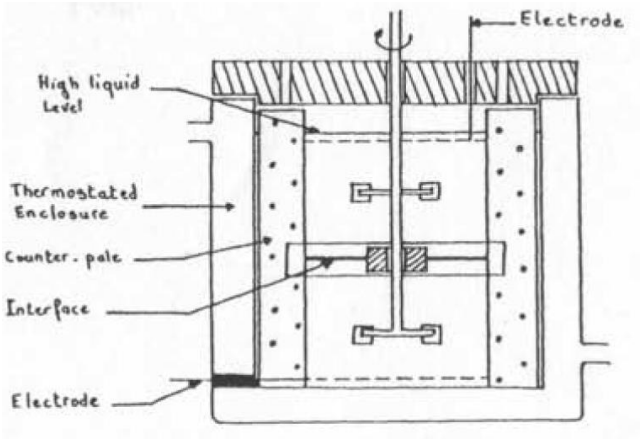


Figure 2.11 Modified Lewis cell used by Hund and Lancelot (1986)

These authors did not offer an explanation of how exactly the charged electrode interacts with the extractant molecules to increase the mass transfer rate. The product from the reaction between Cu(II) and LIX 65N is shown in Figure 2.12. Given that the organic phase is placed on top of the aqueous phase in a modified Lewis cell, it is

difficult to imagine how the charged electrode can influence the orientation of extractant molecules to achieve the orientation required for this reaction.

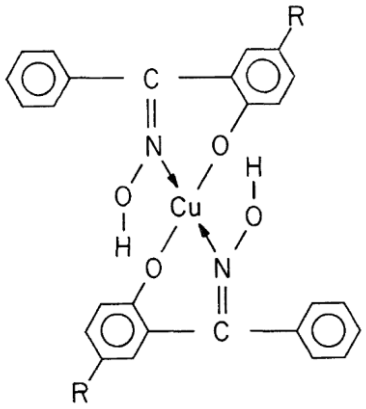


Figure 2.12 Diagram of the product of reaction between Cu(II) and LIX 65N

In a later study, Kuipa and Hughes (1999) argued that the mass transfer enhancement in the presence of an applied field cannot be attributed to the preferential orientation of species at the interface. They pointed out that the electrode polarity would have an effect if the orientation of species was a contributing factor, but they stated that polarity had no effect on the mass transfer rate in their experiments. The conclusion of Kuipa and Hughes (1999) is in direct contrast to that of Hund and Lancelot (1986).

### 2.3.5. Summary

Interfacial phenomena that have been proposed to influence mass transfer across a liquid-liquid interface in the presence of applied fields are (1) Marangoni-type turbulence, (2) movement of electric charge in the organic phase, (3) electromigration of species in the aqueous phase, and (4) orientation of species in the organic phase. It is conceivable that two or more of these phenomena may occur simultaneously in some SX systems.

Marangoni effect is a naturally occurring phenomenon that causes turbulent mixing at a liquid-liquid interface. This phenomenon, which is promoted by local gradients in the interfacial tension, causes increases in mass transfer rates compared with diffusion alone in both non-reactive and reactive mass transfer systems. Subjecting a liquid-liquid interface to electrostatic fields can either enhance or depress the intensity of the Marangoni effect, or induce Marangoni-type turbulence. The occurrence and intensity of field-induced interfacial turbulence is influenced by properties of the phases, such as the differences in the kinematic viscosity and dielectric constant, and the number of charge carriers in the organic phase, as well as properties of the electrostatic fields such

as the applied voltage, electrode polarity, and type of applied field. In the case of reactive mass transfer systems, interfacial turbulence may also be influenced by the type of chemical reaction.

Electrostatic fields can induce movement of electric charge in the organic phase, which may alter the rate of mass transfer in SX systems. The intensity of this phenomenon may be influenced by the applied voltage and electrode polarity, as well as the dielectric constant of the organic phase. It is also likely that the presence of charge carriers in the organic phase is crucial to the occurrence of this phenomenon.

Electromigration may alter the mass transfer rate in SX systems by altering the rate of movement of charged species in the aqueous phase toward a liquid-liquid interface. The effect on the mass transfer rate is dependent on the electrode polarity and the charges of dissolved species. That is, if the species has the opposite charge to an electrode, the species will be attracted toward the electrode. On the other hand, if the species has the same charge as the electrode, the species will be repelled away from the electrode. This can cause the charged species to be attracted to or repelled from a liquid-liquid interface, depending on the electrode configuration.

Electrostatic fields may influence mass transfer rates by inducing the orientation of species in the organic phase in a way that is favourable for chemical reaction at a liquid-liquid interface.

All previous studies on this topic, with one exception, have investigated the effect of DC fields. An investigation of the effect of DC fields will therefore allow comparison to the findings of previous investigators. It is also essential to investigate the effect of the type of electrostatic field by carrying out experiments using transient fields, such as pulsed DC (PDC) and alternating current (AC) to address this gap in the knowledge.

## 2.4. EXPERIMENTAL TECHNIQUES TO STUDY THE EFFECT OF ELECTROSTATIC FIELDS ON INTERFACIAL PHENOMENA

To gain a better understanding of the effects of electrostatic fields on interfacial phenomena requires an experimental technique that allows (1) measurement of mass transfer across a liquid-liquid interface, (2) visual observation of the interfacial region, and (3) application of an electrostatic field across a liquid-liquid interface. Techniques that involve mass transfer across a flat liquid-liquid interface are now reviewed to determine which is the most suitable for the present study.

Given that no standard technique exists for investigating the effect of electrostatic fields on interfacial phenomena, this review was focused on conventional techniques for measuring mass transfer across a liquid-liquid interface including the (1) laminar flow technique, (2) rotating diffusion cell technique, and (3) Lewis cell technique. For each technique, the review comprises the design and method of operation, as well as the significant modifications that have been reported to improve the technique. Finally, the application of each technique to the purpose of the present study is considered, which includes a review of studies that have attempted to adapt these conventional techniques to investigate the effect of electrostatic fields on interfacial phenomena.

### 2.4.1. Laminar Flow Technique

The laminar flow technique involves contacting two immiscible phases over a well-defined interfacial area in the absence of any mixing. The term 'laminar flow' refers to the absence of turbulence within the apparatus. A diagram of a typical laminar flow apparatus is shown in Figure 2.13.

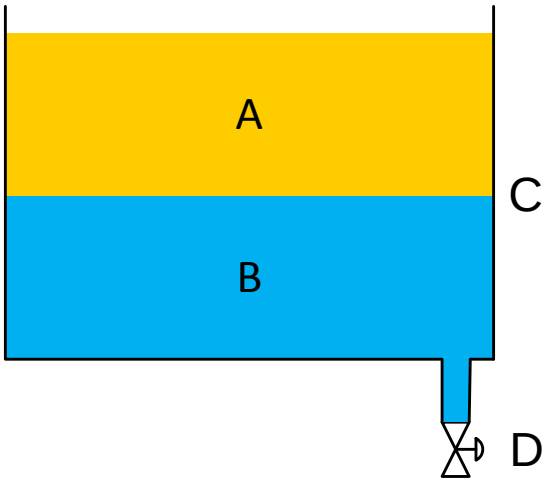


Figure 2.13 Diagram of a typical laminar flow apparatus. A - phase with lower density, B - phase with higher density, C – liquid-liquid interface, D - drain valve

To determine the mass transfer between two phases, the phase with higher density is firstly transferred into the apparatus. The phase with lower density is then slowly transferred into the apparatus to minimise mixing at the liquid-liquid interface between the two phases. The change in concentration of the species of interest can be measured by taking samples from either or both phases at the beginning of an experiment, and at regular time intervals thereafter. The measurements of the concentration of species over time can be used to calculate the mass transfer rate.

#### 2.4.1.1. Modifications to the Technique

The laminar flow apparatus has been modified to be used as a counter current contactor, which was reported by Austin, Banczyk and Sawistowski (1971). The modified apparatus includes a facility to continuously pump the aqueous and organic phases from respective reservoirs in a counter current direction. Very low flow rates are used to maintain laminar flow near the interface. After contacting, the phases are collected in separate raffinate streams, from which the change in concentration of the species of interest can be measured. This eliminates the need to manually remove solution for sampling.

#### 2.4.1.2. Application to the Present Study

The laminar flow technique was used to investigate the effect of electrostatic fields on interfacial phenomena by Sawistowski and co-workers (1971, 1974), and Glitzenstein, Tamir and Oren (1995). Both of these research groups incorporated electrodes on both sides of the interface to facilitate application of an electrostatic field.

The laminar flow technique, however, is not suitable for the present study because it has only limited ability to investigate mass transfer in kinetic-controlled systems. For virtually all systems, except those with very slow chemical reactions, the mass transfer rate is diffusion-controlled in the absence of mixing. According to the extended two-film theory, increases in turbulent mixing of the phases leads to decreases in the thickness of the diffusion regions, which causes the rate controlling process to change from diffusion-controlled to kinetic-controlled. Given that no mixing occurs in the laminar flow technique, this technique does not allow investigation of conditions in which mass transfer is kinetic-controlled in most SX systems. This limitation is inherent to the laminar flow technique, and therefore, this technique is not suitable for the purposes of the present study.

### 2.4.2. Rotating Diffusion Cell Technique

The rotating diffusion cell (RDC) technique, which was developed by Albery et al. (1976), allows measurement of the mass transfer across a liquid-liquid interface that is situated on the surface of a membrane filter.

A diagram of the RDC used by Albery et al. (1976) is shown in Figure 2.14. The apparatus consists of an inner hollow rotating cylinder (B) containing the phase of lower density, which is placed inside a jacketed stationary outer compartment containing the

phase of higher density. The interface between the two phases is located on the surface of either side of a Millipore filter (A), which is dependent on the nature of the filter material. The interfacial area is determined by the permeable area of the filter, which can be modified by applying suitable solutions onto the filter to render the desired area impermeable. The inner cylinder contains a stationary baffle (C), which forces the contained phase to flow out through a gap between the baffle and the filter (E), and back in through slots in the baffle (D). A pulley system (G), driven by a motor, is used to rotate the inner cylinder.

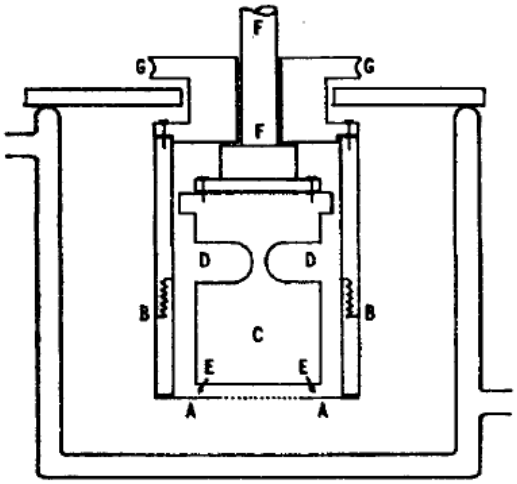


Figure 2.14 A diagram of the rotating diffusion cell (Albery et al. 1976)

To determine the mass transfer between two phases, firstly the filter is wetted with the phase that it is to contain, and temperature-controlled water is pumped through the jacket of the outer compartment. The phase of higher density is transferred into the outer compartment, and the phase of lower density is transferred into the inner cylinder through the hollow stationary shaft (F). The inner cylinder is then rotated at a desired speed which, according to Albery et al. (1976), induces rotating-disc hydrodynamics on both sides of the filter. This assumption facilitates the use of the Levich equation (Levich 1962), Equation 6, to calculate the thickness of the diffusion layer on the surface of the filter.

$$\delta = 0.643\omega^{-1/2}D^{1/3}v^{1/6} \qquad \text{(Equation 6)}$$

where: $\delta$ is the thickness of the diffusion layer, $\omega$ is the rotation speed, $D$ is the diffusion coefficient, and $v$ is the kinematic viscosity.

The change in concentration of the species of interest can be measured in two ways: (1) the pH stat technique, wherein the pH of the aqueous phase is maintained at a desired value by addition of measured amounts of basic solution to neutralise the acid generated

in the aqueous phase from the chemical reaction, or (2) by periodically removing samples from one phase and measuring the concentration by analytical methods such as spectrophotometry.

The measurements of the concentration of species are used to construct a rotating disk plot, which consists of the inverse flux against the inverse square root of the rotation speed. According to Albery et al. (1976), these data can be extrapolated to infinite rotation speed, where there are no stagnant layers on either side of the filter. They claimed that this was a significant advantage of the RDC technique as it allows researchers to account for additional resistances owing to diffusion through the filter and to interfacial transfer reactions.

The overall mass transfer coefficient is determined by the sum of a series of resistances owing to the diffusion in both phases, the chemical reaction, and the membrane filter. Albery et al. (1976) proposed different equations to calculate the overall mass transfer coefficient, depending on the rate determining process.

#### *2.4.2.1. Modifications to the Technique*

Some limitations of the RDC technique have been identified, and attempts have been made to improve the apparatus design. The membrane that separates the two compartments introduces an additional resistance to the mass transfer of species, and characterising the thickness and porosity of the membrane filter is difficult (Danesi 2004). In addition, no study has proven that the hydrodynamics inside and outside the inner cylinder are the same, or that ideal rotating-disc hydrodynamics occur in the inner cylinder (Simonin, Turq & Musikas 1991). These limitations were addressed by Simonin, Turq and Musikas (1991), who developed the rotating stabilised cell (RSC) technique. The main modification of their design is that the aqueous phase was stabilised with a gel of polyacrylamide to prevent convection in this phase, which eliminated the need for a membrane filter altogether. The aqueous phase was placed inside the inner compartment, and this was immersed in a rotating cylinder containing the organic phase. According to the authors, rotating disk hydrodynamics occurs below the rotating cylinder, and pure diffusion occurs in the aqueous phase. A disadvantage of this technique though, is that the addition of gel alters the physical properties of the aqueous phase.

#### *2.4.2.2. Application to the Present Study*

The RDC technique has several limitations that make it unsuitable for the investigation of interfacial phenomena in the presence of electrostatic fields. Only one study (Kuipa & Hughes 1999) has reported the use of the RDC technique to study the effect of applied fields across a liquid-liquid interface. These researchers incorporated stainless steel ring electrodes (0.8 mm thickness, 18 mm OD, 25 mm ID) above and below the interface to facilitate application of a field. The effect of the electrodes on the rotating-disk hydrodynamics is unknown, but it is conceivable that the Levich equation may no longer be valid owing to the modified fluid flow caused by the electrodes.

In addition, the requirements to place the stationary baffle close to the interface and to rotate the inner cylinder, and thus the interface, at high speeds, does not allow good visual observation of the interfacial region. These limitations appear to be inherent to the RDC technique, and therefore, this technique is not suitable for the purposes of the present study.

### 2.4.3. Lewis Cell Technique

The original experimental technique used to measure mass transfer across a flat liquid-liquid interface was conceived by Lewis (1954) and is thus referred to as the Lewis cell. This technique allows measurement of mass transfer over a well-defined and constant interfacial area, while the intensity of mixing in the two bulk phases is varied over the widest possible range.

The Lewis cell is essentially a glass cylinder consisting of two compartments with a volume of approximately 300 mL each (Figure 2.15). A filling plug at the top of the cell (A) allows solution to be added prior to commencing an experiment, and for removing samples during an experiment. A polythene plug (B) is used to support two platinum electrodes that measure the phase conductivity, and is positioned adjacent to the filling plug.

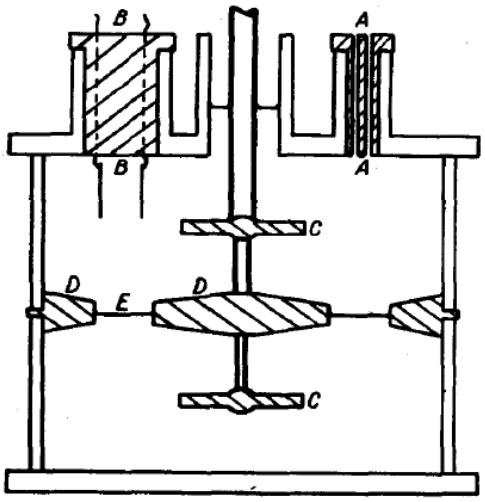


Figure 2.15 A diagram of the Lewis cell. A-filling plug, B-polythene plug supporting electrode, C-stirrer, D-baffles, E-interface (Lewis 1954)

Two baffles (D) are inserted between the two compartments to modify the fluid hydrodynamics. A central circular baffle is used to prevent cavitation, and an outer circular baffle along the wall is used to reduce wall effects on the interface. Both baffles are bevelled to ensure that any liquid that becomes entrained in the opposite phase can move back into its original phase. The interfacial contact area, which is located between these baffles, is approximately 30 $cm^2$. The liquids in each compartment are mixed by separate stirrers (C), and the stirring speeds can be varied independently. The apparatus is placed in a temperature-controlled waterbath to control the temperature during an experiment.

To determine the mass transfer between two phases, firstly the phases and the cell are brought to the desired temperature in a waterbath. The lower compartment is filled with the phase of higher density, and the upper compartment is filled with the phase of lower density. An experiment is commenced when the stirrers, which had previously been set to the desired stirring rate, are turned on. The change in concentration of the species of interest can be measured in two ways: (1) a hypodermic needle is injected through the filling plug and samples are taken from the bulk of one of the phases at the beginning of an experiment, and at regular time intervals thereafter, or (2) two platinum electrodes, which are injected through the polyethylene plug, measure the conductivity of the organic phase, and the change in conductivity is correlated with a change in concentration of the species of interest. The measurements of the concentration of species over time can be used to calculate the mass transfer rate.

#### 2.4.3.1. Modifications to the Technique

Since Lewis's novel study, several limitations of his apparatus have been identified, and many researchers have attempted to make improvements, resulting in many modified designs and methods of operation. Investigators have variously referred to the modified designs as a stirred cell, stirred cell with constant interfacial area, constant interfacial area stirred cell, constant-interface stirred cell, quiescent-interface cell, Lewis-type cell, improved Lewis cell, or modified Lewis cell (MLC). For clarity and consistency, the latter terminology is used throughout the present study. The limitations associated with the measurement of mass transfer and the corresponding improvements are now summarised.

One limitation of Lewis's design is that the range of stirring speeds that can be used without disturbing the interface is narrow, which is owing to undesirable hydrodynamics within the cell. This allows only limited manipulation of the thickness of the diffusion regions and thus, limited investigation of diffusion-controlled systems. The apparatus designed by Nitsch and Hillenkamp (1972) included several modifications to improve the hydrodynamics. Firstly, they incorporated an inner cylindrical insert in both compartments, which are positioned around the stirrer blades. Secondly, they used turbine-type stirring blades that are inclined 45° to the interface. Thirdly, they incorporated steel screens, which are attached to the end of each cylindrical insert and are positioned close to the interface. According to these authors, this modifies the fluid flow, which results in an efficient forced convection within each compartment and thus, allows application of greater stirring speeds without disruption of the interface. The theoretical fluid flow with this modified design is shown in

Figure 2.16.

Later, Danesi et al. (1982) developed the Argonne Modified Lewis Cell for Liquid-Liquid Extraction, abbreviated as ARMOLLEX, shown in Figure 2.17. The authors acknowledged that Nitsch and Hillenkamp's (1972) design enabled the use of high stirring speeds without disruption of the interface. They commented, however, that the large volumes of solution required were undesirable. Danesi et al. (1982) suggested that their apparatus retained all the hydrodynamic advantages of the design of Nitsch and Hillenkamp (1972), but required much smaller volumes of solutions.

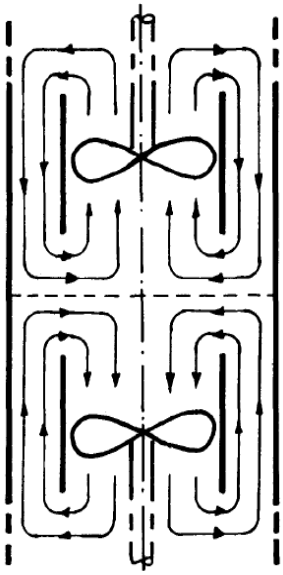

Figure 2.16 The theoretical fluid flow in a modified Lewis cell (Nitsch & Hillenkamp 1972)

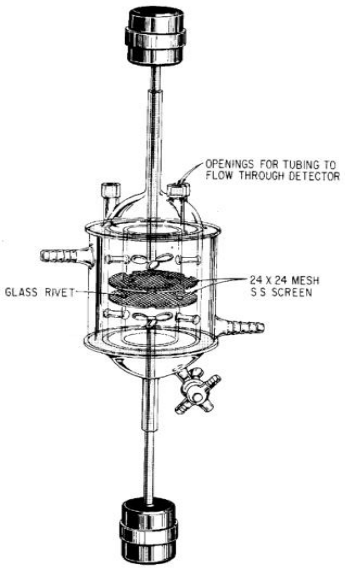


Figure 2.17 The ARMOLLEX cell (Danesi et al. 1982)

Another limitation of Lewis's design is that the position and orientation of the baffles results in a small interfacial area, which makes this design not suitable for studying systems with very slow kinetics (Danesi, Chiarizia & Coleman 1980), and also prevents good visual observation of the interfacial region. This limitation was resolved in the design of Nitsch and Hillenkamp (1972), which incorporated a separate stirring shaft that was inserted from the bottom of the cell. This eliminates the need for a central baffle, which allows a significantly larger interfacial area and thus, improved visual observation of the interfacial region as well as a shorter experimental run time. Another consequence of this modified design is that the MLC was jacketed to facilitate temperature control, as the apparatus could not be immersed in a temperature-controlled waterbath.

A limitation of Lewis's method of operation is that the sampling procedure involves withdrawing a volume of solution from the cell, which can lead to changes in the position of the interface. Sampling from the lower compartment causes the position of the interface to move downward, and it is plausible this may alter the effect of the stirring in each phase on the diffusion regions. For example, as the interface moves closer to the lower stirrer, the thickness of the diffusion region in the solution with higher density may decrease. On the other hand, as the interface moves further away from the upper stirrer, the thickness of the diffusion region in the solution with lower density may increase. Clearly, this could affect the precision of mass transfer

measurement for diffusion-controlled systems. Lewis stated that synthetic solutions with 'approximately the same composition' were injected during experiments to maintain the position of the interface. Given that the concentration of species during an experiment would be different to the initial concentration, this procedure introduces an unmeasurable error.

An improved sampling and analytical technique was conceived by Roddy, Coleman and Arai (1971). Their technique allows continuous, non-destructive measurement of the concentration of the species of interest, which eliminates the need to remove samples as an experiment progresses and thus, maintains the position of the interface. These researchers added a gamma-emitting radioisotope to the aqueous phase and continuously monitored the amount of radioactivity that had transferred into the organic phase by recirculating a small volume from the bulk of the organic phase through a scintillator. Later, Nitsch and Plucinski (1990) further developed this continuous sampling technique by using a spectrophotometer to measure the concentration of the species of interest. This modification eliminated the need to handle radioactive species.

Another limitation of Lewis's method of operation is that there is a lag time between when mass transfer commences and when an experiment commences. Mass transfer occurs as soon as the two phases are contacted, but the experiment is commenced only when the upper compartment is completely filled. It appears that the author made no attempt to account for the additional mass transfer that occurs when the upper compartment is being filled. Nitsch and Hillenkamp (1972) reported a method to eliminate this lag time and thus, allow a more quantitative measurement of mass transfer. In their experiments, the MLC was filled with the two phases, except that neither phase contained the species of interest. The stirrers were then turned on and set to the desired speed, and an experiment was only commenced when a small volume of concentrated solution containing the species of interest was injected into one phase. This procedure relies on the assumption that the phases in both compartments are homogeneously mixed, and that the species of interest are mixed instantaneously.

#### *2.4.3.2. Application to the Present Study*

A few researchers have used MLCs to investigate the effect of applied fields across a liquid-liquid interface. This was first reported by Martin et al. (1983), but they provided no information about the design of their apparatus including how a field was applied.

They also did not include a diagram of their apparatus. Hund and Lancelot (1986) also used a modified Lewis cell, but once again no information about the design of the apparatus was included. A diagram shows that the electrodes were placed at the top and bottom of the cell, but no other information, such as the materials of construction, size, or shape, was provided. Wildberger and Bart (2002) designed an MLC that incorporated a Teflon-coated ring electrode above and below the interface. Ring electrodes, however, would generate a particularly non-uniform electrostatic field and would likely alter the hydrodynamics within an MLC. The size and positioning of the ring electrodes is also not clear, nor is the method of inserting them into the MLC.

The Lewis cell technique can be used to investigate the effects of electrostatic fields on interfacial phenomena. This, however, requires the development of an MLC that incorporates all of the improvements to the design and method of operation that have been reported. In addition, the design must allow application of an electrostatic field across the liquid-liquid interface without altering the hydrodynamics within the MLC.

## 2.5. EFFECT OF ELECTROSTATIC FIELDS ON DROPLET DISPERSION

### 2.5.1. Electrostatically Induced Dispersion

Subjecting a droplet of an electrically conductive liquid, that is suspended in a relatively non-conductive liquid, to an electrostatic field causes the droplet to polarise and elongate along the axis parallel to the applied field (Taylor 1964). A diagram of this phenomenon is shown in Figure 2.18. The electrostatic force exerted on the droplet acts in the opposite direction to the droplet's surface tension and therefore increases in the strength of the applied field result in decreases in the effective interfacial tension (Stewart & Thornton 1967; Kuipa & Hughes 2002). If the strength of the electrostatic force is sufficient to overcome the droplet's surface tension, the droplet will be dispersed into several smaller so-called daughter droplets (O'Konski & Thacher 1953; Hendricks & Schneider 1962; Garton & Krasucki 1964; Taylor 1964). Several researchers have proposed that a certain ratio of the major-to-minor axes of an elongated droplet is required to induce dispersion, but their values differ (Garton & Krasucki 1964; Rosenkilde 1969; Martin et al. 1983). Electrostatic solvent extraction (ESX) utilises the principle of electrostatically induced dispersion of aqueous droplets in a continuous organic phase.

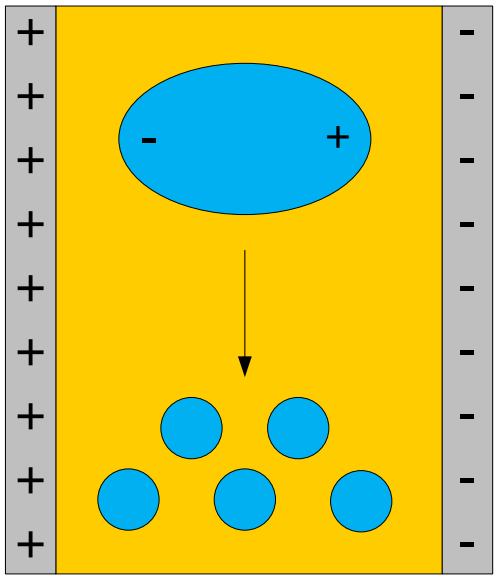

Figure 2.18 Diagram of electrostatically induced dispersion of an aqueous droplet in a continuous organic phase

Electrostatically induced dispersion can be achieved in the presence of different types of electrostatic fields. Most of the early work on this topic was focused on the effect of direct current (DC) fields on droplet dispersion, which subject droplets to a static voltage. More recent research has been aimed at investigating the effect of transient fields, including pulsed direct current (PDC) and alternating current (AC). Transient fields cause droplets to elongate in the direction of the applied field when the field is pulsed on, and contract toward a spherical shape when the field is pulsed off.

In the case of both static and transient fields, the form of droplet polarisation prior to elongation influences droplet dispersion. The most significant forms of polarisation for droplets of an electrically conducting liquid in a relatively non-conducting liquid are orientational polarisation and interfacial polarisation (Pohl 1973). Orientational polarisation occurs when molecules with a permanent dipole moment, such as water, align with an external electrostatic field. The alignment of these polar molecules causes electric stress to be applied to the droplet surface. Interfacial polarisation occurs when electric charges migrate toward a discontinuity of electrical conductivity and permittivity (Melcher & Taylor 1969), such as a liquid-liquid interface. The interaction between this interfacial charge and the external electrostatic field causes electric stress to be applied to the droplet surface. Recent work by Collard (2011) and Steffens (2011) has provided some evidence that interfacial polarisation is the dominant form of polarisation in the presence of electrostatic fields, but it is currently unclear whether this is dependent on the experimental conditions such as the properties of the field. It would also be helpful

to determine whether one form of polarisation induces a greater amount of droplet dispersion and is therefore more favourable for mass transfer.

### 2.5.2. Mechanisms of Droplet Dispersion

The mechanism of droplet dispersion refers to the changes in shape that a droplet undergoes prior to dispersion. Two mechanisms by which droplets disperse under the influence of electrostatic fields have been reported: necking and jetting (Torza, Cox & Mason 1971; Basaran & Scriven 1982; Eow, Ghadiri & Sharif 2003). Necking occurs when a droplet elongates in the direction of the applied field and gradually separates near its centre to form a few smaller droplets (Figure 2.19a). Jetting occurs when a droplet forms conical ends as it elongates and ejects many ultra-fine droplets from its ends while the initial droplet remains relatively large (Figure 2.19b). Previous researchers have reported observing only one of these two dispersion mechanisms under a given set of experimental conditions, so it is unclear whether both necking and jetting can occur concurrently or whether droplets may also disperse by other mechanisms.

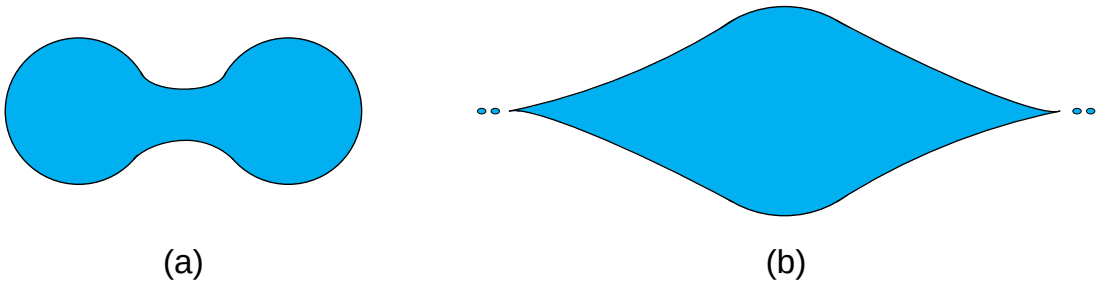


Figure 2.19 Diagrams showing the droplet dispersion mechanisms of (a) necking, and (b) jetting

The droplet dispersion mechanism influences the mass transfer of species between droplets and the continuous phase. In theory, necking should be more favourable for mass transfer because it minimises the formation of ultra-fine droplets, which would likely behave as rigid spheres. In addition, the smaller droplets generated by necking have a larger specific interfacial area than the relatively larger droplets that remain during jetting. In an application of electrostatically induced dispersion, necking would also be the preferred droplet dispersion mechanism as it theoretically produces a narrower droplet size distribution, which means the droplets have similar coalescence time, and minimises the formation of ultra-fine droplets that would likely become entrained in the organic phase. The occurrence of these droplet dispersion mechanisms is influenced by several variables including (1) the properties of the electrostatic field, and (2) the physical properties of the aqueous and organic solutions.

In regards to the former, Torza, Cox and Mason (1971) reported that changes in droplet shape prior to dispersion were significantly different using AC fields compared with that using DC fields, but they offered no explanation for this observation. Scott and his co-workers (Scott 1987; Scott, Basaran & Byers 1990) reported that the dispersion mechanisms in the presence of transient fields are influenced by the relationship between the applied frequency and a droplet's natural frequency. A droplet's natural frequency, which is dependent largely on the droplet's size, is the frequency at which it periodically elongates and contracts about its horizontal axis when moving vertically through another liquid owing to gravity. Despite these various observations, there are currently no generalisations for the effect of the properties of the electrostatic field, such as the type of field, applied voltage or applied frequency, on the dominant droplet dispersion mechanism.

In regards to the latter, Steffens (2011) investigated the effect of a wide range of physical properties on the mechanisms of electrostatically induced droplet dispersion using hydrometallurgical SX solutions. He observed that increases in the viscosity of the organic phase (2.62 cP to 9.02 cP) shifted the predominant dispersion mechanism to jetting, which is consistent with the trend reported by Garton and Krasucki (1964). Steffens observed also that increases in the viscosity (1.5 cP to 3.25 cP) or ionic strength (0 M to 4.8 M) of the aqueous phase shifted the predominant dispersion mechanism to necking. It is notable that in this comprehensive study, Steffens investigated a wide range of values for each physical property that is much greater than the slight variations that would occur in an application of ESX. Although this author pointed out that more quantitative data could be generated using a high-speed imaging system, the effect of the physical properties of the solutions on droplet dispersion is outside the scope of the present study.

The droplet dispersion mechanisms directly influence the size of droplets that are generated in an electrostatically induced dispersion, but most researchers have reported only the effect on the average size of a population of droplets. Numerous researchers have reported that increases in the field strength, regardless of the type of field, lead to decreases in the average droplet size (Bailes & Thornton 1971; Bailes & Thornton 1974; Thornton 1976; Bailes 1977; Bailes 1981; Zhou & Gu 1988; Heckley 2002; Collard 2011; Steffens 2011). In contrast, the effect of the applied frequency of AC fields on droplet sizes is unclear. On one hand, Collard (2011) reported that increases from 35 to 150 Hz caused decreases in the average droplet size from 2.76 to 1.49 mm. On the other hand,

data presented by Steffens (2011) indicates that increases from 20 to 80 Hz had no significant effect on the average droplet size. Therefore, the effect of the applied frequency of AC fields on droplet dispersion clearly requires further investigation. It must be noted that the experimental techniques used by previous researchers to measure droplet sizes have limited accuracy and therefore these findings may only be considered to be anecdotal.

### 2.5.3. Droplet Size Distributions

Measurement of the individual droplet sizes of a population of droplets to generate a droplet size distribution provides a more detailed insight into the effect of electrostatic fields on droplet dispersion. Droplet size distributions may be presented as the percentage of droplets in given size fractions by volume, which is referred to as a volume density distribution, or by number, which is referred to as a population distribution. Only a few studies have generated droplet size distribution data in the presence of DC and AC fields, and none has been reported on the effect of PDC fields. This may be owing to the high cost of a precise measurement technique, such as an imaging system utilising a high-speed camera that allows the recording of high resolution photos of dispersions which is required for such work.

In the case of DC fields, Yamaguchi, Sugaya and Katayama (1988) found that when droplets were released from a distributer into a spray column, a wider volume density distribution was produced in the presence of a field compared with that in the absence of a field (Figure 2.20). Their data suggest that increases in the applied voltage from 0 to 25 kV caused decreases in the minimum droplet size and increases in the volume of smaller droplets. This may be attributed to increases in the electrostatic force that is exerted by the DC field onto droplets, which generates a finer droplet dispersion.

Increases in the applied voltage also caused increases in the maximum droplet size and increases in the volume of larger droplets. At first glance this may appear counter-intuitive given that a greater electrostatic force is applied to droplets, but this may be attributed to electrostatically enhanced coalescence. In addition to electrostatically induced dispersion, previous researchers have reported that electrostatic fields may also be used to enhance coalescence in SX systems (Bailes & Larkai 1981; Bailes 1992). Heckley (2002) reported that low field strength induces coalescence, whereas high field strength induces dispersion. Although field-induced dispersion and coalescence have been treated as largely independent phenomena in the literature, it would be useful to

determine whether dispersion and coalescence occur under the same field conditions, as the results of Yamaguchi, Sugaya and Katayama (1988) suggest.

In the case of AC fields, Broan, Bailey and Williams (1996) reported approximately bimodal droplet size distributions with two distinct peaks (<100 μm and 400 μm) (Figure 2.21). It is plausible that this shape of droplet size distribution indicates that jetting is the dominant dispersion mechanism under these experimental conditions, but the authors did not comment on the dispersion mechanisms. Increases in the applied voltage from 6.0 to 9.0 kV had a non-uniform effect on the proportion of droplets in the smaller size fractions (<100 μm), and the authors provided no explanation. Increases in the applied voltage also resulted in decreases in the proportion of large droplets (>300 μm), which may be attributed to increases in the electrostatic force that is imparted onto droplets and thus a finer droplet dispersion. There is no published work on the effect of the frequency of AC fields on the droplet size distributions, which clearly requires investigation.

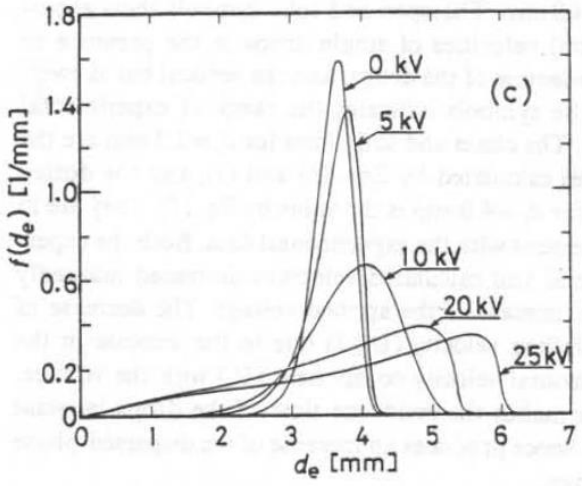


Figure 2.20 Effect of the applied voltage of DC fields on the volume density distribution (Yamaguchi, Sugaya & Katayama 1988)

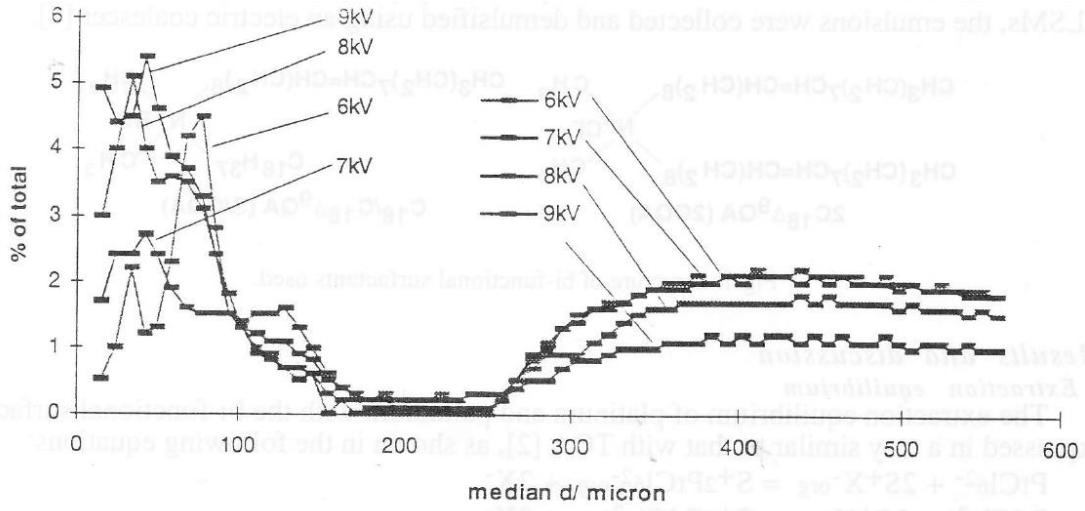


Figure 2.21 Effect of the applied voltage of AC fields on the volume density distribution (Broan, Bailey & Williams 1996)

Two studies (Heckley 2002, Steffens 2011) have compared the effect of DC and AC fields on the droplet size distribution, but their observations are contradictory and they provided no droplet size distribution data to support their observations. Whereas the former stated that AC fields generally produced droplet dispersions with more uniform size distributions than DC fields, the latter stated the opposite. This is peculiar given that both of these researchers were studying hydrometallurgical SX systems with similar physical properties. This clearly requires further investigation.

## 2.6. EFFECT OF ELECTROSTATIC FIELDS ON DROPLET AGITATION

The rate of mass transfer is influenced by the agitation of droplets as they move through the continuous organic phase. In the present study, it is of particular interest to investigate the effect of electrostatic fields on droplet agitation, and how to exploit this field-induced agitation to enhance the rate of mass transfer. Studies on the effect of electrostatic fields on droplet agitation are grouped into the effects on (1) droplet oscillation, (2) droplet speed, and (3) droplet zigzagging.

### 2.6.1. Droplet Oscillation

Liquid droplets that are travelling vertically through an insoluble liquid owing to gravity can exhibit natural droplet oscillation, which is the periodic elongation and contraction of a droplet about its horizontal axis. This is owing to vortex shedding in the wake of a spherical droplet, and occurs when the Reynolds number is greater than 300 (Goldburg & Florsheim 1966) and the Weber number is greater than 3.3 (Hu & Kintner 1955). In theory, droplet oscillation has significant benefits for enhancing mass transfer in SX

because (1) droplet elongation causes periodic increases in the interfacial area, which provides more sites at the liquid-liquid interface for mass transfer to occur, and (2) periodic elongation and contraction enhances mixing within droplets, which facilitates continual replenishment of the interface with fresh reactant species from within a droplet (Figure 2.22).

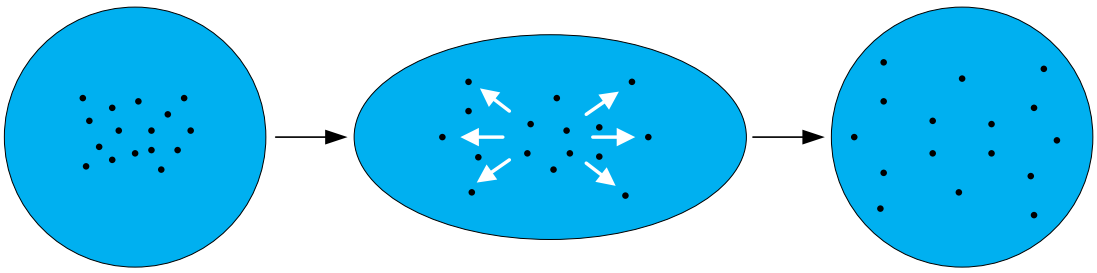

Figure 2.22 Diagram showing that droplet oscillation causes periodic increases in the interfacial area, as well as the movement of fresh reactant species within a droplet towards the interface

The effect of droplet oscillation on mass transfer is dependent on (1) the amplitude of elongation and contraction, and (2) the rate at which this elongation and contraction occurs, which is referred to as the frequency. In regards to (1), it is well accepted that decreases in droplet diameter leads to decreases in the amplitude of natural oscillation in mechanically agitated contactors, which causes droplets to behave more as rigid spheres (Ritcey 2006b). For example, data presented by Nagata and Yamaguchi (1960) indicate that increases in the speed of a mechanical agitator result in decreases in the diameters of the dispersed droplets, but as the droplet size decreases, the rate of mass transfer approaches that caused by diffusion alone. Therefore, at high agitator speeds, dispersed droplets become too small for mechanical agitation to cause mixing inside the droplets. In regards to (2), decreases in droplet diameter lead to increases in the frequency of droplet oscillation (Rayleigh 1879).

In the present study, it is of particular interest to determine whether and, if so, how electrostatic fields influence droplet oscillation and thus affect mass transfer. Although only a few studies on this topic have been reported, the results indicate that electrostatic fields can influence the oscillation of aqueous droplets in a continuous organic phase.

Stewart and Thornton (1967) proposed that static fields can induce natural oscillation in smaller droplets than in the absence of a field. These authors used a high-speed camera to study the behaviour of water droplets that were released from a nozzle charged with a DC voltage and passed through a column containing *n*-heptane towards an earthed electrode. Their data indicate that decreases in droplet size do not lead to decreases in

natural oscillation in the presence of DC fields, which is in direct contrast to natural droplet oscillation that occurs in mechanically agitated contactors. Their data also suggest that the minimum values of both the Weber number and Reynolds number required to induce droplet oscillation in the presence of electrostatic fields are less than those in the absence of a field. These authors, however, only reported observations for relatively large droplet diameters (>2090 μm). Therefore, it is unclear whether droplet oscillation is also induced in smaller droplets (<1000 μm) that are typically encountered in SX applications. Specialised high-speed imaging equipment is required to facilitate reliable observation of droplet oscillation.

Transient fields induce forced droplet oscillations in response to the pulsing of the applied voltage, which is altogether different to natural droplet oscillation. Wham and Byers (1987) reported that PDC fields induced the oscillation of a water droplet that was suspended in a tapered column apparatus containing 2-ethylhexanol. Steffens (2011) and Collard (2011) reported that AC fields induced oscillation of droplets of an aqueous PLS in an organic phase consisting of Shellsol® 2046 diluent. The forced droplet oscillation that is induced by transient fields is different to natural droplet oscillation because the frequency of the former is determined by the frequency of the transient field, whereas the frequency of the latter is determined by the droplet size. Clearly, forced droplet oscillation cannot be achieved by the use of mechanical agitation.

It has been proposed that the frequency of transient fields influences the amplitude of droplet elongation and contraction as well as the frequency of forced droplet oscillation. In the case of PDC fields, the results of Scott, Basaran and Byers (1990) suggest that an optimum frequency maximises the amplitude of droplet deformation for a given droplet size. These authors postulated that this peak deformation amplitude occurred due to the synchronisation of the frequency of natural droplet oscillation and the frequency of forced droplet oscillation induced by the field. In the case of AC fields, Steffens (2011) reported that increases in the frequency from 20 to 50 Hz led to increases in the amount of droplet oscillation. This may be attributed to the increased rate of forced droplet oscillations caused by the shorter cycles of the applied field, but it is unclear if the amount of droplet oscillation refers to the frequency of oscillation or to the proportion of droplets that exhibited oscillation. No study has provided a comparison of the effects of PDC and AC fields on the amplitude of droplet elongation and the frequency of droplet oscillation. It is therefore currently unclear whether the type of transient field influences the nature of droplet oscillation.

The electrostatic field strength and the droplet charge influence forced droplet oscillation. Steffens (2011) reported that increases in the applied voltage from 2 to 5 kV/cm led to increases in the amount of droplet oscillation, which the author attributed to a greater electric force being applied at the interface. Steffens observed that while relatively larger droplets rapidly oscillated in an AC field, a significant number of ultra-fine droplets did not oscillate, which the author attributed to the ultra-fine droplets having insufficient charge. It is currently unclear how the droplet charge and, therefore, the dominant form of polarisation, influences droplet oscillation. The use of a suitable high-resolution imaging technique would allow greatly improved observation of droplet oscillation, which may provide insight into the relationship between droplet charge and droplet oscillation. This would also allow investigation of the effect of electrostatic fields on the relationship between the droplet diameter and the amplitude of droplet elongation and contraction.

A few attempts have been made to determine the effect of droplet oscillation on mass transfer, but it is difficult to quantify because several other factors that influence mass transfer occur simultaneously. In the case of static fields, increases in the applied voltage of a DC field caused increases in the mass transfer coefficient of furfuraldehyde droplets into *n*-heptane, which the authors partly attributed to the greater oscillation of smaller droplets in the presence of a field (Bailes & Thornton 1971; Thornton 1976; Bailes 1981). These authors correctly pointed out, however, that increases in the applied voltage also caused increases in the amount of droplet dispersion and, thus, increase in the interfacial area. In the case of transient fields, Wham and Byers (1987) reported that PDC fields with applied frequencies between 10 and 120 Hz increased the mass transfer coefficient of water into 2-ethylhexanol by up to 35%, although the droplet surface area increased by less than 1%. Similar findings were reported by Scott (1992). These results suggest that the internal mixing induced by forced droplet oscillation has a greater effect on mass transfer than the associated periodic increases in the interfacial area.

### 2.6.2. Droplet Speed

Droplet 'speed' and 'velocity' are used interchangeably in the literature on this topic. Although the velocity strictly requires a direction of motion, for consistency, the same terminology is adopted in this review.

It is well known that the velocity of an object that is immersed in a fluid increases until it reaches a maximum terminal velocity when the downward force owing to gravity is

equal to the upward drag force owing to the resistance from the fluid. In the case of liquid droplets that are immersed in an insoluble liquid, increases in the droplet diameter causes the terminal velocity to initially increase and then plateau. This relationship has been shown for various liquid-liquid systems with a wide range of physical properties (Figure 2.23). In theory, increases in the droplet velocity are beneficial for mass transfer because they (1) induce turbulence in the diffusion region around a droplet, and (2) increase a droplet's Reynolds number and thus promote droplet oscillation (Stewart & Thornton 1967). The use of mechanical agitation to reduce droplet sizes in SX is therefore unfavourable for mass transfer partly because decreases in the droplet size leads to decreases in the terminal droplet velocity.

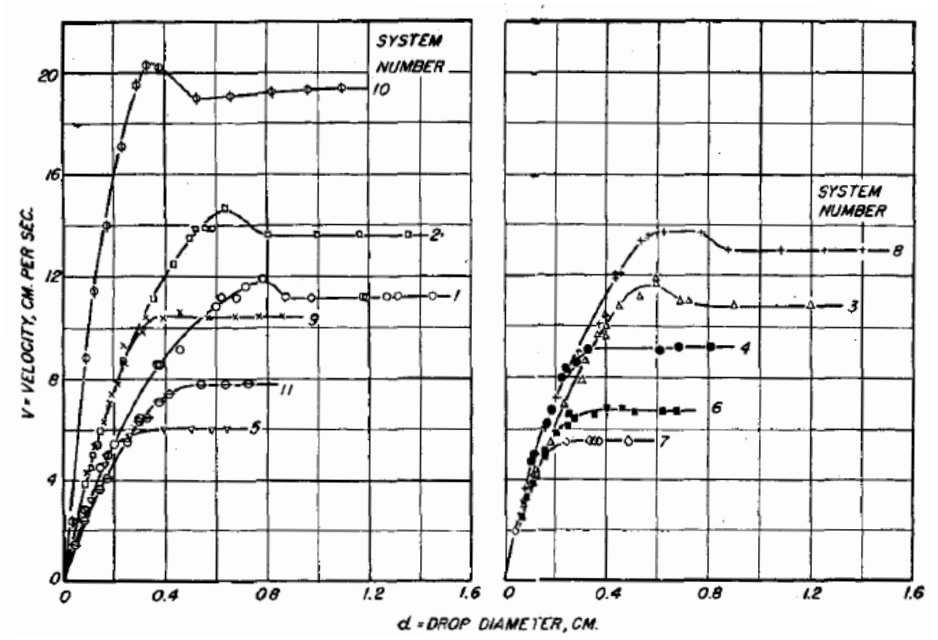


Figure 2.23 Relationship between the droplet diameter and terminal velocity of liquid droplets that are immersed in an insoluble liquid in various systems (Curve 1 – water/benzene, Curve 2 – water/kerosene, Curve 3 – water/Society of Automotive Engineers (SAE) 10W oil, Curve 4 – water/nonyl alcohol, Curve 5 – water/sec-butyl alcohol, Curve 6 – furfural/water, Curve 7 – water/methyl ethyl ketone, Curve 8 – 20% aqueous sucrose/benzene, Curve 9 – water/methyl isobutyl ketone, Curve 10 – water/pentachloroethane, Curve 11 – water/*n*-heptylic acid) (Klee & Treybal 1956)

Subjecting droplets of a conductive liquid, which are suspended in a relatively non-conductive liquid, to an electrostatic field increases the droplet velocity relative to that in the absence of a field. That is, in addition to their movement owing to gravity, droplets can be made to move faster owing to an electrostatic force (Figure 2.24). Stewart and Thornton (1967) reported that increases in the applied voltage of DC fields led to increases in the terminal velocity of charged droplets of water in *n*-heptane by up to 100% relative to that in the absence of a field. This is supported by the findings of

Carleson and Berg (1983) and Vu and Carleson (1986) for water droplets in various other organic liquids.

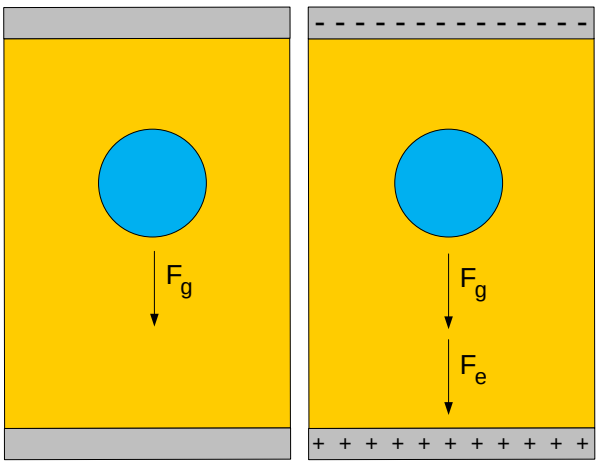


Figure 2.24 Diagrams showing that in the presence of an electrostatic field, droplets are subjected to an electrostatic force that acts in addition to the gravitational force

The enhanced droplet velocity in the presence of DC fields also appears to be dependent on the droplet diameter. Data presented by Stewart and Thornton (1967) indicate that decreases in the droplet diameter lead to increases in the droplet terminal velocity (Figure 2.25a). This is opposite to the general relationship that occurs when droplets are only under the influence of gravity, and therefore appears to be a significant advantage over the use of mechanical agitation. They attributed this to the corresponding increases in the droplet charge-to-mass ratio (Figure 2.25b). These authors, however, only provided data for relatively large droplet diameters (>2090 μm). The same research group later published data for a different liquid-liquid system showing the same relationship between droplet diameter and droplet velocity (Bailes & Thornton 1974), but once again only relatively large droplet diameters were studied (>1600 μm). Therefore, it remains unclear whether this relationship between the droplet diameter and droplet velocity also applies to smaller droplets (<1000 μm) that are typically encountered in SX applications. The droplet velocity must be measured for droplets in this smaller size range to address this gap in the knowledge.

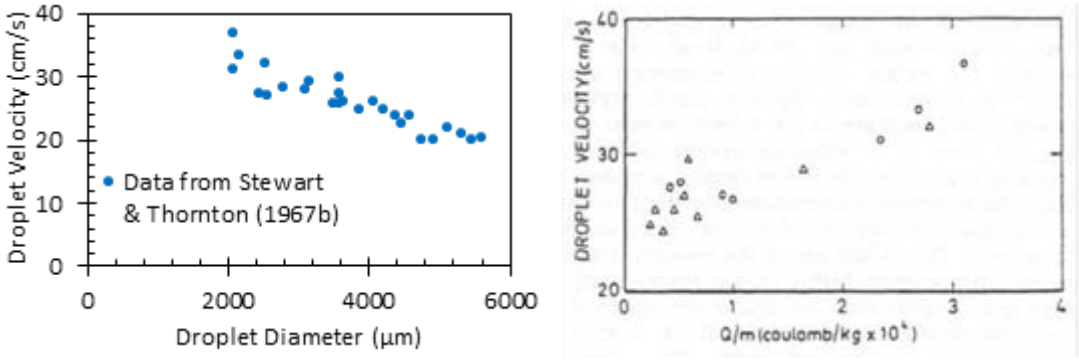


(a) (b)

Figure 2.25 The effect of DC fields on the relationship between the droplet terminal velocity and (a) the droplet diameter, and (b) the charge-to-mass ratio (Stewart & Thornton 1967)

The effect of PDC fields on droplet velocity appears to be similar to that of DC fields. He, Chang and Baird (1990) investigated the effect of PDC fields on droplets of deionized water that were immersed in mineral oil, and found that increases in the applied voltage caused increases in the droplet velocity. In a later work, He, Chang and Baird (1997) compared the effects of DC and PDC fields on droplet velocity. Their results indicate that at low applied voltages (0 – 10 kV) both field types had a similar effect on the droplet velocity, but further increases in applied voltage led to a greater increase in droplet velocity in the presence of PDC fields than with DC fields. The authors seemed to attribute this difference to the cycling nature of the transient field, but their explanation was unclear. No work has been reported on the effect of the applied voltage of other transient fields, such as AC fields, or the effect of the applied frequency of transient fields, on the magnitude of droplet velocity.

Although previous investigators have proposed that enhanced droplet velocity is owing to an electrostatic force, it is currently unclear exactly how this occurs. As discussed in Chapter 2.6.1, forced droplet oscillation has also been attributed to the electrostatic force from an external field, but no study has attempted to differentiate between the conditions required to enhance the droplet velocity or to induce droplet oscillation. Clearly, this requires further investigation.

Two studies (Bailes & Thornton 1974; Bailes 1981) have presented data on the effect of enhanced droplet velocity on mass transfer in the presence of electrostatic fields. Both of these studies reported that increases in the applied voltage of DC fields led to increases in droplet velocity, which corresponded to increases in mass transfer. The authors correctly pointed out, however, that increases in the applied voltage also caused

decreases in droplet size and as well as increases in droplet oscillation, and it is, therefore, difficult to determine the relative contributions of each of these factors towards mass transfer.

### 2.6.3. Droplet Zigzagging

Electrostatic fields can be made to influence the direction of droplets of an electrically conducting liquid as they pass through a relatively non-conducting liquid in a way that cannot be achieved with the use of mechanical agitation. In addition to their vertical movement owing to gravity, droplets can be made to move in a horizontal direction owing to an electrostatic force between droplets and an external field when using parallel-plate electrodes (Figure 2.26). The direction of this field-induced lateral motion alternates periodically, which causes droplets to zigzag through the continuous phase. In theory, zigzagging is beneficial for mass transfer because it (1) increases the residence time of the dispersed phase in the continuous phase (Martin et al. 1983; Yamaguchi, Sugaya & Katayama 1988), and (2) transports the droplets to a new region in the organic phase and thus, replenishes the interface with 'fresh' species in the continuous phase.

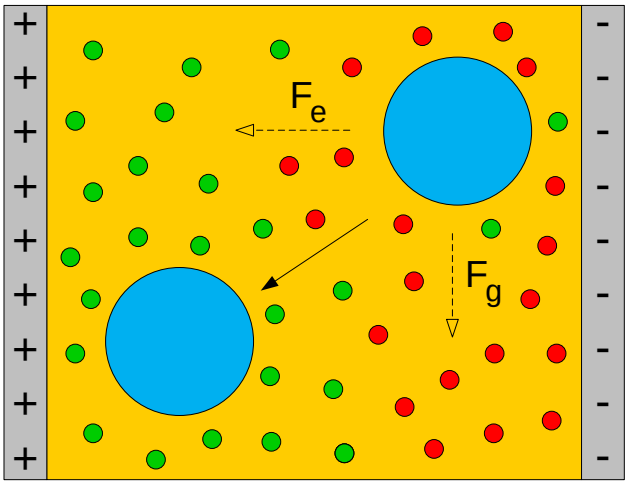


Figure 2.26 Diagram showing that droplet zigzagging can transport aqueous droplets from a region with a high concentration of used extractants (red) to a region with a high concentration of fresh extractants (green)

The nature of droplet zigzagging is dependent on the type of electrostatic field. Heckley (2002) found that both DC and AC fields induced droplet zigzagging but, at comparable field strength, zigzagging was significantly more evident in the presence of DC fields. In the case of DC fields, in which the electrode polarity is constant, the direction of motion of charged droplets only changes upon contact with an earthed electrode and that of uncharged droplets only changes upon contact with a charged electrode (Yamaguchi, Sugaya & Katayama 1988). On the other hand, in the presence of AC

fields, the direction of droplet motion changes in response to the alternating electrode polarity (Reeves et al. 1999), and therefore zigzagging induced by AC fields is significantly more rapid than that induced by DC fields. As a result, whilst zigzagging is more evident in the presence of DC fields, observation of zigzagging in the presence of AC fields requires the use of a suitable high-speed imaging technique.

It is logical that the applied voltage and the amount of droplet charge influence the amount of zigzagging in both DC and AC fields. Gneist and Bart (2003) reported that a low voltage DC field caused droplets to contact a charged electrode, but then simply fall owing to gravity. On the other hand, application of a high voltage DC field caused droplets that had contacted the charged electrode to move in a zigzag motion between the electrodes. It therefore appears that a certain minimum droplet charge is required to induce an electrostatic force that is sufficient to facilitate droplet zigzagging. In addition, both Reeves et al. (1999) and Steffens (2011) observed that increases in the applied voltage of AC fields led to increases in the amount of zigzagging. Steffens (2011) also reported that zigzagging was not evident in some ultra-fine droplets, which was attributed to the droplets having insufficient charge to facilitate interaction with the applied field. Observation of the behaviour of ultra-fine droplets would be greatly improved using a suitable high-resolution imaging technique.

Droplet zigzagging is also influenced by the applied frequency of AC fields. Both Reeves et al. (1999) and Steffens (2011) reported that increases in the applied frequency (from 25 to 100 Hz, and from 20 to 50 Hz, respectively) resulted in decreases in droplet zigzagging. The authors of both studies attributed this to the droplets having less time to undergo the large physical movement of zigzagging. The results of Gneist and Bart (2003) are consistent with this proposal. These authors reported that an AC field with an applied frequency of 30 kHz caused droplets to maintain a constant distance from a charged electrode as they fell through the column. The high applied frequency used by Gneist and Bart (2003) almost certainly provided insufficient time to allow the droplets to undergo horizontal motion. It is conceivable that droplet zigzagging may also be influenced by the applied frequency of other transient fields, such as PDC fields, but no study has been reported on the effect of PDC fields on droplet zigzagging.

The direction of droplet zigzagging between the charged and earthed electrodes may also influence the droplet velocity in the presence of electrostatic fields. Eow, Ghadiri and Sharif (2003) reported that a droplet's velocity was greater when moving from a charged DC electrode towards an earthed electrode than when moving in the opposite

direction. The authors speculated that this could be owing to different amounts of charge transfer between the droplet and the two electrodes, or due to charge leakage, but did not explain how this happens. More work is required to clarify the effect of the direction of droplet velocity in the presence of DC fields, and also to investigate the same relationship in the presence of PDC and AC fields.

No study on the conditions required to induce droplet zigzagging compared to that required to induce droplet oscillation or to enhance droplet velocity has been reported and therefore, the relationship between the three forms of droplet agitation remains unclear. This gap in the knowledge must be addressed as it is essential in optimising mass transfer in ESX. It is conceivable, for example, that the droplet agitation may be dependent on the droplet diameter, the dominant form of polarisation, or the properties of the electrostatic field, but this requires further investigation.

Yamaguchi, Sugaya and Katayama (1989) are the only researchers that have reported on the effect of droplet zigzagging on mass transfer. These authors reported that enhanced extraction efficiency was partly owing to an increased residence time of droplets in the continuous phase. These authors, however, stated that the electrostatic field also caused increases in droplet oscillation, which they correctly pointed out would also influence mass transfer. It is, therefore, difficult to determine the relative contributions of each of these factors towards mass transfer.

## 2.7. EXPERIMENTAL TECHNIQUES TO STUDY THE EFFECT OF ELECTROSTATIC FIELDS ON DROPLET DISPERSION AND DROPLET AGITATION

The aim of this section is to identify an experimental technique that can be used to investigate the effects of electrostatic fields on mass transfer between aqueous droplets and a continuous organic phase. To gain a better understanding of the effects of electrostatic fields on droplet dispersion and droplet agitation requires an experimental technique that allows (1) application of uniform electrostatic fields to induce dispersion and agitation of aqueous droplets in a continuous organic phase (2), visual observation of droplet behaviour, and (3) measurement of droplet size and droplet velocity.

Given that no standard technique exists for investigating the effect of electrostatic fields on droplet dispersion and droplet agitation, this review focuses on techniques for measuring mass transfer between droplets and a continuous phase that have previously been modified to investigate the effect of electrostatic fields. These techniques include

the (1) tapered column technique and (2) droplet column technique. For both techniques, the review comprises the design and method of operation, as well as the significant modifications to improve the technique that have been reported. Finally, the application of each technique to the purpose of the present study is considered to determine which is the most suitable.

### 2.7.1. Tapered Column Technique

The tapered column technique involves suspending a droplet of one phase in the opposite phase by using a suitable flow rate of the continuous phase in a precisely constructed tapered channel (Clinton 1972). The continuous organic phase, which is recirculated through the column, enters through an inlet at the bottom of the column, and exits through an outlet near the top of the column. An aqueous droplet is released from the top of the column and is suspended within the tapered channel by using a suitable flow rate of the organic phase. Mass transfer from the dispersed phase into the continuous phase is measured by analysis of the concentration of solutes in the recirculating continuous phase.

Later, Wham and Byers (1987) adapted the tapered column technique to investigate the effect of electrostatic fields on droplet oscillation by incorporating stainless steel rod electrodes (0.32 cm ∅) on both sides of the tapered channel (Figure 2.27). This electrode design and orientation facilitated application of electrostatic fields to a single aqueous droplet that was suspended within a continuous organic phase. These researchers used a high-speed camera to capture images of droplet behaviour, and were therefore able to observe the changes in the shape of single droplets in the presence of electrostatic fields.

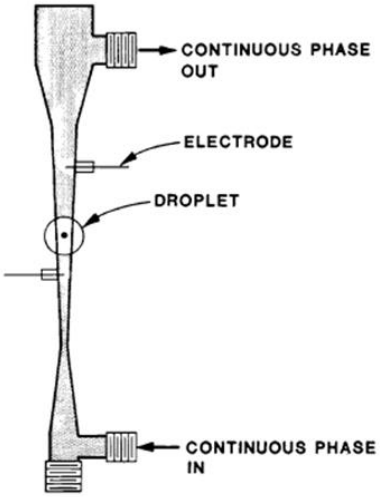


Figure 2.27 Tapered column apparatus used by Wham and Byers (1987)

The tapered column technique allows application of electrostatic fields to induce droplet oscillation, as well as visual observation of droplet oscillation, but is not suitable for investigating droplet dispersion. The flow rate of the continuous organic phase that is required to suspend droplets is dependent partly on the droplet diameter, which would be non-uniform for a droplet population with a range of diameters. As a result, observation of droplet dispersion would not be possible because the droplet population would not be suspended within the column. Also, this technique does not allow investigation of droplet zigzagging. This technique is therefore not suitable for the purposes of the present study.

### 2.7.2. Droplet Column Technique

The droplet column technique involves passing droplets of one phase through a vertical column that is filled with the other phase. The mass transfer between the two phases is measured by the change in concentration of the species of interest in the dispersed phase after it has passed through the continuous phase. This is achieved by sampling the volume of collected droplets and then using an analytical technique that is suitable for the type of solutions and species of interest that is under investigation.

Many researchers have adapted the droplet column technique to investigate the effect of electrostatic fields on droplet dispersion and droplet agitation by incorporating electrodes to facilitate application of a field. The first attempts involved releasing droplets from a charged nozzle at the top of the column and allowing them to move towards an earthed electrode at the bottom of the column (Stewart & Thornton 1967; Bailes & Thornton 1971; Bailes & Thornton 1974). Since these early studies, researchers have reported many alternate designs with modifications to the electrodes including the materials of construction, size and shape, orientation within the column, and the type and thickness of electrode insulation. Parallel-plate electrodes are the most suitable electrode orientation to study the behaviour of droplets in response to a uniform electrostatic field, as this maintains a constant electrode spacing and a relatively uniform field strength in all regions of the field (Figure 2.28).

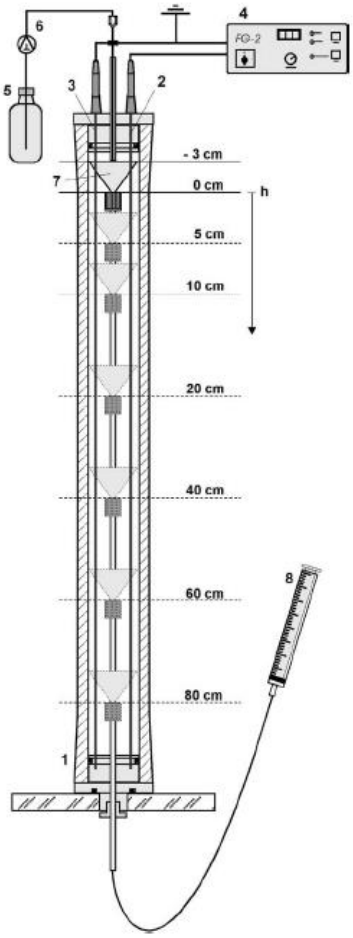


Figure 2.28 Droplet column apparatus with parallel-plate electrodes (1-glass column, 2-charged plate electrode, 3-grounded plate electrode, 4-high voltage power supply, 5-dispersed phase, 6-metering pump, 7-funnel, 8-syringe) (Gneist & Bart 2003)

The droplet column technique also satisfies the other specific requirements to enable investigation of the effects of electrostatic fields on droplet dispersion and droplet agitation. This technique allows good visual observation of droplet behaviour, provided that the droplet column apparatus is constructed using a transparent material, such as glass. In addition, this technique allows measurement of droplet size and droplet velocity by incorporating a suitable imaging technique, such as those reported by previous investigators (Stewart & Thornton 1967; Yamaguchi, Sugaya & Katayama 1988; Eow, Ghadiri & Sharif 2003). The accuracy and reproducibility of these measurements, however, may be improved by the use of more sophisticated imaging equipment.

The main weakness of the droplet column technique is that additional mass transfer occurs when the droplets have coalesced at the end of the column. Some methods have been devised to minimise this, such as collecting droplets in a funnel and removing

them immediately with a syringe (Figure 2.28). If this weakness can be circumvented or minimised, the technique would be suitable for the purposes of the present study as it satisfies all the criteria required for the investigation of the effect of electrostatic fields on droplet dispersion and droplet agitation. And this was pursued in the present study.

## 2.8. CHAPTER SUMMARY

Mass transfer in SX is inherently influenced by processes at the liquid-liquid interface. The application of electrostatic fields across an interface induces phenomena that influence interfacial processes and thus alter mass transfer rates, including (1) the Marangoni effect and Marangoni-type turbulence, (2) movement of electric charges in the organic phase (3) electromigration of species in the aqueous phase, and (4) orientation of species in the organic phase. It is likely that two or more of these phenomena may occur simultaneously in some systems. Currently, it is unclear which is the dominant interfacial phenomenon that influences mass transfer in the Co(II)/Cyanex® 272 system. The modified Lewis cell (MLC) is the most suitable technique to investigate interfacial phenomena in the presence of electrostatic fields.

In organic-continuous systems, electrostatic fields can be used to induce droplet dispersion and droplet agitation, both of which also have a significant effect on mass transfer. Droplets disperse after being polarised in the presence of electrostatic fields, and the main forms of droplet polarisation in ESX are orientational and interfacial polarisation. The two mechanisms of droplet dispersion, which refers to the droplet shape prior to dispersion, are necking and jetting. There is currently insufficient understanding of how the properties of electrostatic fields influence droplet polarisation, dispersion mechanisms and, therefore, the droplet size distributions that are generated in ESX.

Electrostatic fields can influence several forms of droplet agitation including (1) droplet oscillation, (2) droplet speed, and (3) droplet zigzagging. All of these forms of agitation have been attributed to the electrostatic force from an external field, but it is currently unclear exactly how they occur and thus what conditions are required to induce each of these. The droplet column technique is the most suitable technique to investigate droplet dispersion and droplet agitation in the presence of electrostatic fields.

# Chapter 3

# DEVELOPMENT OF LABORATORY EQUIPMENT

## 3.1. INTRODUCTION

This chapter describes the effort to design, construct and commission the two major experimental equipment that were used to investigate the effect of electrostatic fields on mass transfer in solvent extraction (SX).

Two different types of equipment were required to investigate the effect of electrostatic fields on (1) interfacial phenomena, and (2) electrostatically induced dispersion and droplet agitation. The review of experimental techniques in Chapter 2 identified that the most appropriate techniques to achieve this were the (1) Lewis cell and (2) droplet column. For clarity, these two different types of equipment will collectively be referred to as apparatuses in this work. Both of these apparatuses had to be developed for the present study because no suitable apparatus had been developed previously by our research group.

## 3.2. DESIGN AND CONSTRUCTION OF THE MODIFIED LEWIS CELL EXPERIMENTAL SET-UP

### 3.2.1. Design Philosophy

A major requirement of the modified Lewis cell (MLC) used in the present study was the facility to apply an electrostatic field across the liquid-liquid interface and thus enable investigation of interfacial phenomena. Few details regarding how this may be achieved have been reported because this is not a requirement of the conventional uses of an MLC, and little work has been done on the effect of electrostatic fields across a liquid-liquid interface. The only method of applying an electrostatic field in an MLC that has been described in sufficient detail to be easily replicated is to insert ring electrodes on both sides of the interface (Wildberger & Bart 2002). This method, however, is not suitable for the present study because inserting additional objects such as ring electrodes may alter the hydrodynamics within the MLC.

To allow accurate measurement of mass transfer, the MLC should also satisfy the fundamental requirement of the conventional uses of an MLC. That is, it should allow

application of intense stirring that provides homogeneous mixing in each of the bulk phases without causing disruption of the interface.

The MLC should incorporate improvements to the Lewis cell technique that have been reported since Lewis's (1954) novel study. This includes a method to maintain the position of the interface, which ensures that the thickness of the diffusion regions remains constant during an experiment, and eliminates the experimental error associated with continually removing samples and adding new solution. In addition, a method should be incorporated to eliminate lag time between filling the cell with the phases and commencing an experiment, which will allow more accurate measurement of mass transfer.

The materials of construction should (1) be chemically resistant to the aqueous and organic phases used in this work, (2) allow visual observation of the interfacial region, (3) provide a leak-proof seal when all components of the MLC are assembled, and (4) facilitate thorough cleaning of all components of the MLC.

### 3.2.2. Modified Lewis Cell Compartments and Stirrers

In the present study, the MLC was required to provide homogeneous mixing within the bulk of each phase. This was achieved by incorporating internal cylinders on both sides of the interface and by using stirrers with propeller blades oriented at 45°. This design, which is similar to that of Nitsch and Hillenkamp (1972) and Danesi et al. (1982), modifies the direction of fluid flow to create homogeneous mixing within the bulk of both phases.

The MLC has three compartments that are constructed from Pyrex® glass and two stirrers that are constructed from stainless steel (316 Grade). These materials are chemically resistant to the aqueous and organic phases that are used in the present study, and allow clear visual observation of the interfacial region as well as of the phases within the MLC. The MLC was constructed in three separate compartments, rather than in one piece, as these can be assembled and dismantled to facilitate thorough cleaning.

A diagram of the MLC compartments and stirrers is shown in Figure 3.1, and all dimensions of the glass compartments are shown in Appendix A1. The upper compartment (a) contains an outer cylinder (d), and an inner cylinder (e). The inner cylinder is attached to the outer cylinder by three equi-distant glass rods (f). The outer cylinder is surrounded by a jacket (g) that is fitted with barbed ports (h) to allow connection of tubing. The middle compartment (b) consists of a cylinder (i) that is also

surrounded by a jacket (j). The lower compartment (c) mirrors the upper compartment. The stirrers inside the upper (k) and lower compartments (l) are three-bladed propellers oriented at 45° (40-mm blade ∅, 10-mm shaft ∅) (PL010, DAIHAN Scientific). The total volume of solution within the MLC is approximately 800 mL.

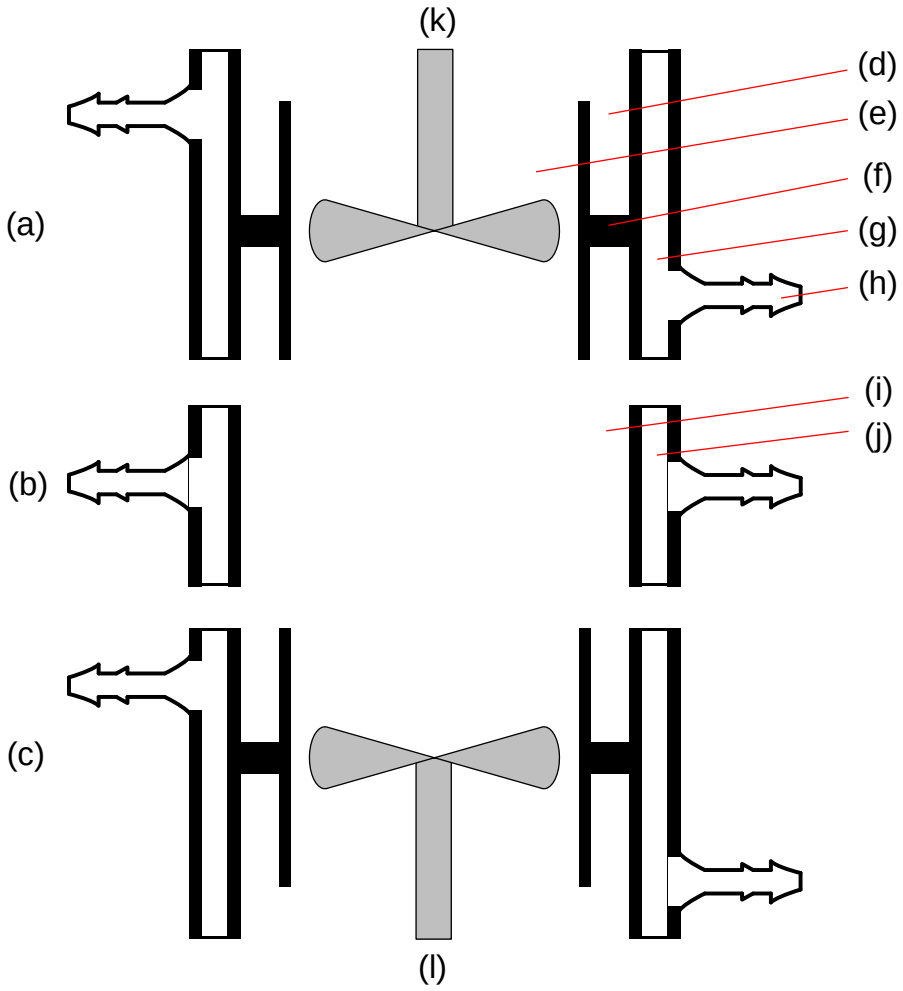


Figure 3.1 Design of the compartments of the modified Lewis cell

### 3.2.3. Modified Lewis Cell Lids

In the present study, the MLC should provide a facility to eliminate lag time between filling the cell with the phases and commencing an experiment, and also provide a leak-proof seal when all components of the MLC are assembled. Both of these requirements were achieved by placing two identical lids below the lower compartment and above the upper compartment.

The MLC lids are constructed from Pyrex® glass. Each lid has a female ground glass joint (24/40) in its centre to enable connection of a stirrer bearing with the corresponding male joint (8050-02, Ace Glass). The lids also have two glass ports (15 mm length, 2.4 mm ID, 4 mm OD) to allow connection of flexible tubing, and a glass

screw cap fitting to allow connection of a PTFE screw cap (GL14) with a silicone septum. The septum was temporarily pierced with a needle to inject a small volume of concentrated solution containing the species of interest from a syringe into one phase after the MLC has been filled with the two phases. This eliminated lag time between filling the cell and commencing an experiment. Diagrams and photographs of the lids are shown in Appendix A2. Flat Viton® o-rings (1 mm thickness, 85 mm ID, 92 mm OD) were placed between the lids and the upper and lower compartments to assist in providing a leak-proof seal.

Initially, a leak-proof seal was achieved by applying a small amount of silicone grease (Z273554, Sigma-Aldrich) between the lids and compartments. This method was used as silicone grease is commonly used to provide a good seal. It was found, however, that upon filling the MLC with the two phases, a haze formed in the organic phase. This was attributed to the partial solubility of the silicone grease in the organic phase. The poisoned organic phase was discarded and Viton® o-rings were used to provide a leak-proof seal for all mass transfer experiments.

### 3.2.4. Wire Mesh Electrodes

The MLC used in the present study was required to enable application of an electrostatic field across the liquid-liquid interface, as well as to satisfy the fundamental requirement of an MLC to allow application of intense stirring in each of the bulk phases without causing disruption of the interface. Placing wire mesh between the upper and middle compartments and between the middle and lower compartments, similar to that used by Nitsch and Hillenkamp (1972) to improve the hydrodynamics, allows both of these requirements to be achieved. This eliminates the need to insert additional objects into the MLC to apply electrostatic fields, such as a ring electrode used by Wildberger and Bart (2002), as the wire mesh simultaneously acts as the electrodes and alters the hydrodynamics to inhibit disruption of the interface.

The main requirements of the electrodes were that they (1) were insulated with a material that is resistant to the aqueous and organic phases used in the present study and provides sufficient dielectric strength to allow application of a high voltage electrostatic field, and (2) could provide a leak-proof seal when placed between the MLC compartments.

The electrodes were constructed using stainless steel wire mesh (316 Grade, 125 μm wire diameter, 190 μm aperture) that had been coated with Parylene C (2 mil thickness,

Parylene Engineering), Polymorph (Altronics), which is a low-melting point polycaprolactone, flat high density polyethylene (HDPE) o-rings (3 mm thickness, 75 mm ID, 95 mm OD), and two moulds made from mild steel (3-mm thickness). Each mould consisted of a ring (95 mm ID, 115 mm OD) that was adhered onto a square plate (115 mm x 115 mm) using an epoxy adhesive (Araldite, Selleys). Holes (8-mm ∅) were drilled into the four corners of the moulds so that bolts and nuts could be used to apply compression between the two moulds. Diagrams of the moulds are shown in Appendix A3.

Granules of Polymorph were placed in boiling water, which allowed the melted Polymorph to be moulded by hand. HDPE o-rings were placed inside the moulds, and a thin layer of the melted Polymorph was placed on both the HDPE o-rings. Holes (10-mm ∅) were drilled into the four corners of a piece of wire mesh (100 mm x 100 mm) to allow the wire mesh to fit around the 8-mm bolts when the wire mesh was compressed between the moulds. The Polymorph was allowed to cool at room temperature for one hour, after which the moulds were dismantled and the wire mesh was removed. The Polymorph did not adhere to the HDPE, but had fused together through the mesh in the shape of the o-rings. A leak-proof seal was achieved by placing flat Viton® o-rings (1 mm thickness, 85 mm ID, 92 mm OD) between the Polymorph layer on the electrodes and the MLC compartments.

Tefzel®-coated stainless steel wire (M22759/16 AWG22, Avial Australia) was soldered onto one corner of the electrodes that had been covered during the insulation coating process and therefore remained uninsulated. Self amalgamating tape (AT87, Advance Tapes) was wrapped around this corner of the electrodes to protect the soldered connection. Connection of the electrodes to high-voltage power supplies was facilitated by connecting the Tefzel®-coated wire to high-voltage cables. Two opposite sides of the wire mesh electrodes were cut along the circumference of the Polymorph layer so that the electrodes could fit between the MLC supports. A photograph of a wire mesh electrode is shown in Figure 3.2, and all dimensions of the wire mesh electrodes are shown in Appendix A4. These wire mesh electrodes satisfied all of the requirements, and were used for all mass transfer experiments.

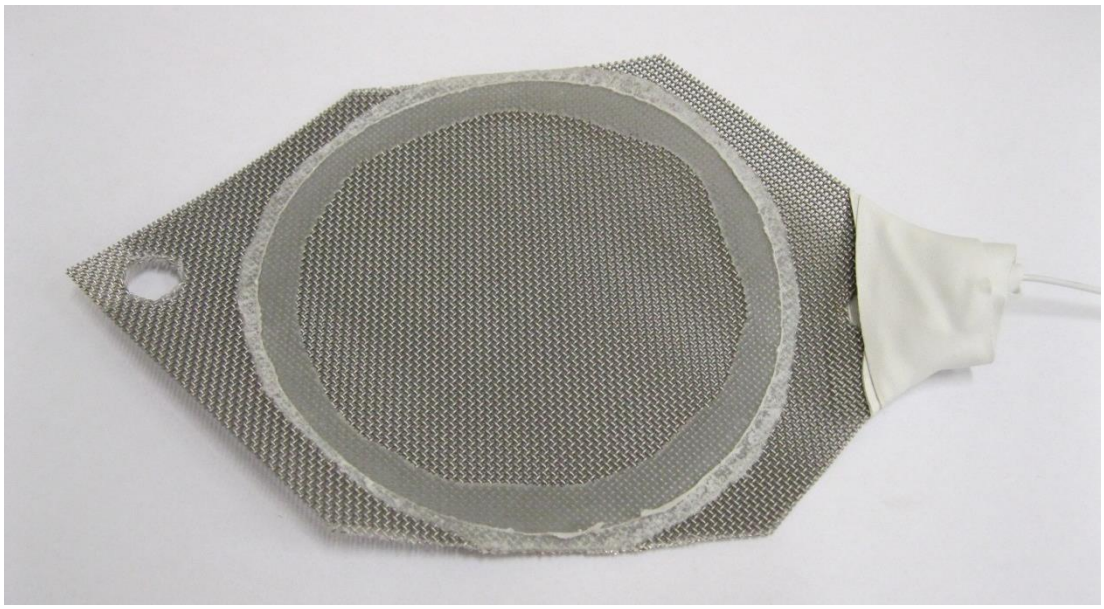

Figure 3.2 Photograph of a wire mesh electrode

The wire mesh size was selected after testing several different mesh sizes. Initial work was carried out using a coarser mesh size (0.56 mm wire diameter, 1.0 mm aperture) as this was readily available and is comparable to the mesh size used in the ARMOLLEX cell designed by Danesi et al. (1982). It was found, however, that these electrodes only prevented disruption of the interface over a narrow range of stirring speed, which was attributed to the mesh size being too coarse. On the other hand, the mesh size used in the MLC allowed application of the required range of stirring speed without disruption of the interface.

The material used for the electrode insulation was selected after testing several different materials and coating processes. Initial work was carried out using PTFE-coated stainless steel wire mesh as this could be purchased commercially pre-coated. It was found, however, that the PTFE coating allowed only a limited range of applied voltage before the onset of electrical arcing and thus, damage of the electrode insulation. This was attributed to the relatively low dielectric strength of PTFE ($1.78 \times 10^7$ V/m). An alternative insulation material was required that provided greater electrical insulation and could be coated onto fine wire mesh without blocking the mesh apertures. This was achieved using Parylene C, which has a relatively high dielectric strength ($2.64 \times 10^8$ V/m) and is coated by a vapour deposition process, which allows a more uniform coating than can be achieved with other processes.

### 3.2.5. Modified Lewis Cell Supports

To provide structural support for the MLC and to provide a leak-proof seal, the glass components of the MLC and the wire mesh electrodes were compressed between two support plates. The support plates consisted of a layer of stainless steel (3 mm thickness, 130 mm x 130 mm) and Viton® (3 mm thickness, 130 mm x 130 mm). A hole (82 mm ∅) was cut in the centre of the support plates, which allowed the MLC lids to rest on the Viton®. Holes (8 mm ∅) were cut in each of the four corners of the support plates, 7 mm from each side, through which threaded vertical rods (stainless steel, 8 mm ∅) were inserted. The position of the support plates was fixed using washers and nuts (stainless steel, 8 mm ∅). A diagram of the dimensions of the support plates is shown in Appendix A5.

The vertical rods were affixed to a metal base that was resting on a table and secured to the table by washers and nuts. The table was bolted to the floor to provide additional stability. The position of the vertical rods was secured by clamping the upper sections to horizontal support rods that had been affixed to a bracket on a nearby wall. A larger threaded vertical rod (stainless steel, 12 mm ∅) was required to provide structural support for the two overhead stirrers that were used in the MLC. The position of the larger vertical rod was secured in the same way as the other four vertical rods. Photographs of the MLC supports are shown in Figure 3.3.

Figure 3.3 Photographs of the MLC supports

### 3.2.6. Sampling and Analytical Technique

In the present study, the position of the interface had to be maintained to ensure that the distance between the stirrers and the interface was constant and thus the thickness of the diffusion regions remained constant. This would also avoid the experimental error associated with continually removing samples and adding new solution into the MLC. This was achieved by using a spectrophotometer (DMS 70, Varian) to continuously monitor the concentration of the species of interest. This non-destructive sampling technique was designed to minimise the volume of solution outside the MLC, and to minimise the time taken for a change in concentration of species to be measured. It also prevented the need to approach the MLC during an experiment for manual sampling, which was desirable given that high voltages were used during experiments.

The organic phase was sampled by pumping solution out of the MLC through one port on the upper lid, through a flow cell (585.3/SOG/10/Z20, Starna Scientific) that was placed in the sample cell holder of the spectrophotometer, and returned into the MLC through the other port on the upper lid. A cartridge peristaltic pump (EW-07519-20, Masterflex®) with an eight-roller pump head was used to reduce occlusion and thus, provide a relatively smooth flow of liquid through the flow cell. Three different tubings were used to carry out sampling: Viton® tubing (3 mm ID x 6 mm ID, 96412-16, Masterflex®) was required to attach to the ports on the upper lid of the MLC, Viton® tubing (1 mm ID x 4 mm OD, 96412-13, Masterflex®) was required to be used with the cartridge pump, and 1.6-mm PTFE tubing (TJ/G/1.5/PTFE, Starna Scientific) that was supplied with the flow cell was required to be used with the flow cell. The two sizes of Viton® tubing were connected using a reducing PVDF barbed fitting (1/8" ID x 1/16" ID, 30703-41, Cole Parmer), and the smaller Viton® tubing was connected to the PTFE tubing by inserting the PTFE into the Viton® tubing and fixing with cable ties.

The concentration of species was determined by measuring the absorbance of solution passing through the flow cell. The spectrophotometer is equipped with a chart recorder output socket, which is an electrical connection that emits an analogue output voltage that is directly proportional to the absorbance of the sample being measured. This chart recorder socket was connected to a LabJack analogue-to-digital converter (U12, LabJack Corporation), and the LabJack was connected to a desktop computer. The associated software (DAQ Factory Express, LabJack Corporation) was used to control the LabJack, as well as to record the data values of the output voltage of the spectrophotometer.

Several adjustments were made to minimise various sources of noise and ripple in the spectrophotometer output voltage signal. Firstly, the wire connecting the chart recorder output socket on the spectrophotometer to the LabJack was replaced with shielded wire, and a resistor (10 kΩ) and a capacitor (0.1 mF) were connected to the LabJack. This filtered the voltage signal by removing interference of random AC voltage from nearby electrical equipment. Secondly, the resolution of the voltage measurement was increased by changing the operating mode of the LabJack from single-ended to differential. The programmable gain amplifier (PGA) was used with a gain of 10 to increase the voltage resolution from 204.8 bit/V to 2048 bit/V. Thirdly, the collection of data points was changed from one sample per second to the average of ten samples per second. This produced the same number of data points, but reduced random fluctuations in voltage. These adjustments provided a consistent relationship between the absorbance of a sample in the spectrophotometer and the spectrophotometer output voltage and thus, allowed accurate measurement of the concentration of the species of interest.

Preliminary work revealed that measurement of the concentration of species in an MLC experiment was hindered by air bubbles entering the flow cell. These air bubbles were attributed to the pulsing action of the cartridge peristaltic pump used to continuously recirculate solution from the MLC through the flow cell. Therefore, the sampling tubing was modified to include an in-line bubble trap (01-0221, GRACE Davison) between the cartridge pump and the flow cell. Viton® tubing was attached to both barbed ports on the bubble trap. This eliminated air bubbles from entering the flow cell.

### 3.2.7. Auxiliary Equipment

In addition to the major components of the MLC, the complete experimental set-up included other auxiliary equipment.

A temperature-controlled waterbath (TH4 Thermoregulator, Ratek Instruments) was used to maintain the temperature of the water within the jackets of the MLC compartments. Peristaltic pumps (7554-20, Cole Parmer) with manual pump controllers (7566-14, Cole Parmer) were used to pump water from the waterbath to the lower barbed ports on each of the three compartments. The temperature-controlled water exited the jacket through the upper barbed ports on each of the compartments, and was returned to the waterbath.

The stirrer shafts were rotated using overhead stirrers (RZR 2021, Heidolph); the stirrer used for the upper compartment was upright, and the stirrer used for the lower

compartment was inverted. The stirrer shafts were attached to the stirrers by connecting flexible tubing (40-mm length) to the end of the stirrer shaft, attaching another shaft (316 Grade stainless steel, 10-mm ∅) to the other end of the flexible tubing, and inserting the secondary shaft into the overhead stirrer. The flexible tubing functioned as a universal joint and thus prevented misalignment of the stirrers.

Peristaltic pumps (7554-20, Cole Parmer) with manual pump controllers (7566-14, Cole Parmer) and Viton® tubing (3 mm ID x 6 mm ID, 96412-16, Masterflex®) were used to transfer aqueous and organic phases into the MLC.

An electrostatic field was generated within the MLC by connecting an insulated high-voltage cable from a high-voltage power supply to one wire mesh electrode, and connecting the other electrode to earth. The power supplies used in this work were a direct current (DC) and an alternating current (AC) that were both constructed by our research group. In the case of a DC field, the desired polarity was set by selecting either a positive or negative diode on the DC power supply. To generate a square-wave pulsed DC (PDC) field, the DC power supply was modified to switch the applied voltage between a desired voltage and zero at a desired frequency and pulse width. This was achieved by connecting a relay (LJTick-Relay, LabJack Corporation) and two opto couplers (OC 250, Voltage Multipliers) to a LabJack (U3-LV, LabJack Corporation).

A high voltage probe (HP-40, Tenma) and a multimeter were used to measure the voltage applied to a charged electrode. The LabJack LJscope application, which functions as an oscilloscope, was used to record the voltage waveforms that were generated. Examples of the recorded voltage waveforms for the three different types of electrostatic fields that were investigated in this work are shown in Figures 3.4 – 3.6. It is evident that there is negligible noise and ripple in the applied voltage in all waveforms, which indicates that the power supplies were functioning as required.

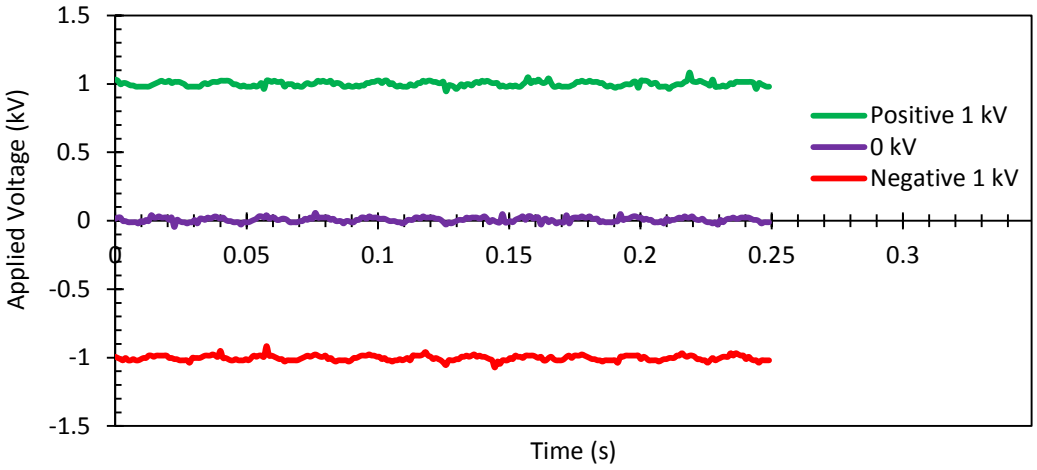


Figure 3.4 Example of voltage waveforms generated by DC fields

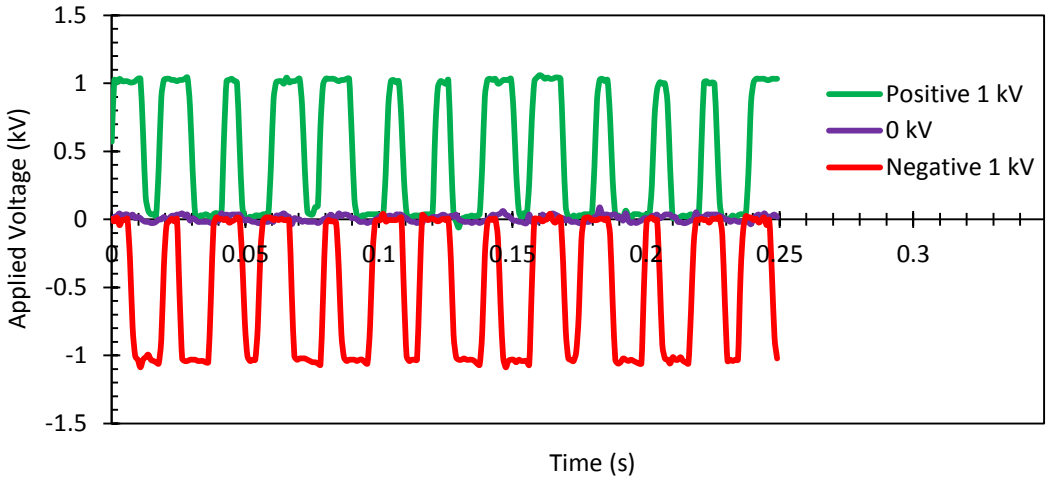


Figure 3.5 Examples of voltage waveforms generated by PDC fields with 50 Hz frequency

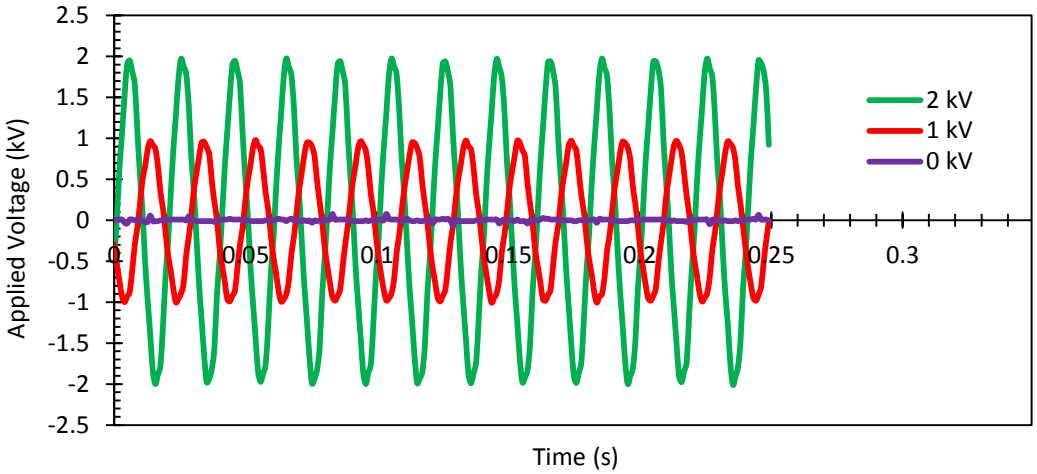


Figure 3.6 Example of voltage waveforms generated by AC fields with 50 Hz frequency

### 3.2.8. Assemble and Disassemble Procedures

To carry out an experiment, the MLC was assembled as follows: The lower lid and stirrer bearing were assembled and placed on the Viton® layer of the lower support plate. The upper lid and stirrer bearing were assembled and attached to the upper stirrer using a universal joint. The lower compartment was placed onto the lower lid, separated by a Viton® o-ring. The upper compartment was placed on top of the lower compartment, and a Viton® o-ring was placed between the upper compartment and the upper lid. The middle compartment was then placed between the upper and lower compartments. The lower wire mesh electrode was then placed between the lower and middle compartments, and the upper wire mesh electrode was placed between the middle and upper compartments. Viton® o-rings were placed on either side of both electrodes.

The support plate above the MLC was carefully pushed down to apply compression between the components of the MLC, but the nuts above the upper support plate were not tightened until the glass compartments and the wire mesh electrodes were aligned. Builders wedges (Builders Edge) were placed between the glass compartments and the four vertical support rods to ensure that the compartments were aligned and equidistant from the vertical support rods. The position of the wire mesh electrodes and all o-rings was then adjusted as required to ensure that they were aligned with the glass compartments. Once all components were properly aligned, the nuts above the upper support plate were tightened with a shifter to apply compression and thus ensure a leak-proof seal. The stirrers in the upper and lower compartments were then positioned by aligning the propeller blades with one of the equi-distant glass rods. The lower stirrer shaft was attached to lower stirrer with another universal joint. Photographs of the assembly procedure of the MLC are shown in Appendix A6.

The MLC had to be completely dismantled after each experiment to allow thorough cleaning and to allow all components to dry before commencing another experiment. After an experiment was completed, all equipment was turned off and the MLC was drained by opening the drain valve that was attached to the tubing connected to the lower lid. The tubing attached to the barbed jacket ports was removed and the water inside the jackets was drained. The nuts above the upper support plate were loosened and the support plate was raised so that all components of the MLC could be removed for cleaning. The wire mesh electrodes were cleaned with methylated spirits and distilled water and were then rinsed with acetone. All other components of the MLC were

cleaned by rinsing with hot tap water, followed by methylated spirits, distilled water, and finally rinsed with acetone. The sampling tubing was drained and then flushed with fresh organic phase.

The MLC experimental set-up is illustrated in Figure 3.7, and photographs of the complete experimental set-up are shown in Appendix A7. The syringe containing a concentrated solution of the species of interest is pink in this diagram to represent the Co(II) and methyl violet solutions that were used in the MLC experiments.

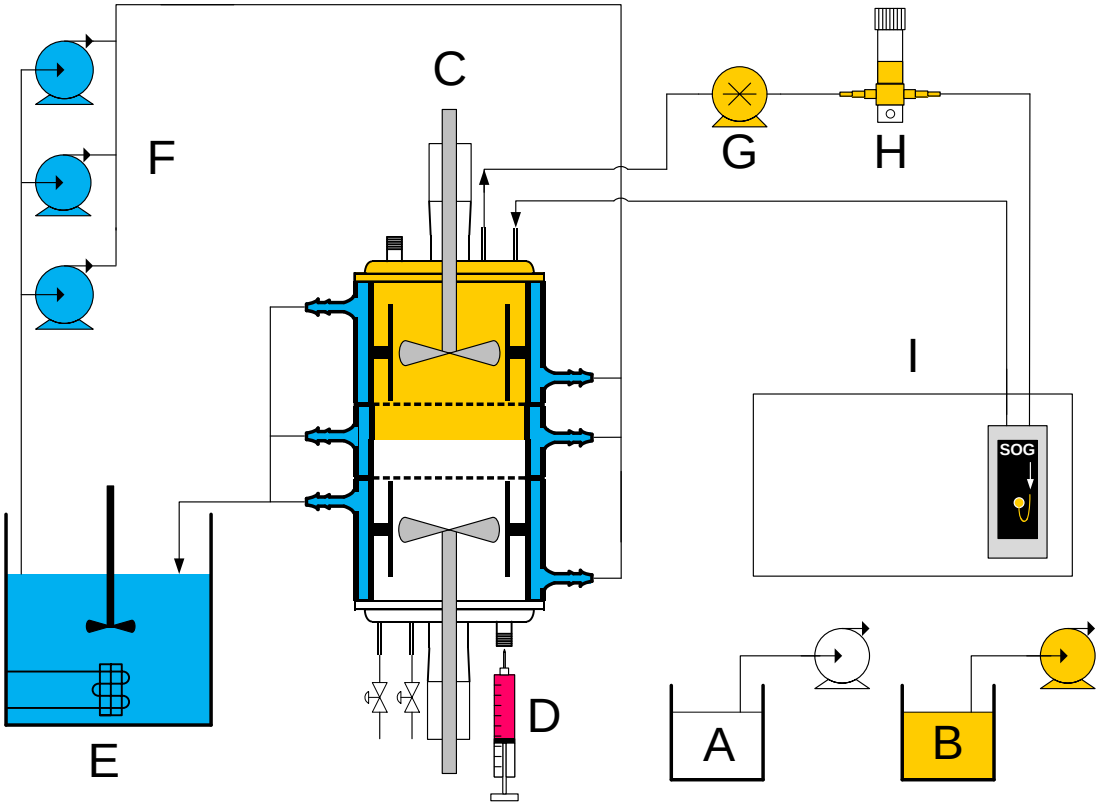


Figure 3.7 Schematic diagram of the MLC experimental set-up (A – aqueous phase reservoir, B – organic phase reservoir, C – modified Lewis cell, D – syringe containing concentrated solution of the species of interest, E – temperature-controlled water bath, F – peristaltic pumps for MLC jacket, G – cartridge pump for sampling, H – air bubble trap, I – spectrophotometer containing flow cell)

## 3.3. COMMISSIONING OF THE MODIFIED LEWIS CELL

The MLC and all auxiliary equipment were commissioned by simulating experimental conditions to ensure that the complete experimental setup operated as required. Given that this apparatus was designed and constructed in this study, it was necessary to develop methods of operating the MLC that would allow experiments to be carried out in a way that achieved the objectives of the present study.

### 3.3.1. Determination of a Method of pH Control

A method of pH control was required to ensure that the pH in an MLC experiment was maintained at conditions that favour the extraction of Co(II) with Cyanex® 272. The pre-neutralisation of Cyanex® 272 with ammonia was trialled as carried out by Lindell et al. (2000) because this is representative of practice in the SX industry. It was found, however, that pre-neutralisation did not work in the MLC because cobalt(II) hydroxide precipitated in the aqueous phase. It appeared that upon contact of the organic and aqueous phases, the un-reacted ammonia transferred into the aqueous phase, which caused an increase in the pH. Several attempts were made to minimise the transfer of ammonia into the aqueous phase, such as reducing the amount of ammonia sparged into the organic phase, but this was unsuccessful. Therefore, an acetic acid/acetate buffer in the aqueous phase was used to control the pH. Theoretical calculations as well as measurements of the pH after maximum Co(II) extraction showed negligible change in the pH, and therefore this method was used for all mass transfer experiments.

### 3.3.2. Determination of a Method to Measure the Concentration of Species

To extract meaningful data from experiments, a method was required to measure the concentration of the species of interest. The two species of interest in the present study were Co(II) and methyl violet. The former was used in all experiments on interfacial phenomena (Chapter 4), and the latter was used in experiments for the characterisation of the MLC (Chapter 3.4).

The ultraviolet-visible (UV-VIS) spectrophotometer was used to measure the concentration of extracted Co(II) in the organic phase as well as the concentration of methyl violet in the organic phase. This necessitated determining the optimum wavelength for measuring the concentration of each of these species in the organic phase. The optimum wavelength was determined by carrying out two wavelength scans (400 nm – 750 nm) to determine the wavelength that produced the maximum absorbance for an organic phase containing extracted Co(II) and methyl violet, respectively. As previously discussed, the technique used to continuously monitor the concentration of the species of interest involved recording the spectrophotometer output voltage, which is directly proportional to the absorbance of the sample being measured.

The spectrophotometer wavelength was set to 750 nm, cuvettes that were filled with fresh organic phase were placed in the sample cell holder and in the reference cell holder, and the spectrophotometer absorbance was zeroed. The cuvette in the sample cell holder was removed from the spectrophotometer, emptied, cleaned with acetone, and filled with an organic phase containing either extracted Co(II) or methyl violet. A wavelength scan was carried out by measuring the spectrophotometer output voltage as the wavelength decreased from 750 nm to 400 nm at a speed of 10 nm/minute.

The results of the wavelength scans are shown in Figures 3.8 and 3.9, respectively. In the case of Co(II), the maximum spectrophotometer output voltage occurred at a wavelength of 633 nm, and therefore this wavelength was used for all experiments that involved measurement of the concentration of the extracted Co(II) in the organic phase. On the other hand, in the case of methyl violet, the maximum spectrophotometer output voltage occurred at a wavelength of 592 nm, and therefore this wavelength was used for all experiments that involved measurement of the concentration of methyl violet in the organic phase.

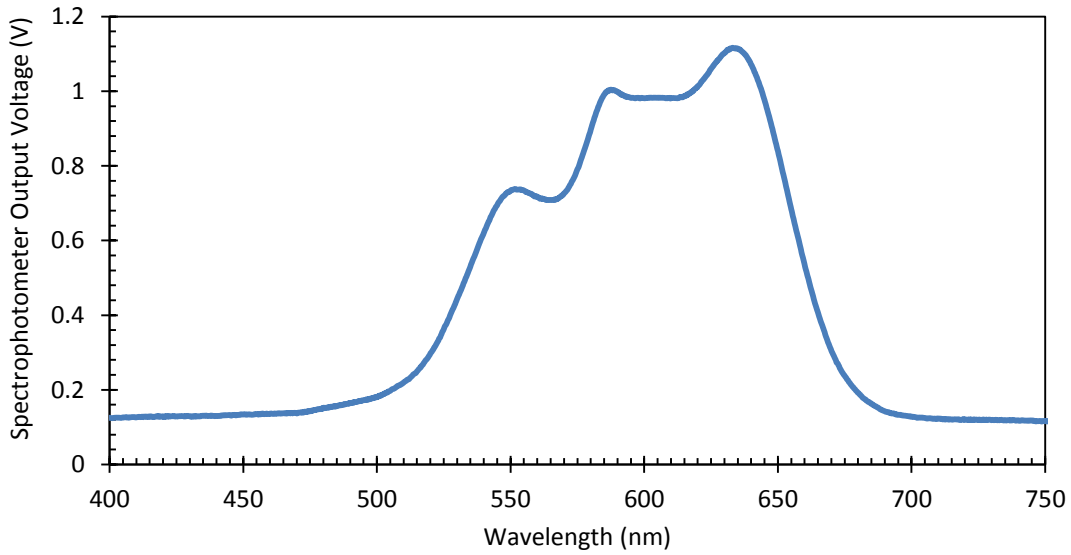


Figure 3.8 Wavelength scan of extracted Co(II) in the organic phase

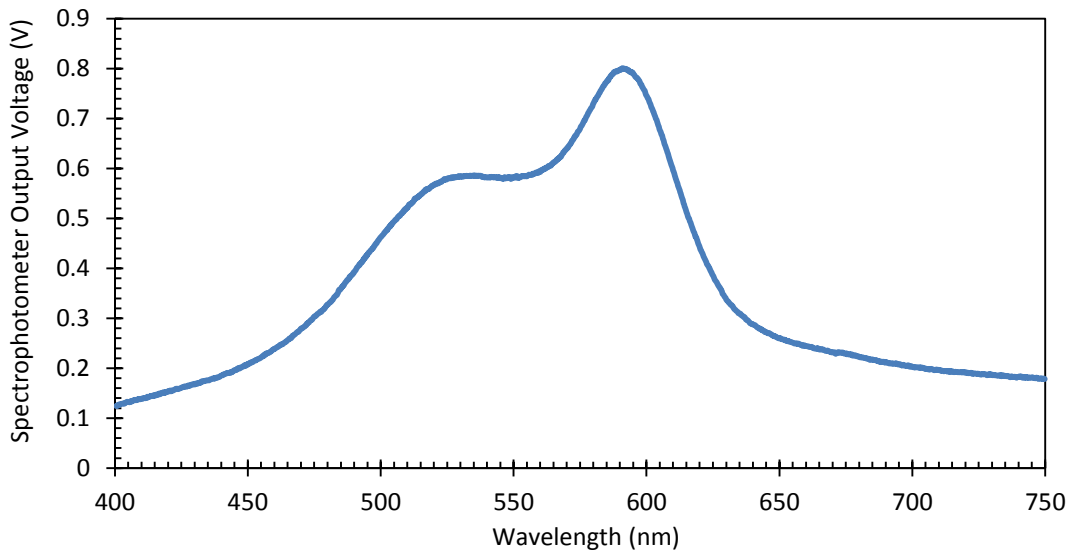


Figure 3.9 Wavelength scan of methyl violet in the organic phase

To facilitate measurement of the concentration of extracted Co(II), and therefore mass transfer rates, the relationship between the concentration of extracted Co(II) in the organic phase and the spectrophotometer output voltage had to be determined. This was determined by preparing and measuring the spectrophotometer output voltage of organic solutions containing known concentrations of extracted Co(II).

Standard organic solutions were prepared by contacting fresh organic phase, containing 10% (v/v) Cyanex® 272 in Shellsol® 2046, with aqueous Co(II) solutions that had been previously prepared from standard aqueous Co(II) solution (10 000 mg/L). Dilution of the aqueous solutions was carried out using distilled water that contained sodium sulphate (0.2 M) and had been adjusted to pH 5.5, which will be referred to as the dilution solution. The sodium sulphate was required to provide enhanced phase disengagement (Fu & Golding 1988), and the pH adjustment was required to prevent precipitation of cobalt(II) hydroxide. Firstly, 10 mL of standard aqueous Co(II) solution was transferred into a 100-mL volumetric flask and filled to the mark with the dilution solution. This 1000 mg/L Co(II) solution was then further diluted to produce solutions containing 10, 20, 30, 40, 50, 60, 70, 80, 90 and 100 mg/L Co(II) by diluting the appropriate amount into 100-mL volumetric flasks and filling to the mark with the dilution solution.

For each aqueous solution (10-100 mg/L Co(II)), 40 mL of an aqueous Co(II) solution and 40 mL of fresh organic phase were transferred into a 250-mL beaker. The phases were mixed vigorously using a magnetic stirrer (approximately 500 rpm) while NaOH (3 M) was added dropwise to increase the pH and thus, promote the mass transfer of

Co(II) ions into the organic phase. The phases were stirred for at least 5 minutes to allow equilibrium to be established, after which time the stirring was stopped and the phases were allowed to disengage. The final pH of the aqueous phase was measured. Sufficient NaOH was added to attain an equilibrium pH of approximately 6.5, which had been determined to be sufficient for 100% extraction of Co(II) into the organic phase. The phases were then heated (~50 °C) to facilitate removal of entrainment.

To measure the spectrophotometer output voltage of each standard solution of Co(II) in the organic phase, cuvettes were filled with fresh organic phase and placed in the sample cell holder and in the reference cell holder, and the spectrophotometer absorbance was zeroed. The cuvette in the sample cell holder was removed from the spectrophotometer, emptied, cleaned with acetone, and filled with a standard solution. The spectrophotometer output voltage was then measured and recorded by the LabJack. The absorbance shown on the spectrophotometer digital display was also recorded for each standard solution.

The results show that a linear relationship exists between the concentration of extracted Co(II) in the organic phase and the absorbance (Figure 3.10) and therefore the Beer-Lambert Law holds under these conditions. These results also confirm that the absorbance is directly proportional to the spectrophotometer output voltage. The equation for the linear trendline from Figure 3.10 was used to convert the spectrophotometer output voltage into concentrations of extracted Co(II) in the organic phase for all mass transfer experiments.

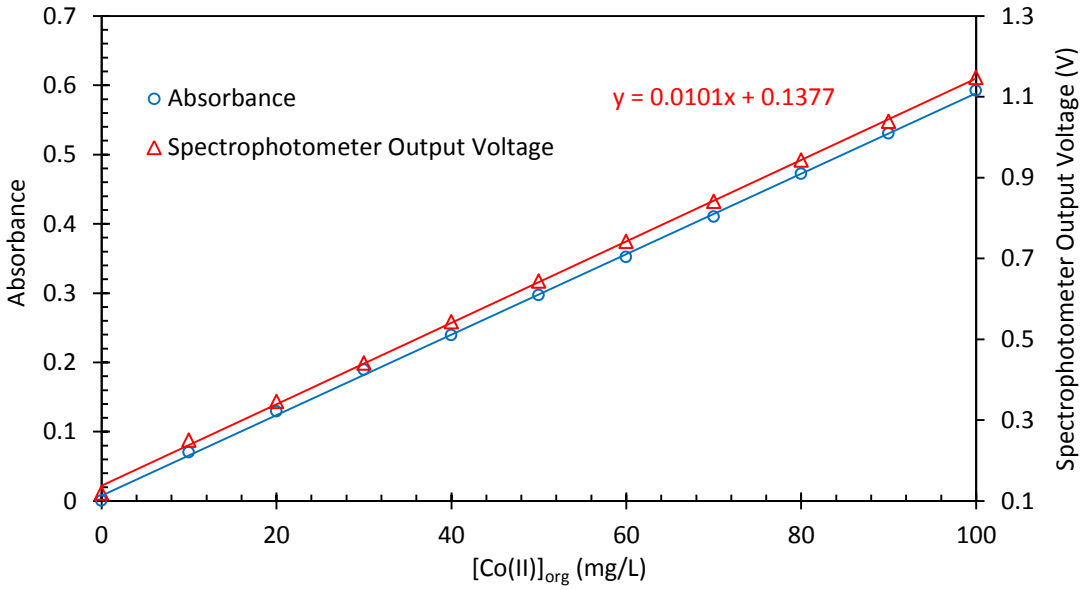


Figure 3.10 Relationship between the concentration of extracted Co(II) in the organic phase and the absorbance and spectrophotometer output voltage

It was unnecessary to obtain the relationship between the concentration of methyl violet in the organic phase and the absorbance because only a relative comparison of the concentrations was required for the characterisation of the MLC, which is described in Chapter 3.4. As a result, the concentration of methyl violet in the organic phase was measured simply from the absorbance measured by the spectrophotometer.

### 3.3.3. Development of a General Procedure for Modified Lewis Cell Experiments

Several types of experiments were carried out using the MLC, but the following general procedure was common to all experiments. This procedure was developed as a result of many attempts to ensure that the MLC operated as required to achieve the objectives of this work.

After assembling the components of the MLC following the procedure described in Chapter 3.2.8, temperature-controlled water was circulated between the waterbath (TH4 Thermoregulator, Ratek Instruments) and the jackets of the MLC compartments using three peristaltic pumps (7554-20, Cole Parmer) with Norprene® tubing (6404-18, Masterflex®). The aqueous phase was then transferred into the MLC as follows: a 75-mm length of Viton® tubing (96412-16, Masterflex®) was attached to a port on the lower lid. A peristaltic pump (7554-20, Cole Parmer) with Viton® tubing (96412-16, Masterflex®) was used to transfer the aqueous phase into the MLC by connecting the two pieces of tubing using a barbed polypropylene connector (4 mm Ø). Another 75-mm length of Viton® tubing (96412-16, Masterflex®), which was connected to a drain valve, was attached to the other port on the lower lid and the valve was closed. The aqueous phase was transferred until it filled the lower compartment and half of the middle compartment. The tubing was then clamped to prevent leaking.

The organic phase was then transferred into the MLC using another peristaltic pump (7554-20, Cole Parmer) with Viton® tubing (96412-16, Masterflex®) through the screw cap port on the upper lid. When the required volume of organic phase had been transferred into the upper half of the MLC, Viton® tubing (96412-16, Masterflex®) was connected to one port on the upper lid and an in-line bubble trap (01-0221, GRACE Davison) was attached between the cartridge pump and the flow cell. The cartridge pump was turned on to flush the sampling tubing with the organic phase, and the tubing returning from the flow cell was then attached to the second port on the upper lid of the MLC. A cuvette containing fresh organic phase was placed in the reference cell

holder, and the spectrophotometer absorbance was zeroed. The stirrers above and below the MLC were turned on and set to the desired rotation speed (resolution ±0.1% of final value).

To begin an experiment, a syringe (5 mL, Terumo) and needle (25G, 0.5 mm x 16 mm, BD) were used to inject a 3-mL solution containing a high concentration of the species of interest into the aqueous phase. This had a negligible effect on the position of the interface. The screw cap on the upper lid was opened during the injection of solution to prevent a build-up of pressure within the MLC, and was closed after injection. The data recording as well as the visual recording was then commenced. A new data recording set was created on the DAQ Factory Express software, and the experiment was filmed using a digital video camera (Sony Handycam).

At the end of an experiment, the organic and aqueous phases were drained from the MLC and separated. All components of the MLC were then dismantled and cleaned following the procedure described in Chapter 3.2.8.

### 3.3.4. Development of a Method for Data Analysis

To facilitate quantitative analysis of mass transfer, a method was developed to process the raw data that were generated from an MLC experiment.

A data series recorded from an MLC experiment consisted of two data sets: the spectrophotometer output voltage, measured in volts, and the run time, measured in seconds (s). For experiments that involved the extraction of Co(II) with Cyanex® 272, the output voltage was converted to a concentration of extracted Co(II) in the organic phase using the relationship derived in Figure 3.10. A graph of time (x-axis) against concentration (y-axis) was then constructed. For experiments that involved the dissolution of methyl violet into the organic solution, a graph of time (x-axis) against output voltage (y-axis) was constructed.

The mass transfer rate was measured by using the LINEST function in Microsoft Excel®, which uses the least squares method, to calculate the slope of the line between a specified time interval. The time interval that was selected was dependent on the experimental conditions, but always comprised one data point per second. It was found that there were some unavoidable random fluctuations in the slopes of the lines and therefore a minimum time interval of 500 consecutive seconds had to be used to calculate the mass transfer rate to eliminate the effect of these small fluctuations in the data on the calculated mass transfer rate.

For experiments that involved the extraction of Co(II) with Cyanex® 272, the mass transfer rate was expressed as mg/L/s, and for experiments that involved the dissolution of methyl violet into the organic phase, the mass transfer rate was expressed as V/s. As mentioned previously, the units for the two mass transfer rates are different because the spectrophotometer output voltage corresponding to the dissolution of methyl violet in the organic phase was not converted to a concentration.

## 3.4. CHARACTERISATION OF THE MODIFIED LEWIS CELL

The MLC was characterised to determine the operating conditions required to cause the mass transfer rate to be limited by either diffusion in one of the phases or the speed of the chemical reaction. This had to be carried out before the MLC could be used to investigate the effect of electrostatic fields on interfacial phenomena. This was achieved by determining the relationship between the initial mass transfer rate and the stirring speed for (1) the reactive mass transfer system of Co(II) with Cyanex® 272, and (2) the non-reactive mass transfer system of methyl violet dissolution into the organic phase.

The initial mass transfer rate is the rate of change of the concentration of the species of interest when it first begins to transfer from one phase into the other. In theory, increases in the stirring speed of one phase, while that of the other phase is constant, causes linear increases in the initial rate of mass transfer when the system is diffusion-controlled, and causes no change in the initial mass transfer rate when the system is controlled by the speed of the chemical reaction which is referred to as kinetic-controlled (Danesi, Chiarizia & Coleman 1980).

To determine the operating conditions required for each limiting step for a reactive mass transfer system requires another set of experiments under comparable conditions to investigate the behaviour of a non-reactive mass transfer system. In the absence of any chemical reactions, a plateau should only occur when the hydrodynamic limit of the apparatus has been reached. To replicate the hydrodynamics within the apparatus as well as possible, the density and viscosity of the solutions should be the same for both mass transfer systems. In the present study, methyl violet was used as the non-reactive mass transfer chemical because it (1) was soluble in both the aqueous and organic phases, (2) did not undergo a chemical reaction with any of the reagents in either phase, (3) did not change the density and viscosity of either phase considerably, and (4) caused a colour change when transferred into the organic phase.

The characterisation of the aqueous phase was achieved by using various stirring speeds in the aqueous phase (70 – 170 rpm) while maintaining a constant stirring speed in the organic phase (170 rpm). Similarly, the characterisation of the organic phase was achieved by using various stirring speeds in the organic phase (70 – 170 rpm) while maintaining a constant stirring speed in the aqueous phase (120 rpm). In each set of experiments, the stirring speed that was maintained constant in one phase was chosen because visual observations from commissioning of the MLC indicated that this speed was sufficient to reduce the diffusion region in that phase to a negligible thickness.

For all experiments involving the reactive mass transfer system, a 3-mL concentrated solution of Co(II) was injected into the aqueous phase, and for all experiments involving the non-reactive mass transfer system, a 3-mL concentrated solution of methyl violet was injected into the aqueous phase. Injecting the same volume of concentrated solutions for both sets of experiments ensured that the position of the interface was the same for all experiments.

### 3.4.1. Characterisation of the Aqueous Phase

The characterisation of the aqueous phase was achieved by carrying out two sets of experiments under comparable conditions except that the stirring speed in the aqueous phase was varied (70 – 170 rpm). The first set of experiments involved the transfer of Co(II) into the organic phase by reaction with Cyanex® 272, and the second set involved the transfer of methyl violet into the organic phase by dissolution (Figure 3.11).

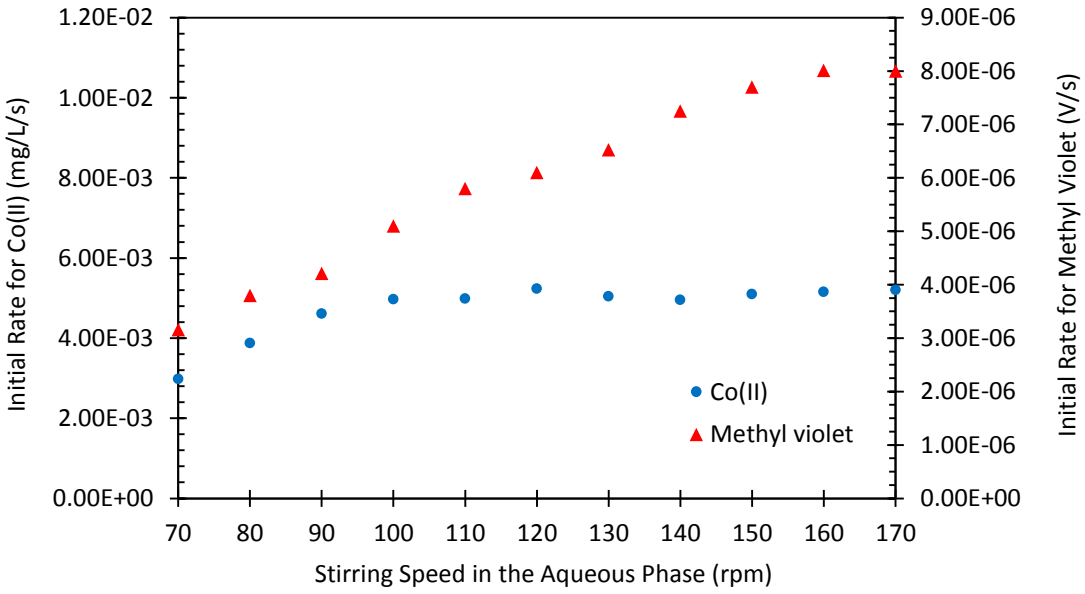


Figure 3.11 Effect of stirring speed in the aqueous phase on the initial mass transfer rate of Co(II) and methyl violet into the organic phase

The data shows that increases in the stirring speed in the aqueous phase from 70 to 100 rpm caused approximately linear increases in the initial mass transfer rate of Co(II) transfer from $3.00 \times 10^{-3}$ to $5.00 \times 10^{-3}$ mg/L/s. Further increases in the stirring speed to 170 rpm, however, had a negligible effect on the initial mass transfer rate in this system. On the other hand, increases in the stirring speed in the aqueous phase from 70 to 160 rpm caused an approximately linear increase in the initial mass transfer rate of methyl violet transfer into the organic phase.

The plateau in the initial mass transfer rate for the reactive mass transfer system is indicative of a shift in the rate controlling process from diffusion-controlled to kinetic-controlled. For the extraction of Co(II) with Cyanex® 272 in the MLC used in the present study, the shift appears to occur when the stirrer speed in the aqueous phase is increased to approximately 100 rpm.

This conclusion is supported by the data for the non-reactive mass transfer system. Under comparable conditions to the experiments with the reactive mass transfer system, increases in the stirring speed well beyond 100 rpm caused linear increases in the initial mass transfer rate for the dissolution of methyl violet into the organic phase. This provides evidence that the plateau in the initial mass transfer rate for the reactive mass transfer system is owing to the speed of the chemical reaction rather than other factors that could imitate a plateau in the initial mass transfer rate such as unfavourable hydrodynamics within the apparatus (Nitsch & Kruis 1978), loss of agitator efficiency, or Marangoni effects and side-reactions (Danesi, Chiarizia & Coleman 1980). These two sets of data suggest that the MLC has correctly identified the operating conditions required to cause the mass transfer process in the reactive mass transfer system to be controlled by the speed of the chemical reaction. Therefore, to allow good observation of the diffusion region in the aqueous phase, a stirring speed of 80 rpm was selected for experiments that require diffusion-controlled conditions in the aqueous phase. On the other hand, a stirring speed of 120 rpm was selected for experiments that require kinetic-controlled conditions in the aqueous phase.

The plateau in the initial rate for the transfer of methyl violet at approximately 160 rpm may be attributed to reaching the hydrodynamic limit of the MLC used in the present study.

### 3.4.2. Characterisation of the Organic Phase

The characterisation of the organic phase was achieved by carrying out two sets of experiments under comparable conditions except that the stirring speed in the organic phase was varied (70 – 170 rpm). The first set of experiments involved the transfer of Co(II) into the organic phase by reaction with Cyanex® 272, and the second set involved the transfer of methyl violet into the organic phase by dissolution (Figure 3.12).

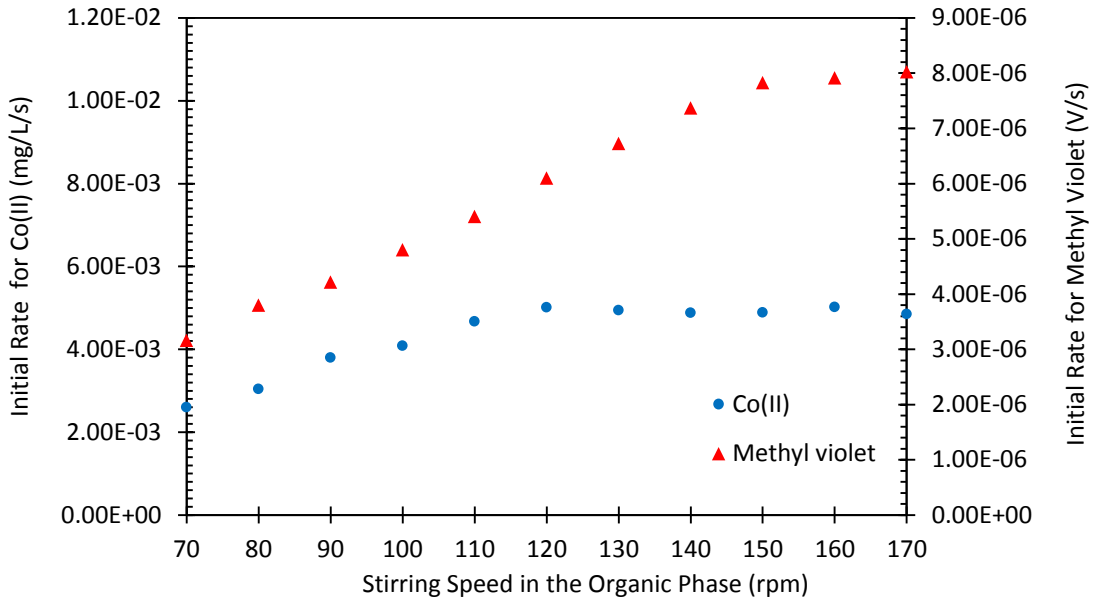


Figure 3.12 Effect of stirring speed in the organic phase on the initial mass transfer rate of Co(II) and methyl violet into the organic phase

The data show that increases in the stirring speed in the organic phase from 70 to 120 rpm caused approximately linear increases in the initial mass transfer rate of Co(II) transfer from $2.50 \times 10^{-3}$ to $5.00 \times 10^{-3}$ mg/L/s. Further increases in the stirring speed to 170 rpm, however, had a negligible effect on the initial mass transfer rate in this system. On the other hand, increases in the stirring speed in the aqueous phase from 70 to 160 rpm caused an approximately linear increase in the initial mass transfer rate of methyl violet transfer into the organic phase.

The plateau in the initial mass transfer rate for the reactive mass transfer system is indicative of a shift in the rate controlling process from diffusion-controlled to kinetic-controlled. For the extraction of Co(II) with Cyanex® 272 in the MLC used in the present study, the shift appears to occur when the stirrer speed in the organic phase is increased to approximately 120 rpm.

Therefore, to allow good observation of the diffusion region in the organic phase, a stirring speed of 80 rpm was selected for experiments that require diffusion-controlled

conditions in the organic phase. On the other hand, a stirring speed of 170 rpm was selected for experiments that require kinetic-controlled conditions in the organic phase.

The differences between these results and those from the characterisation of the aqueous phase can be attributed to the greater viscosity of the organic phase. The initial mass transfer rate at the lowest stirring speed that was investigated (70 rpm) is less for the characterisation of the organic phase (~$2.50 \times 10^{-3}$ mg/L/s) than that for the aqueous phase (~$3.00 \times 10^{-3}$ mg/L/s). In addition, the data indicate that the stirring speed required to shift from diffusion-controlled to kinetic-controlled in the organic phase (120 rpm) is greater than that required to shift the rate controlling process in the aqueous phase (100 rpm). It is evident that a greater stirring speed is required to obtain the same intensity of mixing in the organic phase because its viscosity is greater than that of the aqueous phase.

## 3.5. DESIGN AND CONSTRUCTION OF THE DROPLET COLUMN EXPERIMENTAL SET-UP

### 3.5.1. Design Philosophy

A major requirement of the droplet column used in the present study was the facility to apply a uniform electrostatic field to aqueous droplets in a continuous organic phase and thus enable investigation of droplet dispersion and droplet agitation. To allow a detailed investigation, the experimental set-up should incorporate an imaging technique that allows observation of the behaviour of droplets in an electrostatic field, as well as measurement of the droplet size and the magnitude and direction of droplet velocity.

To provide a fair comparison between various electrostatic field conditions, it was essential that the aqueous droplets were of uniform size prior to entering the electrostatic field.

The droplet column should incorporate improvements to the droplet column technique to allow accurate measurement of mass transfer between aqueous droplets and a continuous organic phase. This includes a technique to minimise additional mass transfer occurring in the pool of collected droplets at bottom of the column.

The materials of construction should (1) be chemically resistant to the aqueous and organic phases used in this work, (2) allow visual observation of the behaviour of droplets dispersed in the continuous phase, and (3) provide a leak-proof seal when all components of the droplet column are assembled.

### 3.5.2. Droplet Column Body

The droplet column was required to allow accurate measurement of mass transfer from aqueous droplets passing through a continuous organic phase. This was achieved partly by ensuring that the shape of the droplet column body facilitated the removal of the aqueous droplets after passing through the continuous organic phase. The droplet column body is constructed from Pyrex® glass as this is chemically resistant to the aqueous and organic phases that are used in the present study, and allows clear visual observation of dispersed droplets in the continuous phase.

A diagram of the droplet column body is shown in Figure 3.13, and all dimensions are shown in Appendix B1. The droplet column body was constructed from a single glass cylinder that was formed into several different sections. A cylindrical section at the top of the column (a) is formed into a rectangular section (c) by means of a transition section (b). The rectangular section allows electrodes to rest against the walls of the column. The rectangular section is formed into a tapered section (e) by means of another transition section (d), and a ground glass cone (CNB5) (f) is attached to the bottom of the tapered section. The transition and tapering sections near the bottom of the column assist aqueous droplets that adhere to the walls to coalesce and move downwards owing to gravity. A leak-proof seal can be achieved by inserting the ground glass cone into the inlet of a standard laboratory syringe filter. The volume of the droplet column body is approximately 200 mL.

The droplet column body was silinated to create a highly hydrophobic layer on the glass surface and thus minimise the adherence of aqueous droplets onto the glass. The droplet column body was cleaned with ethanol and then placed in an oven at 200 °C to remove any adsorbed water. The port at the bottom of the column was sealed with PTFE tape, and the column was filled with a solution of dichloromethylsilane (2 % v/v) in toluene and left in an oven overnight at 80 °C.

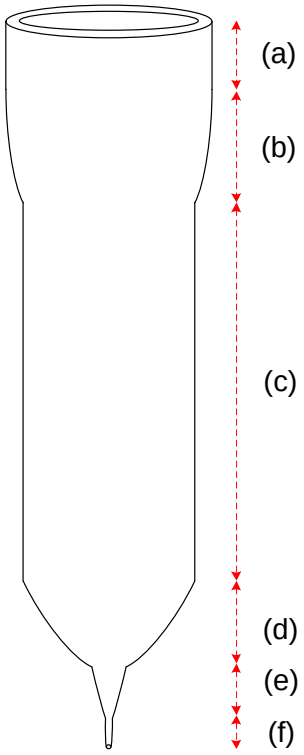


Figure 3.13 Design of the droplet column body

### 3.5.3. Parallel-Plate Electrodes and Droplet Delivery Technique

The droplet column was required to subject droplets of a uniform initial size to a uniform electrostatic field. These requirements were achieved by releasing droplets from a shielded flat-tipped needle within a region of low field strength, and generating an electrostatic field between two parallel-plate electrodes.

Two sets of electrodes were constructed to allow experiments to be carried out with either insulated or uninsulated electrodes. Each set consisted of two identical parallel-plate electrodes that were cut from 3-mm thick stainless steel, and one set was coated with ethylene tetrafluoroethylene (ETFE). This insulation material was used because it (1) has a relatively high dielectric strength (7.88 x $10^7$ V/m), (2) is resistant to the aqueous and organic phases used in the present study, and (3) is cheaper than the Parylene coating that was required for the wire mesh electrodes used in the MLC that were described in Chapter 3.2.4. The ETFE coating thickness was specified as approximately 300 μm, but it was not perfectly uniform owing to the nature of the coating process, and the minimum thickness in any area was specified as 250 μm (Armourcote Hi-Tech Industrial Coatings Pty Ltd). A photograph of a parallel-plate electrode and a diagram showing all of its dimensions is shown in Appendix B2.

A uniform electrostatic field strength was achieved by maintaining a constant spacing between the electrodes. The position of the electrodes was maintained by inserting polypropylene bolts (8 mm ∅, Plastic Fabricators WA) through two holes near the top of both electrodes, and attaching a clamp to the bolts. Connection of the electrodes to high-voltage power supplies was facilitated by soldering Tefzel®-coated stainless steel wire (M22759/16 AWG22, Avial Australia) to a 3-mm hole near the top of both electrodes, and connecting the Tefzel®-coated wire to the power supply.

A uniform initial droplet size was achieved by slowly releasing droplets from a flat-tipped stainless steel needle (35 mm length, 0.6 mm ∅) that was positioned between the electrodes in a region with a low electrostatic field strength and surrounded by a metal cylinder, as shown in Figure 3.14. Tefzel®-coated stainless steel wire (M22759/16 AWG22, Avial Australia) was soldered onto both the stainless steel needle and the metal cylinder, and the wires were connected to earth. This arrangement effectively shielded the needle and thus prevented droplets being ripped off the needle by induced charge from the electrostatic field between the parallel-plate electrodes. Droplets were only substantially influenced by the electrostatic field when they fell through the region of high electrostatic field strength. The aqueous droplets were transferred into the droplet column using a cartridge peristaltic pump (EW-07519-20, Masterflex®) with Norprene® tubing (6404-13, Masterflex®) that was adhered to the needle using super glue (Loctite). The needle and flexible Norprene® tubing was encased in a rigid plastic tube (150 mm length, 8 mm ∅), which was positioned between the two parallel-plate electrodes. The rigid plastic tube was clamped, and the position of the feed needle was controlled by adjusting the height of the clamp.

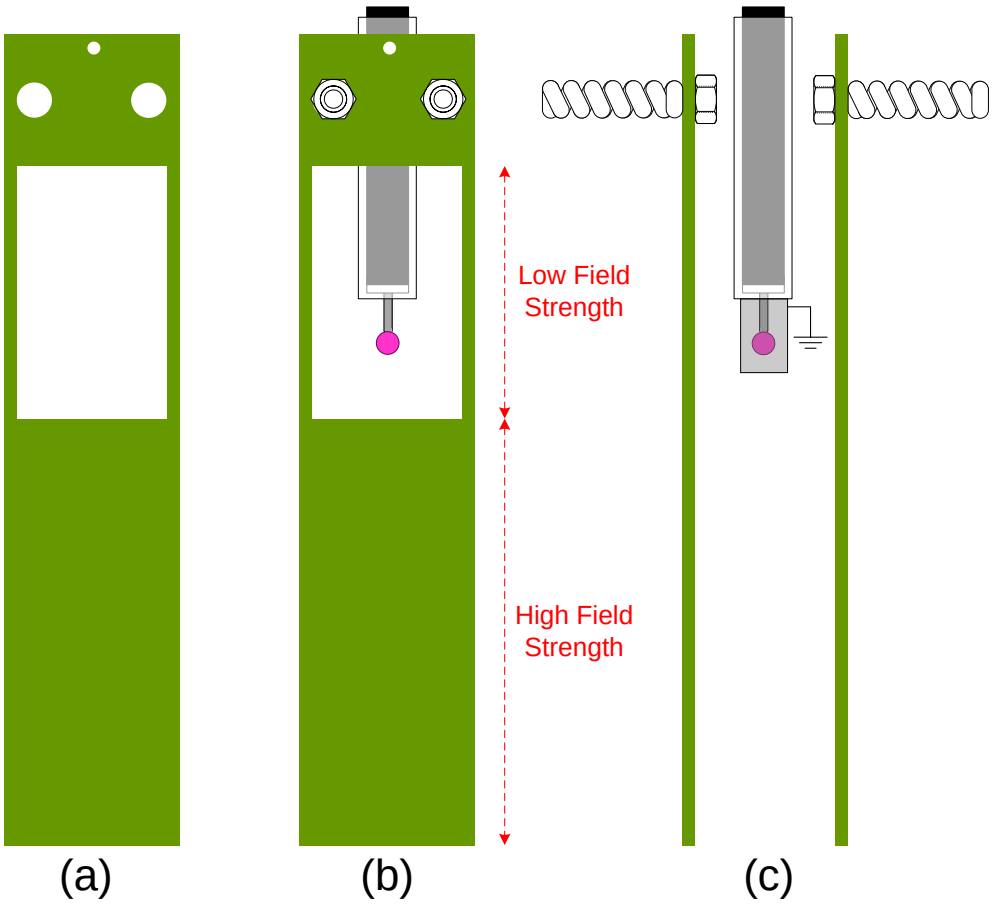


Figure 3.14 Diagrams of (a) one parallel-plate electrode, (b) the arrangement of the parallel-plate electrodes and the droplet delivery needle from the front view, and (c) the arrangement of the parallel-plate electrodes and the droplet delivery needle with earthed metal cylinder from the side view

### 3.5.4. Imaging Equipment

The droplet column was required to provide a facility to observe the behaviour of droplets in the presence of electrostatic fields, as well as to allow measurement of droplet size and the magnitude and direction of droplet velocity. All of these requirements were achieved by incorporating an Oxford Lasers VisiSizer D30V imaging system (IMG0021) into the experimental set-up. This overcame difficulties associated with less precise imaging techniques, and allowed more accurate measurements. For example, this imaging technique prevented the need to add coloured dye, and therefore change the physical properties of solutions, to facilitate observation of droplet behaviour.

Essentially, the imaging system involves using a laser to provide backlighting illumination and a high-speed camera to captures images of droplet behaviour. In the experimental set-up in the present study, the laser and camera were placed on opposite sides of the droplet column. The imaging system uses the Particle/Droplet Image

Analysis (PDIA) technique to measure droplet size and velocity. Each pixel within the field of view of the camera is assigned a 'grey level' value from 0 (black) to 255 (white), and the system analyses the shadow of each droplet to determine the droplet size. The system measures the change in position of droplets between two consecutive images to determine the direction and magnitude of droplet velocity. A more detailed explanation of the methods used by the imaging technique is described in Appendix B3 and B4.

The major components of this system are a firefly pulsed diode laser (FF0500, class IV laser) with RL Diffuser, which provides pulses of infrared laser light; a laser control module, which was used to set the operating variables of the laser and to operate the laser; a high-speed camera (HScam-MC2-500), which has an operating frequency of up to 500 frames per second at 512 x 512 resolution; and an Oxford Lasers PC. The camera was fitted with the Oxford Lasers standard Lens Option 4, and was also equipped with a splash guard to protect the lens. Two specialised computer software packages were supplied with the imaging system: (1) Photron FastCam Viewer, which was used to set the operating variables of the camera, to operate the camera, and to replay recorded images at a reduced frame rate, and (2) VisiSize (v. 6.206), which was used to measure droplet sizes and droplet velocity from a series of recorded images.

### 3.5.5. Sampling and Analytical Technique

The droplet column was required to allow accurate measurement of mass transfer, which included a technique to minimise additional mass transfer occurring in the pool of droplets collected at the bottom of the column. One method that has been previously described, which is to collect droplets in a funnel and remove them using a syringe (Gneist & Bart 2003), cannot be used in the present study given that the entire experimental set-up had to be enclosed to allow safe operation of a class IV laser.

In the present study, accurate measurement of mass transfer was achieved by separating the aqueous phase from the organic phase at the bottom of the column using a 12-port SPE vacuum manifold system (210351, Grace Davison Discovery Sciences) that was fitted with a PES syringe filter (0.45 μm pore size, 30 mm ∅, 32816-84, Cole Parmer) on one of the ports. The droplet column body was positioned directly above the syringe filter to allow the ground glass cone (CNB5) on the bottom of the droplet column body to be inserted into a syringe filter and thus, provide a leak-proof seal. Phase separation was achieved by allowing a small volume of aqueous droplets to coalesce on top of the inlet to the syringe filter, and intermittently turning on the suction to the vacuum

manifold. The hydrophilic syringe filter only allows the aqueous phase to pass through and thus, facilitated separation of the phases. The aqueous phase could then be collected after passing through a needle (PTFE) that was attached to the corresponding port within the vacuum manifold.

Although some additional mass transfer would occur at the interface between the pool of raffinate aqueous phase and the continuous organic phase, it was assumed that this mass transfer is negligible compared to that which occurs during the decent of the aqueous droplets through the continuous organic phase.

The concentration of Co(II) in the aqueous phase raffinate was measured by transferring the Co(II) into a fresh organic phase and measuring the absorbance of the organic phase with a UV-VIS spectrophotometer. Firstly, 10 mL of the aqueous phase raffinate and an appropriate volume of fresh organic phase were transferred into a 250-mL beaker. The volume of fresh organic phase, and therefore the A:O phase ratio, was chosen such that the final concentration of Co(II) in the loaded organic phase was less than 100 mg/L, which had been previously found to be compliant with the Beer-Lambert law (Figure 3.10). The phases were mixed vigorously (~500 rpm) using a magnetic stirrer while NaOH (3 M) was added dropwise to increase the pH and thus promote the mass transfer of Co(II) ions into the organic phase. The phases were stirred for at least 5 minutes to allow equilibrium to be established, after which time the stirring was stopped and the phases were allowed to disengage. Sufficient NaOH was added to attain an equilibrium pH of approximately 6.5, which had been determined to be sufficient for 100% extraction of Co(II) into the organic phase. The final pH of the aqueous phase was measured. The phases were then heated (~50 °C) to facilitate removal of entrainment.

The absorbance of the loaded organic phase was then measured using a UV-VIS spectrophotometer (DMS 70, Varian), and the concentration of Co(II) in the aqueous phase raffinate was calculated using the phase ratio.

### 3.5.6. Droplet Column Supports

The experimental set-up was required to provide structural support for the droplet column body and to facilitate alignment of the laser and camera with the droplet column. This was achieved by fixing the position of the droplet column body, mounting the laser and camera onto separate laboratory support jacks, and placing all of this equipment onto a laboratory optical bench.

The position of the droplet column body was fixed by clamping the column to a steel bar (25 mm ∅, 720 mm length) that had been welded onto an iron support plate (400 mm length x 400 mm width x 15 mm height). The height of the vacuum manifold was adjusted by placing it onto a laboratory support jack (plate size 24 cm x 24 cm, Sigma-Aldrich) that was positioned under the droplet column. A layer of rubber was placed under the support plate to prevent scratching of the laboratory optical bench (1400 mm length x 450 mm width x 25 mm height, UltraLight Series, Thorlabs) and a layer of cork was placed under the laboratory support jack to provide additional electrical insulation.

The laser and camera were mounted onto aluminium railings (500 mm length x 50 mm width x 50 mm height) that were supplied with the imaging equipment. The railings were secured onto separate laboratory support jacks (plate size 12" x 12", DKSH Australia) by drilling an 8-mm hole into the railing and the upper plate of the laboratory support jacks and fastening with stainless steel bolts.

Photographs of the droplet column supports are shown in Appendix B5.

### 3.5.7. Auxiliary Equipment

In addition to the major components of the droplet column, the complete experimental set-up included other auxiliary equipment.

A peristaltic pump (7554-20, Cole Parmer) with a manual pump controller (7566-14, Cole Parmer) and Viton® tubing (3 mm ID x 6 mm ID, 96412-16, Masterflex®) was used to transfer the organic phase into the droplet column. A cartridge peristaltic pump (EW-07519-20, Masterflex®) with an eight-roller pump head and Viton® tubing (1 mm ID x 4 mm OD, 96412-13, Masterflex®) was used to release aqueous droplets through the feed needle.

The experimental set-up was enclosed within an aluminium box (500 mm depth x 800 mm height x 1500 mm length) to ensure that the emissions from the class IV laser were not able to traverse the room. The front side of the box is fitted with hinges so that the box can be opened to set up the equipment inside for an experiment, but it must be closed during an experimental run to prevent laser emission. The inside of the box was spray painted matte black to ensure that the laser emission was not reflected. Two holes (60 mm ∅) were cut in the upper back corners of the aluminium box to allow electrical wires and tubing to be put through from outside, and the holes were then covered to

prevent laser emissions. As an additional safety measure, an earthed wire was connected to a handle on the box to prevent the box from acquiring electrical charge.

An electrostatic field was generated within the droplet column by connecting insulated high-voltage cables from a high-voltage power supply to one or both of the parallel-plate electrodes. The DC and AC power supplies used in this work with the droplet column were the same as that used in the MLC in the present study (Chapter 3.2.7). In the case of a DC or a PDC field, a high-voltage cable was connected to one electrode, and the other electrode was connected to earth. The polarity of the charged electrode was set by selecting either positive or negative on the DC power supply. In the case of an AC field, high-voltage cables were connected to both parallel-plate electrodes.

The droplet column experimental set-up is illustrated in Figure 3.15, and photographs of the complete experimental set-up are shown in Appendix B6. The aqueous phase is shown in pink to represent the Co(II) solution that was used in droplet column experiments.

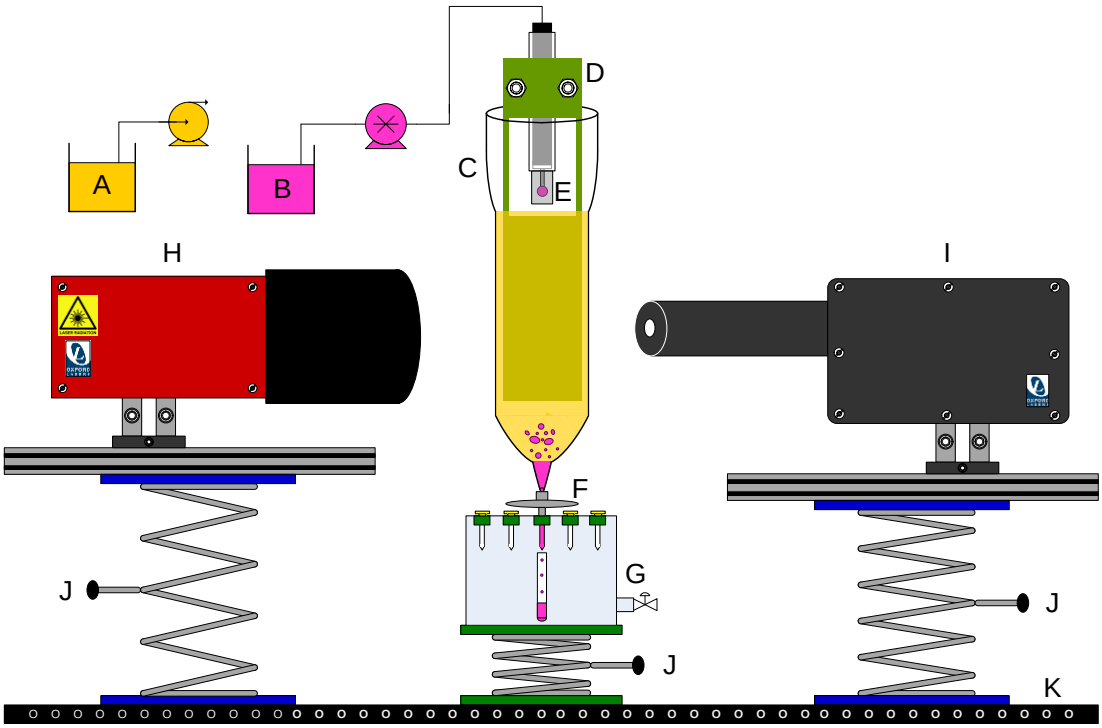


Figure 3.15 Schematic diagram of droplet column experimental set-up (A – organic phase reservoir, B – aqueous phase reservoir, C – droplet column, D – parallel-plate electrodes, E – feed needle, F – syringe filter, G – vacuum manifold, H – laser with diffuser, I – high-speed camera, J – laboratory support jacks, K – laboratory optical bench)

## 3.6. COMMISSIONING OF THE DROPLET COLUMN

The droplet column as well as all auxiliary equipment were commissioned by simulating experimental conditions to ensure that the complete experimental setup operated as required. Given that this apparatus was constructed in this study, it was necessary to develop methods of operating the droplet column that would allow experiments to be carried out in a way that achieved the objectives of the present study.

### 3.6.1. Development of a Procedure for Droplet Column Experiments

During the commissioning of the droplet column it was found that separate sets of experiments had to be carried out to investigate the effect of electrostatic fields on (1) droplet dispersion (Chapter 5), (2) droplet agitation (Chapter 6), and (3) mass transfer (Chapter 7), but the following general procedure was developed and used for all droplet column experiments: The ground glass joint on the bottom of the droplet column was inserted into the female port of a PES syringe filter (0.45 μm pore size, 30 mm ∅, 32816-84, Cole Parmer). A small amount of distilled water was decanted into the bottom of the column and allowed to pass through the syringe filter to wet the filter. The two parallel-plate electrodes were then placed inside the droplet column and separate clamps were used to fix the position of the droplet column, the two parallel-plate electrodes, and the feed needle. The vacuum manifold was assembled with a sample vial placed under a needle within the manifold to collect aqueous raffinate solution.

The assembled vacuum manifold was placed on a laboratory support jack and was elevated so that the male port of the syringe filter was inserted into the port on the vacuum manifold above the sample vial. The organic phase was then slowly transferred into the droplet column using a peristaltic pump (7554-20, Cole Parmer) with a manual pump controller (7566-14, Cole Parmer). Sufficient organic phase was transferred such that the level of the organic phase was within the region of low electrostatic field strength between the electrodes. This ensured that an aqueous droplet would be completely submerged within the organic phase prior to being substantially influenced by the electrostatic field. For experiments to investigate the influence of electrostatic fields, an electrostatic field was generated between the electrodes by turning on the high-voltage power supply and setting the desired applied voltage and, in the case of PDC or AC fields, the applied frequency.

An experiment was commenced by releasing droplets of the aqueous phase (0.50 mL/min) through a feed needle at the top of the column using a peristaltic cartridge pump (EW-07519-20, Masterflex®). The valve for the vacuum supply to the vacuum manifold, which was external from the enclosed aluminium box, was periodically opened to create a vacuum within the manifold and thus transfer the aqueous raffinate, which had coalesced at the bottom of the column, into the sample vial.

Experiments to investigate droplet dispersion and droplet agitation were carried out using the imaging equipment described in Chapter 3.6.2 and 3.6.3. The only difference between the procedure for these sets of experiments was that the laser and high-speed camera were focused lower down the droplet column to investigate droplet agitation. The aqueous raffinate from these experiments was discarded.

In the case of experiments to measure mass transfer, approximately 20 mL of aqueous raffinate was collected to provide a representative sample for analysis of the Co(II) extraction, which required significantly longer experimental run times. The imaging equipment was not required for these experiments.

At the end of an experimental run, all equipment was turned off, and the column was disengaged from the vacuum manifold by lowering the laboratory support jack under the manifold. The organic phase was drained from the column and the column was detached from its clamp and cleaned with methylated spirits, distilled water and acetone. The electrodes remained clamped to maintain constant electrode spacing between experiments, and were also cleaned prior to commencing the next experiment.

### 3.6.2. Commissioning of the Imaging Equipment

Commissioning of the imaging equipment involved firstly becoming familiar with the general use of the equipment, and then developing a procedure to use the equipment for the purposes of the present study. This procedure consisted of capturing images of droplet behaviour using the Fastcam software, and then analysing the captured images to generate size and velocity data using the VisiSize software.

The detailed procedure is as follows: To capture images of droplet behaviour, the laser and high-speed camera were turned on and the operating variables of both were set. The main operating variables of the laser are the pulse duration and pulse frequency, which together determine the intensity of background illumination. These operating variables were set by using a multi-directional dongle to scroll through and adjust values on the electronic display of the laser controller. The main operating variables of the

high-speed camera are the frame rate, which determines the number of images captured per second, and the lens magnification, which determines the size of the field of view. The camera frame rate was set on the Fastcam software, and the lens magnification was set by removing the splash guard covering the lens and manually adjusting the zoom dial. The range of values for the main operating variables and the values that were found to be most suitable, and were therefore used in the present study, are summarised in Table 3.1.

Table 3.1 Settings for the main operating variables of the laser and high-speed camera

| Setting | Minimum | Maximum | Used in this Study |
|---|---|---|---|
| Laser Pulse Duration (μs) | 0.02 | 100 | 0.35 |
| Laser Pulse Separation (μs) | 0.01 | 9999.99 | 40 |
| Camera Frame Rate (fps) | 50 | 500 | 500 |
| Camera Lens Magnification | 1.0 | 7.0 | 2.0 |
| Camera Field of View (μm) | 2982 x 2220 | 20956 x 15596 | 10460 x 7784 |

Droplets were released into the column and, if necessary, the position of the laser and camera were adjusted so that the background illumination was uniform and droplets were in the field of view of the camera. A series of images were captured by selecting 'record' on the Fastcam software. The maximum memory of the camera allowed 8188 consecutive frames to be recorded. Given the selected camera frame rate (500 fps), the maximum experimental run time was therefore limited to 16.38 s.

After a series of images were captured using Fastcam, analysis of the captured images to generate size and velocity data was carried out using VisiSize. Firstly, the VisiSize software was calibrated using the appropriate calibration file for the selected lens magnification (2.0), which was provided by the manufacturer of the imaging system. Next, the series of images that had been captured from an experimental run were uploaded. The VisiSize image analysis parameters, which includes the analysis, rejections, and velocity panels, were then set. The VisiSize image analysis parameters place constraints on the software when processing images and thus, influence the accuracy of the size and velocity data that are generated. It was therefore necessary to determine the optimum values for each of the parameters to extract meaningful and reliable data.

The parameters on the analysis panel are: the minimum and maximum diameter, the minimum and maximum velocity, and the number of separate fractions between the minimum and maximum values for both the diameter and velocity. A minimum droplet

diameter of 43 μm was used as this is the minimum droplet size that can be accurately measured with the lens magnification used in this study (2.0). The appropriate maximum droplet diameter and maximum droplet velocity were dependent on the experimental conditions and therefore had to be determined for each set of experimental conditions. These were determined by carrying out several preliminary experimental runs setting an excessively large maximum droplet size and droplet velocity initially and reviewing the recorded frames to check that the maximum droplet size and velocity were accurately reported. The maximum number of separate fractions between the minimum and maximum diameters and velocities that the software would permit (140) was used to provide the greatest possible resolution in the data.

The parameters on the rejections panel are: focus rejection, border rejection, repetition rejection, and shape rejection. Each of these parameters can be either enabled or disabled, except the shape rejection, which also requires input of a shape factor parameter. The depth of field correction allows sizing of droplets that are partly out of focus by analysing the shadow around a droplet. Border contact rejection allows droplets to be excluded from sizing because they are partly in contact with one or more of the edges of the field of view. Repetition rejection allows droplets to be excluded from sizing because they appear to be stationary between consecutive images. This prevents sizing of droplets that, for example, adhere to the glass surface of the droplet column. Shape rejection allows droplets to be excluded from sizing because they are highly non-spherical. The shape factor parameter is a measure of the minimum sphericity of a droplet that is required to allow sizing of a droplet, and ranges from 0 for completely non-spherical, to 1.0 for a perfect sphere. A relatively low shape factor parameter (0.4) was used in the present study because a significant number of droplets were elongated and oscillated and thus had a relatively low sphericity.

A description of the parameters on the velocity panel, and the most suitable values for the present study, are shown in Table 3.2. The VisiSize software calculates the magnitude and direction of droplet velocity by matching droplets between consecutive images. The parameters on the velocity panel are directly responsible for the amount of droplet mismatching, wherein two droplets appear to be the same droplet in consecutive images but actually are not. An example of droplet mismatching is shown in Appendix B7. Clearly, droplet mismatching generates inaccurate velocity data and therefore the settings of the parameters on the velocity panel were chosen to minimise the amount of droplet mismatching, although droplet mismatching could not be completely eliminated.

Table 3.2 Parameters on the VisiSize Velocity Panel

| Parameter | Description | Used in this Study |
|---|---|---|
| Mode of Velocity Measurement | VisiSize measures velocity by one of three methods: double exposed images, image pairs, or interframe | Image Pairs |
| Direction of Droplet Velocity | The general direction of the majority of droplets within the field of view | Down |
| Maximum Angle of Deviation | The maximum angle droplets could deviate from a directly vertical path between two consecutive images | No Limit |
| Maximum Search Radius | The maximum radius (in microns/pixel) that a droplet could travel between two consecutive images | 30 |
| Maximum Area Ratio | The maximum ratio of the area of a droplet in two consecutive images | 1.1 |
| Maximum Halo Area Ratio | The maximum ratio of the area of the halo surrounding a droplet in two consecutive images | 1.1 |
| Maximum Shape Factor Ratio | The maximum ratio of the shape factor of a droplet in two consecutive images | 1.5 |

After setting all of the VisiSize parameters, a run was carried out by selecting 'Start Run' on the VisiSize software. VisiSize then processed the series of images that had been uploaded and generated size and velocity data.

The software also reported the system performance parameters, which provide an indication of the reliability of the data that were generated. These parameters include: the percentage of droplets that are too far out of focus to be measured, the percentage of droplets whose shape is too non-spherical to be measured, the number of particles measured per frame, and the average intensity of the background illumination. The latter was defined as the most important parameter in the operation manual of the VisiSize software and had to be maintained within an acceptable range (140–200) to generate reliable data. For a new set of experimental conditions, a preliminary experimental run was always carried out to ensure that the system performance parameters were compliant with those specified in the operation manual. If necessary, fine adjustments were made to the position or operating variables of the laser and camera, and further preliminary experimental runs were carried out until the desired values of the system performance parameter were achieved, prior to commencing a set of experiments.

For each experimental run, the VisiSize software generated two data files that were compatible with Microsoft Excel: (1) VisiSize Analysis Report (TXT file), and (2) Individual Particle Data (VSP File). The former displayed the percentage of droplets in each of the 140 size fractions by volume and by number as well as a summary of the

system performance parameters. The latter displayed the diameter and velocity of each individual droplet that was measured as well as a unique combination of the frame and particle number, which allowed droplets to be identified when reviewing recorded images. Examples of a VisiSize Analysis Report and an Individual Particle Data file are shown in Appendices B8 and B9, respectively.

### 3.6.3. Determination of Limitations of the Droplet Column Experimental Set-Up

Commissioning of the droplet column experimental set-up revealed that the experimental conditions that could be used to generate meaningful and reproducible data were restricted by limitations of the imaging equipment as well as properties of the electrostatic fields.

One limitation was the range of applied voltage that could be investigated. The minimum applied voltage used in experiments was that required to induce sufficient droplet dispersion to generate a population of daughter droplets for analysis using the imaging technique. Increases in the applied voltage caused increases in the number of droplets that were generated, but this also led to decreases in the ability of the imaging equipment to distinguish between individual droplets. Many droplets were overlapping and therefore were not sized owing to shape rejection or were sized inaccurately. An example of an excessive number of droplets is shown in Appendix B10. This significantly reduced the number of droplets that were included in the sizing analysis. As a result of these limitations, the minimum and maximum applied voltages were chosen such that a minimum of 10 000 droplets were recorded and characterised for a given camera field of view.

Given that one aim of the present study was to compare the droplet dispersion behaviour induced by various types of electrostatic fields, sufficient electrostatic field strength was required to generate a droplet dispersion that could be analysed using the imaging technique. It was found that continual dispersion in the presence of DC and PDC fields could only be achieved using uninsulated electrodes, whereas continual dispersion in the presence of AC fields could be achieved using insulated electrodes. This is attributed to the insulation throttling off the electrostatic field in the case of DC and PDC fields and is consistent with the findings of Collard (2011) and Steffens (2011).

For almost all experiments with uninsulated electrodes, a 3-cm electrode spacing was required to prevent aqueous droplets simultaneously contacting both electrodes and

thus, arcing between the electrodes, whilst still generating a suitable droplet dispersion. The exception to this was in the case of negative PDC fields, which required significantly greater field strength. Given that the maximum applied voltage was limited by the capabilities of the high voltage DC power supply, increases in the electrostatic field strength could only be achieved by reducing the spacing between the charged and earthed electrodes. Therefore, investigation of the effect of negative PDC fields required that the electrode spacing was reduced to 2 cm.

Given the limited capability of the high voltage AC power supply used in the present study, a droplet dispersion that was suitable for analysis using the imaging technique could only be generated using an electrode spacing of 1 cm.

The experimental conditions that were used to investigate the effect of electrostatic fields on droplet dispersion and agitation are summarised in Table 3.3.

Table 3.3 Summary of the experimental conditions that were used to investigate the effect of electrostatic fields on droplet dispersion and droplet agitation

| **Type of Electrostatic Field** | **Electrode Insulation** | **Electrode Spacing (cm)** | **Range of Applied Voltage (kV/cm)** |
|---|---|---|---|
| Positive DC | Uninsulated | 3 | 4.00 – 4.37 |
| Negative DC | Uninsulated | 3 | -4.12 – -4.50 |
| Positive PDC | Uninsulated | 3 | 5.00 – 5.67 |
| Negative PDC | Uninsulated | 2 | -8.75 – -9.75 |
| AC | Insulated | 1 | 2.50 – 3.50 |

## 3.7. CHAPTER SUMMARY

To allow investigation of the effect of electrostatic fields on interfacial phenomena, a modified Lewis cell (MLC) was designed, constructed and commissioned. The MLC developed in the present study incorporates all of the improvements to the design and method of operation that have been reported. This includes a method to maintain the position of the interface, and a method to eliminate lag time between filling the cell with the phases and commencing an experiment. In addition, the MLC has the facility to apply an electrostatic field across the liquid-liquid interface without altering the hydrodynamics within the apparatus.

The MLC was characterised and it was found that the rate controlling process for the extraction of Co(II) with Cyanex® 272 shifts from diffusion-controlled to kinetic-controlled with a stirring speed in the aqueous phase of 100 rpm. This reactive mass transfer system also shifts from diffusion-controlled to kinetic-controlled with a stirring speed in the organic phase of 120 rpm.

To allow investigation of the effect of electrostatic fields on electrostatically induced dispersion and droplet agitation, a droplet column was designed, constructed and commissioned. This experimental set-up includes a high-speed imaging system that allows measurement of droplet size and the magnitude and direction of droplet velocity. It was found that continual dispersion in the presence of DC and PDC fields could only be achieved using bare metal electrodes, whereas continual dispersion in the presence of AC fields could also be achieved using insulated electrodes.

# Chapter 4

# STUDY ON THE EFFECT OF ELECTROSTATIC FIELDS ON INTERFACIAL PHENOMENA

## 4.1. INTRODUCTION

One of the major gaps in the knowledge on this research topic that was identified in the review of literature is the effect of electrostatic fields on interfacial phenomena (Chapter 2.3), particularly the transport of the species across the diffusion layers between immiscible liquids that are in contact with each other as is the case in solvent extraction. While it has been reported that several electrostatically induced interfacial and intra-facial phenomena such as (1) Marangoni-type turbulence, (2) movement of electric charge in the organic phase, (3) electromigration of species in the aqueous phase, and (4) orientation of species in the organic phase, supposedly influence the rate of transport of the dissolved species from one phase to another, available experimental details, both in terms of methodology and generated data are cursory, inconsistent and even contradictory. This chapter describes the present investigator's attempt to determine how electrostatic fields affect the transport and extraction of Co(II) species with Cyanex® 272 as extractant using a purpose-built modified Lewis cell (MLC).

## 4.2. MATERIALS AND METHODS

### 4.2.1. Reagents

The following reagents were used in the work that is described in this chapter: acetic acid (Analytical Reagent (AR), Chem-Supply), sodium hydroxide (AR, Chem-Supply), standard aqueous Co(II) solution (10,000 mg/L, Australian Chemical Reagents), cobalt sulphate heptahydrate (AR, Chem-Supply), sodium sulphate (AR, BDH), ShellSol® 2046 (Industrial Grade, Shell Chemicals), Cyanex® 272 (Industrial Grade, Cytec Australia), sulphuric acid (98%, Sigma Chemicals), methyl violet 6B (34054, BDH) and ethanol (AR, 100% denatured, Chem-Supply). All reagents were used as supplied.

### 4.2.2. Analytical Techniques

All pH measurements made were with a bench-top pH meter (Orion 3 Star, Thermo Electron Corporation) using a glass body electrode (LoT402-611-DPA-S7/40, Mettler-Toledo).

The measurement of the conductivity of aqueous phases was carried out using a pre-calibrated handheld conductivity meter (Aqua-CPA, TPS) with the k=10 conductivity sensor (122221, TPS). The measurement of the conductivity of organic phases was carried out using a pre-calibrated digital conductivity meter (model 1152, Emcee Electronics). The meters were calibrated and operated using methods supplied by the manufacturer, which are described in Appendix C1 and C2.

The measurement of the dielectric constant of aqueous and organic phases was carried out using a dielectric constant meter (Alpha TDR-5000, Zadow Electronics). The meter was calibrated and operated using the methods supplied by the manufacturer, which are described in Appendix C3.

The determination of the concentration of extracted Co(II) in the organic phase was carried out using a UV-VIS spectrophotometer (DMS 70, Varian). The spectrophotometer was calibrated prior to carrying out a mass transfer experiment by measuring the absorbance of a standard organic solution with a known concentration of extracted Co(II).

### 4.2.3. Preparation of Test Solutions

The aqueous phase consisted of Co(II) ions in an acetic acid/acetate buffer with a pH of 5.5. This was prepared by preparing two separate aqueous solutions: (1) a concentrated Co(II) solution, and (2) a buffer solution, and the two were mixed when an experiment was commenced by injecting 3 mL of concentrated Co(II) solution into the buffer solution. The concentrated Co(II) solution was prepared by dissolving cobalt sulphate heptahydrate in distilled water, transferring to a volumetric flask and filling to the mark with distilled water. The buffer solution was prepared by dissolving the required volume of acetic acid and mass of sodium hydroxide pellets in a volumetric flask with distilled water. Sodium sulphate (0.2 M) was added to the buffer solution to increase the ionic strength and, thus, the rate of phase separation, as well as to avoid third phase formation (Fu & Golding 1988). The solution was mixed vigorously to ensure that the neutralisation reaction went to completion. The solution was allowed to cool to room temperature, after which the pH was measured to ensure that it was 5.5.

The flask was then filled to the mark with distilled water. The calculations for the composition of the buffer solution and the concentrated Co(II) solution are shown in Appendices C4 and C5.

The appropriate concentration of Co(II) in the aqueous phase (300 mg/L) was determined by several considerations. Firstly, it was desirable to simulate the Co(II) concentration that is typical of that in the pregnant liquor streams (PLS) generated from nickel laterite pressure acid leach (PAL) operations. Secondly, injection of a concentrated Co(II) solution should allow visual observation of a pink colour in the bulk aqueous solution owing to formation of a Co(II)-acetate complex. Thirdly, the volume injected could not be too great to significantly change the position of the interface. Finally, a smaller volume of injection requires a stock solution with a greater concentration, but increases in the concentration of the stock solution leads to increases in the error of replicating the Co(II) concentration in the bulk aqueous phase owing to the use of a syringe.

The presence of acetate in the aqueous phase will not impede the extraction of Co(II) ions with Cyanex® 272 because the stability constant (log K) of the Co(II)-acetate complex with 0.1 M acetate (0.61) (Gu, Wasan & Li 1986) is significantly less than that of the Co(II)-Cyanex® 272 complex in sulphate media (7.6) (Sole & Hiskey 1992).

The organic phase (10% (v/v) Cyanex® 272) was prepared by transferring the required volume of Cyanex® 272 into a volumetric flask and filling to the mark with ShellSol® 2046.

The stripping solution was prepared by transferring the required volumes of sulphuric acid (24.5 g/L) and cobalt sulphate (20.5 g/L Co(II)) into a volumetric flask and filling to the mark with distilled water. The stripping solution was used to strip the loaded organic phase from experiments following the procedure described in Appendix C6.

### 4.2.4. Procedures for Investigating the Effect of Electrostatic Fields on Interfacial Phenomena

The aim of this work was to determine how electrostatic fields affect the transport and extraction of Co(II) species with Cyanex® 272. This was achieved by using a purpose-built MLC to investigate the effect of electrostatic fields on the (1) diffusion process in the organic phase, (2) diffusion process in the aqueous phase, and (3) chemical reaction at the interface. MLC experiments were carried out using the general procedure described in Chapter 3.3.3, and the appropriate stirring speeds that were used to study

each of these processes, which had been determined in the characterisation of the MLC described in Chapter 3.4, are summarised in Table 4.1.

Table 4.1 Summary of experimental conditions for investigating the effect of electrostatic fields on interfacial phenomena

| **Set of Experiments** | **Aqueous Stirring Speed (rpm)** | **Organic Stirring Speed (rpm)** |
|---|---|---|
| Effect of electrostatic fields on the diffusion process in the organic phase | 120 | 80 |
| Effect of electrostatic fields on the diffusion process in the aqueous phase | 80 | 170 |
| Effect of electrostatic fields on the chemical reaction | 120 | 170 |

To investigate the effect of electrostatic fields, one wire mesh electrode was connected to a high-voltage power supply, while the other electrode was earthed. Three different fields types were investigated: DC fields, in which the charged electrode had a static voltage; PDC fields, in which the charged electrode pulsed between zero and a set applied voltage at a frequency of 50 Hz; and AC fields, in which the charged electrode cycled between negative and positive polarity at a frequency of 50 Hz. A high voltage probe (HP-40, Tenma) was connected to the charged electrode and used with a multimeter to allow accurate measurement of the applied voltage. The desired voltage and, in the case of DC and PDC fields, the desired polarity, were selected when the high-voltage power supply was turned on.

Two ways of applying electrostatic fields were used: (1) application at the beginning of the experiment when the concentrated Co(II) solution was injected into the aqueous phase, and (2) application after a high concentration of extracted Co(II) species had accumulated in the organic or aqueous diffusion regions. In the case of the latter, an electrostatic field was only turned on after a constant mass transfer rate was achieved for a period of 1000 consecutive seconds. In all experiments, the applied voltage was only changed when the mass transfer rate had stabilised in the presence of a field for at least 1000 consecutive seconds.

### 4.2.5. Data Analysis

The effect of electrostatic fields on interfacial phenomena was investigated qualitatively by visual observations as well as quantitatively by comparing the mass transfer rate in the presence of various types of electrostatic fields with that in the absence of a field.

The data generated from MLC experiments were processed using the method developed in Chapter 3.3.4. In all experiments, the mass transfer rate was calculated from the slope of the plot of concentration against time for a period of 1000 consecutive seconds, but the time period chosen was dependent on the experimental conditions.

In experiments in the absence of a field, or where the field was on from the beginning of an experiment when the concentrated Co(II) solution was injected into the aqueous phase, the mass transfer rate was calculated from the slope of the line after a conveniently measurable concentration of Co(II) in the bulk of the organic phase was reached and the rate had stabilised. The rate varied at very low Co(II) concentrations owing to the delay required for the species to migrate into the bulk of the organic phase, and then through to the spectrophotometer.

In experiments where the field was turned on after a high concentration of Co(II) had accumulated in either the organic or aqueous diffusion regions, the time interval that was used to calculate the mass transfer rate in the presence of some given field conditions was 200 seconds after the field conditions were changed. This ensured that the mass transfer rate was a true indication of the effect of the new field conditions, rather than a temporary effect from changes in the field conditions.

## 4.3. RESULTS AND DISCUSSIONS

The main findings in this part of the study are: (1) DC and PDC fields enhanced the transport of the Cyanex® 272-extracted Co(II) species across the organic diffusion region by nearly 2.5 times owing to electrostatic attraction, (2) AC fields had no effect on the transport of these extracted species across the organic diffusion region, (3) electrostatic fields had no effect on the reaction of Co(II) and Cyanex® 272. Details follow.

### 4.3.1. Effect of Electrostatic Fields on the Diffusion Process in the Organic Phase

The effect of electrostatic fields on the diffusion process in the organic phase was investigated by applying electrostatic fields across the organic diffusion region under

various experimental conditions and observing how they affect the mass transfer of the extracted species across this region.

Two ways of applying electrostatic fields were used: (1) application after a high concentration of extracted Co(II) species had accumulated in the organic diffusion region, and (2) application at the beginning of the experiment so that no extracted Co(II) species had reached the organic diffusion region. In the first case, the concentration of the extracted Co(II) species in the organic diffusion region was substantially higher than that in the bulk and thus, a concentration gradient existed when the electrostatic field was applied. In the second case, the concentration of the extracted Co(II) species in both the organic diffusion region and the bulk of the organic phase was zero and, therefore, no concentration gradient existed when the electrostatic field was applied. In both cases, the stirring speed in the organic phase was only 80 rpm, allowing a sufficiently thick organic diffusion region for visual observation of the processes in the region, and providing a conveniently measureable rate of transport of the extracted species across it. The stirring speed in the aqueous phase was maintained at 120 rpm to render the aqueous diffusion region essentially non-existent. In effect, the rate of transport of the cobalt species from the aqueous to the organic phase may be attributed wholly to the rate of their transport across the organic diffusion region. A detailed discussion of the mechanics and characterisation of the modified Lewis cell used in the present study including the determination of these conditions is in Chapter 3.4.

The results show that both DC and PDC fields enhanced the diffusion of the extracted species across the organic diffusion region while AC had no effect. These are shown qualitatively in Figure 4.1. The effects were immediately observable. The application of either DC or PDC fields (1 kV) induced a rapid upward movement of the accumulated extracted Co(II) from the organic diffusion region into the bulk of the organic phase, resulting in a proportionate darkening of the blue colour of the organic bulk. Remarkably, the effect was the same whether the applied field was positive or negative.

When the electrostatic fields were applied from the beginning of the experiments when no Co(II) species had reached the organic diffusion region, no accumulation of extracted Co(II) in the region was observed rendering the region indistinguishable from the bulk. This indicated a much faster transport of the extracted species across the region than natural diffusion. Again, the results were the same with either DC or PDC applied fields. In contrast, the application of AC fields led to accumulation of extracted

species in the organic diffusion region, which is similar to that when no field was applied. These observations may be seen in Figure 4.2.

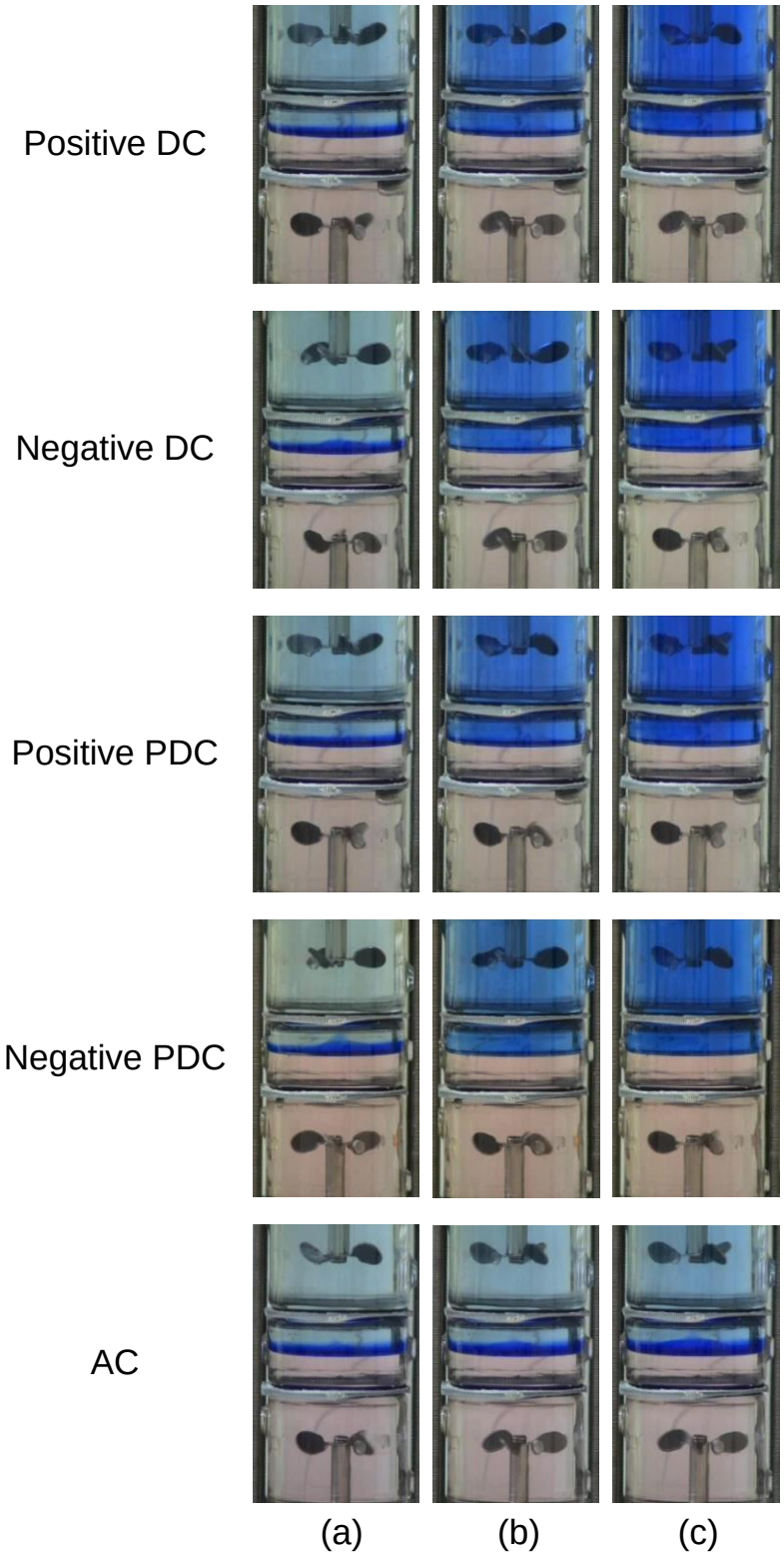


Figure 4.1 Photographs showing the effect of electrostatic fields (±1 kV) on the movement of extracted Co(II) in the organic phase from the diffusion region into the bulk at time intervals after the field was turned on: (a) 0 s, (b) 1200 s, and (c) 3600 s

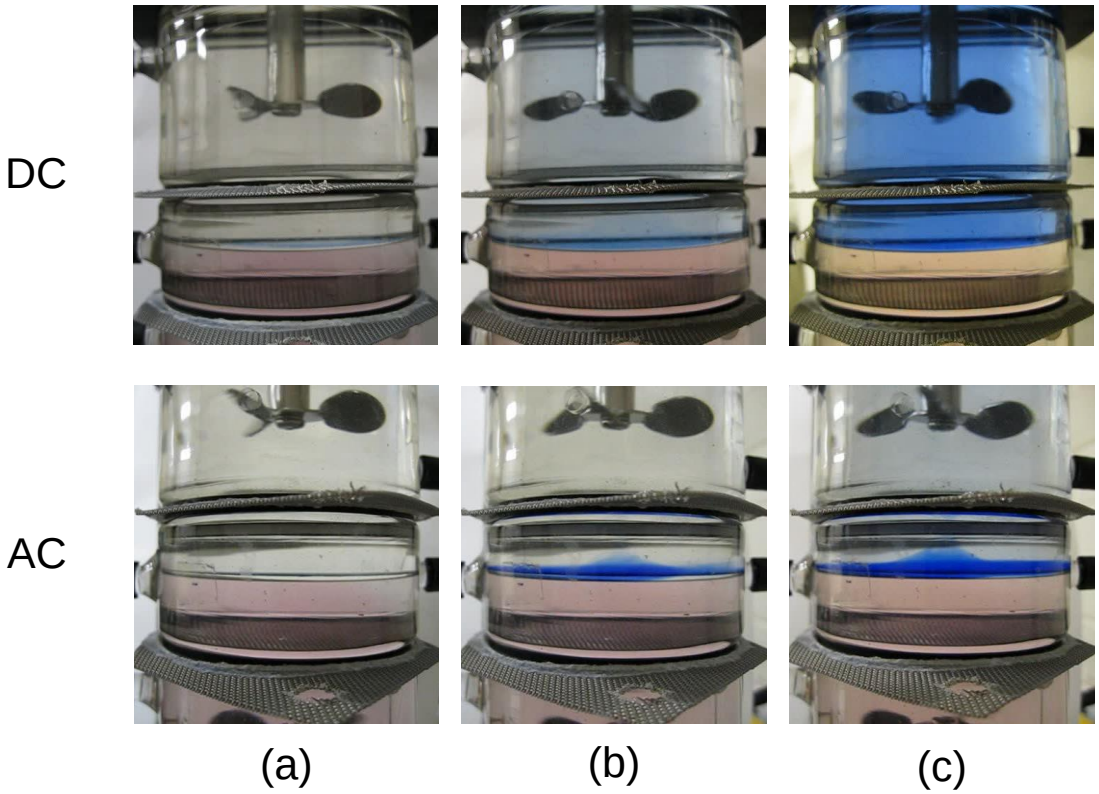


Figure 4.2 Effect of electrostatic fields when the electrostatic field (1 kV) was applied from the beginning of the experiment at time intervals after the field was turned on: (a) 0 s, (b) 1200 s, and (c) 3600 s

It was then thought that if the enhanced transport of the extracted species was indeed solely due to the applied fields, then the same phenomena should occur even if the bulk of the organic phase was not stirred at all. Thus, a set of experiments was carried out at comparable conditions to those of the first set of experiments such that a high concentration of extracted Co(II) species was first allowed to accumulate in the organic diffusion region before the electrostatic field was applied. The only difference was that the stirring of the organic phase was stopped before the field was applied. Under these conditions, the transport of extracted species across the organic diffusion region as well as in the bulk of the organic phase may be attributed solely to the effect of electrostatic fields and natural diffusion.

The results, summarised in Figure 4.3, are unmistakeable. The application of a 1-kV DC field resulted in a rapid upward dissipation of the accumulated extracted Co(II) species from the organic diffusion region. The dissipation appeared like rising blobs of the extracted species, which may be attributed to the non-uniformity of the electrostatic field owing to the structure of the wire mesh electrode. Within 60 s, the entire region between the interface and the upper electrode was homogenously coloured.

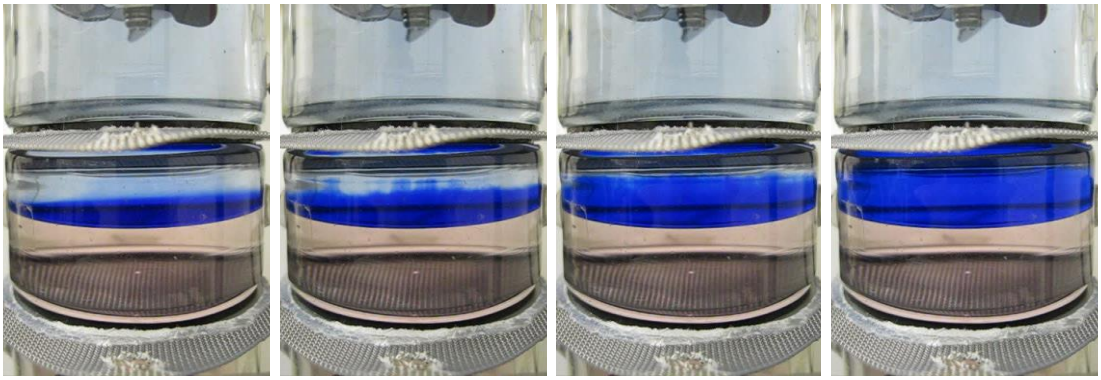


Figure 4.3 Photographs showing the effect of a positive 1-kV DC field on the movement of extracted Co(II) in the organic phase from the diffusion region in the absence of stirring after (a) 0 s, (b) 10 s, (c) 30 s, and (d) 60 s

This field-enhanced transport of the extracted species extended to the bulk of the organic phase as shown in Figure 4.4. The apparent congregation of the extracted species around the shaft of the stirrer indicated that electrostatic attraction was the driving force of this field-enhanced mass transport because the metal stirrer, which had to be connected to ground to allow the dissipation of extraneous charges, was acting as a supplementary ground electrode.

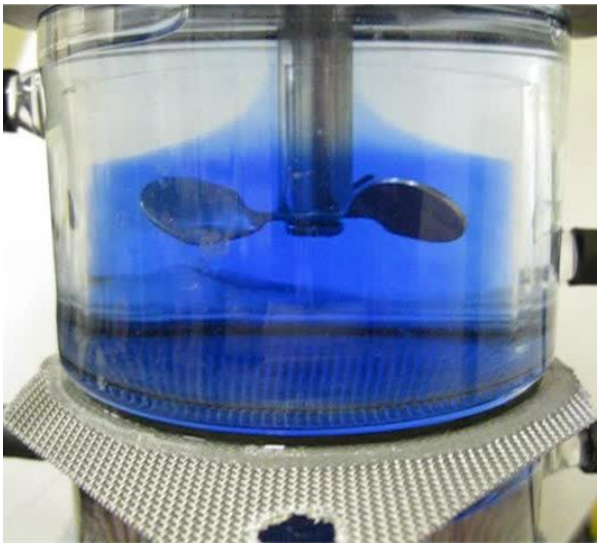

Figure 4.4 Photograph of the organic phase in the absence of stirring taken 1800 s after a 1-kV DC field was applied to the upper electrode

Measurements of the mass transfer confirmed these visual observations. Figure 4.5 shows the effects of applying 1-kV DC, PDC and AC fields on the change in the concentration of the extracted Co(II) in the bulk of the organic phase. In addition, representative plots for higher voltages and opposite polarities are also shown. In all

cases, the electrostatic fields were applied from the beginning of the experiments allowing for a direct comparison of the mass transfer rates. For comparison, a plot of the Co(II) concentration that was determined under comparable conditions except that no electrostatic field was applied is also shown. Clearly the results show that DC and PDC fields, either positive or negative, enhanced the mass transfer of Co(II) at comparable levels while AC field had no effect at all.

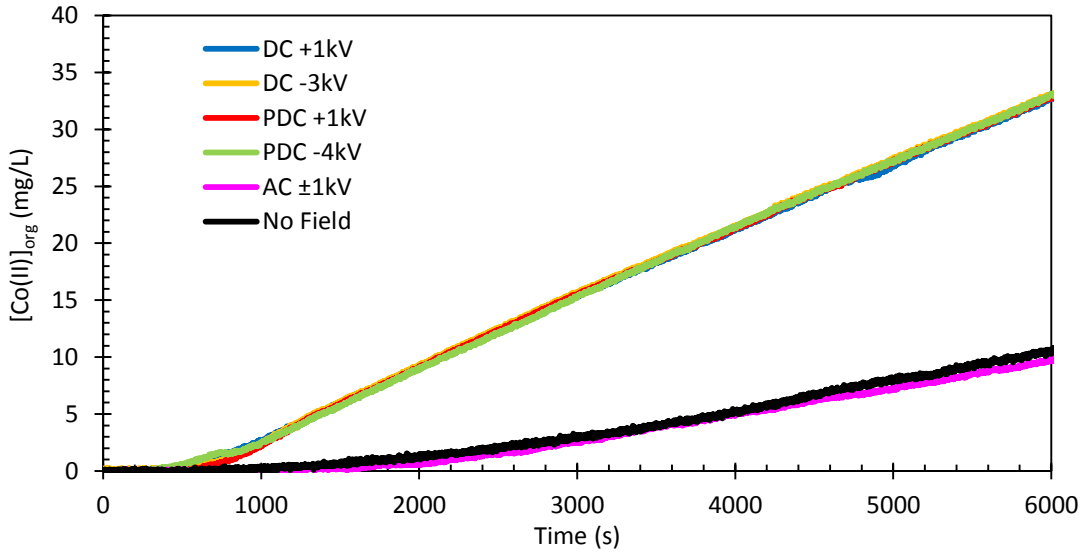


Figure 4.5 Plot of the change in concentration of extracted Co(II) in the organic phase over time when the electrostatic field was applied from the beginning of an experiment

The slopes of the curves for both DC and PDC fields were calculated at 1000-second intervals starting at 2000 s from the start of the experiments, when a conveniently measurable concentration of Co(II) in the bulk of the organic phase was reached. It showed that, for DC and PDC fields, either positive or negative, the slopes were identical within experimental error. For example, the slopes for positive DC and positive PDC were 5.83 x $10^{-3}$ and 5.90 x $10^{-3}$ respectively, remaining constant up to 6000 s and then started to decrease. In the case of a 1-kV DC field, for example, the slope at 7000 s had decreased to 5.47 x $10^{-3}$ and at 10 000 s, it had dropped to 4.98 x $10^{-3}$. This may be attributed to a significant depletion of the Co(II) in the aqueous phase. Mass balance showed that at 6000 s, the cobalt concentration in the aqueous phase had decreased by approximately 30 mg/L (~10% extraction) and at 10,000 s, it had decreased by 53 mg/L (~18% extraction).

In comparison, the slopes of the AC curve and that with no applied field were both 2.41 x $10^{-3}$, which remained constant even after 10,000 s. At this point, only 20 mg/L of the cobalt had been extracted into the organic phase, which equated to only 7% decrease in

the concentration of the Co(II) in the aqueous phase. Based on the data generated from the application of DC and PDC fields, this change in concentration was too small to affect the rate of mass transfer. The enhancement factor, calculated as the ratio of the slope of either the DC or PDC field to the slope of no applied field or with AC field, is approximately 2.5.

The application of higher voltages up to 4 kV, either negative or positive and either DC or PDC, had no further effect on the rate of mass transfer of the extracted cobalt species. Representative plots for higher voltages are also shown in Figure 4.5.

The application of higher AC fields up to 4 kV also had no effect on the rate of mass transfer of the extracted Co(II) species as shown in Figure 4.6. The slope of the plot of the cobalt concentration under these conditions is identical to that generated without an applied field, which means that the transport across the organic region of the extracted Co(II) species was solely by natural diffusion.

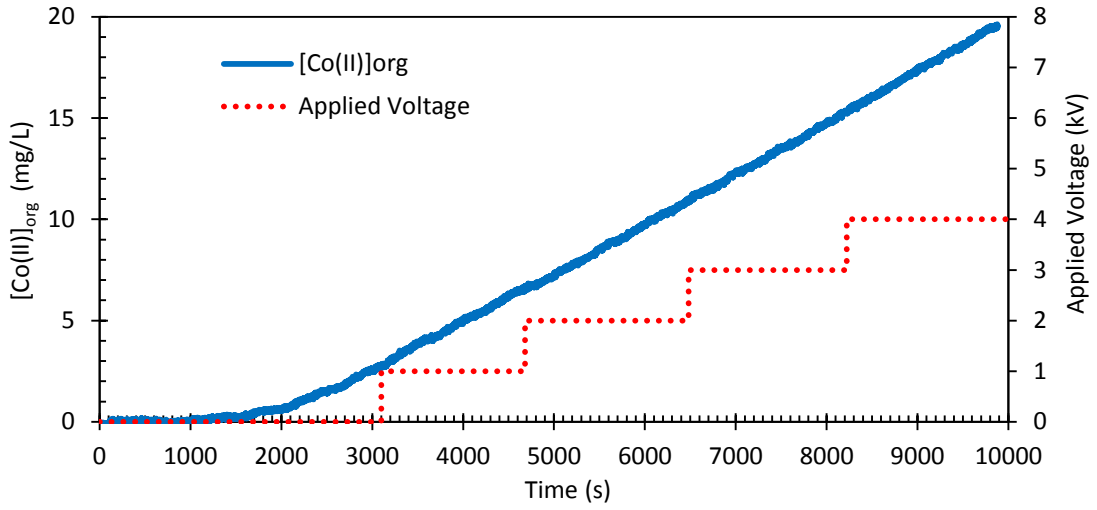


Figure 4.6 Plot of the concentration of the extracted Co(II) at various AC voltages over time when the electrostatic field was applied after extracted Co(II) species had accumulated in the organic diffusion region

The use of voltages lower than 1 kV was not attempted in this study as it has been established previously (Heckley 2002; Collard 2011; Steffens 2011) that no droplet dispersion can be achieved when such low voltages are used. Given that the ultimate goal of electrostatic solvent extraction (ESX) is to optimise both droplet dispersion and agitation, the use of less than 1 kV voltage was outside the scope of this study.

Given these experimental data and observations, it appeared likely that the field-enhanced mass transfer of the extracted Co(II) species across the organic diffusion region was owing to electrostatic attraction between the charged electrode and the

extracted species. Only DC or PDC fields caused enhanced mass transfer because the extracted species are polar (Figure 4.7) and the transport was unidirectional toward the charged electrode. It worked with either a positive or a negative charge because the extracted species can correspondingly orient themselves. It did not work with AC fields because the alternating direction of the field would correspond to an alternating direction of the migration of polar species, resulting in no net effect on the migration of the extracted species.

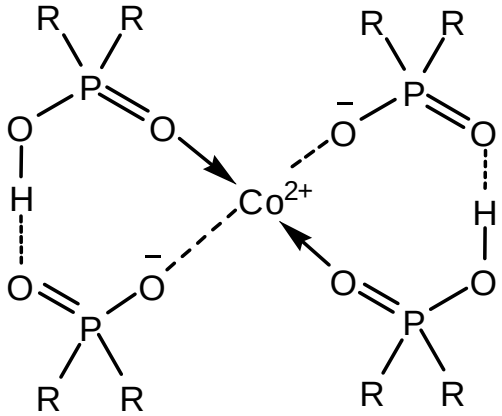


Figure 4.7 Diagram of the tetrahedral Co(II) complex with the dimerised form of Cyanex® 272, the extracted Co(II) species as indicated by the characteristic blue colour of the loaded organic phase

These data and observations indicated too that other interfacial phenomena that were suggested previously to be factors in enhancing mass transfer between two immiscible liquids under the influence of electrostatic fields were unlikely to be a significant factor in the transport of extracted Co(II) species across the organic diffusion region when using Cyanex® 272 as extractant. Favourable orientation of species in the organic phase (Hund & Lancelot 1986) could not have been a major factor because, if it was so, the enhancement of mass transfer could have only happened with either positive or negative DC or PDC fields but not both. Electromigration of species in the aqueous phase (Martin et al. 1983; Wildberger and Bart 2002) could not have been a major factor given that the increases in the mass transfer rate were clearly owing to enhanced migration of extracted Co(II) across the organic diffusion region and into the bulk of the organic phase. Turbulence induced by the movement of electric charges within the organic phase (Austin, Banczyk & Sawistowski 1971; Iyer & Sawistowski 1974; Glitzenstein, Tamir & Oren 1995) could not have been a major factor because AC fields had no effect on the mass transfer rate, which is in contrast to the expected increased movement of electric charges in the presence of AC fields owing to the continually changing direction of the field. Finally, Marangoni-type turbulence (Austin, Banczyk &

Sawistowski 1971; Iyer & Sawistowski 1974; Hund & Lancelot 1986; Kuipa & Hughes 1999) could not have been a major factor because AC fields had no effect on the mass transfer rate, which is in contrast to the expected local gradients in the density of electric charges at the interface induced by AC fields.

The apparent maximum field-enhanced rate of mass transfer is rather perplexing. It may be owing to a combination of factors such as the formation of an electrical double layer around the charged electrode and hydrodynamic limitations in the MLC used in the present study. While probing this phenomenon is undoubtedly interesting, it is outside the scope of the present study.

No direct comparison of the results of the present study can be made with previous studies as no directly comparable study could be found in the literature. It is however important to note that the work of Gneist and Bart (2003), which is the only previous study to investigate the effect of transient fields on interfacial phenomena, reported that mass transfer rates were enhanced by DC fields and diminished by AC fields in comparison to that in the absence of a field. They proposed that Marangoni-type turbulence is responsible for these effects of electrostatic fields on mass transfer, which is in contrast to the findings of the present study. Their experimental method, however, was significantly different from the present study as they investigated non-reactive mass transfer from aqueous droplets that were suspended in a continuous organic phase. Hence, the overall mass transfer could not be attributed solely to any single interfacial process.

In summary, the diffusion of Cyanex® 272-extracted Co(II) species in the organic phase is enhanced by approximately 2.5 times with the application of 1 kV of either DC or PDC fields whether the applied field is negative or positive apparently owing to electrostatic attraction of the extracted species. Higher voltages up to 4 kV had no further effect. The application of comparable strengths of AC fields had no effect at all.

### 4.3.2. Effect of Electrostatic Fields on the Diffusion Process in the Aqueous Phase

The effect of electrostatic fields on the diffusion in the aqueous phase was investigated by applying electrostatic fields across the liquid-liquid interface and measuring the change in the concentration of the extracted Co(II) under experimental conditions such that the mass transfer rate was controlled only by the diffusion of the species in the aqueous phase. This was achieved by using suitable stirring speeds in both the aqueous

phase (80 rpm) and organic phase (170 rpm). Under these conditions, two distinct regions were visible in the aqueous phase immediately after Co(II) ions were injected (Figure 4.8): (1) a diffusion region on the aqueous side of the interface, which was colourless indicating negligible concentration of Co(II) ions, and (2) the bulk of the aqueous phase, which was pink owing to a high concentration of Co(II) ions. The entire organic phase was homogenously yellowish, which was the natural colour of the solvent, but gradually changed to blue as the experiment progressed, indicating an increasing concentration of the extracted Co(II). That is, as determined in Chapter 3.4.2, the stirring rate in the organic phase was sufficiently fast such that its diffusion region is rendered negligible. This means that any extracted Co(II) ions are immediately transferred into the bulk of the organic phase. It follows that any changes in the rates of mass transfer, as a result of changes in the applied voltage, could only be attributed to the effect of electrostatic field on the diffusion process of the Co(II) ions in the aqueous diffusion region.

Figure 4.8 Photograph of the phases in the absence of a field under operating conditions used to investigate the effect of electrostatic fields on the diffusion in the aqueous phase. For illustration purposes, the pink colour in the bulk of the aqueous phase is enhanced

In addition, to determine the effect of the orientation of the charged electrode on this diffusion process, two sets of experiments were carried out: one using a charged upper electrode with a grounded lower electrode, and one using its opposite orientation. In both sets, the applied voltage was increased stepwise at 1-kV intervals when the rate of mass transfer had apparently remained at steady state for at least 500 consecutive s.

The results, summarised in Figures 4.9 and 4.10, show that the application of high voltages (1 - 4 kV), regardless of the type (positive DC, negative DC, AC, positive PDC, negative PDC), had negligible effect on the rates of mass transfer of the extracted Co(II) species and hence, on the diffusion process in the aqueous diffusion region. This was true whether the upper (Figure 4.9) or lower electrode (Figure 4.10) was charged. The slight differences in the actual rates may be attributed to slight differences in the hydrodynamics within the MLC in individual experiments owing to equipment limitations as well as random experimental errors. These include, for example, known slight fluctuations in the speed of the stirrers, unavoidable slight differences in the actual positions of the liquid-liquid interface between individual experiments, and analytical errors.

At first glance, these were bewildering results given the earlier studies of Martin et al. (1983) and Wildberger and Bart (2002), on the effect of electrostatic fields on the extraction of Cu(II) with LIX 65N and Zn(II) with D2EHPA, respectively. They reported that electrostatic fields affect the rate of movement of species in the aqueous phase toward the interface but they provided little experimental details, both in terms of methodology and results, making any comparison difficult.

In contrast, the data generated in the present study, that include the effect of practically all types of applied field, a wide of range of field strengths, and both possible electrode orientations, are extensive and unambiguous. These results suggest that, consistent with the theory, no significant electrostatic field could be sustained within the aqueous phase owing to its high conductivity allowing a rapid dissipation of the charge. For example, the conductivity of the aqueous solution used in this study was 5.13 S/m. Its permittivity was approximately $7.17\times10^{-10}$ F/m. Therefore, its relaxation time constant, which is a measure of the time required to dissipate any charge placed in a material (Hendricks 1973), and is calculated as the ratio of its permittivity to its conductivity, was $1.40 \times 10^{-10}$ s. In contrast, the organic phase used in this study had a permittivity of $1.24\times10^{-11}$ F/m and a conductivity of $3.00 \times 10^{-11}$ S/m and thus, a charge relaxation time constant of 0.413 s, which is nine orders of magnitude larger than that of the aqueous phase. This means that, for practical purposes, a significant strength of electrostatic field can only be sustained within the organic phase. The conductivities of both the aqueous and organic phases used in this study are typical of those encountered in hydrometallurgical solvent extraction applications and thus, these results would be relevant to them.

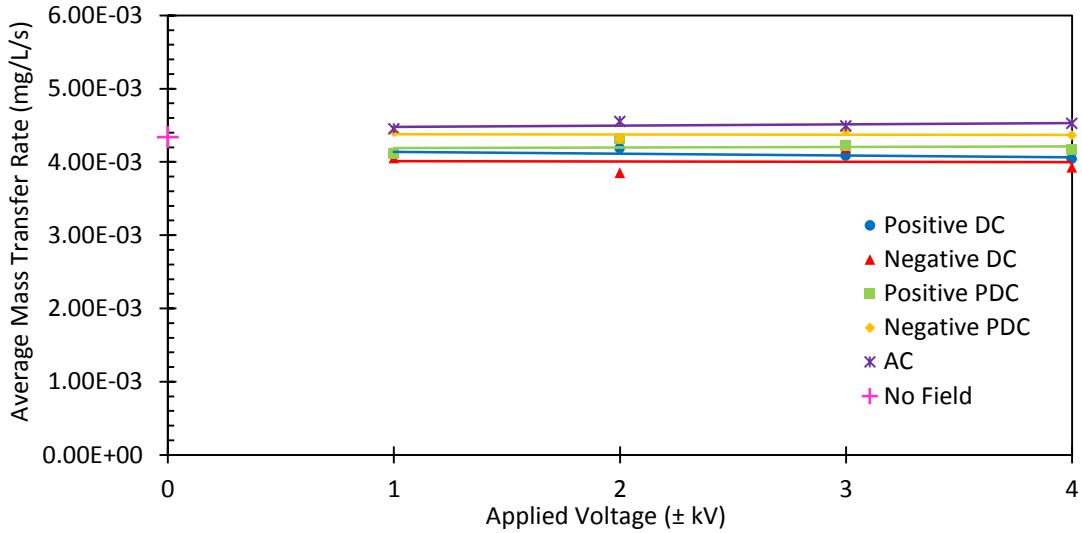


Figure 4.9 Effect of electrostatic fields on the mass transfer in the presence of an aqueous diffusion region but no organic diffusion region (charged upper electrode)

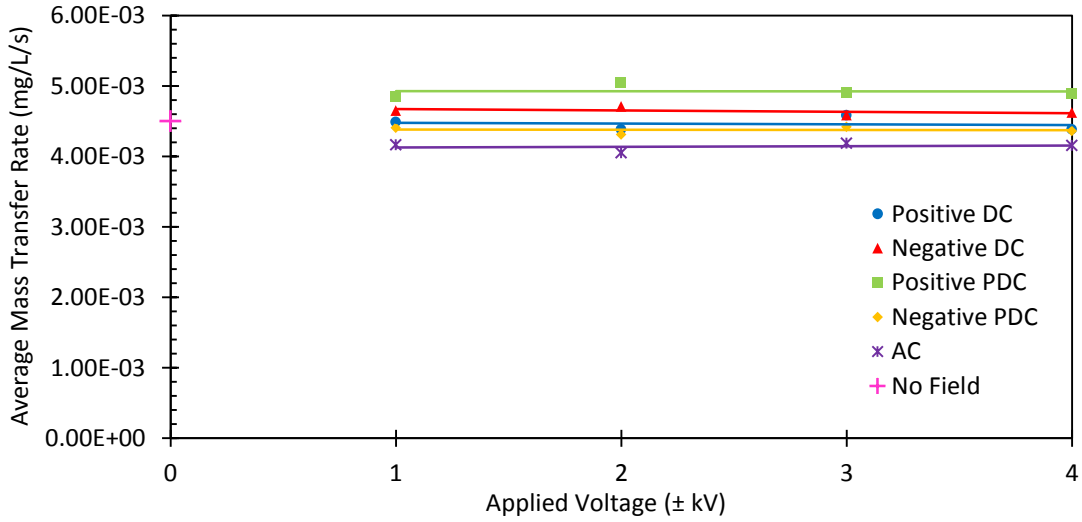


Figure 4.10 Effect of electrostatic fields on the mass transfer in the presence of an aqueous diffusion region but no organic diffusion region (charged lower electrode)

In summary, no electrostatic field can be sustained in aqueous solution as its high conductivity leads to fast dissipation of charge and thus, electrostatic fields cannot be made to influence the transport of dissolved metal species in this phase.

### 4.3.3. Effect of Electrostatic Fields on the Rate of the Chemical Reaction

The effect of electrostatic fields on the rate of the chemical reaction between Co(II) and Cyanex® 272 was investigated by applying electrostatic fields across the liquid-liquid interface and measuring the changes in the concentration of the extracted Co(II) in the bulk of the organic phase. The stirring speeds used in both the aqueous phase (120 rpm)

and organic phase (170 rpm) were such that no diffusion regions existed in either phase. The upper electrode was the charged electrode for all of these experiments, effectively subjecting the interface to an electrostatic field. Therefore, any change in the mass transfer rate, as a result of changes in the applied voltage, can only be attributed to its effect on the rate of the chemical reaction.

The effect of positive DC fields on the change in the concentration of extracted Co(II) in the bulk of the organic phase and hence, the rate of the chemical reaction, is shown in Figure 4.11. Clearly, the mass transfer rate was unchanged in spite of the substantial changes in the applied voltage, showing that positive DC fields had no effect on the rate of the chemical reaction.

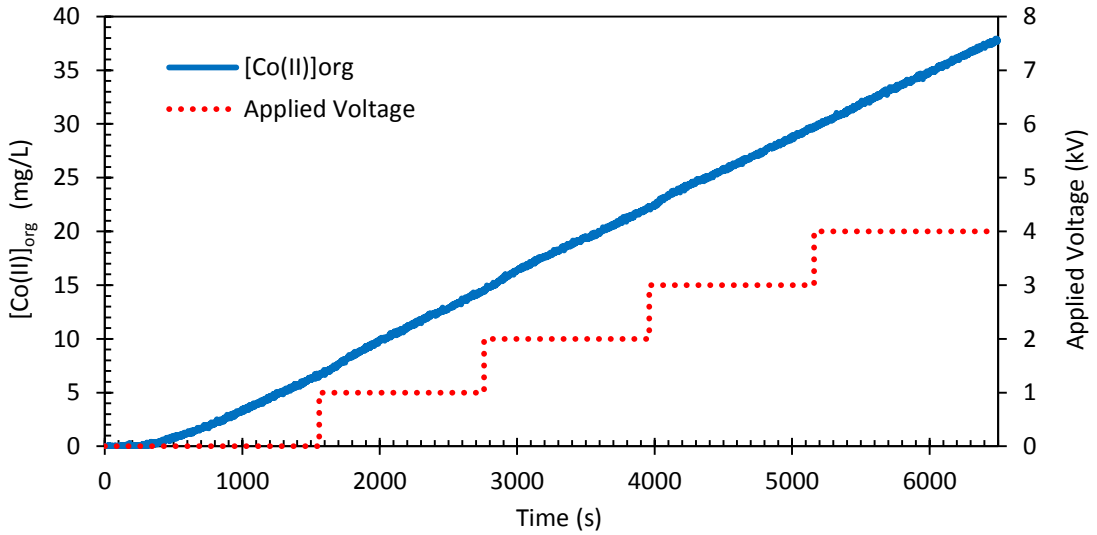


Figure 4.11 Effect of a positive DC field on the rate of the chemical reaction

Similar results were obtained when other types of fields (negative DC, positive PDC, negative PDC, AC) were used. These are summarised in Figure 4.12. As in the previous section, the slight differences in the rates of mass transfer between each set of data were owing to the limitations of the technique including random experimental errors. These results show clearly that electrostatic fields, regardless of their type, had no effect on the rate of the chemical reaction between Co(II) and Cyanex® 272.

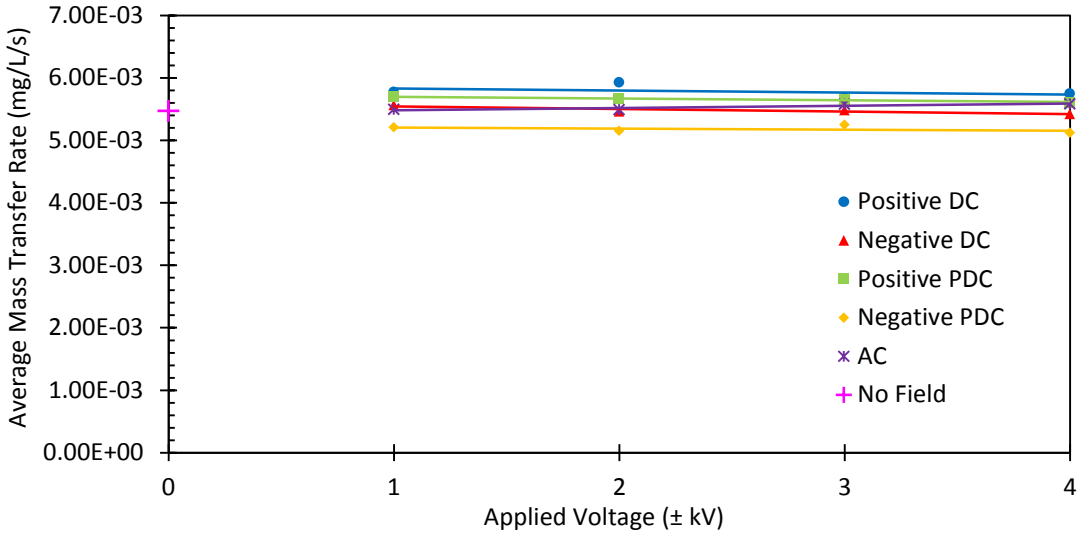


Figure 4.12 Effect of electrostatic fields on mass transfer with negligible diffusion regions

It should be noted that a previous study on the extraction of Zn(II) with D2EHPA by Wildberger and Bart (2002) mentioned some influence of DC fields on the rate of the chemical reaction, which they attributed to electromigration of species in the aqueous phase. There was, however, little experimental detail provided, either in terms of methodology or generated data, and thus, no comparison can be made.

## 4.4. CHAPTER SUMMARY

The effect of electrostatic fields on the interfacial phenomena in the extraction of Co(II) with Cyanex® 272 was investigated using a modified Lewis cell (MLC) that was developed in the present study for this purpose. It was found that:

- The application of 1 kV of DC and PDC fields, either positive or negative, enhanced the rate of transport of the extracted species across the organic diffusion region by approximately 2.5 times owing to electrostatic attraction but further increases in the applied voltage up to 4 kV had no further effect. The application of comparable strengths of AC fields had no observable effect at all.
- Electrostatic fields had no effect on the mass transfer of the dissolved Co(II) in the aqueous diffusion region apparently because the applied field cannot be sustained in this region as the high conductivity of this phase facilitated fast dissipation of charges.
- Electrostatic fields had no effect on the chemical reaction between Co(II) and Cyanex® 272.

# Chapter 5

# STUDY ON THE EFFECT OF ELECTROSTATIC FIELDS ON DROPLET DISPERSION

## 5.1. INTRODUCTION

This chapter describes the study on the effect of various types of electrostatic fields (DC, pulsed DC, and AC) as well their properties such as field strength and, in the case of transient fields, frequency, on droplet dispersion. The focus was on determining how electrostatic fields effect and affect droplet dispersion. This was achieved by carrying out droplet dispersion experiments at systematically varied experimental conditions in relation to the types and properties of electrostatic fields and observing and measuring the characteristics of the dispersions. Several conflicting views in the literature were resolved and new useful insights have been gained.

## 5.2. MATERIALS AND METHODS

### 5.2.1. Reagents, Test Solutions and Equipment

The following reagents were used in the work that is described in this chapter: acetic acid (AR, Chem-Supply), sodium hydroxide (AR, Chem-Supply), standard Co(II) solution in nitric acid matrix (10,000 mg/L, Australian Chemical Reagents), cobalt sulphate heptahydrate (AR, Chem-Supply), sodium sulphate (AR, BDH), ShellSol® 2046 (Industrial Grade, Shell Chemicals), Cyanex® 272 (Industrial Grade, Cytec Australia), and sulphuric acid (98%, Sigma Chemicals). All reagents were used as supplied.

Two test solutions were used: a buffered (pH 5.5) Co(II) solution (300 mg/L) as the aqueous feed and Cyanex® 272 in ShellSol® 2046 as the solvent. This choice was to ensure consistency of the properties of the aqueous solution in both mass transfer experiments such as those in Chapters 4 and 7, and characterisation of droplet dispersion and agitation in the present and the following chapter (Chapter 6).

The droplet column that was developed in Chapter 3.5 including its auxiliary equipment, which is illustrated in Figure 3.15, was used in this part of the study.

### 5.2.2. Preparation of Test Solutions

The aqueous test solution consisted of Co(II) ions (300 mg/L) in an acetic acid/acetate buffer with a pH of 5.5. This was prepared by transferring the required volume of acetic acid, and masses of sodium hydroxide pellets and cobalt sulphate heptahydrate into a volumetric flask and dissolving in a minimum amount of distilled water. A mass of sodium sulphate was also added to make its concentration in the final solution 0.2 M. This was to increase the ionic strength to facilitate good phase separation as well as to avoid third phase formation (Fu & Golding 1988). The volume was then adjusted so that it was just under the required volume. The solution was mixed thoroughly, allowed to equilibrate at room temperature and made to the final volume. The pH was measured and recorded.

The organic solution was prepared by transferring the required volume of Cyanex® 272 (10% v/v) into a volumetric flask and filling to the mark with ShellSol® 2046. The stripping solution was prepared by transferring the required volumes of sulphuric acid (24.5 g/L) and cobalt sulphate (20.5 g/L Co(II)) into a volumetric flask, allowing the solution to equilibrate, and filling to the mark with distilled water.

### 5.2.3. Analytical Techniques

All pH measurements were carried out using a bench-top pH meter (Orion 3 Star, Thermo Electron Corporation) equipped with a glass body electrode (LoT402-611-DPA-S7/40, Mettler-Toledo).

The concentrations of the cobalt in the test solutions were determined by ICP (Varian VISTA-PRO Simultaneous ICP-OES) following the procedures recommended by the manufacturer. Calculations for the composition of the aqueous solutions used in droplet column experiments are shown in Appendix C7.

### 5.2.4. Determination of the Effects of Electrostatic Fields on Droplet Dispersion

The determination of the effects of electrostatic fields on droplet dispersion was carried out by conducting several sets of droplet dispersion experiments under comparable conditions while the types of electrostatic fields (negative and positive DC, negative and positive PDC and AC), their strengths, and frequency, in the case of the transient fields (PDC and AC), were systematically varied. For example, in the case of positive PDC field, a set of four droplet dispersion experiments was carried out under comparable conditions except that each was at different field strength, and then, another set was

similarly carried out at different frequencies while the strength of the applied field was kept constant. The focus of this part of the study was on understanding how electrostatic fields effect and affect droplet dispersions.

The range of values of the field properties (strength and frequency) were chosen such that a significant variation of the characteristics of the dispersion were clearly observable while keeping the range of the droplet size that was produced within the constraints of the imaging equipment as discussed in Chapter 3.6.2. At the same time, to allow appropriate comparison among the various sets of variables, the range of field strengths and, in the case of transient fields, frequencies, of each type of field that yielded an approximately comparable droplet size distribution to those of the others were chosen. To achieve this, several exploratory dispersion experiments were first carried out to determine the range of droplet sizes in the resulting dispersion as a function of the field types and properties. The resulting dispersions were then recorded and preliminary analyses, both visual and quantitative, were carried out. Once replicable results for a particular set of experimental conditions were achieved, a set of final experiments for this set of experimental conditions was carried out.

### 5.2.5. Procedures for Droplet Dispersion Experiments

The droplet dispersion experiments were carried out following the general procedures for droplet column experiments described in Chapter 3.6.1. The imaging equipment was used following the procedures described in Chapter 3.6.2. The laser and high-speed camera were positioned such that a good visual observation of the behaviour of the droplets was achieved. The dispersion of the feed droplets (primary droplets) was best observed when they are positioned in between the top end of the electrodes. On the other hand, the dispersion of secondary droplets was best achieved when they are positioned approximately halfway down the column between the electrodes.

### 5.2.6. Data Acquisition and Analysis

Videos of the dispersions were recorded at 500 f/s, which are essentially a series of 500 consecutive high quality still photos of the dispersion per second. This allowed replaying the videos at various speeds from frame by frame up to the full speed of the camera facilitating detailed visual analysis of the dispersions. This also allowed ensuring that the settings of the camera are appropriate for a given set of experimental conditions such as, for example, the out of focus as well as overlapping droplets are correctly identified and treated as such.

The videos were imported into VisiSize, which is an image analysis software, to generate and analyse individual droplet data, droplet distributions and characteristic measures of the dispersions. The droplet size distributions were analysed in two ways as they provide a complimentary picture of the dispersion: (1) volume density distribution, which refers to the total volume of the droplets in a given size fraction as a percentage of the total volume of all the droplets in the sample and (2) population distribution, which is the total number of droplets in a given size fraction as a percentage of the total number of droplets. The software was set to distribute the values over 140 size fractions. The actual size ranges for each of the 140 fractions vary between experimental conditions as the software calculates them based on the largest and smallest droplets of the particular dispersion.

The volume density distributions were generated by plotting the droplet diameter against the percentage of droplets by volume in each of the 140 size fractions that were generated by the VisiSize software. The population distributions were initially generated in the same manner but the distribution over 140 fractions appeared to be too thinly spread and overlapping because of the disproportionate abundance of small droplets compared to the large droplets and thus, the trends were not easily visible (Figure 5.1).

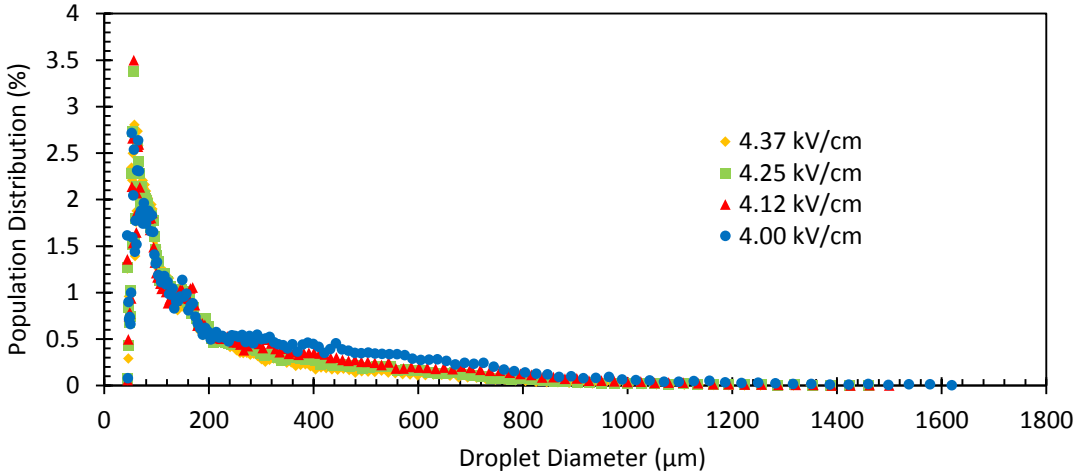


Figure 5.1 Effect of the field strength of positive DC fields on the population distribution for the 140 size fractions generated by VisiSize

To allow a clearer analysis and presentation of the population distribution, the individual droplets were sorted from smallest to largest droplet diameter and distributed over six selected size fractions (<100 µm, 100 – 200 µm, 200 – 300 µm, 300 – 400 µm, 400 – 500 µm, and >500 µm). This allowed the plotting of the field strength or frequency against the number of droplets in each of the six size fractions as a percentage of the total number of droplets. An example is shown in Figure 5.2.

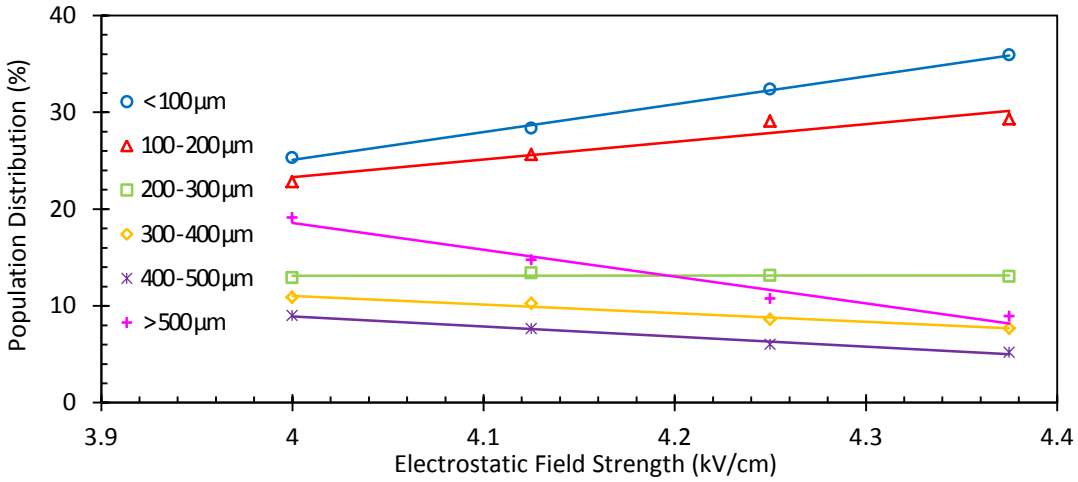


Figure 5.2 Effect of the field strength of positive DC fields on the population distribution for six selected size fractions

Two characteristic measures of the dispersion were generated and used in the analyses: the Sauter mean ($d_{32}$), which is the diameter of the droplet whose ratio of volume to surface area is the same as the entire dispersion (Equation 7), and volume-weighted mean ($d_{43}$), which is the mean diameter ($d$) weighted by the volume (Equation 8).

$$d_{32} = \frac{\sum d^3}{\sum d^2} \qquad \text{(Equation 7)}$$

$$d_{43} = \frac{\sum d^4}{\sum d^3} \qquad \text{(Equation 8)}$$

Sometimes referred to as the true measure of fineness of a particle size distribution, Sauter mean is relevant to processes wherein the surface area is a major factor. The volume-weighted mean is also relevant to solvent extraction as it is sensitive to the presence of particles with large volumes, which is a factor in phase holdup and thus provides complimentary information to Sauter mean.

Preliminary experiments revealed some variations in the droplet distributions for a given set of experimental conditions. To generate a more representative profile, ten experimental runs were recorded for each set of these sets of experimental conditions. That is, each data point in this chapter is an average of ten experimental runs.

The imaging equipment was optimised to record the size of a minimum of 10 000 droplets as a representative of the total population of droplets per experiment. A typical spread of the data in all these experiments is shown in Figures 5.3 and 5.4. The average standard error shown is typical of all data sets. For tidiness and clarity of the graphs, error bars are not included in each of the graphs in this part of the study. Additional data from droplet dispersion experiments are shown in Appendix D.

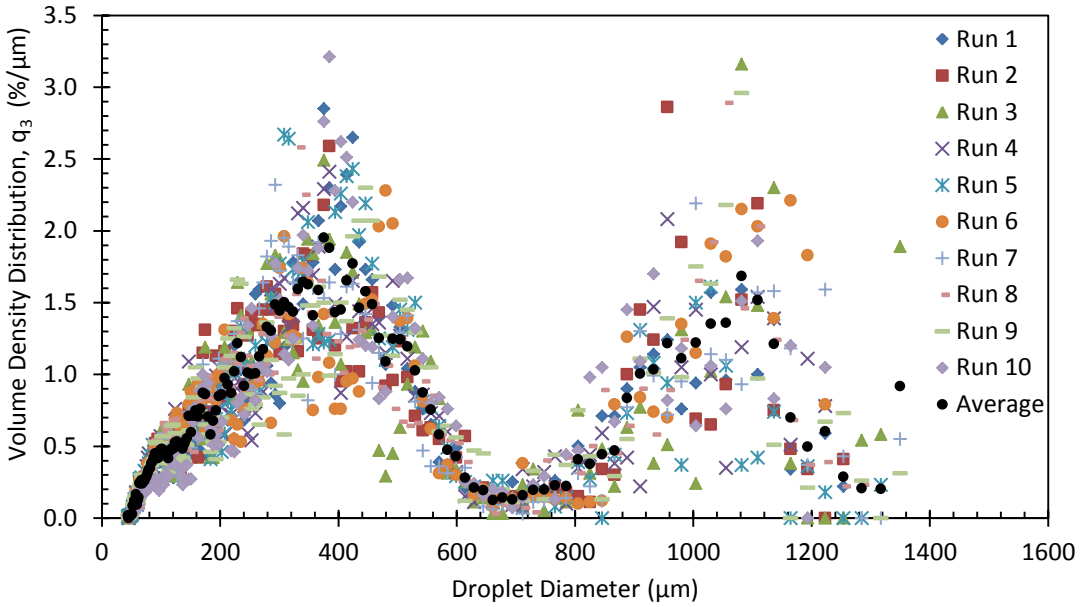


Figure 5.3 Raw data from experiments to investigate the effect of AC fields (3.50 kV/cm, 60 Hz) on the volume density distribution

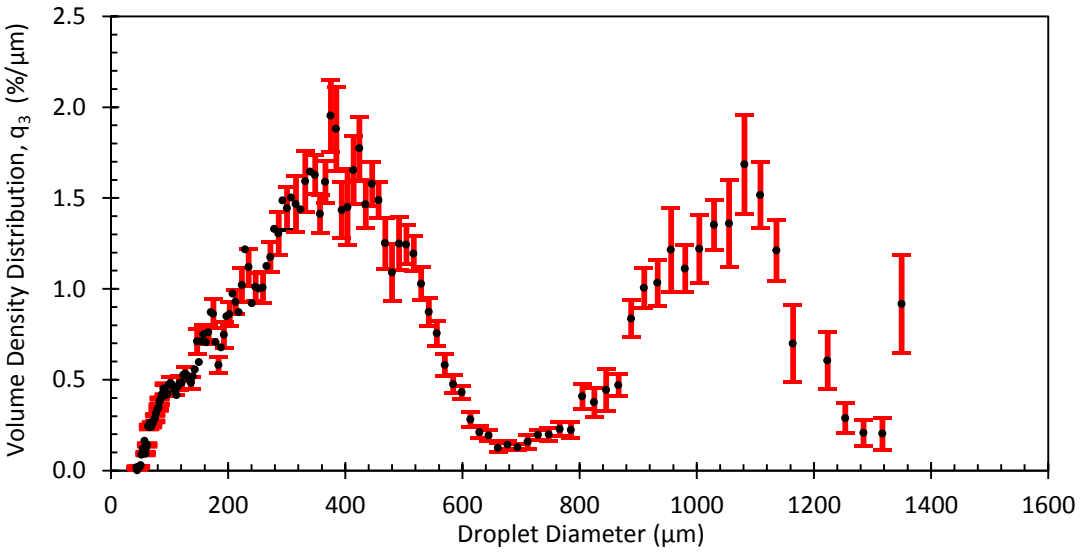


Figure 5.4 Average values from experiments to investigate the effect of AC fields (3.50 kV/cm, 60 Hz) on the volume density distribution with error bars of ±1 standard error

Visual analysis of the effect of electrostatic fields on droplet dispersion mechanisms was carried out by using the FastCam software to replay recorded images of droplet dispersion at reduced speeds (1 – 25 frames per second in most cases). This facilitated detailed observation of the dispersion behaviour. Screenshots of droplet behaviour, including successive images to show changes in droplet behaviour, were captured. When necessary, a grid mesh was used to provide scale.

## 5.3. RESULTS AND DISCUSSION

The use of a high speed camera equipped with a laser backlighting and image analysis software has facilitated detailed visual analyses of the behaviour of aqueous droplets under the influence of electrostatic fields, as well as quantitative analysis of their size distributions.

The results show that as the feed droplets (primary droplets) come under the influence of the electrostatic field between the two parallel-plate electrodes, they start to elongate, which is a manifestation of orientational polarisation (Figure 5.5) but the nature of this elongation is different for different types of fields. With DC fields, the amplitude of elongation of the droplets steadily increased with increases in the strength of the applied field until they dispersed supposedly when a sufficiently strong field was reached. On the other hand, with transient fields, either PDC or AC, the ends of the droplets parallel to the direction of the electrostatic field alternated between a conical and rounded shape at a rate that was in apparent synchrony with the frequency of the applied field. An example is shown in Figure 5.6(a). When a sufficiently strong field was applied, the droplets then dispersed. These behaviours indicated that the elongations of the droplets and eventual dispersion were a consequence of the attractive force between the applied field and the droplets and the differences in the mode of their elongation were a consequence of the different waveforms of the voltage, whether steady or transient. It was evident that the alternating shapes of the droplets under the influence of transient fields occurred at the maximum (conical ends) and minimum (rounded ends) points of the voltage cycles.

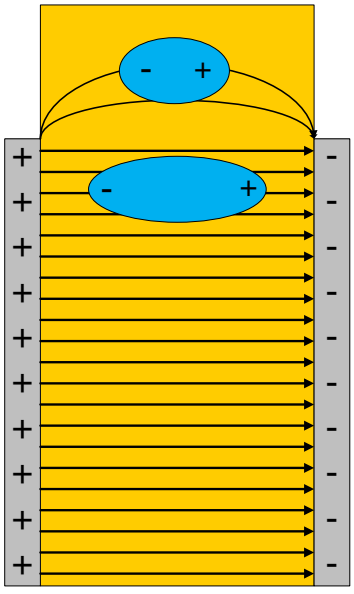


Figure 5.5 Diagram of primary droplet entering the electrostatic field

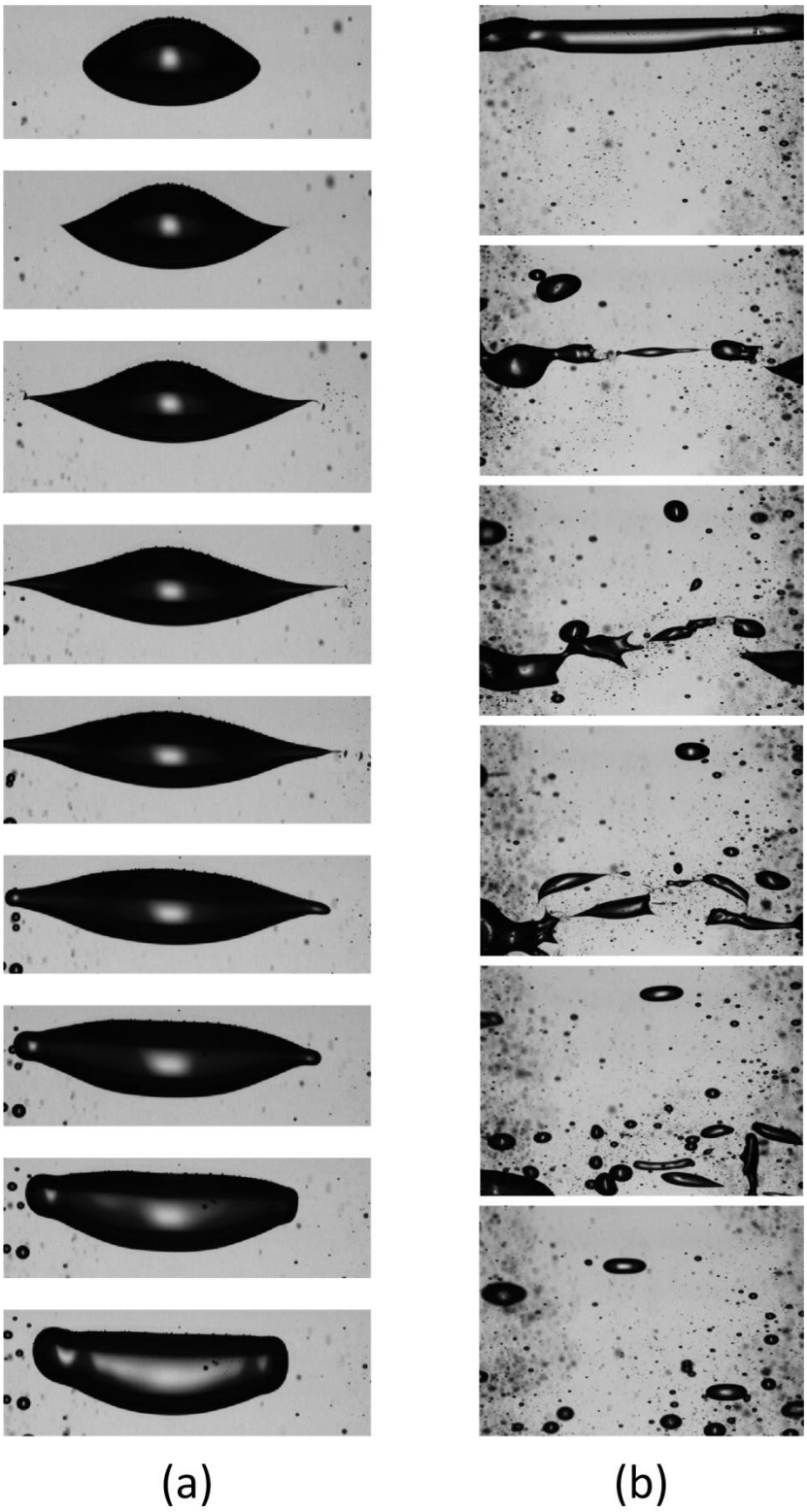


Figure 5.6 Effect of an AC field (3.5 kV/cm, 60 Hz) on the dispersion behaviour of an aqueous feed droplet (a) as it comes under the influence of electrostatic field, and (b) as it moves through the electrostatic field and generates a population of secondary droplets

The dispersions of the primary droplets forming a population of secondary droplets had no discernible pattern (Figure 5.6(b)). That is, they occurred through various

mechanisms of dispersion in apparent random fashion. These included both previously known mechanisms of droplet dispersion, namely necking (Figure 5.7(a)), which is largely owing to orientational polarisation, and jetting (Figure 5.7(b)), which is consistent with a combination of orientational and interfacial polarisation, as well as previously unreported mechanisms of dispersions. One of these mechanisms involves the formation of several protrusions towards various directions that progressively extend until the droplet disperses. This is referred to in the present study as irregular dispersion mechanism. Figure 5.8(a) shows an example of this dispersion mechanism.

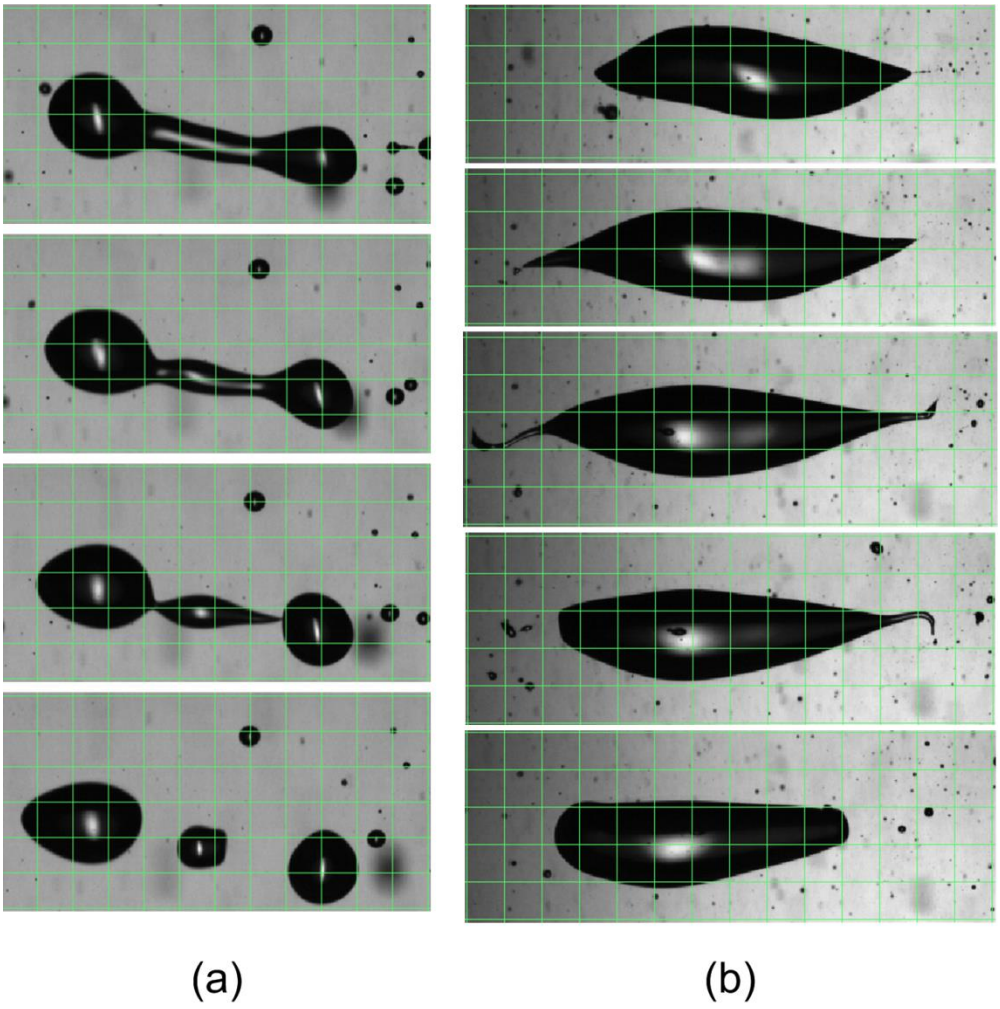


Figure 5.7 Examples of (a) necking-type dispersion, and (b) jetting-type dispersion, induced by DC fields (grid = 500 μm)

Another previously unknown dispersion mechanism that was observed, although only with DC or PDC fields, was what appeared to be an explosive dispersion of a droplet leading to the formation of emulsion-like ultra-fine droplets that eventually disappear by coalescing to form larger droplets. Hence, this is referred to as emulsion-like formation mechanism. This happens when a droplet is situated between two larger and elongated droplets that are each contacting its nearby electrode and hence, presumably acting as

extensions of the electrodes creating a localised region with substantially higher field strength. This is consistent with the acquisition of interfacial charge and hence, interfacial polarisation. A photo of this mechanism of droplet dispersion is shown in Figure 5.8(b).

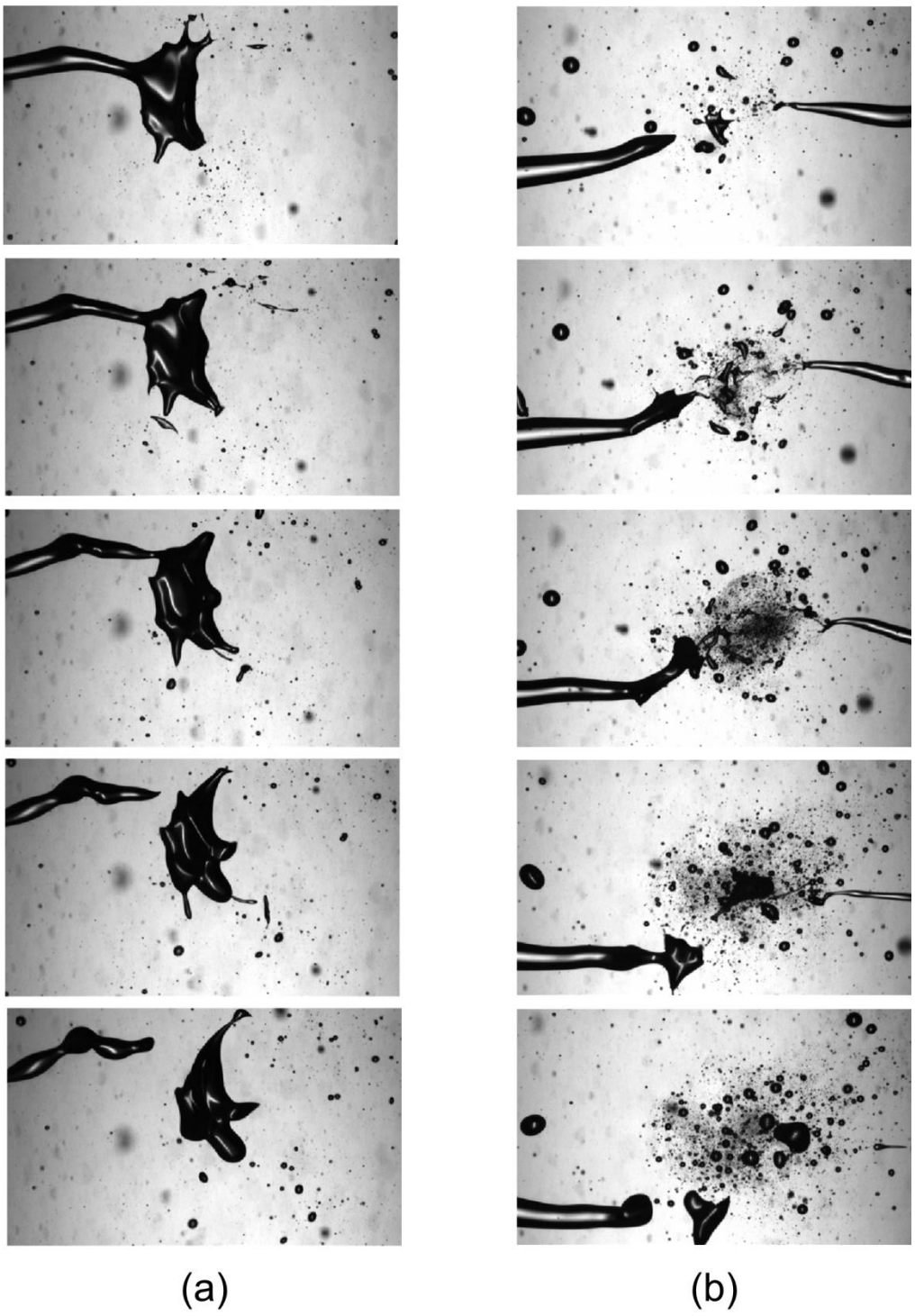


Figure 5.8 Examples of (a) irregular dispersion, and (b) emulsion-like formation, induced by DC fields

Another distinct mechanism that was observed, which has not been reported previously, involves the dispersion of a droplet through a combination of two or more of these dispersion mechanisms and hence, referred to as combination dispersion mechanism. For example, the dispersions of a droplet through a combination of necking and jetting or jetting and irregular dispersion mechanisms were quite common.

These behaviours occurred regardless of the type of the applied field (DC, PDC or AC). Given that it is generally agreed in the literature that droplet dispersion occurs either by necking or jetting only, these observations were unexpected but are of practical significance in the development of electrostatic solvent extraction applications.

Another previously unreported behaviour of a population of droplets that are under the influence of electrostatic fields was the co-occurrence of dispersion and coalescence of droplets within a given set of experimental conditions. Given the current thinking in the literature that droplets either disperse or coalesce depending on the strength of the applied field, with the former favoured at high field strength and the latter at low field strengths, which means they are seen as mutually exclusive, this observation was unexpected too but relevant and useful in the development of electrostatic solvent extraction applications.

In contrast to the dispersion of primary droplets, the dispersion of the secondary droplets was found to be quite patterned and predictable. For example, there were distinct differences in the manner by which the different types of electrostatic fields effected the dispersion of these droplets. Typical droplet distributions generated by dispersion of secondary droplets are shown in Figure 5.9. Given that these resulting dispersions largely determine the final droplet size distribution in a given set of experimental conditions, their characterisation was critical to understanding the effect of electrostatic fields on mass transfer in electrostatic solvent extraction and, thus, the focus of this part of the study.

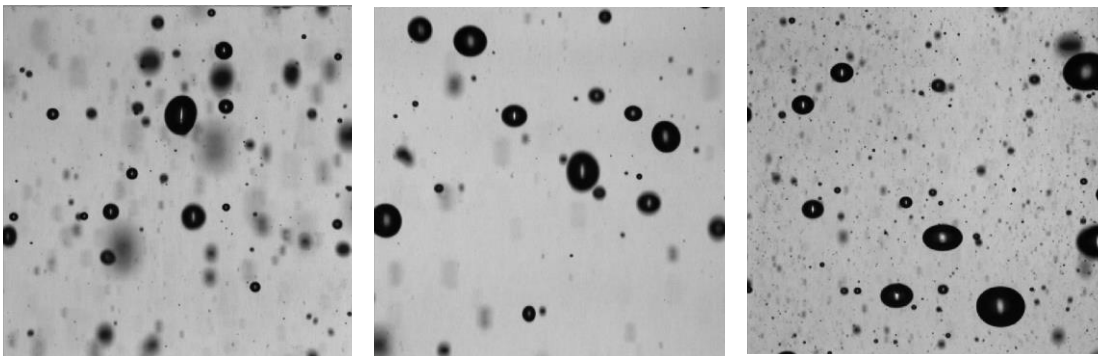

(a) (b) (c)

Figure 5.9 Typical resulting dispersions of secondary droplets and droplet distributions generated by (a) DC fields, (b) PDC fields, and (c) AC fields

In general, the droplet size distributions were largely a function of the strength of the applied field but, in the case of transient fields, the frequency had significant effect too. For clarity, a detailed discussion of the effects of each type of field on droplet dispersion is discussed in separate sections as follows.

### 5.3.1. Effect of DC Fields on Droplet Dispersion

The appropriate strengths of DC fields for this part of the work were found to be 4.00 – 4.37 kV/cm and −4.12 – −4.50 kV/cm for positive and negative fields respectively. Increases in the field strength within these ranges resulted in decreases in droplet size. These are evident in the values of the Sauter mean diameters, which changed from 558 μm at 4.00 kV/cm to 401 μm at 4.37 kV/cm and from 586 μm at −4.13 kV/cm to 464 μm at −4.50 kV/cm (Figures 5.10 and 5.11). A similar trend has been reported by a number of investigators (Bailes & Thornton 1971; Bailes & Thornton 1974; Thornton 1976; Bailes 1977; Bailes 1981; Zhou & Gu 1988; He, Chang & Baird 1997) even though they used aqueous and organic phases that are different from those in the present study and most of them focused on the behaviour and characteristics of single droplets only rather than a population of droplets, which was the focus of the present study as it is most practically relevant to the application of electrostatic dispersion in solvent extraction. They invariably attributed this trend to the increasing electrostatic force that is imposed on the droplets.

Closer analysis of the droplet population showed that increases in the field strength, whether positive (Figure 5.10) or negative (Figure 5.11) caused approximately linear increases in the number of droplets in the small-sized fractions (<100 μm, and 100 – 200 μm) and, correspondingly, linear decreases in the number of droplets in the medium-sized (300 – 400 μm, 400 – 500 μm) and large-sized fractions (>500 μm) while

the number of droplets in the intermediate-sized fraction (200 – 300 µm) remained relatively constant. This suggested relative stability of these droplet sizes over the ranges of field strengths that were investigated.

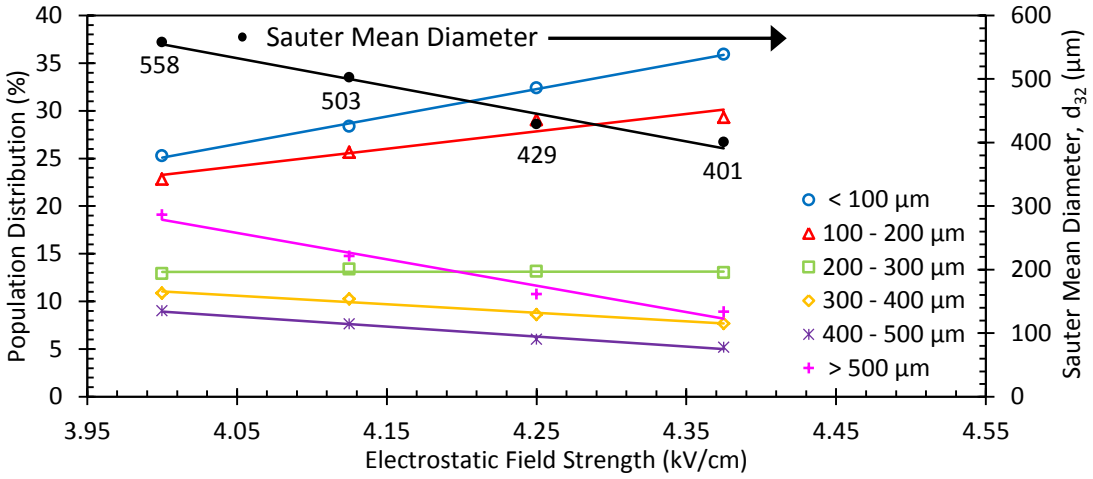


Figure 5.10 Effect of the electrostatic field strength of positive DC fields on the population distribution (primary y-axis) and the Sauter mean diameter (secondary y-axis)

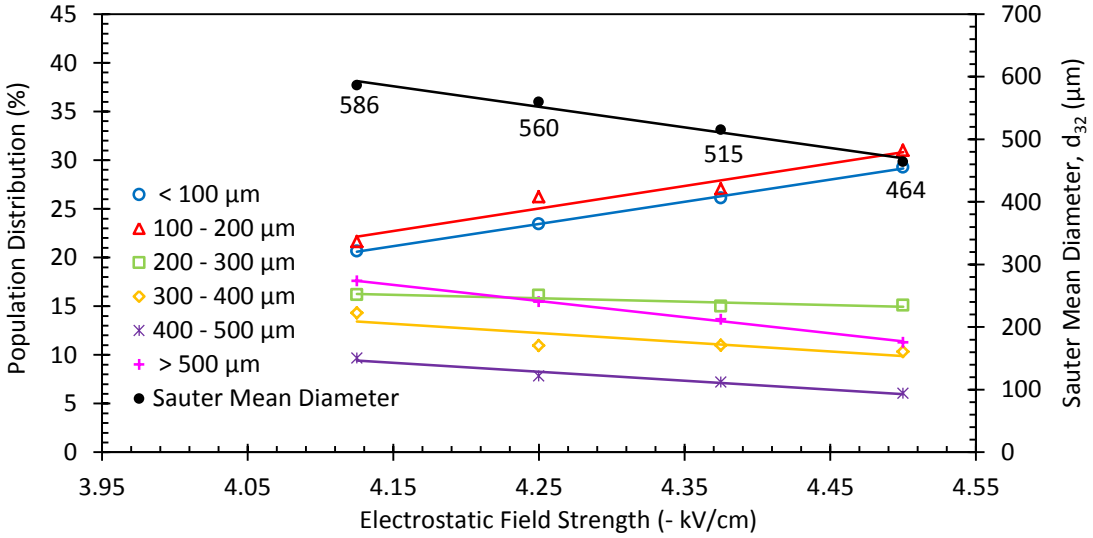


Figure 5.11 Effect of the electrostatic field strength of negative DC fields on the population distribution and the Sauter mean diameter

Increases in the field strengths also resulted in narrower droplet size distributions as shown by the larger decreases in the volume densities of the large droplets than the increases in the volume densities of the small droplets (Figures 5.12 and 5.13).

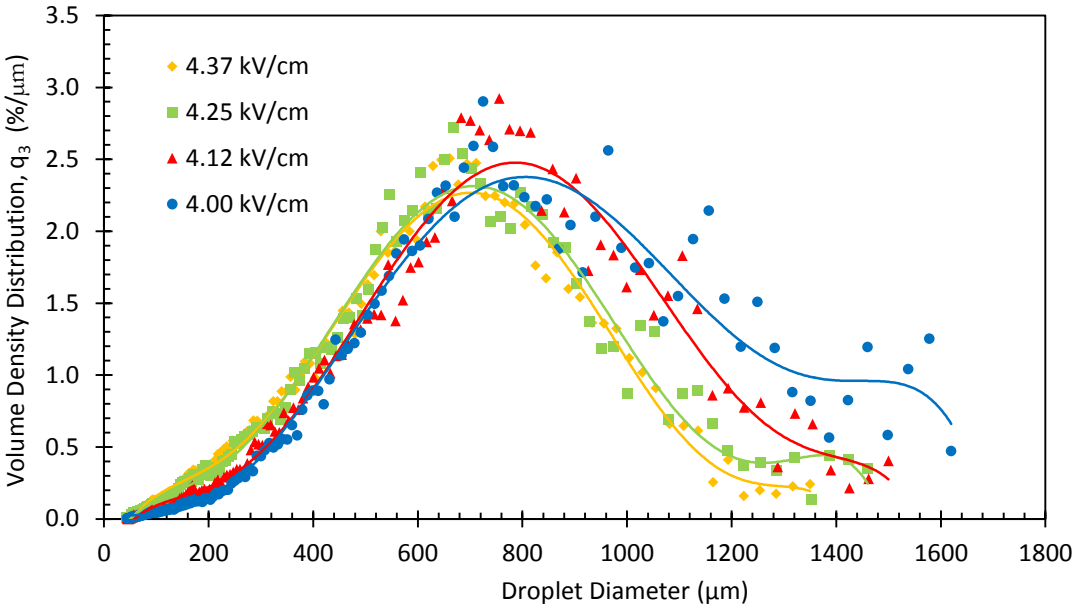


Figure 5.12 Effect of the field strength of positive DC fields on the volume density distribution

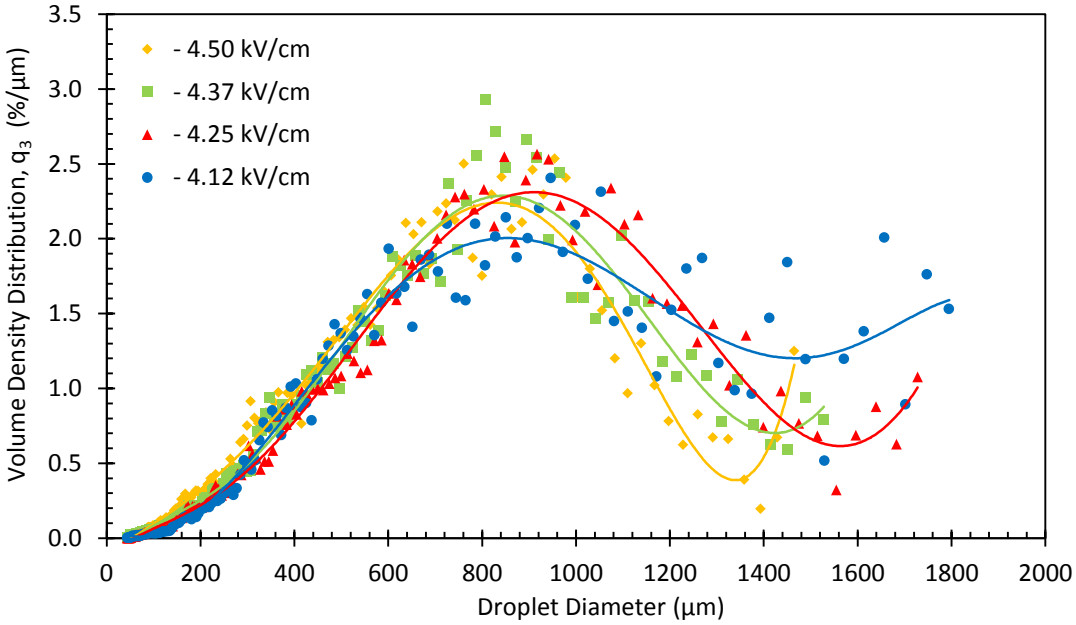


Figure 5.13 Effect of the field strength of negative DC fields on the volume density distribution

This narrowing trend of the droplet size distributions with increases in the applied field is in contrast to that of the study of Yamaguchi, Sugaya and Katayama (1988) who reported that increases in the field strength resulted in wider droplet size distributions. Although there are considerable experimental differences between theirs and the present study such as, for example, they used deionised water as the aqueous phase and cyclohexane as the organic phase, a different electrode configuration, and they dealt with much larger feed droplets (~3000 – 4000 µm), which then expanded to

approximately 1 – 6000 μm, it is difficult to assess whether these can account for the contrasting trend as they provided insufficient details. For example, they described their droplet sizing technique simply as measuring the drop profiles recorded in photographs. Capturing a substantially wider droplet size distribution such as theirs within a given set of experimental conditions is difficult, even with currently available advanced imaging technologies. No other study that investigated the effect of DC fields on the spread of a droplet size distribution has been reported.

The evidently much finer droplet dispersions that were generated under the influence of positive fields than those of negative fields under comparable field strengths (Figures 5.10, 5.11, 5.12 & 5.13) was at first perplexing as it suggested that positive DC fields exerted higher electrostatic force than negative DC fields. No previous study comparing the effects of polarities of DC fields has been reported and, thus, no comparison could be made. The observation, however, made sense when two models of electrostatically induced polarisation of droplets—orientational and interfacial—that are discussed in Chapter 2, were considered. Since comparable droplet sizes would have comparable amounts of polar species and thus strength of orientational polarisation, this difference in dispersion behaviour may only be attributed to a difference in the extent of interfacial polarisation. It is proposed that positive DC fields induce a greater amount of interfacial polarisation because: (1) a larger proportion of droplets have an overall negative charge owing to the greater mobility of electrons, and (2) a positively charged active electrode, which is the case when a positive DC field is used, generates a higher electrostatic force than an induced positive charge on the earthed electrode, which is the case when a negative DC field is used.

It is helpful to recall that interfacial polarisation occurs when electric charges migrate towards a discontinuity of electrical conductivity and permittivity, such as a liquid-liquid interface (Melcher & Taylor 1969). This is the case at the interfaces of aqueous droplets that are suspended in poorly conducting organic liquids. Under these conditions, ions and electrons are the only charged species that can migrate in an electrostatic field since protons are tightly held to the nuclei of atoms. There may be an equal number of positively and negatively charged ions in the organic phase used in the present study, but the amount of these will be negligible given the low dissociation constant of the extractant. The $pK_a$ of Cyanex® 272 is 6.37 (Sole & Hiskey 1992). It is therefore reasonable to think that, under the conditions used in the present study, some electrons are able to migrate through the poorly conducting organic phase and accumulate at the

liquid-liquid interface, causing the aqueous droplets to acquire a greater amount of negative charges. Hence, greater proportions of droplets have an overall negative charge and, consequently, are more responsive to a positively charged electrode.

The difference in the field strength between the actively charged electrode and the induced charged grounded electrode may be explained as follows. In the experimental set up in the present study, applying a charge to one of the parallel-plate electrodes induces an opposite charge on the other electrode. If the organic phase between the electrodes was a perfect conductor, the charge on both electrodes would be equal. Since the organic phase is a poor conductor, given its very low conductivity ($3.00 \times 10^{-11}$ S/m), the induced charge on the earthed electrode would be less than that applied to the active electrode. As a result, the positive charge induced on the earthed electrode, which was the case when negative DC fields was used, would be less than the positive charge on the positively charged active electrode, which was the case when positive DC fields was used. If a droplet has a net negative charge, then it is logical that negative DC fields would induce less dispersion than positive DC fields of equivalent field strength, because a lower effective electrostatic force is exerted onto it.

The considerable spread of the droplet size distributions generated with either positive or negative DC fields may be attributed to the occurrence of several mechanisms of droplet dispersion. It was clear that, similar to the dispersion of the primary droplets, the dispersion of secondary droplets under the influence of DC fields occurred through all the various mechanisms of dispersion, including necking, jetting, irregular, emulsion-like formation, and combination with approximately comparable prevalence.

### 5.3.2. Effect of PDC Fields on Droplet Dispersion

The suitable ranges of field strengths for the study of the effect of these types of fields at 50 Hz, which was used as the base frequency given it is the frequency of the mains power supply in Australia, were found to be 5.00 – 5.67 kV/cm and −8.75 – −9.75 kV/cm for positive and negative PDC fields, respectively.

#### *5.3.2.1. Effect of the Strength of PDC Fields*

The trends of the effect of the strength of PDC fields, whether positive (Figure 5.14) or negative (Figure 5.15) are similar to those of DC fields. Specifically, increases in the field strength resulted in finer dispersed droplets. For instance, the trends of the population distributions in each size fraction (<100 μm, 100 – 200 μm, 200 – 300 μm, 300 – 400

μm, 400 – 500 μm, and >500 μm) as well as the Sauter mean were similar. Clearly, these results indicate that, similar to DC fields, the droplet size is a function of the strength of the electrostatic force and that there is a range of droplet size that is stable under a given field strength.

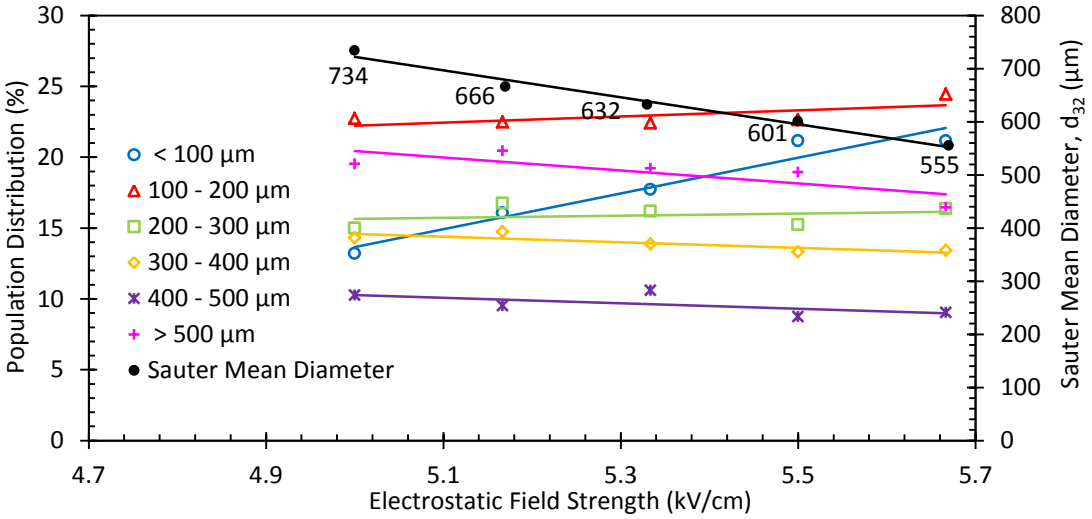


Figure 5.14 Effect of the electrostatic field strength of positive PDC fields (50 Hz) on the population distribution and the Sauter mean diameter

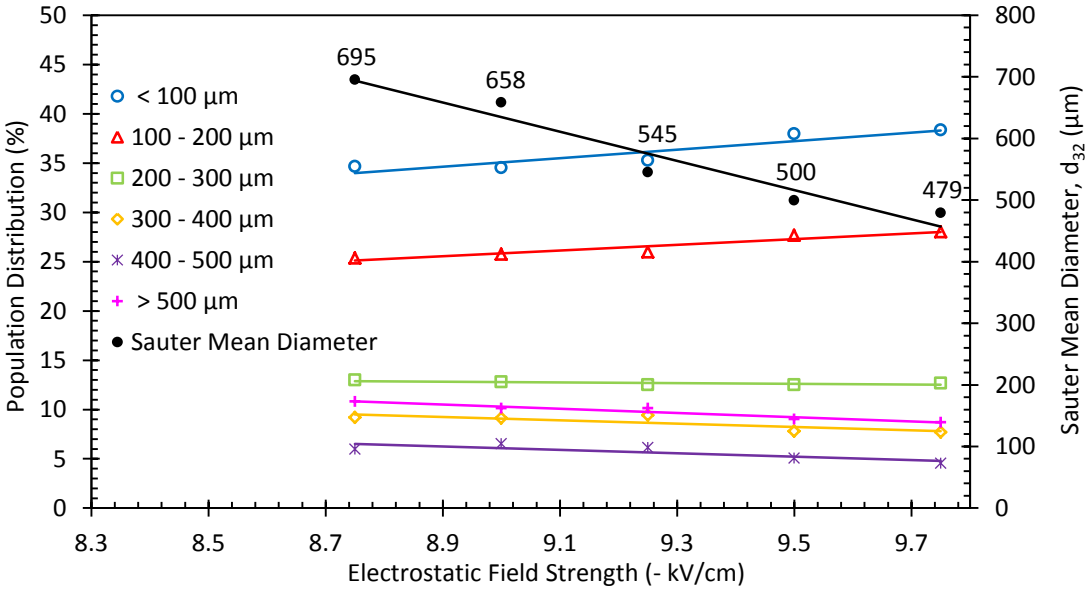


Figure 5.15 Effect of the electrostatic field strength of negative PDC fields (50 Hz) on the population distribution and the Sauter mean diameter

Similar too to DC fields, increases in the field strength of PDC fields within the range investigated resulted in narrower size distributions owing to larger decreases in the number of large droplets than the increases in the smaller droplets. These are evident in both the population distributions (Figures 5.14 and 5.15) as well the volume density distributions (Figures 5.16 and 5.17). For example, the maximum droplet diameter

decreased from 2319 to 1713 µm and from 2435 to 1825 µm for positive and negative PDC fields, respectively.

In addition, similar to the trend observed in DC fields but to a much greater extent, PDC fields (5.0 – 5.67 kV/cm) were more effective in dispersing droplets than negative PDC fields (−8.75 – −9.75 kV/cm). This is clearly evident in the substantially different minimum field strengths (+5.0 kV/cm vs −8.85 kV/cm) required to generate the minimum number of dispersed droplets. This is also clearly evident when the population distributions generated with DC fields (Figures 5.10 and 5.11) are compared with those of PDC fields (Figures 5.14 and 5.15). It is also clearly evident in the volume density distributions (Figures 5.12, 5.13, 5.16 and 5.17). These results are further evidence that a higher proportion of droplets acquire negative charge making them more responsive to interfacial polarisation with a positive electrode and a positively charged active electrode exerts a higher electrostatic force than the induced positive charge of an earthed electrode.

There are, however, significant differences in the effects of PDC and DC fields. Most glaring among these is that, as observed in Chapter 3.6.3, PDC fields, particularly negative fields required significantly higher field strengths (−8.75 – −9.75 kV/cm PDC fields vs −4.12 – −4.50 kV/cm DC fields) to disperse droplets.

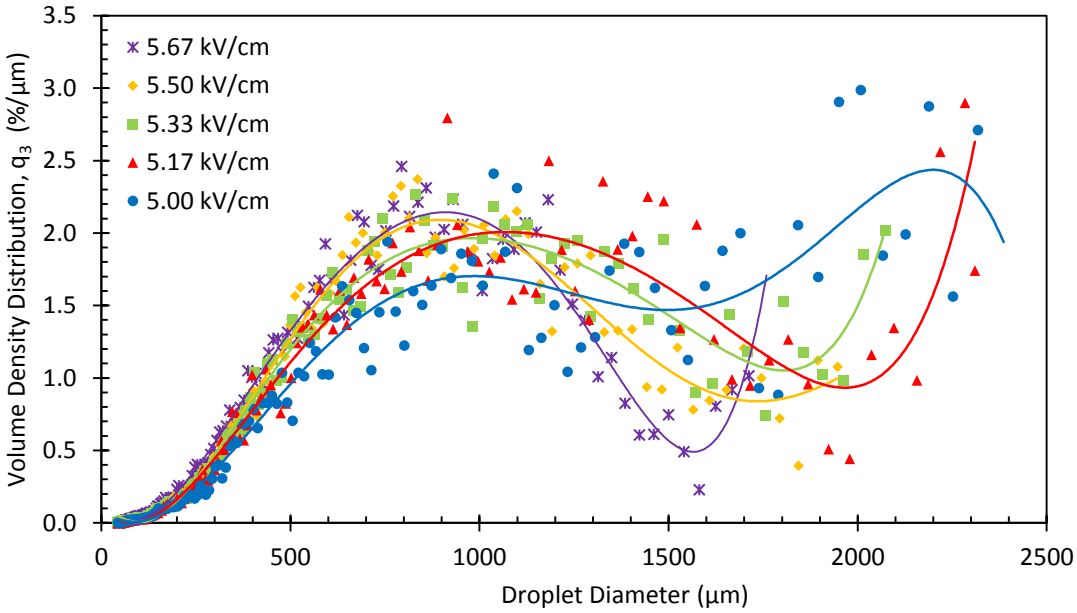


Figure 5.16 Effect of the electrostatic field strength of positive PDC fields (50 Hz) on the volume density distribution

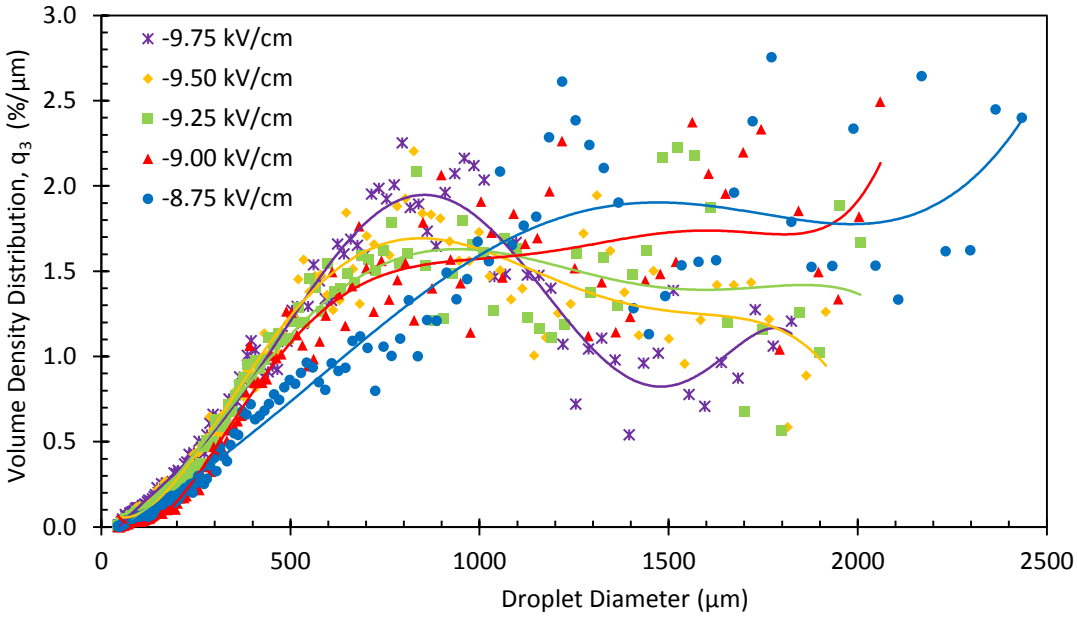


Figure 5.17 Effect of the electrostatic field strength of negative PDC fields (50 Hz) on the volume density distribution

Another major difference was that PDC fields, either positive or negative, produced a much wider spread of droplet sizes than DC fields. This can be clearly seen, for example, by comparing the volume density distributions that were generated using PDC fields (Figures 5.16 and 5.17) with those that were generated using DC fields (Figures 5.12 and 5.13). A further difference between PDC and DC fields was that much larger changes in field strengths were needed when using PDC fields to effect observable changes in the droplet size distribution. For example, a 0.17 kV/cm interval was needed when using positive PDC fields compared to only 0.13 kV/cm when using positive DC fields and a 0.25 kV/cm interval was needed when using negative PDC fields compared to only 0.13 kV/cm when using negative DC fields.

It should be noted that these results are in contrast to those of He, Chang and Baird (1997) who reported that PDC and DC fields with comparable field strengths produced virtually the same droplet sizes. This difference was traced to the manner in which these investigators carried out their experiments. They fed the aqueous solutions through an unshielded nozzle located in between two parallel electrodes and thus, the feed droplets that they measured were essentially being ripped out by the electrostatic force. Clearly, the same field strength, whether DC or PDC, would have exerted comparable electrostatic force and hence, generated equivalent droplet sizes. This was easily replicated in the current work when the shielding of the feed nozzle was momentarily removed.

Clearly, the results of the present study show that PDC fields, particularly negative fields, are less effective than DC fields in dispersing droplets. This was found to be due to the difference in the nature of the electrostatic force that is generated by these fields. Whereas DC fields apply a steady electrostatic force, PDC fields apply an intermittent electrostatic force owing to the periodic relaxation time between pulses. This relaxation time appears to hinder the migration of charges through the organic phase and allows some interfacial charge to periodically dissipate from droplet surfaces and thus, weaken interfacial polarisation and consequently weakening its contribution to droplet dispersion. It was therefore clear that an investigation of the effect of the frequency of the applied field was warranted.

#### *5.3.2.2. Effect of the Frequency of PDC Fields*

The investigation was carried out at constant field strengths of 5.17 kV/cm and −9.50 kV/cm for positive and negative PDC fields, respectively, and the frequencies were systematically varied between 20 and 60 Hz. Figures 5.18 and 5.19 show the relationship between the frequency and the Sauter mean diameters for positive and negative PDC fields, respectively. The most prominent feature of the plots is that a frequency of 40 Hz produced the finest droplets, whether the applied field was positive or negative. The use of either lower or higher frequencies than this value yielded larger droplets.

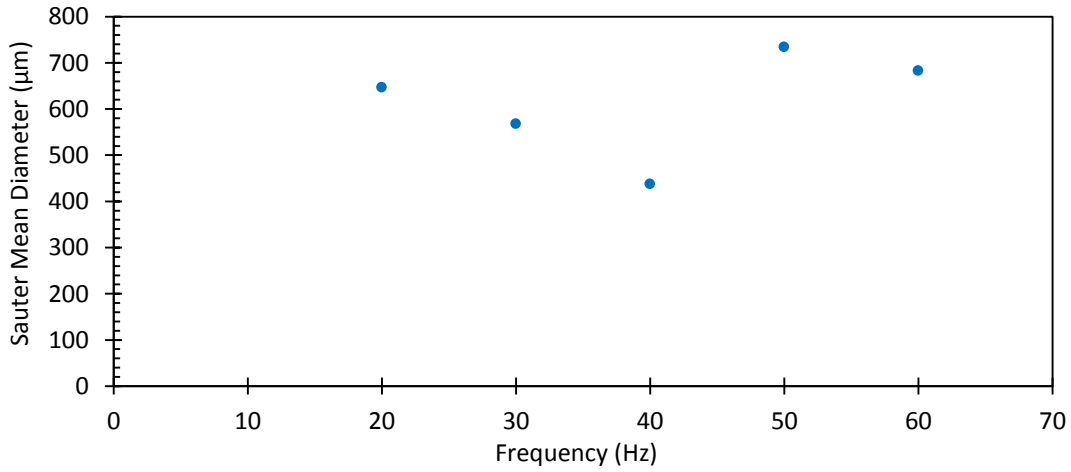


Figure 5.18 Effect of the frequency of positive PDC fields (5.17 kV/cm) on the Sauter mean diameter of the droplet distribution

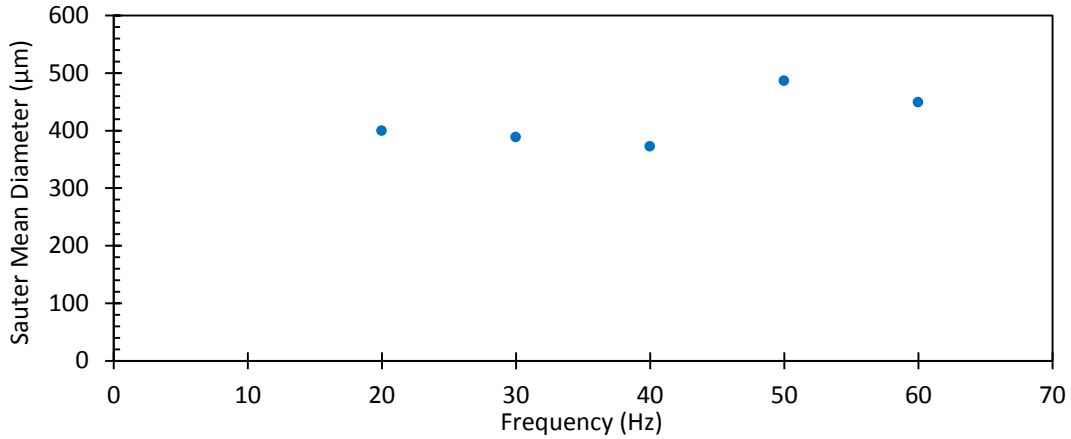


Figure 5.19 Effect of the frequency of negative PDC fields (-9.50 kV/cm) on the Sauter mean diameter of the droplet distribution

Analyses of the videos of the dispersions revealed that the length of time that the field is on and off (pulses), and thus the period by which a droplet is subjected to electrostatic stress and relaxation, as well as the rate by which these occur as shown diagrammatically in Figure 5.20, have a significant effect on the dispersion of droplets. That is, at 40 Hz, the droplets achieved what appeared to be their maximum elongation for the given field strength at a fast enough rate to lead to dispersion and consequently slightly favoured necking and irregular mechanisms of dispersion over jetting. At lower frequencies, they appeared to still achieve their maximum elongation but in what appeared to be a gentler manner of elongation. This appeared to slightly favour jetting over irregular or necking dispersion mechanisms leading to the production of both fine and large droplets. Higher frequencies, on the other hand, provided insufficient time for the droplets to achieve maximum elongation and thus, were less favourable to necking and irregular mechanisms of dispersion.

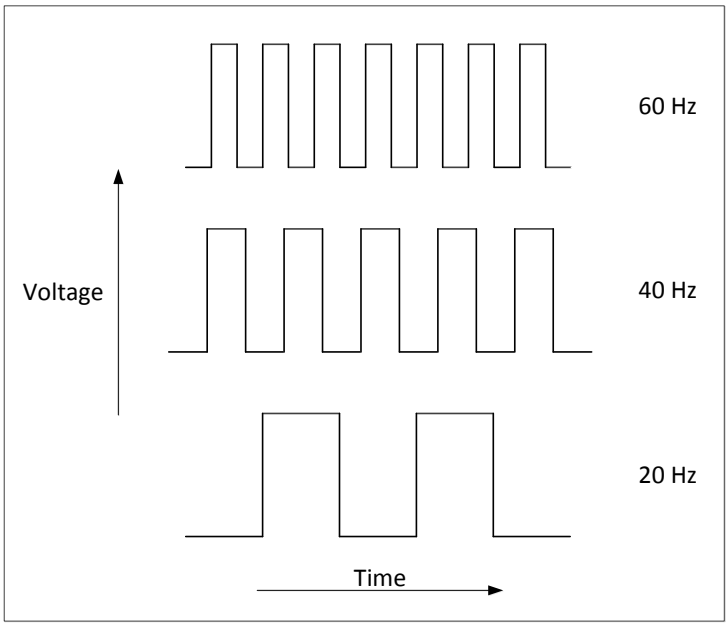


Figure 5.20 Relative difference in the theoretical voltage waveforms generated by PDC fields at various frequencies

Overall, PDC fields, even with higher field strength, yielded significantly larger droplets than DC fields. For example, as shown in Figure 5.10, the Sauter mean diameter of the dispersion obtained at 4.37 kV/cm DC was 401 μm. In contrast, the Sauter mean diameter of the dispersion at 5.17 kV/cm PDC was 438 μm. The trend is the same with corresponding negative fields.

Furthermore, PDC fields yielded wider droplet dispersions than DC fields. This can be clearly seen when the volume density distributions for PDC fields (Figures 5.21 and 5.22) are compared with those of DC fields (Figures 5.12 and 5.13).

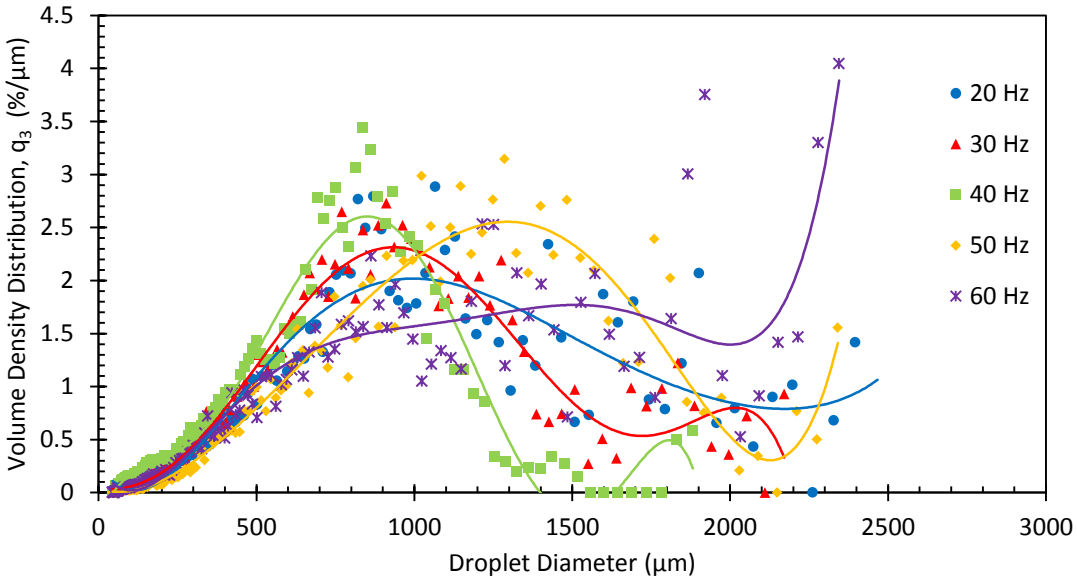


Figure 5.21 Effect of the frequency of positive PDC fields (5.17 kV/cm) on the volume density distribution

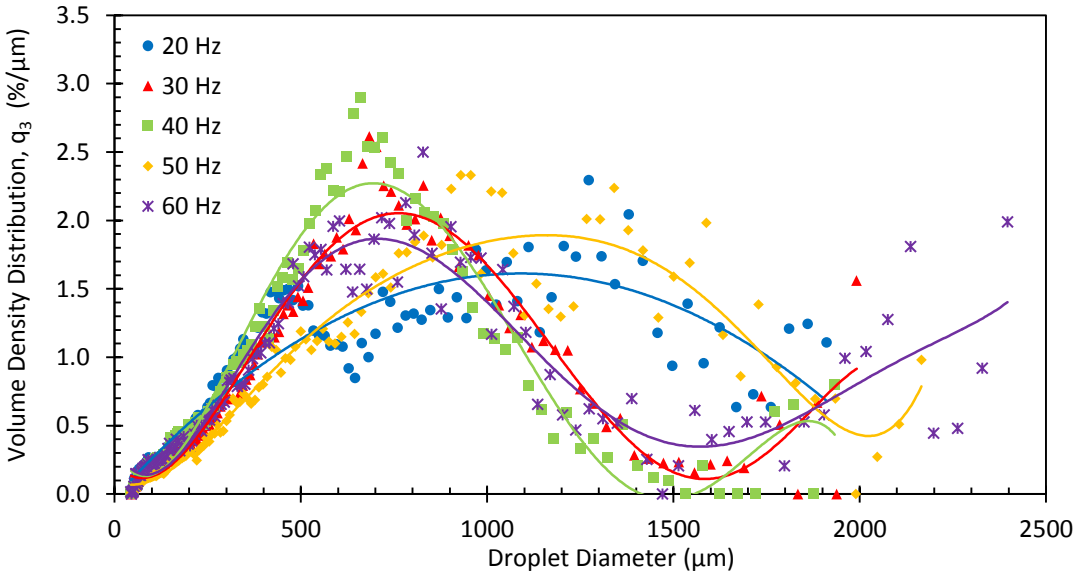


Figure 5.22 Effect of the frequency of negative PDC fields (-9.50 kV/cm) on the volume density distribution

This was clearly owing to the different nature of the electrostatic force generated by these types of fields. It appeared that the intermittent relaxation of the electrostatic stress that is imposed on the droplets as well as on the migration of charges, which is essential in the operation of interfacial polarisation, makes PDC less effective in dispersing droplets than DC fields.

### 5.3.3. Effect of AC Fields on Droplet Dispersion

The appropriate range of AC fields at 50 Hz, which is the frequency of the mains power supply in Australia and therefore used as the default, was found to be 2.5 – 3.5 kV/cm,

which is considerably lower than either DC (~4.0 – 4.5 kV/cm) or PDC fields (≥5.0 kV/cm), giving it a distinct practical advantage in relation to electrostatic solvent extraction. Similar to DC and PDC fields, the size of the dispersed droplets was found to be largely a function of the field strength, indicating that the droplet dispersion is a result of the electrostatic force imparted on the droplet. Unlike DC and PDC fields, however, wherein the droplets were observed to disperse through all various dispersion mechanisms, the dispersion of droplets under AC fields occurred mainly by necking and jetting and one can be made to predominate over the other by adjusting the frequency of the field. Details follow.

#### *5.3.3.1. Effect of the Strength of AC Fields*

As with other field types, increases in the strength of AC fields resulted in decreases in droplet size as the plots of the Sauter mean diameter against field strength (Figure 5.23) as well as the volume density distribution (Figure 5.24) clearly show. Unlike DC and PDC fields, however, wherein this trend was primarily owing to decreases in the number of medium and large droplets (>300 μm) accompanied by increases in the number of small (<200 μm) droplets (Figures 5.10, 5.11, 5.14 and 5.15), the trend in AC fields was primarily owing to decreases in the number of large droplets (>500 μm) accompanied by increases in the medium sized (~300 – 400 μm) droplets. The number of the small (<200 μm) sized droplets hardly changed (Figure 5.23). The overall effect was a much narrower droplet size distribution.

The same figures show that the whole range of AC field strength that was investigated generated far greater proportion (>50%) of the smallest sized droplets (<100 μm) as well as those in second smallest sized (100 – 200 μm) range (~30%) than DC and PDC fields, whether negative or positive. For example, the highest percentage of droplets in the smallest sized range with DC (Figures 5.10 and 5.11) and PDC (Figures 5.14, 5.15) fields were approximately just over a third (~35%) and they were only achieved at the highest field strengths with either types of fields. This difference in droplet size distribution was also evident in the total number of droplets that fitted within the camera field of view per measurement. For instance, all AC fields strengths used generated around 70 000 droplets per measurement. In contrast, DC and PDC fields generated only between 11 000 – 30 000 droplets over the range of field strengths used. In addition, AC fields (Figure 5.23) produced far fewer of the large droplets (>500 um) than DC (Figures 5.10 and 5.11) and PDC (Figures 5.14 and 5.15) fields. Clearly,

therefore, AC fields generated much smaller droplets than any of the other fields types investigated, which essentially constitute all electrostatic field types.

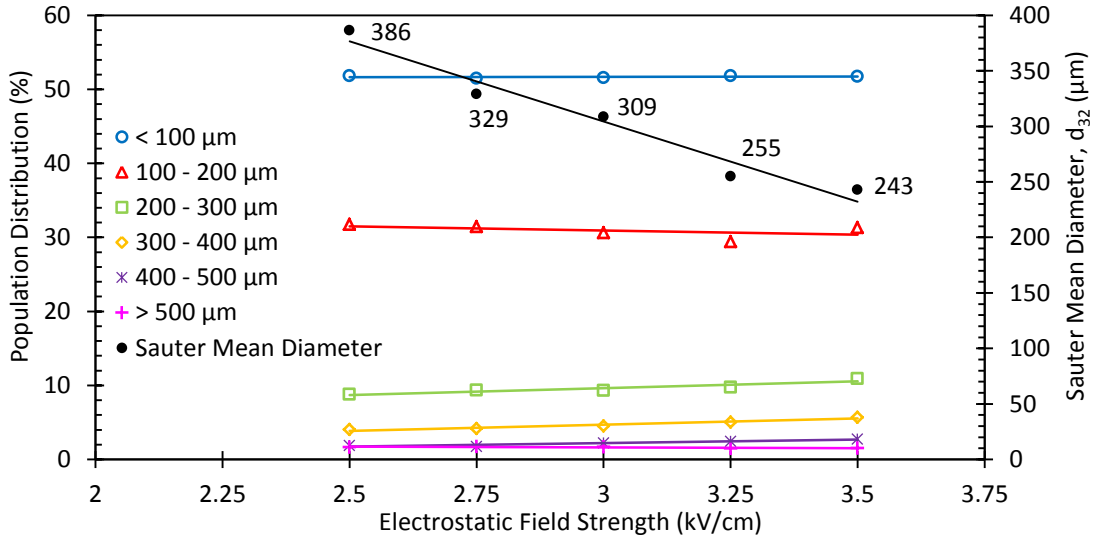


Figure 5.23 Effect of the electrostatic field strength of AC fields (50 Hz) on the population distribution and the Sauter mean diameter

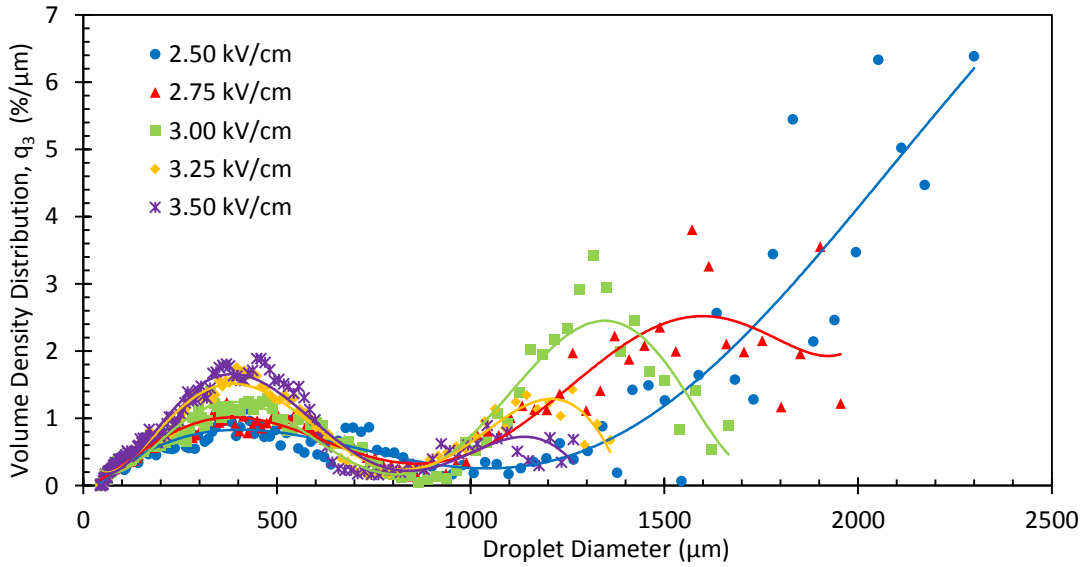


Figure 5.24 Effect of the electrostatic field strength of AC fields (50 Hz) on the volume density distribution

Unlike DC and PDC fields, wherein all mechanisms of droplet dispersion were observed, the dispersion of droplets under the influence of AC fields occurred mainly by either necking or jetting and, sometimes, through a combination of necking and jetting. As with the other field types, however, there was no observable relationship between the prevalence of a particular droplet dispersion mechanism and field strength.

### 5.3.3.2. *Effect of the Frequency of AC Fields*

The effect of variation of frequency on population distribution is summarised in Figure 5.25 and shows that decreases in the frequency from 50 to 20 Hz resulted in slight increases in the droplet size but an increase in the frequency from 50 to 60 Hz had no significant effect. Visual analysis of the recorded videos of the dispersions revealed that the former was largely owing to the higher amplitude of elongation of the droplets as a consequence of the longer period that they were subjected to an electrostatic force of one polarity before shifting to the opposite polarity. Figure 5.26 shows, for example, the relative amplitudes of elongation of droplets at (a) 20 Hz and (b) 60 Hz. It is therefore understandable that the overall effect was more evident in the number of smallest and largest droplets in the population distribution (Figure 5.25).

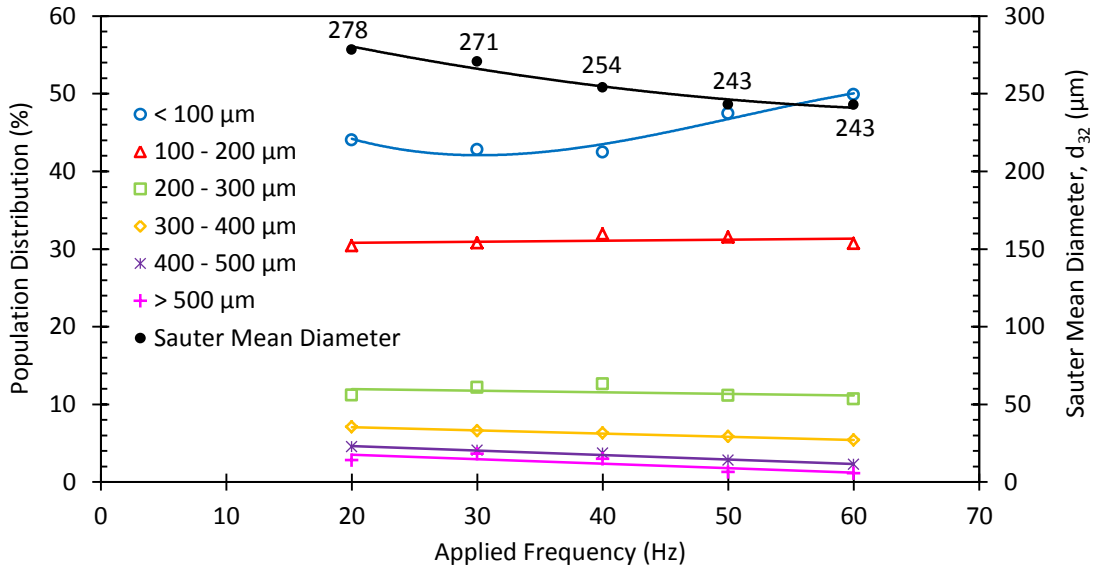


Figure 5.25 Effect of the frequency of AC fields (3.5 kV/cm) on the population distribution and the Sauter mean diameter

The lack of significant difference in the droplet size of those under 50 Hz and 60 Hz appeared to be owing to hydrodynamic hindrance. As this relates to droplet motion, its discussion is deferred to the following chapter.

Figure 5.26 also shows the presence of un-elongated droplets, which was evident at any given instance during the dispersion experiment. The main difference between the elongated and un-elongated droplets was their mode of motion. Thus, this too is discussed in the following chapter.

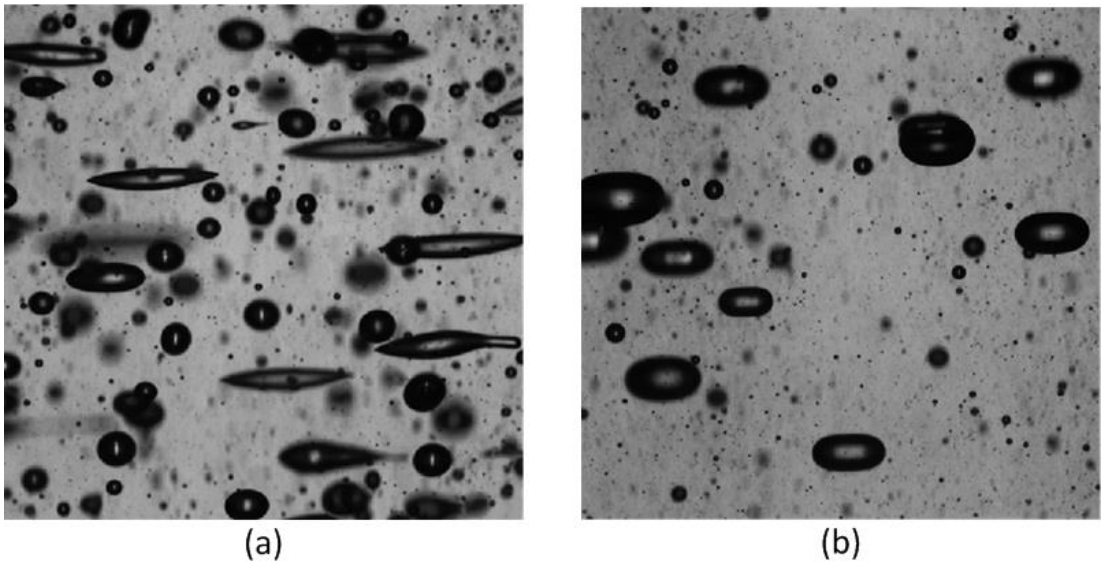


Figure 5.26 Typical droplet dispersions produced by AC fields (3.5 kV/cm) at the peak of the voltage cycle showing the maximum amplitudes of droplet elongation with (a) 20 Hz, and (b) 60 Hz

Changing the frequency of the applied field shifted the mechanism by which droplets dispersed. The use of low frequencies favoured necking, resulting in narrower droplet size distribution, while the use of high frequencies favoured jetting, resulting in wider droplet size distribution. This shift in the mechanism of droplet dispersion is clearly evident in the volume density distribution (Figure 5.27). At 20 Hz, for example, both the left and right side of the curve moved toward the centre while the opposite happened at 60 Hz.

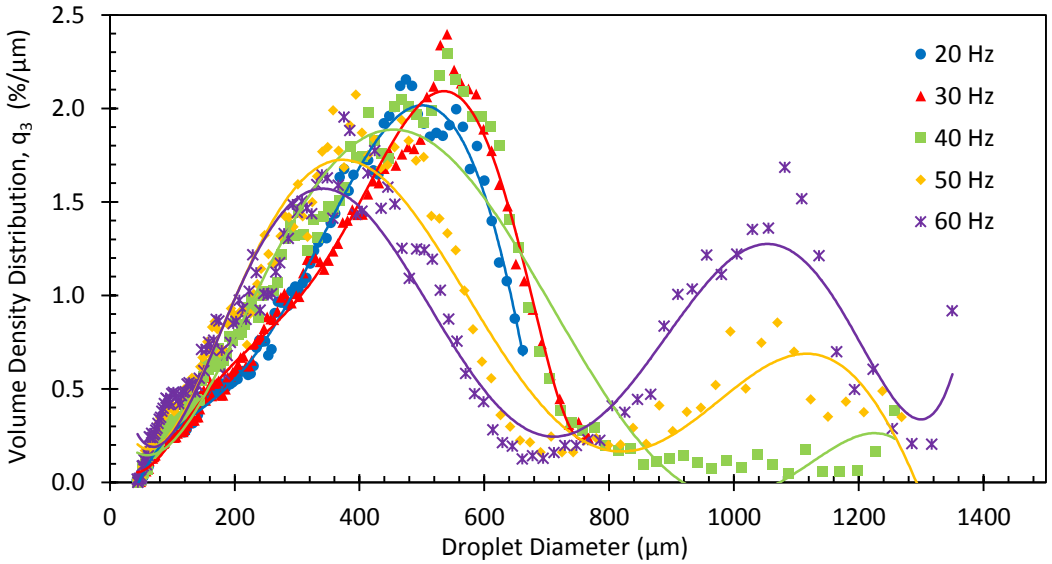


Figure 5.27 Effect of the frequency of AC fields (3.5 kV/cm) on the volume density distribution

This behaviour was observed to be a direct consequence of the period for which a droplet is subjected to electrostatic stress (polarised) and hence the amplitude and period of elongation. The reason is, since the size of a droplet is a function of the strength of the field, a droplet is either stable or not under a given field strength. If not, it will disperse and, under the influence of AC fields, it does so mainly by necking or jetting. Subjecting it to a low frequency is essentially allowing it to achieve much higher amplitude of elongation over a longer period of time, which understandably aids orientational polarisation and hence, necking. Conversely, at high frequency, the period for which a droplet is subjected to electrostatic stress is too short and thus, the amplitude of elongation that it can achieve in a given cycle may also be lower. This leaves jetting as a way of gaining stability.

The presence of some large droplets at the lowest frequency (20 Hz), wherein necking was clearly the dominant mechanism of droplet dispersion, was owing to the occurrence of some highly elongated large droplets that exhibited jetting prior to necking within one voltage cycle. An example is shown in Figure 5.28. This series of photographs show that one conical end of an elongated droplet ejected ultra-fine droplets before dispersing by necking forming three medium-sized daughter droplets. Under AC fields, this droplet dispersion behaviour was observed only at frequencies below 50 Hz and its prevalence increased with decreases in frequency.

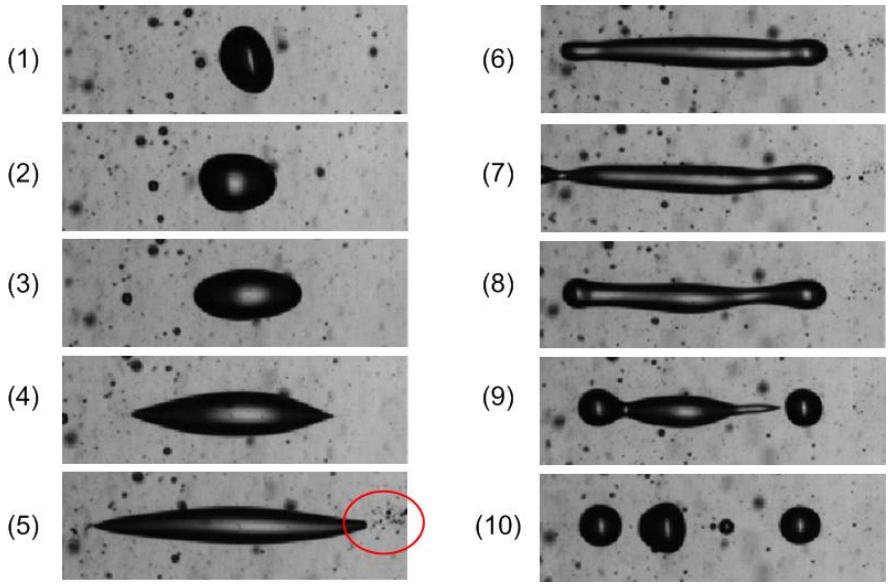


Figure 5.28 A droplet with a large amplitude of elongation sometimes exhibited jetting (shown in the red circle) prior to necking within one voltage cycle in the presence of an AC field (3.5 kV/cm, 20 Hz)

It follows that the apparent difference in the effect of the frequency of AC fields to those of PDC may be attributed to their different waveforms. PDC fields (Figure 5.20)

essentially subject droplets as well as incident electrons to periodic electrostatic force and relaxation and hence the effect on dispersion mechanism, as discussed in the previous section. AC fields on the other hand, which cycle between positive and negative polarities passing only fleetingly to zero voltage, as shown diagrammatically in Figure 5.29. In terms of electrostatic force, this means the droplets are constantly subjected to electrostatic force but at periodically changing polarity. It is reasonable to suggest that the continually changing polarity, and thus the direction of migrating charges, would result in greater migration of electrons to the liquid-liquid interface, favouring interfacial polarisation than that, for example, in the presence of PDC fields and hence more effective droplet dispersion.

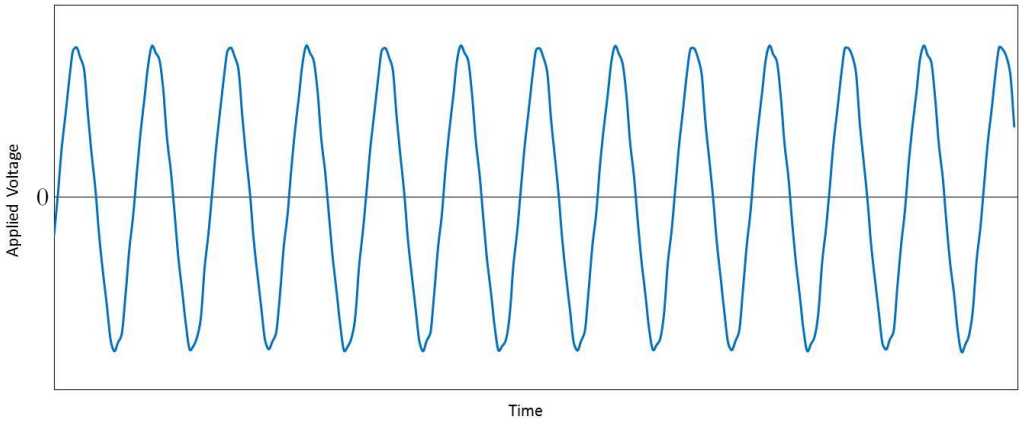


Figure 5.29 Typical voltage waveforms generated by AC fields

The dispersion of droplets mainly by necking and jetting under influence of AC fields may explain the general view in the literature that these are the only mechanisms by which electrostatic fields disperse droplets. Another contributing factor may be the fact that most studies were focussed on the application of the phenomenon rather than the mechanism by which it happens. A further factor may be that the availability of high speed cameras with laser backlighting is relatively recent. In fact, no study using this technique has been reported yet in the literature except for that of the present author.

## 5.4. CHAPTER SUMMARY

In this chapter, the effect of various types of electrostatic fields (negative and positive DC, negative and positive PDC and AC) and their properties on droplet dispersion were investigated. The main findings are:

- All electrostatic field types—positive and negative DC, positive and negative PDC and AC—allowed the dispersion of aqueous droplets in an organic phase

owing to the imposition of orientational polarisation beyond that which the surface tension could withstand. Interfacial polarisation, when present, provided additional favourable force. This was evident in the relationship between type, strengths of the applied field, droplet sizes and size distributions, which decreased with increases in field strength.

- In addition to previously known mechanisms by which droplets disperse under the influence of electrostatic fields, namely necking and jetting, two additional mechanisms were observed in all field types, namely irregular and combination, and one additional mechanism under DC and PDC fields only, namely emulsion-like formation.
- The co-occurrence of dispersion and coalescence was observed in various dispersion experiments, which is contrary to the general view in the literature that a given field strength causes either dispersion or coalescence.
- The droplet size was observed to be largely a function of the field strength as there was always a range of droplet sizes for a given field strength but the frequency of the field, in the case of transient fields, had a small but measurable effect on both droplet size and spread of the dispersion. This indicated that how long and how often a droplet is subjected to a given strength of electrostatic stress contribute to its stability and the mechanism by which it disperses. The optimum frequency for PDC was 40 Hz and for AC was 20 Hz, which subject droplets to comparable stress. In the case of AC fields, for example, decreases in frequency favoured necking, resulting in slightly larger droplets but narrower size distribution. The opposite favoured jetting, leading to slightly finer droplets but wider size distribution.
- DC fields were more effective in inducing droplet dispersion than PDC fields, indicating that steady fields are more effective in imparting polarisation, either orientational or interfacial, and the relaxation time in transient fields appeared to allow the dissipation of interfacial charges hindering interfacial polarisation.
- Positive DC and PDC fields generated finer droplets with narrower size distributions than their corresponding negative fields owing to a greater contribution of interfacial polarisation.
- Overall, among all five field types, AC fields provided much finer droplets and narrower distributions at far lower field strengths.

# Chapter 6

# STUDY ON THE EFFECT OF ELECTROSTATIC FIELDS ON DROPLET AGITATION

## 6.1. INTRODUCTION

This chapter describes the study on the effects of various types of electrostatic fields (positive DC, negative DC, positive PDC, negative PDC, and AC) on droplet agitation, which refers to droplet oscillation, speed and zigzagging. Droplet speed refers to the speed of linear motion of a droplet regardless of its direction from totally horizontal to totally vertical. Droplet zigzagging refers to the periodically sharp turning linear motion, and is measured as the horizontal component of droplet speed.

The study was carried out by observing and measuring the droplet oscillation, speed, and zigzagging over a range of field strengths and, in the case of transient fields, frequencies. This knowledge is critical in determining the electrostatic field conditions that induce maximum droplet agitation, which is essential in the design and development of a commercial application of electrostatic solvent extraction (ESX).

## 6.2. MATERIALS AND METHODS

### 6.2.1. Reagents, Test Solutions and Equipment

The reagents used in this part of the work are the same as those in Chapter 5. For the convenience of the readers, they are copied here as follows: acetic acid (AR, Chem-Supply), sodium hydroxide (AR, Chem-Supply), standard Co(II) solution in nitric acid matrix (10 000 mg/L, Australian Chemical Reagents), cobalt sulphate heptahydrate (AR, Chem-Supply), sodium sulphate (AR, BDH), ShellSol® 2046 (Industrial Grade, Shell Chemicals), Cyanex® 272 (Industrial Grade, Cytec Australia), and sulphuric acid (98%, Sigma Chemicals). All reagents were used as supplied.

Two test solutions were used: a buffered (pH 5.5) Co(II) solution (300 mg/L) as the aqueous feed and Cyanex® 272 in ShellSol® 2046 as the solvent. This choice was to ensure consistency of the properties of the aqueous solution in both mass transfer experiments, such as those in Chapters 4 and 7, and characterisation of droplet dispersion in the previous chapter and droplet agitation in the present chapter.

The droplet column that was developed in Chapter 3.5 including its auxiliary equipment, which is illustrated in Figure 3.15, was used in this part of the study.

### 6.2.2. Preparation of Test Solutions

These too were prepared in the same way as those in Chapter 5 and copied here for the readers' convenience. The aqueous test solution consisted of Co(II) ions (300 mg/L) in an acetic acid/acetate buffer with a pH of 5.5. This was prepared by transferring the required volume of acetic acid, and masses of sodium hydroxide pellets and cobalt sulphate heptahydrate into a volumetric flask and dissolving in a minimum amount of distilled water. A mass of sodium sulphate was also added to make its concentration in the final solution 0.2 M. This was to increase the ionic strength to facilitate good phase separation as well as to avoid third phase formation (Fu & Golding 1988). The volume was then adjusted so that it was just under the required volume. The solution was mixed thoroughly, allowed to equilibrate at room temperature and made to the final volume. The pH was measured and recorded.

The organic solution was prepared by transferring the required volume of Cyanex® 272 (10% v/v) into a volumetric flask and filling to the mark with ShellSol® 2046. The stripping solution was prepared by transferring the required volumes of sulphuric acid (24.5 g/L) and cobalt sulphate (20.5 g/L Co(II)) into a volumetric flask, allowing the solution to equilibrate, and filling to the mark with distilled water.

### 6.2.3. Procedures for Droplet Agitation Experiments

This set of experiments was designed to allow the observation and measurement of the effects of electrostatic fields on droplet oscillation, speed, and zigzagging. The experiments were carried out following the general procedures for droplet column experiments described in Chapter 3.6.1. The raffinates were not collected because these experiments did not involve measurement of mass transfer. The imaging equipment was used following the procedures described in Chapter 3.6.2. The laser and high-speed camera were positioned approximately two-thirds down the electrodes to allow good visual observation of droplet agitation within the population of secondary daughter droplets.

An additional set of experiments was carried out to measure the speed of droplets in the absence of a field to allow comparison with those under the influence of electrostatic fields. This was achieved by using the same procedures as those under the influence of

electrostatic fields except that, after generating the dispersion, the field was turned off and the droplet speed was measured. This ensured that the droplet dispersion in this set of experiments had a comparable size distribution to those in the presence of electrostatic fields and thus, allowed a good comparison of droplet speeds.

### 6.2.4. Analytical Techniques

The analytical techniques used in this part of the study were the same as those in Chapter 5.

### 6.2.5. Data Acquisition and Analysis

The FastCam software of the imaging equipment was used to replay recorded images of droplet oscillation at reduced speeds (1 – 25 frames per second). This facilitated clear observation of droplet oscillation and enabled measurement of the rate of oscillation under the various experimental conditions that were investigated. The amplitudes of elongation of the droplets were measured as the ratio of a droplet's major-to-minor axis. The frequency of oscillation was measured by calculating the number of frames required to complete a full oscillation, given that the camera frame rate was known. Screenshots of droplet behaviour, including successive images to show changes in droplet behaviour, were captured. When necessary, a grid mesh was used to provide scale.

The effect of electrostatic fields on the droplet speed was determined by plotting the droplet diameter against the average speed as a function of the field strength, and, in the case of transient fields, as a function also of the frequency. The average droplet speeds were determined using the VisiSize software (Chapter 3.6.2 discusses how the software is used). The average speeds of the droplets in this part of the work refer to the linear motions of the droplets regardless of their direction.

The effect of electrostatic fields on droplet zigzagging was determined by observing the droplets and calculating the horizontal component of the speeds of the droplets. For brevity and clarity, the horizontal component of the droplet speeds will be referred to simply as the horizontal velocity. The average horizontal velocities of the droplet population were then plotted as a function of the field strength and, in the case of transient fields, as a function also of the frequency. The horizontal velocities were calculated using the magnitude and angle of the droplet's velocity (Equation 9), which had been measured using the VisiSize software as described in Appendix B4. The magnitude and angle data were extracted from the Individual Particle Data (IPD) files

that were generated by the VisiSize software for each experimental run. In the case of DC and PDC fields, which do not involve an alternating electrode polarity, the average horizontal velocities towards the charged and earthed electrodes were also plotted.

$$V_{Horizontal} = \left| \frac{\pi \times \sin\theta}{180} \times V_{Measured} \right| \qquad \text{(Equation 9)}$$

Preliminary experiments revealed that there were observable variations in the data generated for the same set of experimental conditions and, therefore, ten experimental runs were recorded for each of these sets to generate a representative profile. The imaging equipment was optimised to record the diameters of a minimum of 10 000 droplets as a representative of the total population of droplets per experiment. The average values for each size fraction from ten experimental runs were used to determine the effect of the experimental conditions on the droplet speed and horizontal velocity and therefore, each curve in the graphs represents the average of ten experimental runs. Figures 6.1 and 6.2 show a typical spread of the data in these experiments. For the sake of readability, error bars are no longer included in each of the graphs.

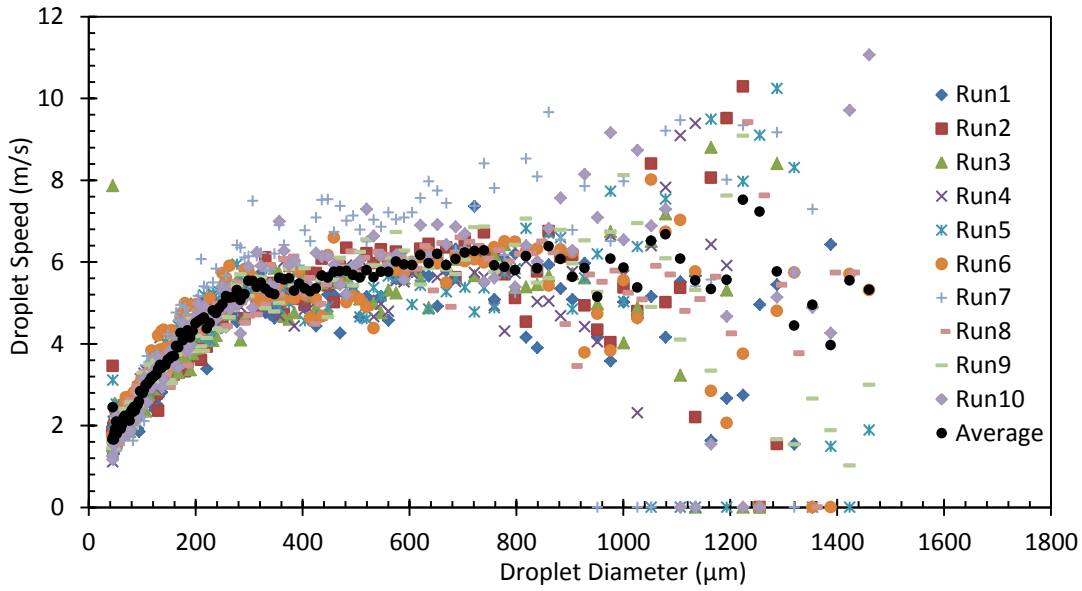


Figure 6.1 Raw data from experiments to investigate the effect of a DC field (4.25 kV/cm) on the droplet speed

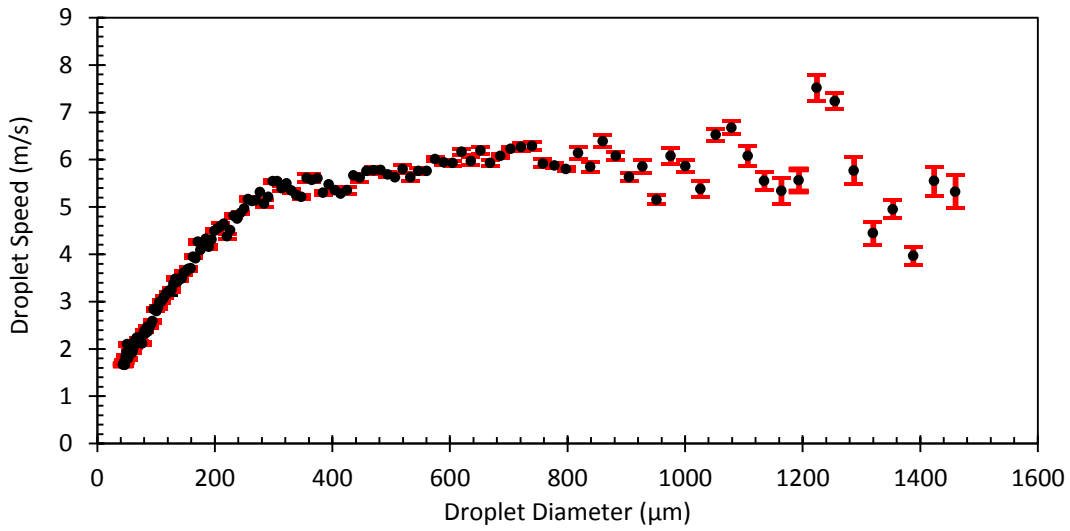


Figure 6.2 Average values from experiments to investigate the effect of a DC field (4.25 kV/cm) on the droplet speed with error bars of ±1 standard error

## 6.3. RESULTS AND DISCUSSIONS

The main effects of electrostatic fields on droplet agitation are to induce droplet oscillation, as well as alter droplet linear speed and direction. The former is largely owing to orientational polarisation while the latter is largely owing to interfacial polarisation. Orientational polarisation arises owing to the polar species in the droplets. Interfacial polarisation arises owing to accumulated charges on the surface of the droplets either through contact with electrodes or migration of incidental charges across poorly conducting liquids such as solvents.

For clarity, the three main effects of electrostatic fields on droplet agitation are discussed in separate sections as follows:

### 6.3.1. Effect of Electrostatic Fields on Droplet Oscillation

Theoretically, droplet oscillation enhances mass transfer in SX in two main ways. Firstly, the periodic droplet elongation causes periodic increases in the interfacial area, providing more sites at the liquid-liquid interface for mass transfer to occur. Secondly, the periodic elongation and contraction enhances mixing within droplets facilitating continual replenishment of the interface with fresh reactant species from within a droplet.

The effect of electrostatic fields on droplet oscillation was investigated by observing, recording and analysing the behaviour of droplets under the influence of electrostatic fields over a range of field strengths and, in the case of transient fields, a range of

frequencies also. The main finding was that droplets oscillated between a spherical and elongated shape in response to the electrostatic force imparted by transient fields. It follows that droplets oscillate only when the applied field is either PDC or AC.

#### *6.3.1.1. Effect of DC Fields on Droplet Oscillation*

Droplets elongated but did not oscillate when subjected to a range of either positive (4.00 – 4.37 kV/cm) or negative (−4.12 – −4.50 kV/cm) DC fields (Figure 6.3). Increases in the field strength led to increases in both the population of elongated droplets and the amplitude of elongation. Generally, the amplitude of elongation increased with the droplet diameter. Changing the polarity of the applied fields had no observable effect. This behaviour is consistent with the so-called orientational polarisation as the cause of the droplet elongation.

Orientational polarisation refers to the alignment of the polar species in the direction of the electrostatic field lines of an external field (Inculet 1973, Pohl 1973). The electrostatic force exerted by the aligned species acts against the droplet's interfacial tension. Since larger droplets have greater amounts of polar species and, hence, stronger electrostatic force between them and the external field, it makes sense that they exhibited greater elongation.

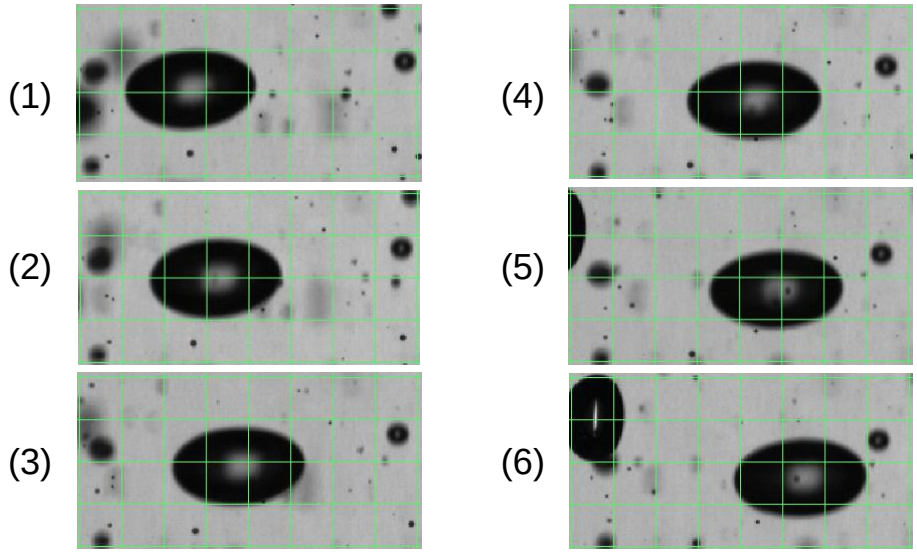


Figure 6.3 A constantly elongated droplet under the influence of a positive DC field (4.12 kV/cm) as it falls through the column (grid = 500 μm).

As the elongation of droplets under DC fields is a consequence of a constant electrostatic force that is imposed on the droplets, the lack of oscillation under this field type was therefore not unexpected. This finding is in contrast to that reported by Stewart and Thornton (1967), who claimed that DC fields induced droplet oscillation. It

is difficult to reconcile the difference because while they mentioned observing an oblate-prolate type oscillation with a spherical shape as an intermediate, they provided neither details nor visual evidence. It should be noted, however that there were significant differences in the experimental methods between theirs and the present study. For example, they used droplets of pure water with very low conductivity (AnalaR grade), which were charged as they were introduced into the column, while the present study used droplets of aqueous solution with substantially high ionic strength, which is typical of aqueous feed to hydrometallurgical SX, and were introduced into the column uncharged. Also, while they studied the behaviour of single relatively large droplets at a time—a minimum of ~0.21 cm diameter, which is approximately the maximum of those observed in the present study—the current work studied the behaviour of a large population of droplets. It is difficult to identify whether any of these factors could account for the difference. While it is of academic interest to determine whether any of these could explain the different finding, it is outside the scope of the present study, given it is directed towards understanding the behaviour of populations of droplets under conditions that are applicable to hydrometallurgical SX.

The occurrence of droplet behaviours that were not consistent with the general trend, such as large droplets that were not elongated and small droplets with significantly higher amplitude of elongation than larger droplets, is worth mentioning. At this point of this thesis, it is sufficient to say that this was found to be partly owing to the non-uniform conditions that each droplet is subjected to. The difficulty of maintaining uniform electrostatic field conditions across condensed fluids is well recognised in the field of electrohydrodynamics, and is perhaps aptly summarised by Melcher and Taylor (1969), when they wrote in a comprehensive review of the topic that electrostatic effects in fluids are known for their vagaries. It is not hard to imagine that when a population of droplets is subjected to a given electrostatic field, some droplets would be subjected to higher field effects owing to their position relative to the electrodes as well as relative to other droplets that could be shielding them or otherwise. It is also worth mentioning at this point of this thesis that the possibility of the existence of a different form of polarisation, such as interfacial polarisation as mentioned in the previous chapter, may also be a contributing factor.

#### *6.3.1.2. Effect of PDC Fields on Droplet Oscillation*

Subjecting droplets to a range of field strengths (5.00 – 5.67 kV/cm and -8.75 – -9.75 kV/cm) and frequencies (20 – 60 Hz) of PDC fields resulted in droplet oscillation. Increases in the strength of the applied field resulted in increases in both the amplitude of oscillation and the population of oscillating droplets. Similarly, the amplitude of oscillation increased with increases in the droplet diameter owing to increases in the amount of polar species within the droplet. This indicated that, as with DC fields, the droplet elongation is primarily owing to orientational polarisation.

Increases in the pulsing frequency of the applied field resulted in increases in the frequency of oscillation, indicating that droplet oscillation is a direct consequence of the periodic polarisation of the droplet owing to the periodic application of electrostatic force. For example, when a pulsing frequency of 50 Hz was applied, the droplets required 10 frames to complete one oscillation when recorded at 500 frames per second. This clearly showed that the periodic pulsing of the electrostatic force induced the periodic elongation and contraction of the droplets.

Photographic analysis revealed that the maximum amplitude of elongation of the oscillating droplets increased with decreases in the pulsing frequency. This is shown, for example, in Figure 6.4, which is a comparison of the amplitude of elongation of droplets at low (20 Hz) and high (60 Hz) frequencies. The photographs also show that the droplets that were subjected to lower frequencies formed conical ends when they reached the maximum amplitude of oscillation. This indicated that this pulsing period allowed the droplets more time to respond to the electrostatic force that is imparted before the field is pulsed off and the droplet relaxes. These observations indicated that hydrodynamic factors affect the amplitude of oscillation of droplets and hence, mass transfer. Therefore, to achieve optimum mass transfer in terms of droplet oscillation, a compromise between the strength and frequency of the applied field would need to be determined.

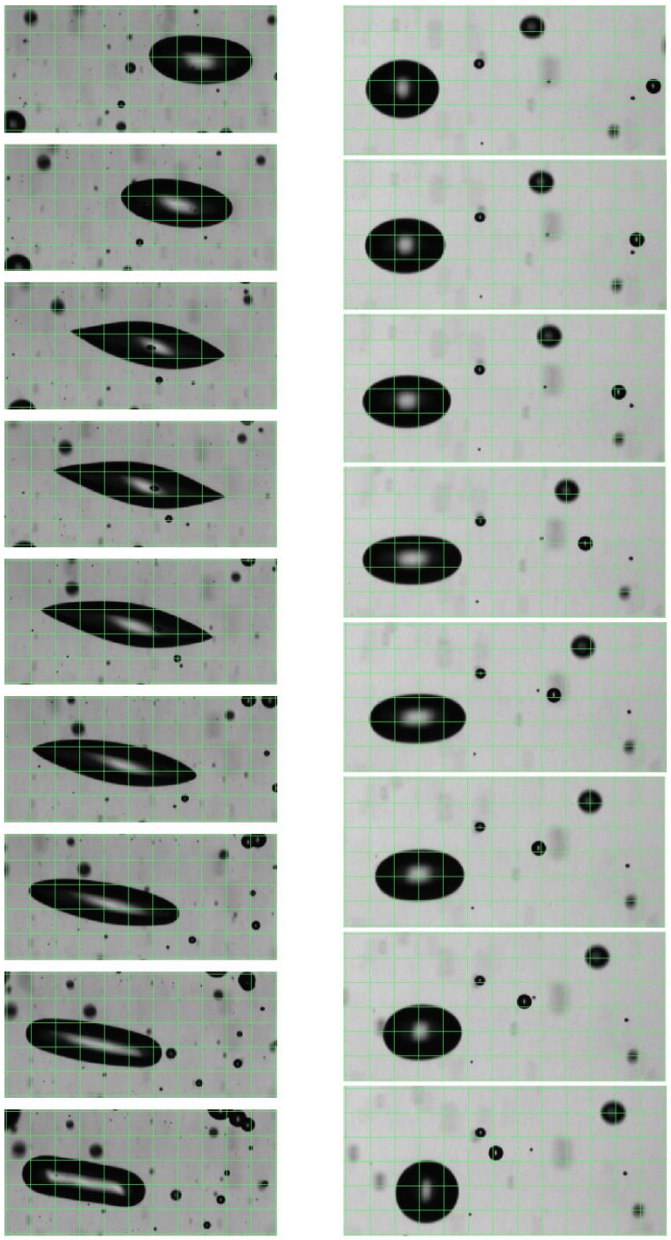


Figure 6.4 Droplet oscillation in the presence of PDC fields (5.33 kV/cm) with a frequency of (a) 20 Hz, and (b) 60 Hz (grid = 500 μm)

The possibility that natural droplet oscillation was a contributing factor to these observations was explored by carrying out a separate set of experiments under comparable conditions except that the applied field was turned off after a dispersion had been generated to allow recording of droplet behaviour in the absence of a field. Any droplet oscillation that occurs under these conditions could, of course, be attributed only to natural droplet oscillation. None was observed, clearly indicating that natural oscillation was not a significant factor under these experimental conditions.

#### 6.3.1.3. Effect of AC Fields on Droplet Oscillation

Similar to the effect of PDC fields, droplets oscillated when subjected to the influence of AC fields, and the amplitudes of their oscillation were generally proportional to their diameters. Increases in the field strength (2.50 – 3.50 kV/cm) resulted in increases in both the amplitude of the oscillation and the population of oscillating droplets. This indicated that the oscillation under the influence of AC fields is owing to the periodic cycling of the polarity and, hence, the periodic electrostatic force between the applied field and the droplets.

Variation of the frequency of AC fields had two notable effects. Firstly, increases in the frequency (20 – 60 Hz) of the applied field resulted in increases in the frequency of oscillation. This is similar to the effect of PDC fields. The difference, however, was that, for the same applied frequency, the oscillation frequency under the influence of AC fields was double of that under the influence of PDC fields. For example, when recording at 500 frames per second, a droplet under the influence of an AC field (50 Hz) required 5 consecutive frames to complete one oscillation. On the other hand, a droplet under the influence of a PDC field (50 Hz) required 10 consecutive frames to complete one oscillation. This is logical, given that, in AC fields, the voltage cycles from zero to positive and then to negative in one cycle, whereas in PDC fields, the voltage cycles only from zero to either positive or negative. This is clear evidence that droplet oscillation is induced directly by the periodic cycling of the electrostatic force.

Secondly, decreases in the frequency (60 – 20 Hz) resulted in increases in the maximum amplitude of oscillation. Figure 6.5 shows a comparison of the maximum amplitude of elongation of comparably sized droplets under comparable experimental conditions except that one was at low frequency (20 Hz) while the other was at high frequency (60 Hz). Clearly, decreases in the frequency led to increases in the length of the voltage cycles and hence the time that the droplets experience electrostatic force from the external field. Thus, similar to that in PDC fields, hydrodynamic factors play a role in optimising the effect of frequency on droplet oscillation and, hence, mass transfer.

The photographs in Figure 6.5 also show that, generally, the larger the droplet, the higher its amplitudes of elongation. In addition, a higher proportion of larger droplets exhibited oscillation than smaller droplets. These are further evidence that greater amounts of polar species within the droplet with increases in its diameter lead to greater orientational polarisation.

As with PDC fields, the oscillation of droplets under the influence of AC fields is characteristic of orientational polarisation. It is clear, therefore, that both the elongation of droplets under the influence of steady fields, such as DC fields, and periodic elongation and relaxation of droplets in response to the application of transient fields, as in the case of PDC and AC fields, are owing to electrostatically induced orientational polarisation.

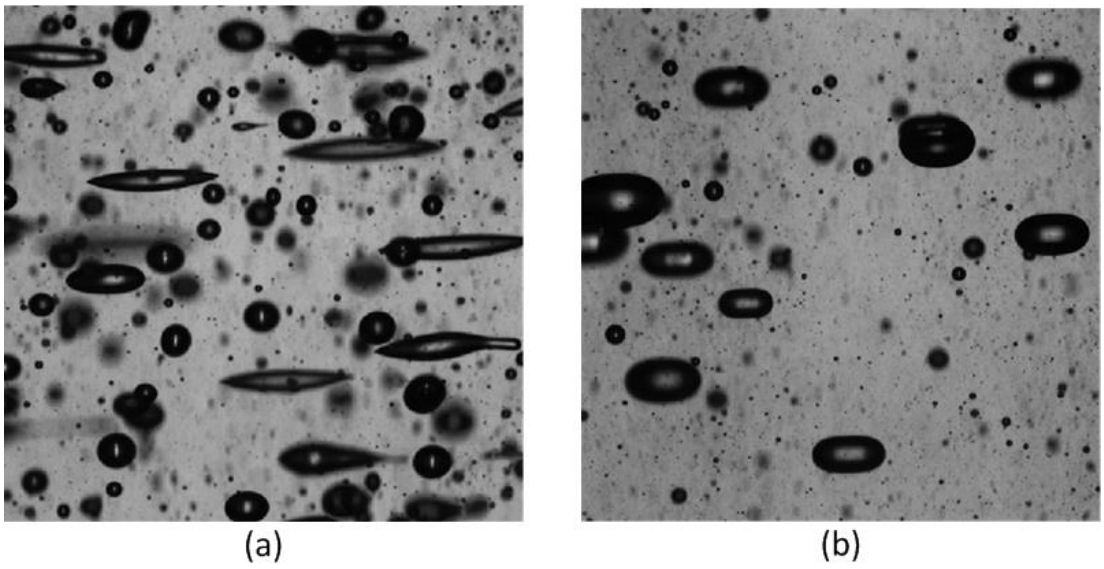


Figure 6.5 Typical droplet dispersions showing the maximum elongation of droplets typically induced by AC fields (3.5 kV/cm) at the peak of the voltage cycle with a frequency of (a) 20 Hz, and (b) 60 Hz

One distinct difference between the effects of PDC and AC fields in terms of droplet oscillation was that, under comparable conditions, AC fields generated a higher proportion of oscillating droplets than PDC fields. Similar to PDC fields, however, droplets that were not oscillating were also observed. It is reasonable to suggest that similar to DC and PDC fields, this may be at least partly attributed to the non-uniformity of the actual environment that each droplet is subjected to.

Finally, another significant observation in this part of the study was that some droplets of comparable spherical diameter exhibited noticeably different amplitudes of elongation within the same experiment (Figure 6.6). Given that these droplets have approximately the same number of polar species, this observation cannot be attributed to differences in the amount of orientational polarisation. Both observations indicate that another form of polarisation was in operation.

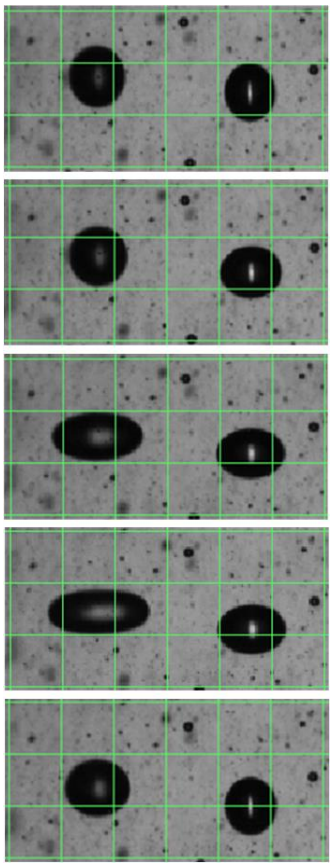

Figure 6.6 Two droplets with comparable spherical diameters exhibit different amplitudes of elongation when oscillating in the presence of an AC field (3.5 kV/cm, 60 Hz) (grid = 500 μm)

This will become more evident when the effect of the electrostatic fields on droplet speed and zigzagging is considered in the sections that follow (Chapter 6.3.2 and 6.3.3).

### 6.3.2. Effect of Electrostatic Fields on Droplet Speed

The speed of a droplet refers to its linear motion regardless of its direction, which may be horizontal, vertical or anything in between. The literature review revealed that an increase in the speed of the dispersed droplets has two main benefits for enhancing mass transfer in SX. Firstly, it increases the turbulence in the diffusion region of the continuous phase around a droplet and, secondly, it increases a droplet's Reynolds number, promoting droplet oscillation.

The effect of electrostatic fields on the droplet speed was investigated by measuring the speed of the droplets under the influence of electrostatic fields over a range of field strengths and, in the case of transient fields, a range of frequencies. It was found that the droplet speed was enhanced in the presence of electrostatic fields owing to an electrostatic force imparted by the external fields. This electrostatic force may be seen as analogous to gravitational force when no field is applied. In essence, similar to the effect

of gravitational force, droplets reach a terminal speed that is induced by the electrostatic force under a given set of conditions.

#### 6.3.2.1. *Effect of DC Fields on Droplet Speed*

The effects of DC fields on the speed of droplets were investigated by observing their behaviour and measuring their speed under the influence of a range of positive (4.00 – 4.37 kV/cm) and negative (-4.12 – -4.50 kV/cm) field strengths.

Analyses of the recorded videos revealed that the application of DC fields led to higher droplet speeds compared to those in the absence of a field. Measurements of the speeds showed that the droplets reached a field-induced terminal speed that is analogous to but of greater magnitude than that achieved under the influence of gravity only. These are shown in Figures 6.7 and 6.8 for positive and negative fields, respectively.

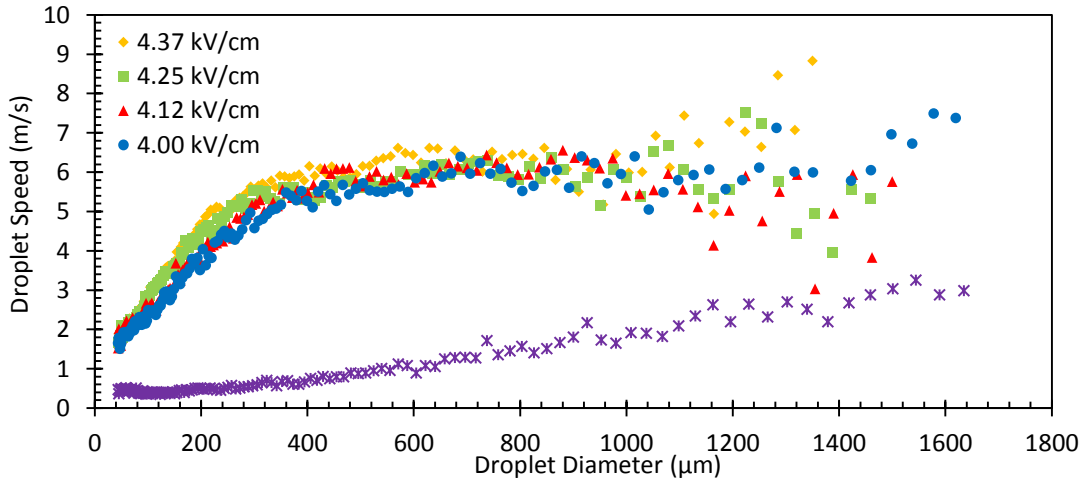


Figure 6.7 Effect of the field strength of positive DC fields on droplet speed

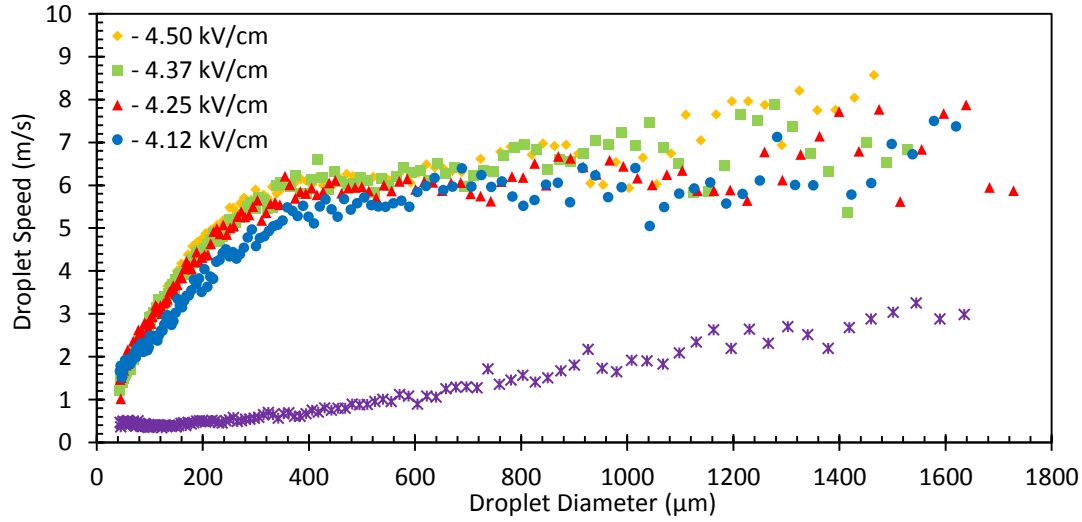


Figure 6.8 Effect of the field strength of negative DC fields on droplet speed

The relationship between the droplet diameter and speed for a given field strength was not uniform over the range of droplet diameters measured. There are three distinct regions on both graphs: (1) increases in the droplet diameter to approximately 400 μm caused steep increases in the droplet speed, (2) further increases in the droplet diameter up to approximately 1000 μm caused the droplet speed to plateau, and (3) much further increases in the droplet diameter generated scattered data. The shape of the curve in the first and second regions of each data set is analogous to the relationship between the droplet diameter and its terminal speed under the influence of gravity shown in Chapter 2 (Figure 2.23). It is therefore proposed that the effect of the electrostatic force from DC fields is analogous to that of the gravitational force in the absence of a field, except that droplets achieve a terminal speed that is greater than that achieved in the absence of a field. The data in the third region of the graphs are scattered because an insufficient number of droplets larger than approximately 1000 μm was generated to provide representative data in this droplet size range.

These data are in contrast to those reported by Thornton and co-workers (Stewart & Thornton 1967, Bailes & Thornton 1974), which indicate that increases in droplet diameter resulted in decreases in the terminal speed. It should be noted, however, that these authors studied the behaviour of much larger droplets (>1600 μm ∅) that were being fed from the top of the column. This difference may be attributed to the difference in the strength of drag force experienced by droplets, given that larger droplets would be subjected to a significantly greater drag force than that of the smaller droplets, which were the focus of the present study. The data in the present study show that the relationship between the diameter and the speed for droplets that are typically encountered in SX applications (<1000 μm ∅) is opposite to the trend that these previous investigators have reported.

The data in Figures 6.7 and 6.8 also revealed that increases in the strength of DC fields, whether positive or negative, resulted in increases in the speed for most droplet sizes. This trend is consistent with the findings of previous researchers (Stewart & Thornton 1967, Carleson & Berg 1983, Vu & Carleson 1986) although they studied single droplets only. This relationship between the strength of the field and the speed of the droplet may be attributed to increases in the interfacial polarisation of the droplets and, hence, increases in the electrostatic force between the charged droplets and the electrodes. As mentioned previously, interfacial polarisation arises from the accumulation of charges on the surface of the droplets. This in turn arises because of incidental charges,

particularly electrons given they are more mobile than charged chemical species, that migrate across the poorly conducting organic phase and accumulate at the interfaces of the dispersed conductive droplets.

Analyses of the recorded videos also revealed that within the same set of experimental conditions, two distinct motions of droplets were observed. That is, while most droplets moved horizontally between the parallel-plate electrodes with relatively high speeds Figure 6.9), some droplets simply fell vertically towards the bottom of the column at much lower speed, apparently owing only to the influence of gravity. This has not been reported previously.

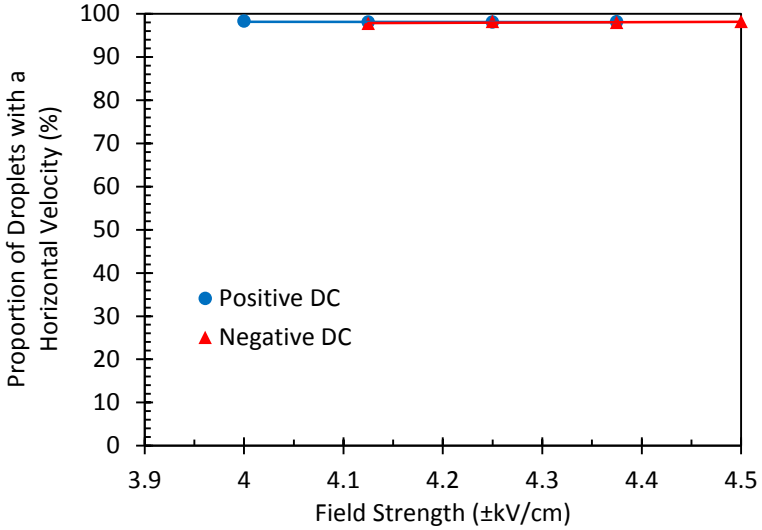


Figure 6.9 Proportion of droplets with a horizontal velocity in the presence of DC fields

It was speculated at this point of the study that this was partly owing to shielding, which means that some droplets are not subjected to the same polarising effect. That is, it appeared that the speed of the droplet is at least partly owing to interfacial polarisation and because the number of migrating charges in the continuous organic phase is limited, not all droplets acquire a charge and, hence, not all droplets exhibit interfacial polarisation.

Another significant trend was that, for large droplets (>1000 μm ∅), their speeds were in inverse proportion to the amplitude of their elongation. That is, large droplets that had high speeds were not elongated as they moved horizontally toward the electrodes. An example is shown in Figure 6.10. In these photos, the large droplet (droplet A - 1050 μm ∅) has approximately the same speed as an intermediate-sized droplet (droplet B - 390 μm ∅). The fast moving large droplet is not elongated towards the electrode. In

fact, it is slightly distorted vertically owing to the drag force from the horizontal motion. On the other hand, slower moving large droplets generally exhibited greater amplitudes of elongation. On closer examination, it was found that the high speeds of the large droplets are a consequence of a contact between these droplets and one of the electrodes, which then drive them to the opposite electrode. It therefore appeared that these droplets acquire a charge when they contact the electrode, leading to a high charge-to-mass ratio. The acquisition of charge of droplets has been previously observed by Stewart and Thornton (1967), although in their study the droplets acquired charge in a different way. In their work, the droplets were introduced through a charged nozzle, which was essentially the active electrode fixed at the top of the column. They observed that increases in the charge on the nozzle resulted in increases in the speed that the droplets were moving towards the earthed electrode that was at the bottom of the column. They concluded that increases in the charge-to-mass ratio leads to increases in the droplet velocity.

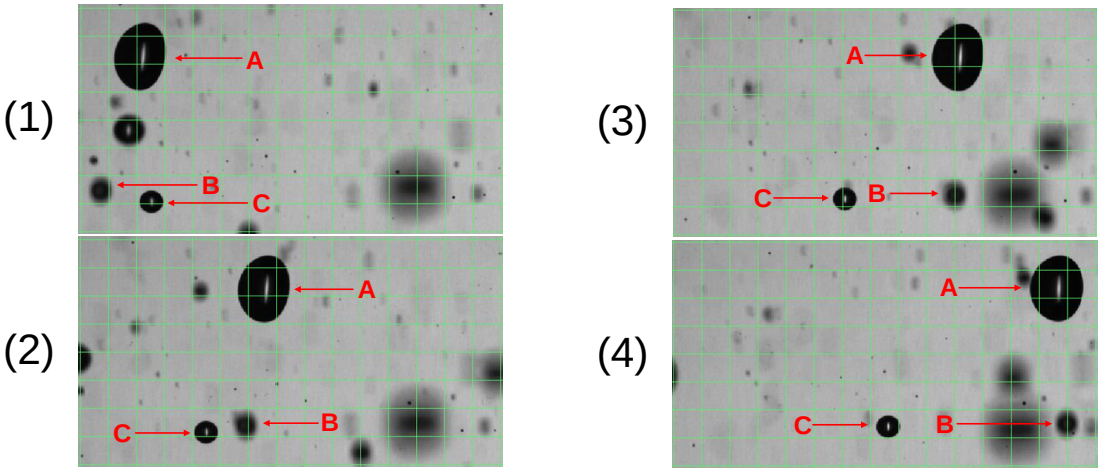


Figure 6.10 The large droplet A (1050 μm ∅) retains a spherical shape as it has a high velocity that is similar to that of the intermediate-sized droplet B (390 μm ∅), whereas droplet C (360 μm ∅) has a much slower velocity, in the presence of a DC field (4.12 kV/cm) (grid = 500 μm)

It therefore appeared that droplets can acquire and accumulate charges either through direct contact with bare electrodes or through the accumulation of incidental migrating charges through the poorly conducting organic phase. These accumulated charges lead to an increase in the charge-to-mass ratio. When subjected to electrostatic force, these droplets are interfacially polarised and the strength of this polarisation is proportional to their charge-to-mass ratio. For example, shown in Figure 6.10 are droplets B and C, which are of comparable size. Neither of them is elongated and hence both appeared to be shielded from orientational polarisation. Droplet B, however, had a much higher

speed. It appeared, therefore, that it had a higher charge-to-mass ratio and thus exhibited greater interfacial polarisation.

These results are in contrast to those of Stewart and Thornton (1967), who suggested that increases in the droplet speed induce droplet oscillation. They, however, did not provide experimental data so it is difficult to reconcile the difference.

#### *6.3.2.2. Effect of PDC Fields on Droplet Speed*

Subjecting droplets to the influence of a range of positive (5.00 – 5.67 kV/cm) and negative (-8.75 – -9.75 kV/cm) PDC field strengths and frequencies (20 – 60 Hz) provided further evidence of the occurrence of two different forms of droplet polarisation, resulting in two different forms of droplet agitation: one is oscillation and the other is linear motion.

Many of the behavioural trends under the influence of PDC fields are similar to those of DC fields. These include higher droplet speeds under the influence of applied fields than that in the absence of a field, the droplets reach a field-induced terminal speed that is analogous to but of greater magnitude than that achieved under the influence only of gravity, increases in the field strength over the range used had little effect on the speed of the droplets, and the use of either positive or negative field made no difference to these trends.

As with DC fields, many droplets moved between the parallel-plate electrodes with relatively high speeds although a small but significant proportion just fell down vertically, travelling at much slower speeds apparently under only the influence of gravity. The trend that increases in the field strength of PDC fields resulted in increases in the speed of the droplets was also observed by He, Chang and Baird (1997), although their work involved measuring only the initial velocity of single droplets being released from a charged nozzle, which is effectively the active electrode, and moving towards an earthed plate at the bottom of the column and thus travelling in the direction of gravity.

Measurements of the speeds of the droplets confirmed these observations. Increases in the strength of the applied field, either positive (Figure 6.11) or negative (Figure 6.12), resulted in increases in the speeds of the droplets, but these increases were smaller than those induced by comparable increases in the field strength of DC fields. This difference may be attributed to the differences in the nature of the applied fields. In the case of DC fields, the electrostatic force is exerted onto droplets continuously, whereas in the case of PDC fields, the periodic pulsing of the electrostatic force reduces the effective

electrostatic force and thus causes smaller increases in the speeds of droplets. This indicated that transient electrostatic force is less effective in achieving electrostatically induced linear motion of droplets than that of a constantly operating electrostatic force. In addition, the speed of the droplets that were travelling horizontally between the two electrodes increased and decreased periodically. This was clearly owing to the pulsing voltage of PDC fields, which causes periodic switching on and off of the electrostatic attraction between the applied field and the droplets.

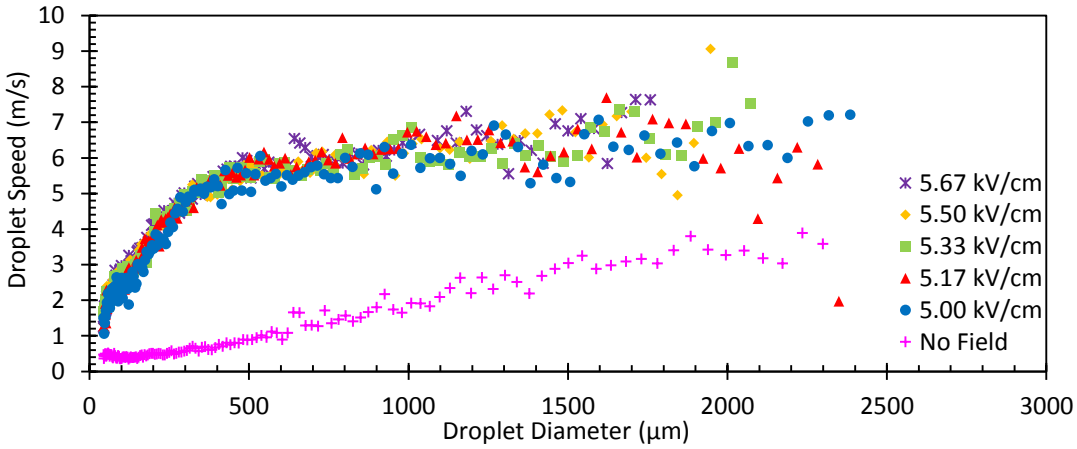


Figure 6.11 Effect of the field strength of positive PDC fields (50 Hz) on droplet speed

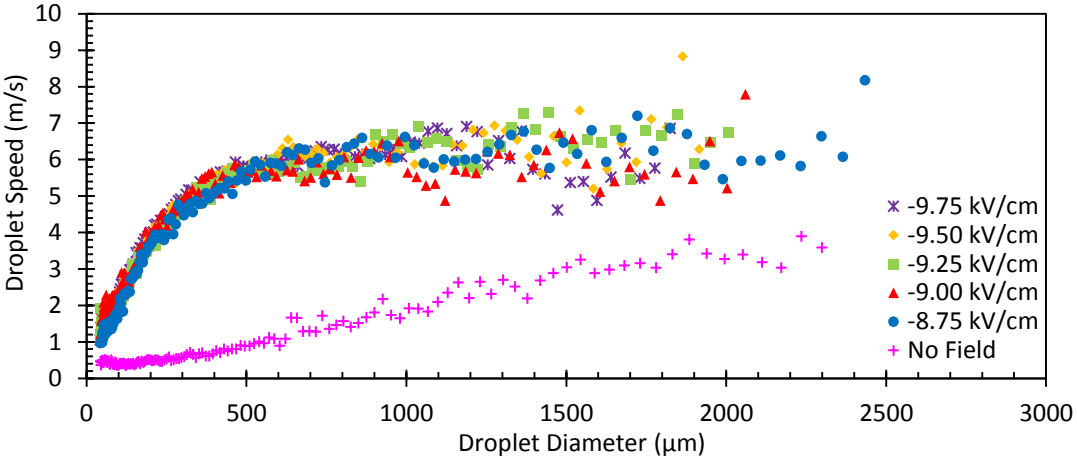


Figure 6.12 Effect of the field strength of negative PDC fields (50 Hz) on droplet speed

The relationship between the droplet diameter and the average speeds for a given PDC field strength was also the same as that for DC fields. That is, there are three distinct regions on both graphs: (1) increases in the droplet diameter to approximately 400 μm caused steep increases in the droplet velocity, (2) further increases in the droplet diameter to approximately 1000 μm caused a more gradual increase in the droplet velocity, and (3) further increases in the droplet diameter generated scattered data. The speeds plateaued at approximately the same speeds as with DC fields, which provides

further evidence that droplets reach a terminal speed in the presence of electrostatic fields owing to the effect of the drag force, as discussed previously. Thus, the effect of the electrostatic force of PDC fields is analogous to that of the gravitational force in the absence of a field. The data in the third region of both graphs are scattered because these experimental conditions generate only a few droplets larger than approximately 1000 μm and, thus, no significance may attributed to this part of the data.

There is another effect of PDC fields that was different to those of DC fields. That is, unlike DC fields, a particular frequency (40 Hz) over the range investigated (20 – 60 Hz) induced the highest average droplet speed over the whole range of droplet sizes that was measured. This was true with both positive (Figure 6.13) and negative (Figure 6.14) fields. Coupled with the observed periodic increase and decrease in the speed, this indicated that this frequency provides a sufficient period that the electrostatic force is in operation for the droplets to gain adequate momentum to continue their motion through the period that the electrostatic force is off. The use of higher applied frequencies appears to provide insufficient time for the droplets to achieve such momentum while the relaxation time of lower frequencies appears too long for the droplets to maintain their speed.

It should be noted that, as discussed in Chapter 5.3.2, greater field strengths of PDC fields were required to induce comparable droplet dispersions to those achieved under the influence of DC fields. Given that the droplet speed is partly dependent on the droplet diameter, similar droplet diameters were required to provide fair comparison.

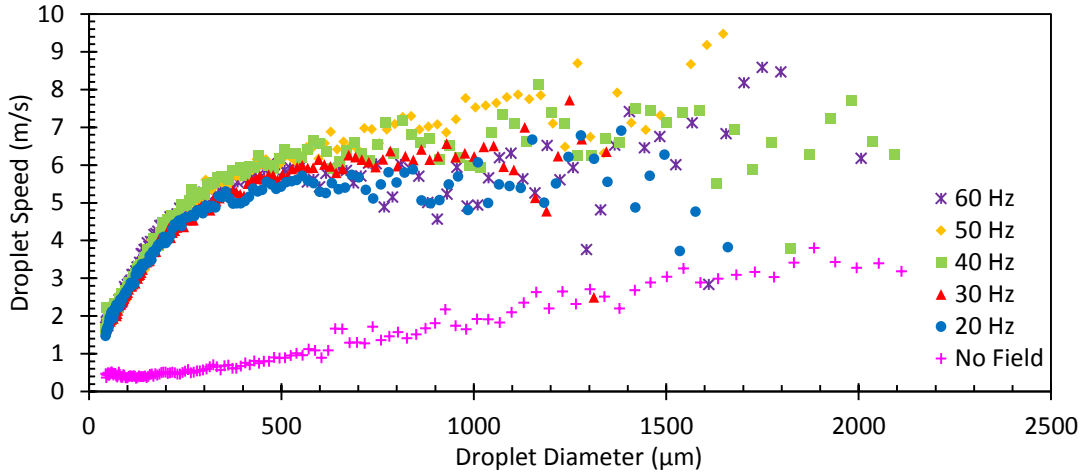


Figure 6.13 Effect of the frequency of positive PDC fields (5.67 kV/cm) on droplet speed

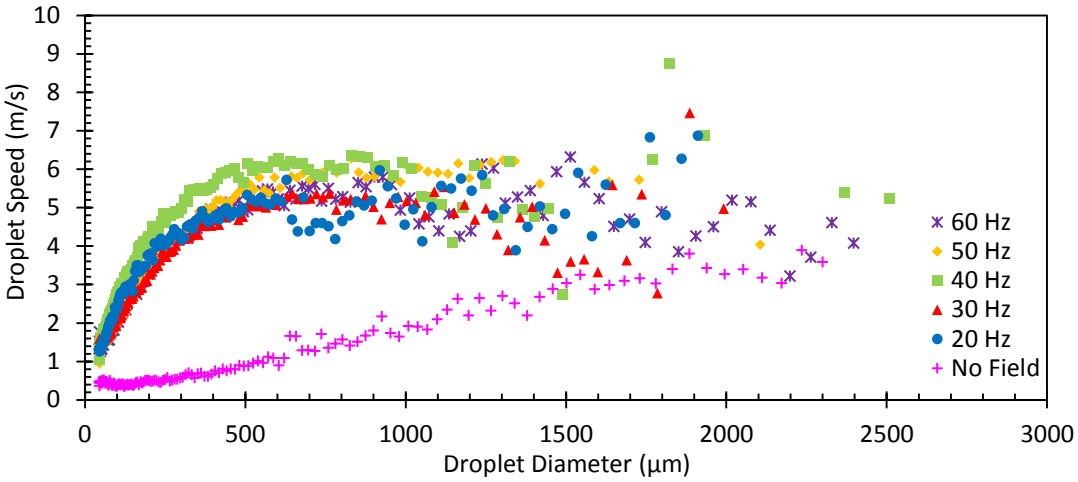


Figure 6.14 Effect of the frequency of negative PDC fields (-9.50 kV/cm) on droplet speed

### *6.3.2.3. Effect of AC Fields on Droplet Speed*

Subjecting droplets to AC fields of various field strengths (2.50 – 3.50 kV/cm) and frequencies (20 – 60 Hz) generated further evidence of the occurrence of two forms of droplet polarisation—orientational and interfacial—that influence droplet agitation.

Analysis of the recorded videos revealed that, under the influence of AC fields, some droplets were moving horizontally between the electrodes while others were moving only vertically. The droplets that were moving horizontally were continually reversing direction at apparently the same rate as the frequency of the applied field. The smaller droplets (<500 μm) were observably more able to reverse direction quickly than larger droplets. This behaviour was unique to AC fields and clearly owing to the alternating polarity of the electrodes in these fields. As a consequence, however, the droplets under the influence of AC fields that were moving horizontally appeared to have slower speeds than those under the influence of DC or PDC fields.

Measurements of the average speeds of the droplets as a function of the strengths of the applied field and droplet size confirmed the above observations. As shown in Figure 6.15, there are only small differences between the speeds of the droplets that were under the influence of AC fields and those that were not at all subjected to electrostatic fields, and the differences exist only for small droplets of up to approximately 500 μm in diameter. Moreover, for comparably sized droplets, the speeds of those under AC fields were clearly much lower than those of DC (Figures 6.7 and 6.8) and PDC (Figures 6.13 and 6.14) fields even if the differences in the strengths of the applied fields are factored in. Clearly, these data indicate that while droplets respond to AC fields in the same way that they do to DC or PDC fields, they are unable to reach a field-induced terminal

velocity owing to the cycling of the voltage, which provides insufficient time for droplets to accelerate before they change direction.

Shown also in Figure 6.15 is that, for a given field strength, increases in the droplet diameter led to increases in their average speeds but, for large droplets (≥500 μm), there was negligible difference in the speeds of those under the influence of electrostatic fields and those that were not. Visual analysis of the videos revealed that droplets of this size tended to simply fall down the column in the same way as those that were not subjected to electrostatic fields and comparably sized droplets appeared to have comparable speeds, indicating that their fall was simply owing to gravity. The difference, however, between those that were subjected to electrostatic fields and those that were not, was that the former were oscillating at a rate that was in apparent synchrony with the frequency of the field. This behaviour is consistent with orientational polarisation becoming the dominant form of polarisation, which makes sense because, as the droplet size increases, the amount of polar species contained within them increases, leading to increases in the attractive force between them and the applied field.

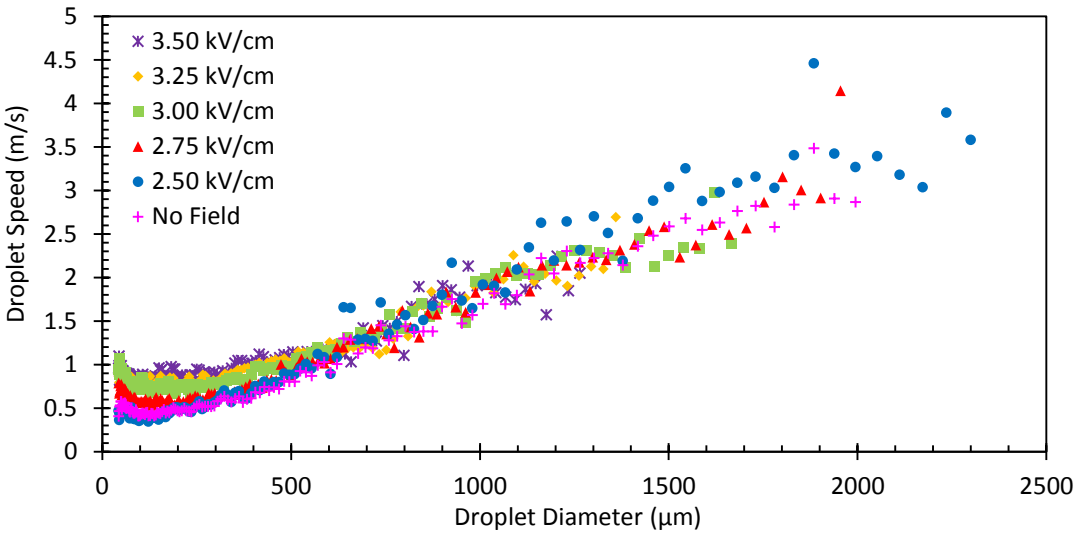


Figure 6.15 Effect of the field strength of AC fields (50 Hz) on droplet speed

For a given droplet size, increases in the frequency of AC fields resulted in decreases in their speed (Figure 6.16). This is further proof that the horizontal motion of droplets is a direct consequence of the attractive force between an oppositely charged electrode and droplet. In the case of AC fields, the charge of each electrode is continually alternating. As the frequency increases, the period of time by which a droplet can move in one direction decreases and, hence, its overall speed.

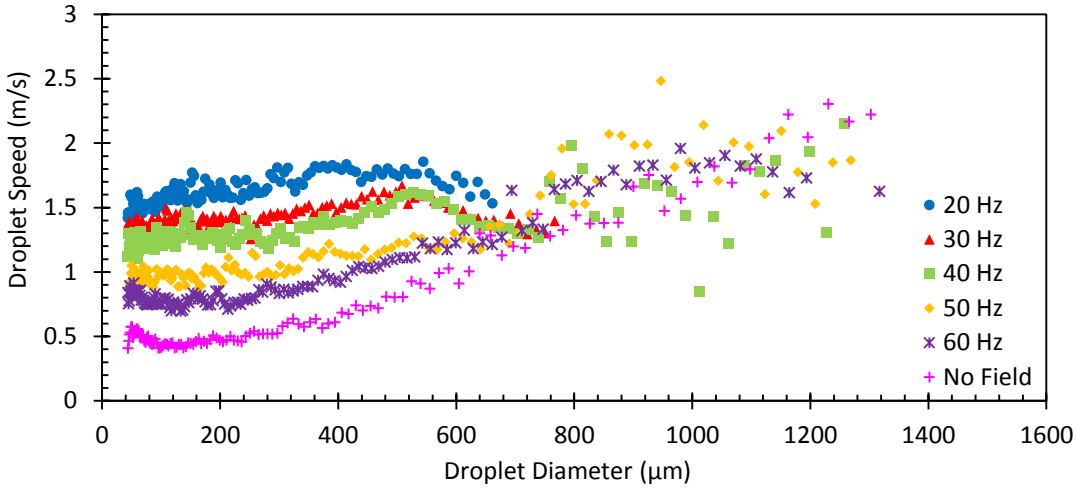


Figure 6.16 Effect of the frequency of AC fields (3.50 kV/cm) on droplet speed

The scatter of the data for droplets larger than approximately 600 μm may be attributed to the fact that, as mentioned previously, the linear motion of the droplets of these sizes was predominantly owing to gravity although, in contrast to those not subjected to gravity only, they were oscillating, which does not contribute to the measured speed.

### 6.3.3. Effect of Electrostatic Fields on Droplet Zigzagging

Zigzagging is an important property of droplets under the influence of electrostatic fields as it can be used to enhance the mass transfer in two major ways. Firstly, it increases residence time of the dispersed phase and thus provides longer time for the desired reaction, and secondly, it transports the droplets to a new region in the organic phase and thus aids in the interfacial replenishment.

The effect of electrostatic fields on droplet zigzagging was investigated by observing their motions and measuring the horizontal component of their velocity under the influence of various electrostatic fields over a range of field strengths and, in the case of transient fields, a range of frequencies as well. The horizontal component refers to any linear motion that is not directly vertical. For brevity and clarity, the horizontal component of the droplet velocity will be referred to simply as the velocity of the droplets henceforth in this thesis.

#### *6.3.3.1. Effect of DC Fields on Droplet Zigzagging*

Subjecting droplets to a range of positive (4.00 to 4.37 kV/cm) and negative (–4.12 to –4.50 kV/cm) DC fields caused them to move towards one electrode and, upon contact, reversed their direction towards the opposite electrode resulting in their zigzagging motion between the charged and earthed electrodes. This indicated that, upon contact

with an electrode, a droplet acquires the same charge as that of the electrode and thus is repelled towards and attracted by the opposite electrode. A small proportion of droplets (~ 1%), mainly the larger sizes (>500 μm), however, were observed to simply fall vertically down the column. Similar to the observations in the previous section, whilst the zigzagging droplets maintained their spherical shape, the non-zizagging droplets were elongated along the horizontal axis indicating that they were orientationally polarised. These observations indicate that, under the influence of DC fields, the acquisition of charge leads to a high charge-to-mass ratio leading to interfacial polarisation, and consequently, zigzagging motion of droplets. Previous investigators (Yamaguchi, Sugaya & Katayama 1988; Heckley 2002; Gneist & Bart 2003) have also mentioned observing some zigzagging of droplets under the influence of DC fields although, as this was not the main focus of their studies, they provided little information.

Figures 6.17 and 6.18 show the effect of positive and negative DC fields, respectively, on the velocities of the droplets. It is clear that the average velocities of droplets that were moving towards the positive electrode were higher than those moving towards the negative electrode. This was true whether the positively charged electrode was the active electrode (~4.4 m/s vs ~3.4 m/s), as in the case when the applied field was positive (Figure 6.17), or the earthed (induced charge) electrode (~5.0 m/s vs ~3.6 m/s), as in the case when the applied field was negative (Figure 6.18). This indicated that the negatively charged droplets had higher amounts of charge, and hence higher electrostatic attraction with the electrode, than the positively charged droplets. It is proposed that, under a given set of conditions, droplets acquire a greater amount of negative charge than positive charge owing to the higher mobility of negative charges (electrons) than positive charges.

The apparently higher average velocities of the entire population of droplets when under the influence of negative DC fields (~4.2 m/s) than those under positive DC fields (~3.8 m/s) were owing to the finer droplet dispersions generated by negative DC fields at comparable field strengths, as shown in Chapter 5.3.1 (Figures 5.10-5.13). This was evident when corrected for the droplet diameter, as shown in Figures 6.19 and 6.20.

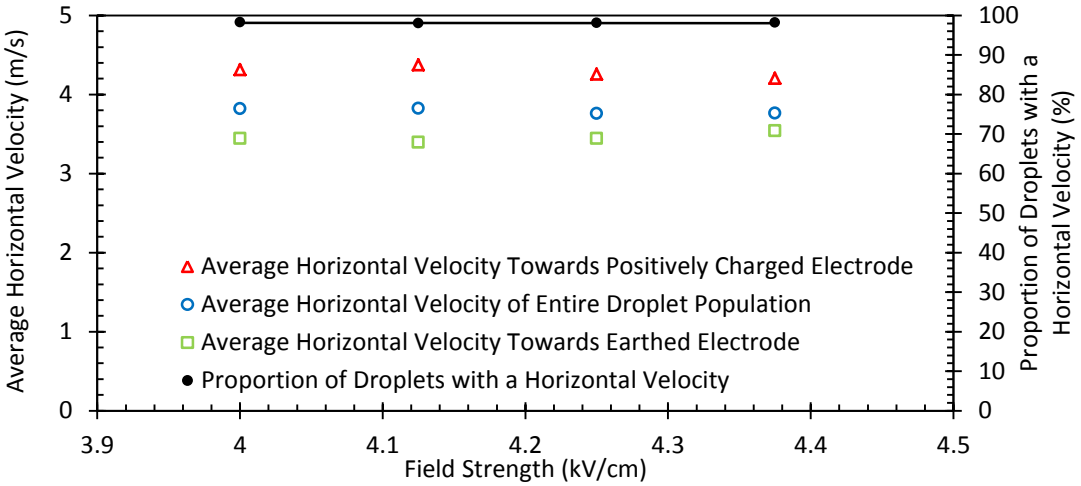


Figure 6.17 Effect of the field strength of positive DC fields on the average horizontal velocity

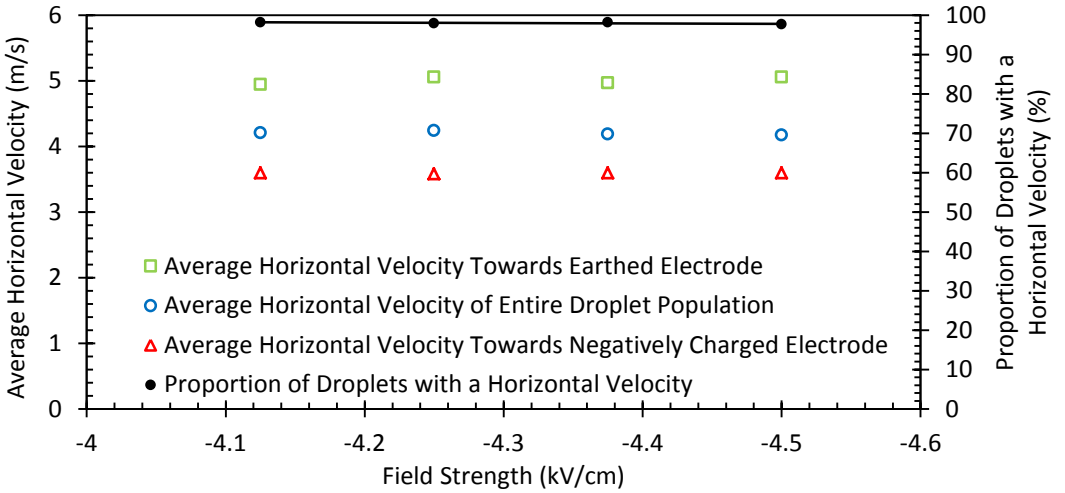


Figure 6.18 Effect of the field strength of negative DC fields on the average horizontal velocity

In contrast, Eow, Ghadiri and Sharif (2003) reported that the average velocity in the presence of positive DC fields was greater for droplets moving towards the earthed (negative) electrode. They speculated that this could be owing to different amounts of charge transfer upon contact of a droplet with the two electrodes or to charge leakage from the droplet after contacting the electrode. They, however, provided little experimental data. For example, they provided no description of their sizing technique and they made no attempt to determine the effect of switching the polarities of the electrodes. They also provided no justification for their speculations.

Increases in the strength of the applied DC fields, either positive (Figure 6.19) or negative (Figure 6.20), had no observable effect on the average horizontal velocities of the smallest droplets (<100 μm) but resulted in increases in those of all other droplet sizes. This indicated that larger droplets are able to acquire higher amounts of charge,

resulting in higher interfacial polarisation and thus stronger electrostatic forces between them and the electrodes.

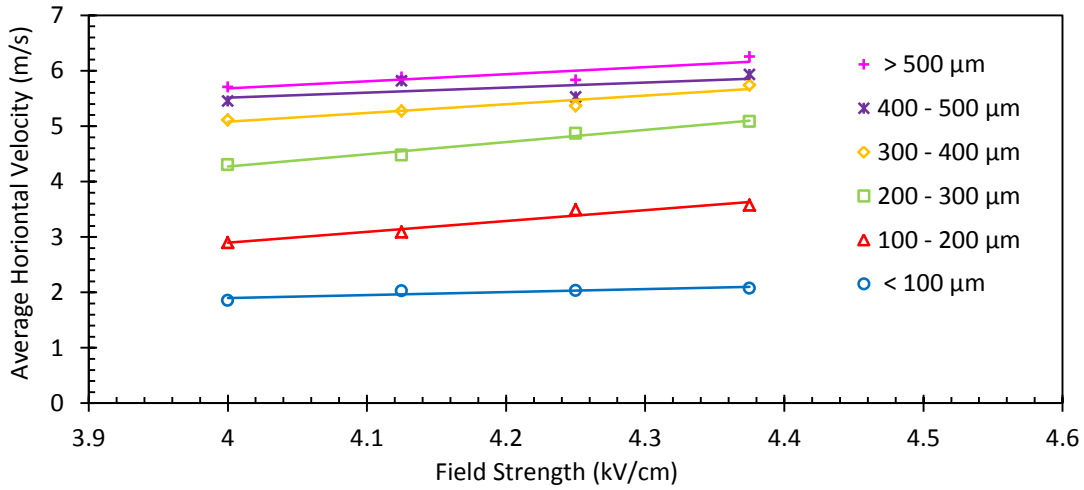


Figure 6.19 Effect of the field strength of positive DC fields on the average horizontal droplet velocity for given size fractions

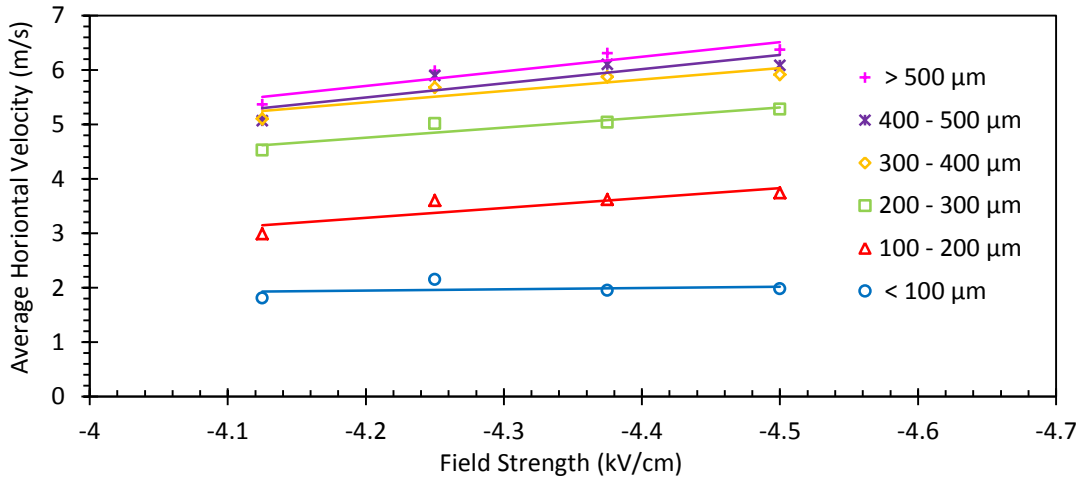


Figure 6.20 Effect of the field strength of negative DC fields on the average horizontal droplet velocity for given size fractions

### *6.3.3.2. Effect of PDC Fields on Droplet Zigzagging*

The investigation on the effect of PDC fields on droplet zigzagging was carried out in the same way as those of DC fields but, as discussed previously, higher field strengths (5.00 – 5.67 kV/cm and −8.75 − –9.75 kV/cm) had to be used. Consequently, however, negative PDC fields generated finer droplet dispersions and this must be taken into consideration when comparing the effect of these two different polarities.

Overall, the effects of PDC fields on droplet zigzagging were similar to those of DC fields. Subjecting droplets to a range of positive and negative PDC fields caused them to move towards one of the electrodes and, upon contact with the electrode, reverse direction towards the opposite electrode resulting in their zigzagging motion. The

average velocity was highest for droplets that were moving towards the positive electrode, whether it was the active (applied charge) electrode (Figure 6.21) or earthed (induced) electrode (Figure 6.22), and for a given size of droplet, the average velocity was relatively constant over the range of field strengths that was investigated. Similar to DC fields, a very small proportion of droplets (~1%) simply fell vertically down the column and, unlike the zigzagging droplets, which were largely spherical, these non-zigzagging droplets were periodically elongated along the horizontal axis. These results are further evidence that the zigzagging motions of droplets was owing to the electrostatic attraction and repulsion between the electrodes and charged droplets, which are subjected to interfacial polarisation and that the two forms of polarisation of droplets always occur together although one predominates over the other, depending on the specific experimental conditions.

At a glance, it would appear that, in contrast to that of DC fields, the average velocity of the entire droplet population was higher with positive PDC fields (~4.10 m/s) than with negative PDC fields (~3.15 m/s), as shown in Figures 6.21 and 6.22, respectively. This was not the case. It was simply because negative PDC fields generated significantly finer dispersions and, thus, slower overall average velocities. When corrected for the difference in droplet size distribution, it was clear that, consistent with the observation in the previous section, the velocities of the droplets under the influence of applied negative PDC fields were higher than those under the influence of positive PDC fields. This is further evidence that droplets were able to acquire negative charges more easily than positive charges, which is consistent with the known higher mobility of negative charges (electrons).

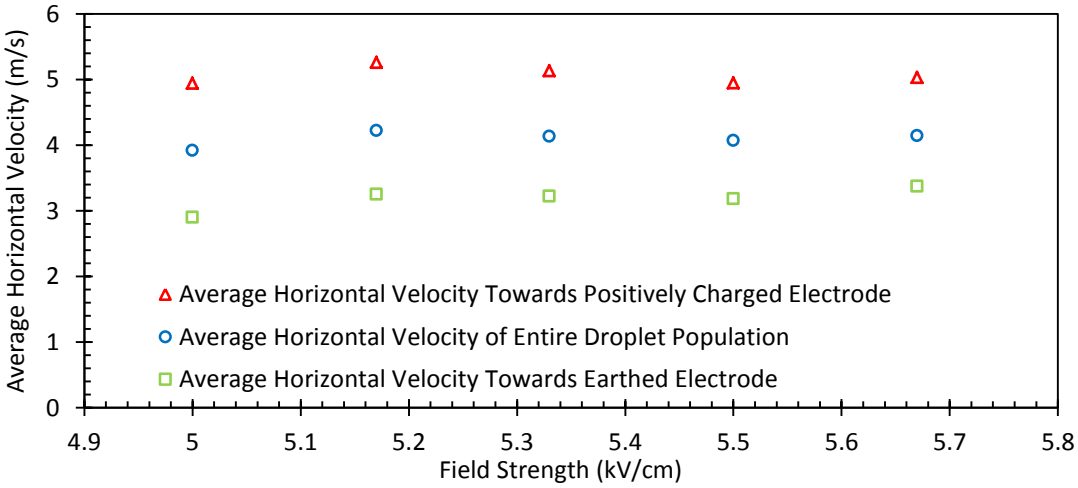


Figure 6.21 Effect of the field strength of positive PDC fields (50 Hz) on the average horizontal droplet velocity

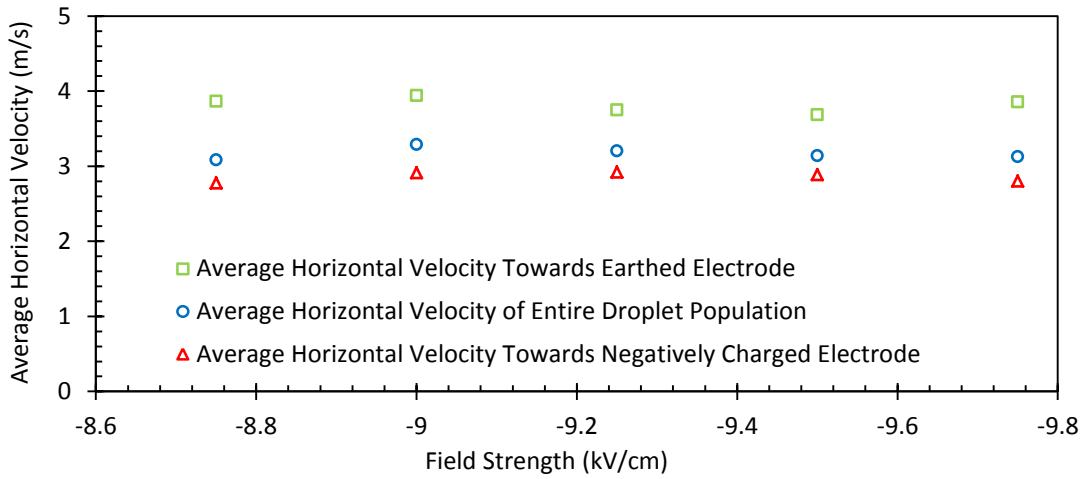


Figure 6.22 Effect of the field strength of negative PDC fields (50 Hz) on the average horizontal droplet velocity

Variation of the frequency of the applied field from 20 to 60 Hz, which is the most convenient and practical range to work with, revealed a maximum velocity of the droplets at 40 Hz for both positive (Figure 6.23) and negative (Figure 6.24) PDC fields. This indicated that this frequency exerted the maximum effective electrostatic force upon the droplets over this range of frequencies. That is, at higher frequencies the time that a voltage, and hence the electrostatic force, was applied was too short, and at lower frequencies the electrostatic force was not applied often enough. This was consistent with visual observations. Unlike DC fields, wherein the movement of the droplets towards the electrode was steady, the movement of the droplets under the influence of PDC fields was staggered. Hence, the overall distance travelled per unit time was significantly affected by the periods at rest.

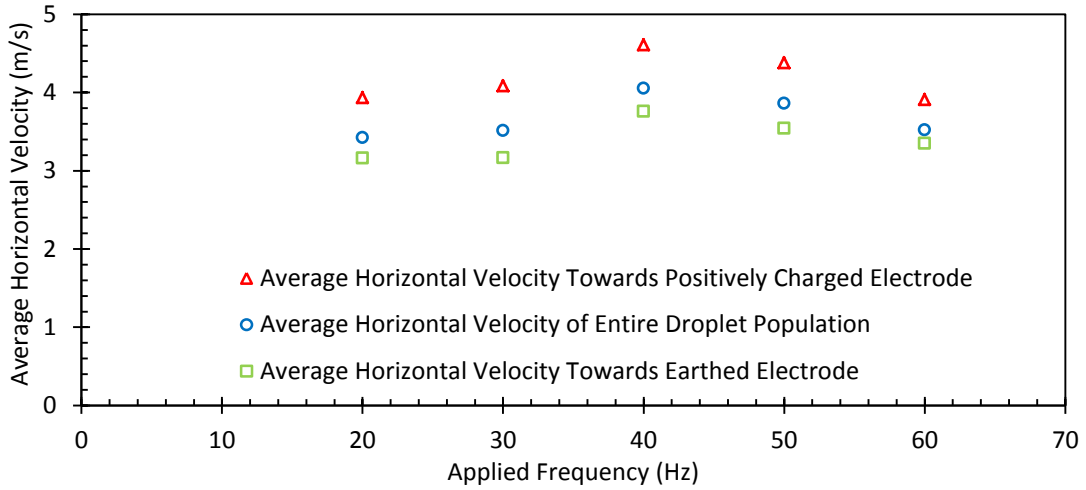


Figure 6.23 Effect of the frequency of positive PDC fields (5.67 kV/cm) on the average horizontal droplet velocity

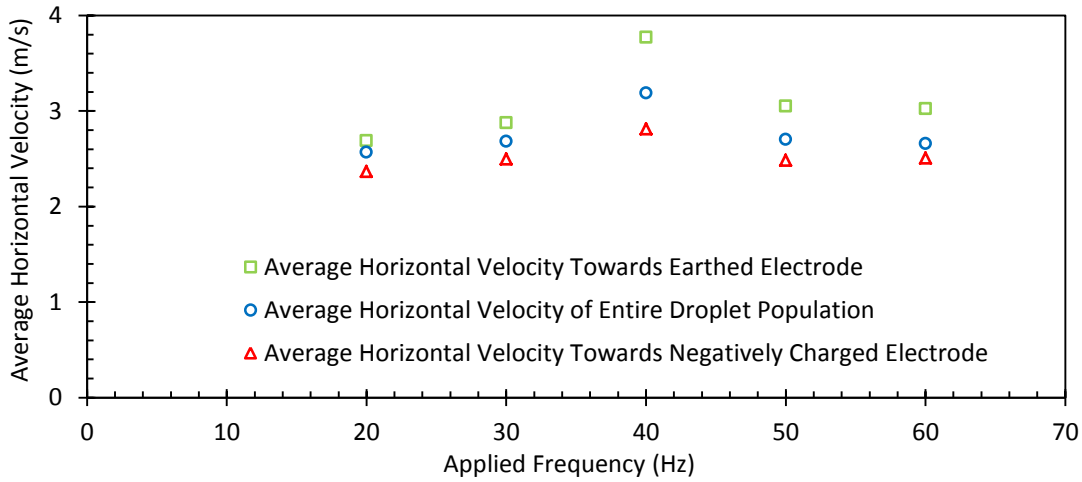


Figure 6.24 Effect of the frequency of negative PDC fields (-9.5 kV/cm) on the average horizontal droplet velocity

#### *6.3.3.3. Effect of AC Fields on Droplet Zigzagging*

The effect of AC fields on droplet zigzagging was investigated by observing their motion and measuring the horizontal component of their velocity under the influence of a range of field strengths (2.50 – 3.50 kV/cm) and frequencies (20 – 60 Hz). Similar to DC and PDC fields, AC fields induced droplets to zigzag between the electrodes and, although with some differences, they provided further proof of the main mechanism of this motion.

Firstly, the droplets changed direction at apparently the same rate as the frequency of the field and did so without contacting an electrode. Consequently, they zigzagged considerably more frequently in the presence of AC fields than those in the presence of DC or PDC fields. Given that, as with DC and PDC fields, a small proportion of droplets were not zigzagging, this observation reinforced the earlier observation that the zigzagging motion of droplets is owing to the electrostatic force between the electrodes and the charged droplets.

Secondly, while the majority of the zigzagging droplets were doing so in synchrony, a small proportion was doing so also but towards the opposite direction. This behaviour suggested that the overall charge on droplets may be either positive or negative, and that the majority of the droplets had a negative charge, which is consistent with the higher mobility of electrons.

Thirdly, at low field strength (2.5 kV/cm), the horizontal distance travelled by zigzagging droplets often gradually decreased as they moved through the organic phase but increases in the field strength minimised the occurrence of this behaviour. This

suggested that charges on the droplets dissipated as they move though the organic phase and that, at low field strengths, the rate of the dissipation of charge is greater than the rate of accumulation of new charge.

Fourthly, increases in the strength of AC fields (2.5 – 3.5 kV/cm) resulted in nearly linear increases in the average horizontal velocity for all size fractions (Figure 6.25). This suggested that increases in the field strength resulted in increases in the amount of incidental charges and thus their acquisition by the droplets, leading to greater interfacial polarisation. Further evidence of the migration of incidental charges across the poorly conducting organic phase and their accumulation on the droplet surface was the occurrence of droplets that were zigzagging but cease doing so and non-oscillating droplets that suddenly start oscillating. This can only be attributed to the incidental accumulation and dissipation of charges on the droplets.

The slight tapering of the curves in Figure 6.25 may be attributed to droplets approaching their maximum horizontal velocity that can be achieved for a given frequency. That this is much more pronounced as the size of the droplets decrease is further evidence of the observation in the previous section that the amount of charge that droplets can accumulate increases with their size. The data for droplets >500 µm at 3.25 and 3.5 kV/cm were too small to be given much significance.

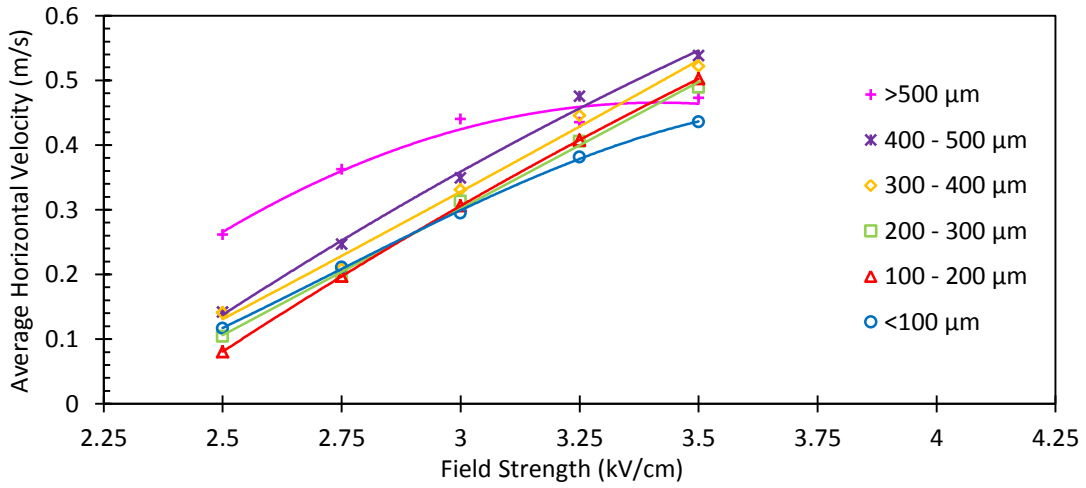


Figure 6.25 Effect of the field strength of AC fields (50 Hz) on the average horizontal velocity of droplets in given size fractions

Increases in the frequency of AC fields resulted in decreases in the average velocity of the droplets (Figure 6.26). This was clearly owing to the shorter time for the droplets to move prior to changing direction as they do so in synchrony with the frequency. In the case of DC or PDC fields on the other hand, the droplets change direction only after

contacting an electrode. The effect of frequency on the average horizontal velocity is further proof of this. As shown in Figure 6.26, decreases in frequency, which equate to longer times before the droplets have to change direction, led to higher average velocity.

The slight differences in the average horizontal velocities of differently sized droplets indicate slight differences in the effective electrostatic force exerted onto them. At the lowest frequency (20 Hz), the droplets with the fastest horizontal velocity were those in the medium size fractions (200 – 300 μm, 300 – 400 μm, 400 – 500 μm), and the slowest were those in the smallest (<100 μm) and largest (>500 μm) size fractions. This suggested that the horizontal velocity in the presence of AC fields was not only dependent on the electrostatic force owing to the amount of droplet charge but also the hydrodynamic hindrance, which is dependent on the mass of a droplet. It appeared that droplets in the medium size fractions exhibit a good compromise between the amount of charge that they can acquire and their mass, resulting in the highest average horizontal velocity within the droplet population. The difference was much smaller at high frequencies because their average velocities were much lower.

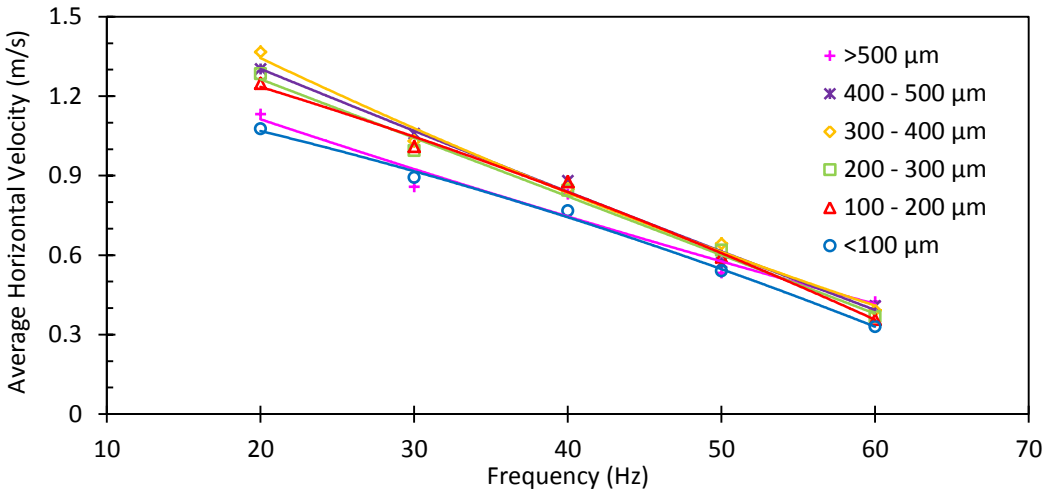


Figure 6.26 Effect of the frequency of AC fields (3.50 kV/cm) on the average horizontal velocity of droplets in given size fractions

## 6.4. CHAPTER SUMMARY

In this chapter it was found that:

- Electrostatic agitation may be effected in three ways: droplet oscillation, linear speed and zigzagging. Oscillation refers to the periodic elongation and relaxation of the droplet. Linear speed refers to the speed of the droplet regardless of its direction, which can be totally horizontal or vertical and anything in between. It was calculated as the total speed of the droplets and simply referred to as speed.

Zigzagging has two aspects: the frequency of change in direction and velocity, which was calculated as the horizontal component of the speed.

- The oscillation of droplets under the influence of electrostatic fields was clearly a direct consequence of their intermittent orientational polarisation by the electrostatic force of a transient field. Hence, steady fields effected no oscillation.
- Although droplets oscillated in synchrony with the frequency of the field, hydrodynamic factors appeared to have an influence. As the frequency increased, the amplitude of elongation decreased and, hence, the intensity in terms of agitation.
- It appeared that a small amount of electric charge migrates through the organic phase that is subjected to electrostatic fields and some droplets acquire charges, leading to increases in their charge-to-mass ratio and, consequently, interfacial polarisation.
- The dominant form of droplet agitation was found to be dependent on the relative amount of orientational and interfacial polarisation. Purely orientational polarisation led to droplet oscillation. Predominance of interfacial polarisation led to high linear speed and zigzagging.
- The droplet diameter always had a significant effect on droplet agitation, be it oscillation or linear motion and zigzagging. Increases in the droplet diameter resulted in higher amplitudes of elongation owing to higher amounts of polar species and thus orientational polarisation, and increases in the terminal velocity owing to higher capacity to acquire charges.
- Under DC and PDC fields, droplets changed direction only upon contact with an electrode, indicating the acquisition of charges. Under AC fields, droplets changed direction in synchrony with the frequency of the field.
- For a given population of droplets under the influence of a transient field, a proportion of droplets oscillated while falling almost totally vertically down the column, a proportion of droplets moved horizontally between the two electrodes at high speeds in a zigzagging fashion while remaining spherical, and a proportion of droplets manifested both motions but in varying degrees. These observations clearly indicated the occurrence of two forms of polarisation: orientational and interfacial.

# Chapter 7

# EFFECT OF ELECTROSTATIC FIELDS ON MASS TRANSFER IN ELECTROSTATIC SOLVENT EXTRACTION

## 7.1. INTRODUCTION

This chapter describes the attempt to relate the results of the investigations on the effects of electrostatic fields on droplet dispersion, as well as the oscillation, speed and zigzagging of the droplets in the resulting dispersions. The focus was to understand how the variables of electrostatic fields influence the mass transfer in the extraction of Co(II) with Cyanex® 272 as extractant and thus the considerations for the design of contactors in electrostatic solvent extraction (ESX).

Given the findings in Chapters 5 and 6 indicating that the use of AC fields appeared to be the most favourable for the application of ESX, and the practical difficulties and inherent weaknesses in using either DC or PDC fields, only AC fields were investigated in this part of the study.

## 7.2. MATERIALS AND METHODS

### 7.2.1. Reagents, Test Solutions and Extraction Apparatus

To minimise experimental variability, the reagents and test solutions used in this part of the study were the same as those in Chapters 5 and 6 for the reasons stated previously. For the convenience of the readers, they are copied here as follows: acetic acid (AR, Chem-Supply), sodium hydroxide (AR, Chem-Supply), cobalt sulphate heptahydrate (AR, Chem-Supply), sodium sulphate (AR, BDH), ShellSol® 2046 (Industrial Grade, Shell Chemicals), Cyanex® 272 (Industrial Grade, Cytec Australia), and sulphuric acid (98%, Sigma Chemicals). All reagents were used as supplied.

Two test solutions were used: a buffered (pH 5.5) Co(II) solution (300 mg/L) as the aqueous feed and Cyanex® 272 in ShellSol® 2046 as the solvent.

The droplet column that was developed in Chapter 3.5 including its auxiliary equipment (Figure 3.15) except the imaging apparatus was used in this part of the study as the extraction apparatus.

### 7.2.2. Analytical Techniques

The determination of the concentration of extracted Co(II) in the organic phase was carried out using a UV-VIS spectrophotometer (DMS 70, Varian) following the recommended procedures by the manufacturer including the calibration method. The calibration was carried out daily prior to commencing the extraction experiments.

The concentrations of the cobalt in the test solutions were determined by ICP (Varian VISTA-PRO Simultaneous ICP-OES) following the procedures recommended by the manufacturer. Calculations for the composition of the aqueous solutions used in droplet column experiments are shown in Appendix C7.

### 7.2.3. Procedure for Mass Transfer Experiments

The effect of electrostatic fields on mass transfer of Co(II) from the aqueous to the organic phase was investigated by carrying out a series of extraction experiments under systematically varied electrostatic field conditions using the droplet column that was developed in Chapter 3 and used in Chapters 5 and 6. A separate set of experiments was also carried out in the absence of a field to provide a baseline and thus quantify the effect of electrostatic fields on mass transfer. For each set of experimental conditions, a minimum of three experimental runs was carried out to ensure reproducibility of the data.

The experiments were carried out following the general procedure for droplet column experiments described in Chapter 3.6.1. The imaging equipment was not and could not be used in these experiments because doing so would require the closure of the laser compartment when the experiment is started for the safety of the operator. Unlike the experiments in Chapters 5 and 6, in which the laser compartment can be enclosed fully from the beginning to the end of each run, these experiments necessitated the periodic draining of the disengaged aqueous phase to minimise further mass transfer and to collect a sufficient amount of sample for analysis.

To determine the amount of mass transfer of cobalt, samples of the raffinate (20 mL) were withdrawn from the total raffinate generated in each test and assayed for the residual cobalt. The mass transfer was determined by mass balance.

### 7.2.4. Data Acquisition and Analysis

The mass transfer in each experiment was determined by calculating the difference in the concentration of Co(II) in the aqueous feed and raffinate solutions and hence the

percentage extraction under a given set of experimental conditions. For experiments carried out in the presence of electrostatic fields, the Co(II) extraction was plotted against either the field strength or the applied frequency. The average value of Co(II) extraction was plotted along with error bars of ±1 standard deviation for each set of experimental conditions.

## 7.3. RESULTS AND DISCUSSIONS

This part of the study was meant to determine how the variable properties of AC fields affect mass transfer. It was not the intention to compare the mass transfer between mechanically and electrostatically agitated systems. While this comparison would be valuable, it was outside the scope of the present study as its inclusion would have led to an impractically large scope for the nature of the study. This was evident in the experience in developing the experimental techniques in Chapter 3.

### 7.3.1. Mass Transfer in the Absence of Electrostatic Field

The results of the mass transfer experiments in the absence of electrostatic fields are summarised in Table 7.1. The mass transfer was small but easily measurable and with a high degree of reproducibility. The close to 90% remaining cobalt in the feed that could only be extracted by the use of much more favourable experimental conditions, such as wider interfacial area and more vigorous droplet speed and zigzagging, allowed for a wide variation of the properties of electrostatic fields in determining their effect on mass transfer.

Table 7.1 Mass transfer in the absence of electrostatic field

| Run Number | Co(II) Extraction (%) |
|---|---|
| 1 | 12.7 |
| 2 | 13.0 |
| 3 | 12.8 |
| Average | 12.8 (±0.15) |

These results confirmed the suitability of the experimental technique, including the apparatus that was developed for this purpose (Chapter 3), and provided a basis for the determination of the effects of electrostatic fields on mass transfer.

### 7.3.2. Effect of the Field Strength on Mass Transfer

The results of the experiments to determine the effect of field strength on mass transfer are summarised in Figure 7.1.

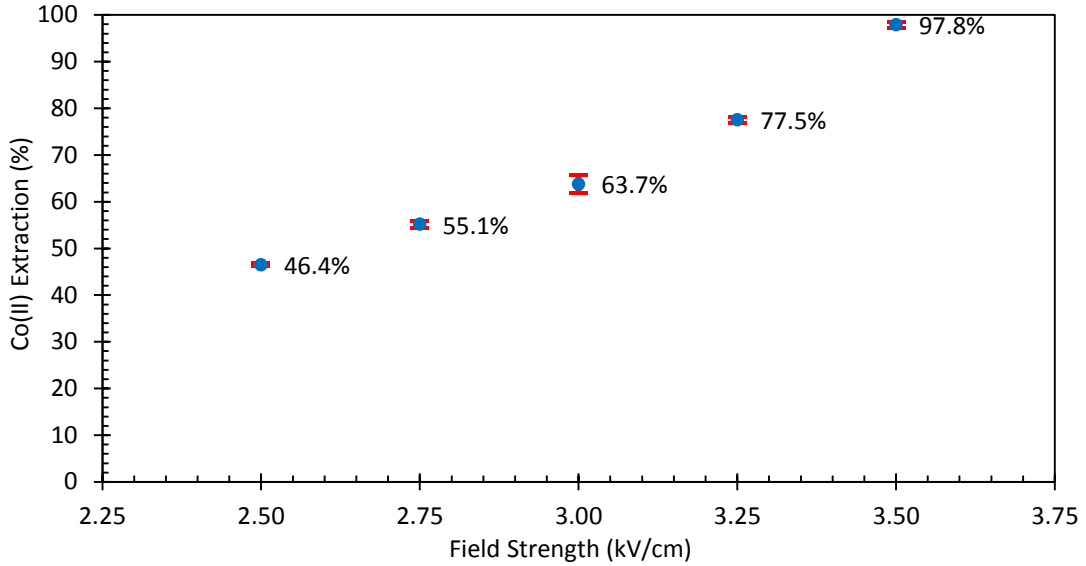


Figure 7.1 Effect of field strength of AC fields (50 Hz) on the extraction of Co(II)

It is clear that the application of electrostatic fields enhanced the mass transfer dramatically. For example, the extraction of cobalt (~45%) of Co(II) at the lowest field strength (2.50 kV/cm) was substantially higher than that in the absence of a field (~13%). A 1-kV increase in the strength of the applied voltage (2.5 to 3.5 kV/cm) resulted in more than doubling of the mass transfer from 46% to 98% (Figure 7.1).

Given the results in Chapters 5 and 6, this nearly linear relationship between mass transfer and field strength, may be attributed to three contributing factors associated with the field strength namely the interfacial area of the dispersion, droplet speed and zigzagging. It was found, for example, in Chapter 5 that, with AC fields, an increase of 0.5 kV in the applied voltage from 2.5 to 3.0 kV/cm resulted in a 20% decrease in the Sauter mean diameter and thus the droplet surface area. At the same time, the population of droplets increased by 52%. Thus, overall, these changes equated to an estimated 22% increase in the total surface area of the dispersion. Then, in Chapter 6, it was found that the same change in the applied voltage resulted in approximately 22% increase in the droplet speed and 172% increase in zigzagging. These figures are summarised in Table 7.2.

Clearly, these trends are consistent with the basic relationships between these properties of the dispersion and mass transfer. It is, however, difficult to quantify the individual

contributions of these properties to mass transfer as it is difficult to isolate them from each property given they are characteristic of the dispersion under a given set of experimental conditions.

Table 7.2 Effect of increase in field strength from 2.5 to 3.0 kV/cm

| Variable | 2.5 kV/cm | 3.0 kV/cm | %Change |
|---|---|---|---|
| Mass transfer (%) | 46.4 | 63.7 | 37 |
| Sauter mean (μm) | 386 | 309 | −20 |
| Droplet surface area ($mm^2$) | 0.47 | 0.30 | −36 |
| Number of droplets | 44,788 | 68,227 | 52 |
| Total surface area ($mm^2$) | 17.29 | 21.08 | 22 |
| Speed (m/s) | 0.49 | 0.84 | 71 |
| Zigzagging (m/s) | 0.11 | 0.30 | 172 |

Other properties of droplet dispersion that increased with increases in the field strength were the amplitude of droplet elongation and the population of the oscillating droplets (Chapter 6.3.1.3). The former, in turn, results in an increase in surface area while the latter results in greater agitation. Again, the basic principles of mass transfer indicate that both changes are favourable to mass transfer and these trends are thus consistent with underpinning theories.

### 7.3.3. Effect of the Frequency on Mass Transfer

The effect of the frequency of the applied field on mass transfer is summarised in Figure 7.2. The inverse relationship between the frequency and mass transfer mirrors the relationships between the frequency and the droplet speed and also, between the frequency and the droplet zigzagging. That is, as observed in Chapter 6, increases in the frequency of the applied field resulted in decreases in droplet speed and zigzagging. Figure 6.16 shows that an increase in the frequency from 20 to 60 Hz (200%) resulted in approximately 40% decrease in the speed of the droplets. The same increase in frequency resulted in approximately 67% decrease in zigzagging (Figure 6.26). These trends are consistent with fundamental principles of mass transfer.

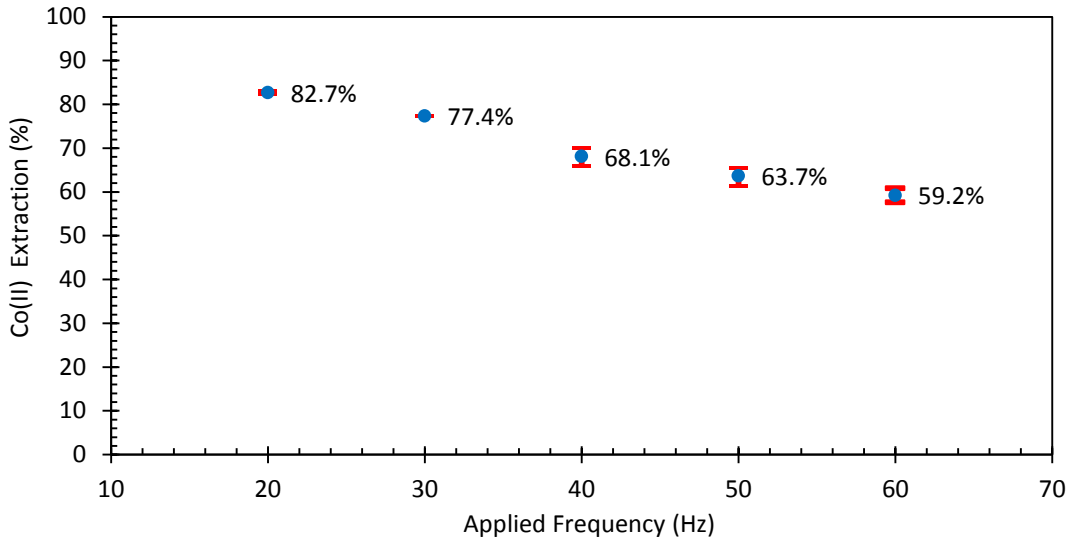


Figure 7.2 Effect of frequency of AC fields (3.0 kV/cm) on the extraction of Co(II)

At a glance, this inverse relationship between the frequency and the mass transfer of cobalt would appear to be inconsistent with the basic principles of mass transfer because increases in the frequency would have meant increases in the droplet motion. As observed in Chapter 6.3.1.3, droplets oscillated in synchrony with the frequency of the field. Hence, an increase in the frequency would have resulted in proportionate increase in the oscillation of the droplets, which equates to more a vigorous agitation. The visual analysis of the dispersion revealed a possible explanation for this apparent inconsistency. That is, as the voltage cycles in AC fields, a droplet elongates and its amplitude attempts to synchronise with the cycling voltage if given sufficient time. As the frequency of the cycling of voltage increases, however, the hydrodynamic resistance sets in until it reaches a point that it becomes essentially non-oscillating.

This inverse relationship between the frequency of applied field and the mass transfer of cobalt also appeared at first glance to be inconsistent with basic principles of mass transfer in terms of the relationship between mass transfer and interfacial area. As shown in Figure 5.25, an increase in the frequency from 20 to 60 Hz resulted in 13% decrease in the Sauter mean, which meant a corresponding increase in the interfacial area by a comparable value (13%), which should have favoured mass transfer. The same figure provides a clue to this apparent quirk. As shown, the main reason for the small decrease in Sauter mean was the increase in the populations of the smallest range of droplet size. Conversely, the main reason for the small increases in the Sauter mean with decreases in the frequency was the consequent higher amplitude of elongation of the oscillating droplets rather than actual size difference. That is, at relax state, say zero

field, there was no actual difference in the size of the droplets in the respective distribution. Thus, the actual differences in the interfacial areas among these various frequencies would have been minimal, which is consistent with the measured mass transfer.

Clearly, the effect of the frequency of the applied field on mass transfer was mainly owing to its effect on the droplet speed, zigzagging and amplitude of elongation, which all increased with decreases in frequency and hence, the mass transfer trend.

The practical implication of these results is that the use of high voltage with low frequency AC fields appeared to be the most favourable in electrostatic solvent extraction. Both DC and PDC fields require bare electrodes which is a serious hazard to operating personnel. DC fields do not facilitate droplet oscillation, which is a distinct weakness. PDC fields require substantially high field strength to effect dispersion than either DC or AC, which is obviously a distinct disadvantage in terms of operational cost and occupational health and safety considerations.

## 7.4. CHAPTER SUMMARY

The main findings in this chapter may be summarised as follows:

- Increases in the strength of the applied field resulted in increases in the interfacial area, droplet speed and droplet zigzagging and, consequently, increases in mass transfer of cobalt.
- Increases in the frequency of the applied field resulted in decreases in droplet speed and droplet zigzagging and, consequently, decreases in mass transfer of cobalt. Increases in the frequency also led to increases in the oscillation of droplets but decreases in the amplitude of elongation. Although this resulted in apparently slightly smaller droplets and thus larger interfacial area, which should have favoured mass transfer, its overall effect on mass transfer was negligible
- These results are consistent with the basic principles of mass transfer.

Thus, AC fields with high voltage and low frequency would be the most suitable for electrostatic solvent extraction, both in terms of mass transfer and operational considerations including safety.

# Chapter 8

# CONCLUSIONS AND RECOMMENDATIONS

## 8.1. CONCLUSIONS

The commercial applications of solvent extraction (SX) in hydrometallurgy have been increasing and expanding since its introduction in the middle of the past century. This trend is set to continue, given the increasing need to process low grade and complex ores necessitating the use of more vigorous leaching conditions and thus generating highly contaminated pregnant liquor solutions. SX is the only commercially proven technique for purifying these solutions. It is also the only purifying technique that can be used for the separation of chemically similar species such as, for example, nickel and cobalt and the rare earth metals whose productions are increasing too.

The current SX technology, however, has weaknesses and a major one is the use of mechanical agitation. Recognised since the early days of SX commercial applications, it has been the subject of extensive efforts but it is now clear that it has inherent limitations particularly in regards to mass transfer.

A promising alternative is the use of electrostatic fields to intimately contact the aqueous and organic phases and hence called electrostatic solvent extraction (ESX). It is particularly attractive as it promises to circumvent the limitations of conventional SX associated with mechanical agitation while retaining its strengths and distinct advantages over other separation techniques, resulting in enhanced mass transfer, low shear mixing, enhanced phase disengagement, and lower power consumption. Efforts to develop ESX have already yielded several significant advancements, including the achievement of a volumetric throughput that is comparable to conventional pulse column at pilot scale. In spite of this, however, no commercial application of the technique has been achieved. This may be attributed to the still scarce technical data and some inconsistent and even conflicting reports particularly in regards to how electrostatic fields influence interfacial phenomena, and effect and affect droplet dispersion and droplet agitation and hence mass transfer under experimental conditions that are relevant to hydrometallurgical SX.

To assist in addressing this gap in the knowledge of the technique, the present study was aimed to further the understanding of the main factors that influence mass transfer in ESX. Specifically, it was aimed to:

- determine how electrostatic fields influence the interfacial phenomena and the mass transfer across the aqueous-organic interface under conditions that are relevant to hydrometallurgical SX,
- determine how the properties of electrostatic fields effect and affect the droplet dispersion, the droplet agitation in the resulting dispersions and the mass transfer within the dispersions, and
- determine the most suitable electrostatic field conditions for practical applications of ESX.

To assist in the effort of the research group to develop an application of the technique for the purification of cobalt and nickel and ensure relevance to hydrometallurgical SX applications, the extraction of Co(II) with Cyanex® 272 was used as the test system.

The literature review revealed that, to achieve these objectives, two different experimental methods had to be developed: a modified Lewis cell for the investigation on the effect of electrostatic fields on interfacial phenomena and mass transfer across the aqueous-organic interface, and a droplet column for the investigation on how electrostatic fields effect and affect droplet dispersion, droplet agitation and mass transfer within dispersions. Since both had to be purpose built, their design, construction and commissioning became a significant part of this study.

The investigation on the effect of electrostatic fields on interfacial phenomena and mass transfer across the aqueous-organic interface revealed that:

- Electrostatic fields with fixed polarity such as DC and PDC, either negative or positive, enhanced the mass transfer of Co(II) species across the organic diffusion region owing to electrostatic attraction between the extracted species and the electrodes. As such, AC fields had no effect on mass transfer across this diffusion region.
- Electrostatic fields had no effect on the mass transport of Co(II) species across the aqueous diffusion region because no field could be sustained in this region owing to its high conductivity leading to fast dissipation of charges.

- Electrostatic fields had no effect on the rate of the chemical reaction between Co(II) and Cyanex® 272 at the aqueous-organic interface.

The investigation on how electrostatic fields effect and affect droplet dispersion revealed that:

- All electrostatic field types—positive and negative DC and PDC, and AC—can be used to disperse aqueous droplets in the organic phase by imposing orientational and interfacial polarisation beyond that which their surface tension can withstand. This is evident in the relationship between the strengths of the applied field and droplet sizes, which decreased with increases in field strengths. DC and PDC fields, however, could only be sustained when using bare electrodes as otherwise, the set-up acted as a capacitance. The continuous organic phase was therefore the only insulation.
- The droplets dispersed through previously known mechanisms, namely necking and jetting but also through three distinct mechanisms that have not been reported previously. These are referred to, in this work, as irregular, combination and emulsion-like formation to be descriptive.
- Although the size of the dispersed droplets was found to be largely a function of the field strength, the frequency of transient fields (PDC and AC) had a small but measurable effect, as it was found to influence the amplitude of droplet elongation and hence its susceptibility to dispersion. The elongation, however, was also influenced by hydrodynamic factors, such that too high a frequency prevented the droplet from elongating fully while too low a frequency led to too gentle elongation. Neither of them is favourable to droplet dispersion. The optimum frequency for PDC was 40 Hz and for AC was 20 Hz, which subject droplets to comparable stress.
- Positive DC and PDC fields generated finer droplet dispersions with narrower size distributions than their corresponding negative fields owing to a greater amount of interfacial polarisation. At comparable field strengths, however, AC fields yielded the finest dispersed droplets and narrowest distribution.

The investigation on how electrostatic fields effect and affect droplet agitation revealed that:

- Electrostatic agitation consists of droplet oscillation, speed (of linear motion) and zigzagging (horizontal component of linear speed and frequency of change of direction).
- Droplet oscillation is a manifestation of orientational polarisation as it occurred only in the presence of transient fields (PDC and AC) and hence, an intermittent electrostatic force imparted by the field, at a rate that was in synchrony with the frequency of the field, and increased with increases in the field strength. Increases in the droplet size led to increases in the amplitude of oscillation owing to greater amounts of polarisation.
- The horizontal motion (zigzagging) of droplets is a manifestation of interfacial polarisation as it was far more prevalent in DC and PDC fields, which had no insulation and droplets changed direction only upon contact with electrodes, indicating the acquisition of the electrode's charge. In addition, zigzagging droplets were usually not elongated.
- The charge-to-mass-ratio of droplets influences their polarisation when subjected to electrostatic fields. Droplets with high charge-to-mass ratio are both orientationally and interfacially polarised while droplets with low charge-to-mass ratio are largely orientationally polarised only.

The investigation on the effect of electrostatic fields on mass transfer within dispersions revealed that:

- As predicted, based on the results of the characterisation of the effects of electrostatic fields on droplet dispersion and agitation, increases in the strength of the applied field resulted in increases in the mass transfer of Co(II) as these conditions would have led to increases in interfacial area and droplet agitation (oscillation, speed and zigzagging).
- Increases in the frequency of the applied field resulted in decreases in the mass transfer of Co(II) indicating that the droplet speed, amplitude of oscillation and zigzagging, which all decreased with increases in frequency, had a more significant effect on mass transfer than the slight increase in interfacial area owing to the production of slightly finer droplets.

Overall, therefore, the use of high voltage and low frequency AC fields would be the most suitable for ESX applications as they provide the largest interfacial area and most intense agitation at the lowest field strengths with highest degree of insulation.

## 8.2. RECOMMENDATIONS

Whilst the present study has achieved its objectives, there were a number of unexpected observations that are relevant towards the development of commercial application of ESX and therefore a useful subject of future work. These include:

- Droplets were observed to both coalesce and disperse at strengths that were used to disperse the feed droplets, which was totally unexpected given that it is in contrast to the common view in the literature that a given field strength would either disperse or coalesce droplets and therefore these are considered to be mutually exclusive. Obviously, an understanding of this phenomenon would be relevant to ESX.

- The imaging technique that was used in the present study as well as all currently available techniques allow only a limited range of droplet sizes to be investigated under a given set of experimental conditions. It would be helpful to extend the present work to a range of much smaller droplets below the minimum size of the current study as they proved useful in enhancing mass transfer in ESX.
- The generation of emulsion-like formation of dispersed droplets that almost immediately disappeared to form larger droplets was also totally unexpected but exploiting it in ESX to enhance mass transfer may prove particularly useful.

- Some peripheral observations in the present study suggested that the electrode configuration and spacing may have a significant influence on droplet dispersion and agitation. The knowledge on this would be useful in the design of an ESX contactor.

- Investigate interfacial phenomena, droplet dispersion and droplet agitation in other SX systems. Although the data generated in the present study are relevant to other hydrometallurgical SX applications, it is not certain that they are fully transferable.

# REFERENCES


Albery, WJ, Burke, JF, Leffler, EB & Hadgraft, J 1976, 'Interfacial transfer studied with a rotating diffusion cell', *Journal of the Chemical Society, Faraday Transactions 1: Physical Chemistry in Condensed Phases,* vol. 72, pp. 1618-1626.

Austin, LJ, Ying, WE & Sawistowski, H 1966, 'Interfacial phenomena in binary liquid-liquid systems', *Chemical Engineering Science*, vol. 21, no. 11, pp. 1109-1110.

Austin, LJ, Banczyk, L & Sawistowski, H 1971, 'Effect of electric field on mass transfer across a plane interface', *Chemical Engineering Science*, vol. 26, no. 12, pp. 2120-2121.

Bailes, PJ 1977, 'Electrostatic extraction for metals and non-metals', *Proceedings of the International Solvent Extraction Conference*, Toronto, Canada, pp. 233-241.

Bailes, PJ 1981, 'Solvent extraction in an electrostatic field', *Industrial and Engineering Chemistry Process Design and Development*, vol. 20, no. 3, pp. 564-570.

Bailes, PJ 1992, 'Electrically augmented settlers and coalescers for solvent extraction', *Hydrometallurgy*, vol. 30, no. 1-3, pp. 417-430.

Bailes PJ & Larkai, SKL 1981, 'An experimental investigation into the use of high voltage DC fields for liquid phase separation', *Transactions of the Institution of Chemical Engineers*, vol. 59, no. 1, pp. 229-237.

Bailes, PJ & Thornton, JD 1971, 'Electrically augmented liquid-liquid extraction in a two-component system. Single droplet studies', *Proceedings of the International Solvent Extraction Conference*, The Hague, Netherlands, pp. 1431-1439.

Bailes, PJ & Thornton, JD 1974, 'Electrically augmented liquid-liquid extraction in a two-component system. Multidroplet studies', *Proceedings of the International Solvent Extraction Conference*, Lyon, France, pp. 1011-1027.

Basaran, OA & Scriven, LE 1982, 'Profiles of electrified drops and bubbles', *Proceedings of the Second International Colloquium on Drops and Bubbles*, California, United States, pp. 322-329.

Broan, C, Bailey, A & Williams, T 1996, 'Advances in fundamental understanding of electrostatic pseudo liquid membrane systems', paper presented to the International Congress on Membranes and Membrane Processes, Yokohama, Japan, 18-23 August.

Clinton, SD 1972, 'Mass transfer of water from single aqueous sol droplets fluidized in a partially miscible alcohol', PhD thesis, Oak Ridge National Laboratory, Tennessee.

Collard, JM 2011, 'Separation and purification of dissolved metals using electrostatic pseudo liquid membrane (ESPLIM)', PhD thesis, Curtin University of Technology, Kalgoorlie.

Danesi, PR 2004, 'Solvent extraction kinetics' in Rydberg, J, Cox, M, Musikas, C & Choppin, GR (eds.), *Solvent Extraction Principles and Practice*, 2nd edn, Marcel Dekker, New York, 243-250.

Danesi, PR, Chiarizia, R & Coleman, CF 1980, 'The kinetics of metal solvent extraction', *C R C Critical Reviews in Analytical Chemistry*, vol. 10, no. 1, pp. 1-126.

Danesi, PR, Cianetti, C, Horwitz, EP & Diamond, H 1982, 'ARMOLLEX: An apparatus for solvent extraction kinetic measurements', *Separation Science and Technology*, vol. 17, no. 7, pp. 961-968.

Fu, X & Golding, JA 1988, 'Equilibrium and mass transfer for the extraction of cobalt and nickel from sulfate solutions into bis(2,44-trimethylpentyl) phosphinc acid – Cyanex 272', *Solvent Extraction and Ion Exchange*, vol. 6, no. 5, pp. 889-917.

Garton, CG & Krasucki, Z 1964, 'Bubbles in insulating liquids: stability in an electric field', *Proceedings of the Royal Society of London*, vol. A280, pp. 211-226.

Glitzenstein, A, Tamir, A & Oren, Y 1995, 'Mass transfer enhancement of acetic acid across a plane kerosene/water interface by an electric field', *The Canadian Journal of Chemical Engineering*, vol. 73, no. 1, pp. 95-102.

Gneist, G & Bart, HJ 2003, 'Influence of high-frequency AC fields on mass transfer in solvent extraction', *Journal of Electrostatics*, vol. 59, no. 2, pp. 73-86.

Goldburg, A & Florsheim, BH 1966, 'Transition and Strouhal number for the incompressible wake of various bodies', *The Physics of Fluids*, vol. 9, no. 1, pp. 45-50.

Gu, ZM, Wasan, DT & Li, NN 1986, 'Ligand-accelerated liquid membrane extraction of metal ions', Journal of Membrane Science, vol. 26, no. 2, pp. 129-142.

He, W, Chang, JS & Baird, MHI 1990, 'Liquid-liquid dispersion under pulsed electric fields in a horizontal cell', Proceedings of the Industry Applications Society Annual Meeting, pp. 774-777.

He, W, Chang, JS & Baird, MHI 1997, 'Enhancement of interphase mass transfer by a pulsed electric field', *Journal of Electrostatics*, vol. 40-41, pp. 259-264.

Heckley, PS 2002, 'Extraction and separation of cobalt from nickel laterite leach solutions using the ESPLIM technique', PhD thesis, Curtin University of Technology, Kalgoorlie.

Hendricks, CD & Schneider, JM 1962, 'Stability of a conducting droplet under the influence of surface tension and electrostatic forces', *American Journal of Physics*, vol. 31, no. 6, pp. 450-453.

Hendricks, CD 1973, 'Introduction to electrostatics', in Moore AD (ed.), *Electrostatics and its Applications*, John Wiley & Sons, New York, pp. 8-28.

Hu, S & Kintner, RC 1955, 'The fall of single liquid drops through water', *American Institute of Chemical Engineers (AIChE) Journal*, vol. 1, no. 1, pp. 42-48.

Hund, M & Lancelot, F 1986, 'Interfacial transfer under electrostatic field in solvent extraction*', Proceedings of the International Solvent Extraction Conference*, Munich, Germany, pp. 511-517.

Inculet, II 1973, 'Static electrification of dielectrics and at materials' interfaces', in Moore AD (ed.), *Electrostatics and its Applications*, John Wiley & Sons, New York, pp. 86-114.

Iyer, PVR & Sawistowski, H 1974, 'Effect of electric field on mass transfer across a plane interface', *Proceedings of the International Solvent Extraction Conference*, Lyon, France, pp. 1029-1045.

Klee, AJ & Treybal, RE 1956, 'Rate of rise or fall of liquid drops', *American Institute of Chemical Engineers (AIChE) Journal*, vol. 2, no. 4, pp. 444-447.

Kuipa, PK & Hughes, MA 1999, 'Influence of high voltage electric fields applied across a horizontal liquid-liquid interface on the rate of metal extraction using a rotating diffusion cell', *Separation Science and Technology*, vol. 34, no. 13, pp. 2643-2661.

Kuipa, PK & Hughes, MA 2002, 'Behavior of interfacial tension at an oil-water interface in the presence of an applied electrical field', *Proceedings of the International Solvent Extraction Conference*, Cape Town, South Africa, pp. 53-57.

Levich, VG 1962, *Physiochemical Hydrodynamics*, Prentice-Hall, New Jersey, USA.

Lewis, JB 1954, 'The mechanism of mass transfer of solutes across liquid-liquid interfaces. Part I: the determination of individual transfer coefficients for binary systems', *Chemical Engineering Science*, vol. 3, no. 6, pp. 248-259.

Lide, DR (ed.), 2002, *CRC Handbook of Chemistry and Physics*, 82nd edn, CRC Press LLC, Boca Raton, USA.

Lindell, E, Jaaskelainen, E, Paatero, E & Nyman, B 2000, 'Effect of reversed micelles in Co/Ni separation by Cyanex 272', *Hydrometallurgy*, vol. 56, no. 3, pp. 337-357.

Marangoni, C 1871, 'Ueber die ausbreitung der tropfen einer flussigkeit auf der oberflache einer anderen' (Of the expansion of drops of a liquid on the surface of another liquid), Poggendorff's Annalen Der Physik und Chemie, vol. 143, no. 7, pp. 337-354.

Maroudas, NG & Sawistowski, H 1964, 'Simultaneous transfer of two solutes across liquid-liquid interfaces', *Chemical Engineering Science*, vol. 19, no. 11, pp. 919-931.

Martin, L, Vignet, P, Fombarlet, C & Lancelot, F 1983, 'Electrical field contactor for solvent extraction', *Separation Science and Technology*, vol. 18, no. 14-15, pp. 1455-1471.

Melcher, JR & Taylor GI 1969, 'Electrohydrodynamics: A review of the role of interfacial shear stresses', *Annual Review of Fluid Mechanics*, vol. 1, pp. 111-146.

Mohan, V, Padmanabhan, K & Chandrasekharan, K 1983, 'Marangoni effects under electric fields', *Advances in Space Research*, vol. 3, no. 5, pp. 177-180.

Nagata, S & Yamaguchi, I 1960, 'Mass transfer and chemical reaction in liquid-liquid agitation systems', *Memoirs of the Faculty of Engineering, Kyoto University*, vol. 22, pp. 249-276.

Nitsch, W & Hillekamp, K 1972, 'Zur kinetic der zinkionenextraktion aus wasser in dithizon-beladene solventien' (The kinetics of zinc ion extraction from water into dithizone-loaded solvents), *Chemiker-Zeitung*, vol. 96, no. 5, pp. 254-261.

Nitsch, W & Kruis, B 1978, 'The influence of flow and concentration on the mass transfer mechanism in chelating liquid/liquid-extractions', *Journal of Inorganic and Nuclear Chemistry*, vol. 40, no. 5, pp. 857-864.

Nitsch, W & Plucinski, P 1990, 'Two-phase kinetics of the solubilization in reverse micelles', *Journal of Colloid and Interface Science*, vol. 136, no. 2, pp. 338-351.

Pohl, HA 1973, 'Nonuniform field effects: Dielectrophoresis', in Moore AD (ed.), *Electrostatics and its Applications*, John Wiley & Sons, New York, pp. 336-362.

O'Konski, CT & Thacher, HC 1953, 'The distortion of aerosol droplets by an electric field', *The Journal of Physical Chemistry*, vol. 57, pp. 955.

Oxford Lasers Imaging Division, 2010, *Oxford Lasers Sizing System User Manual.*

Rayleigh, Lord 1879, 'On the capillary phenomena of jets', *Proceedings of the Royal Society of London*, vol. 29, pp. 71-97.

Reeves, MJ, Bailey, AG, Howard, AG, & Broad, CJ 1999, 'Factors influencing operational efficiency of an electrostatic solvent extraction system', *Proceedings of Electrostatics 1999, Institute of Physics Conference Series Number 163*, Cambridge, United Kingdom, pp. 257-260.

Ritcey, GM 1980, 'Crud in solvent extraction processing - a review of causes and treatment', *Hydrometallurgy*, vol. 5, no. 2-3, pp. 97-107.

Ritcey, GM 2002, 'Some design and operating problems encountered in solvent extraction plants', *Proceedings of the International Solvent Extraction Conference*, Cape Town, South Africa, pp. 871-878.

Ritcey, GM 2006a, *Solvent Extraction. Principles and Applications to Process Metallurgy, vol.* 2, 2nd edn, G.M. Ritcey & Associates Incorporated, Ottawa.

Ritcey, GM 2006b, *Solvent Extraction. Principles and Applications to Process Metallurgy, vol.* 1, 2nd edn, G.M. Ritcey & Associates Incorporated, Ottawa.

Roddy, JW, Coleman, CF & Arai, S 1971, 'Mechanism of the slow extraction of iron(III) from acid perchlorate solutions by di(2-ethylhexyl)phosphoric acid in *n*-octane', *Journal of Inorganic and Nuclear Chemistry*, vol. 33, no. 4, pp. 1099-1118.

Rosenkilde, CE 1969, 'A dielectric fluid drop in an electric field', *Proceedings of the Royal Society of London*, vol. A312, pp. 473-494.

Scott, TC & Wham RM 1989, 'An electrically driven multistage countercurrent solvent extraction device: the emulsion-phase contactor', *Industrial and Engineering Chemistry Research*, vol. 28, no. 1, pp. 94-97.

Scott, TC, DePaoli, DW & Sisson, WG 1994, 'Further development of the electrically driven emulsion-phase contactor', *Industrial and Engineering Chemistry Research*, vol. 33, no. 5, pp. 1237-1244.

Scott, TC, Basaran, OA & Byers, CH 1990, 'Characteristics of electric-field-induced oscillations of translating liquid droplets', *Industrial and Engineering Chemistry Research*, vol. 29, no. 5, pp. 901-909.

Simonin, J, Turq, P & Musikas, C 1991, 'Rotating stabilised cell: a new tool for the investigation of interfacial extraction kinetics between liquid phases', *Journal of the Chemical Society, Faraday Transactions*, vol. 87, no. 17, pp. 2715-2721.

Sole, KC & Hiskey, JB 1992, 'Solvent extraction characteristics of thiosubstituted organophosphinic acid extractants', *Hydrometallurgy*, vol. 30, no. 1-3, pp. 345-365.

Steffens, MJ 2011, 'Development of an electrostatically assisted solvent extraction column', PhD thesis, Curtin University of Technology, Kalgoorlie.

Stewart, G & Thornton, JD 1967, 'Charge and velocity characteristic of electrically charged droplets. Part 2: Preliminary measurements of droplet charge and velocity', *Institute of Chemical Engineers Symposium Series*, vol. 26, pp. 37-42.

Sternling, CV & Scriven LE 1959, 'Interfacial turbulence: Hydrodynamic instability and the Marangoni effect', *American Institute of Chemical Engineers (AIChE) Journal*, vol. 5, no. 4, pp. 514-523.

Taylor, G 1964, 'Disintegration of water drops in an electric field', *Proceedings of the Royal Society of London*, vol. A280, pp. 383-397.

Ullmann's Encyclopedia of Industrial Chemistry (online service), 2012, Wiley-Blackwell.

Wham, RM & Byers, CH 1987, 'Mass transport from single droplets in imposed electric fields', *Separation Science and Technology*, vol. 22, no. 2-3, pp. 447-466.

Whitman, WG 1923, 'The two-film theory of gas absorption', *Chemical and Metallurgical Engineering*, vol. 29, no. 4, pp. 146-148.

Wildberger, A & Bart, HJ 2002, 'Influencing the rate of mass transfer in reactive extraction using high voltage', *Proceedings of the International Solvent Extraction Conference*, Cape Town, South Africa, pp. 251-256.

Yamaguchi, M, Sugaya, H & Katayama, T 1988, 'Hydrodynamic behavior of dispersed phase in a spray column with an electric field for liquid-liquid extraction', *Journal of Chemical Engineering of Japan*, vol. 21, no. 2, pp. 179-183.

Zhou, Q & Gu, ZM 1988, 'Studies on the extraction of $Eu^{3+}$ by means of electrostatic pseudo liquid membrane', *Water Treatment*, vol. 3, pp. 127-135.

# APPENDICES

## APPENDIX A: ADDITIONAL INFORMATION FOR MODIFIED LEWIS CELL EXPERIMENTS

### A1: Diagrams and Photographs of the Glass Compartments of the MLC

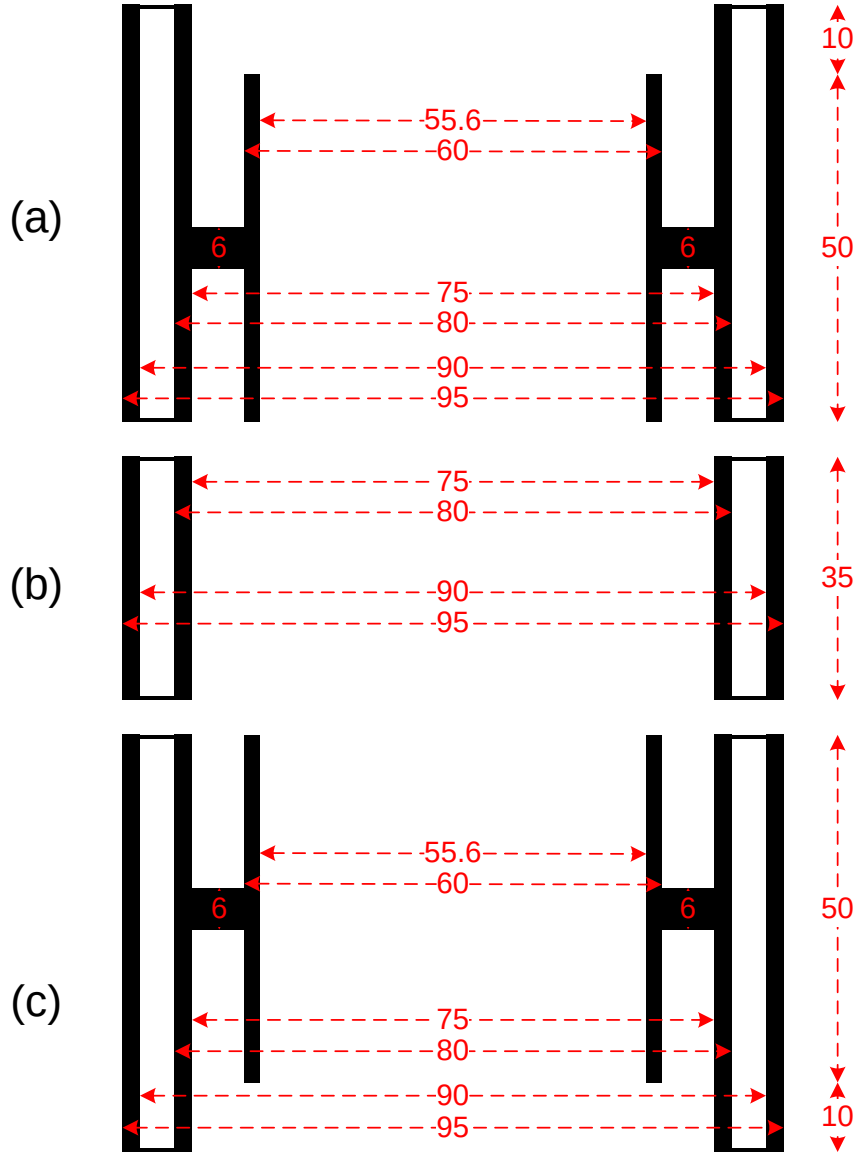


All dimensions are in millimetres. This diagram does not show the barbed ports on the jacket in each compartment, as well as the third glass rod (6 mm Ø) which attaches the inner cylinder to the outer cylinder in the upper and lower compartments. The three glass rods were equi-distant around the inner cylinder.

The dimensions shown on the above diagram are those that were provided to the glassblower that manufactured the MLC (Custom Blown Glassware Australia). These

dimensions are approximate owing to the nature of manufacturing a custom piece of glassware and thus, the actual dimensions may be slightly different from those shown above. For example, the internal diameter of the middle compartment (specified as 75 mm) was actually 74.3 mm when measured with a vernier caliper.

Middle Compartment

Side View

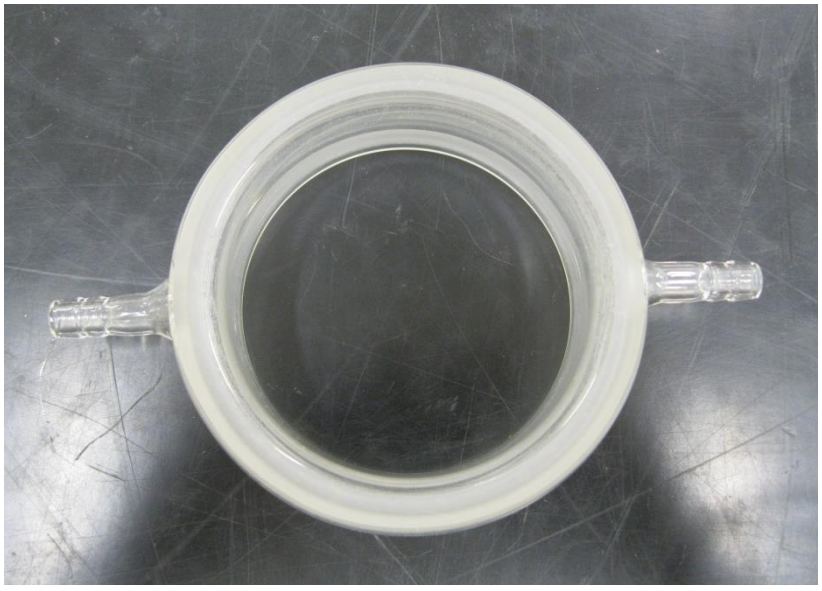

Top View

Upper and Lower Compartments

Side View

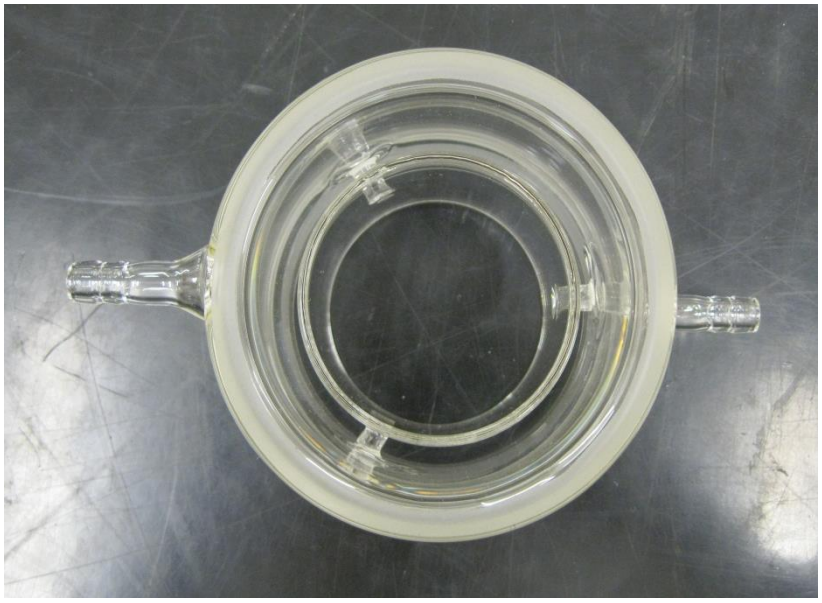

Top View

## A2: Diagrams and Photographs of the MLC Lids

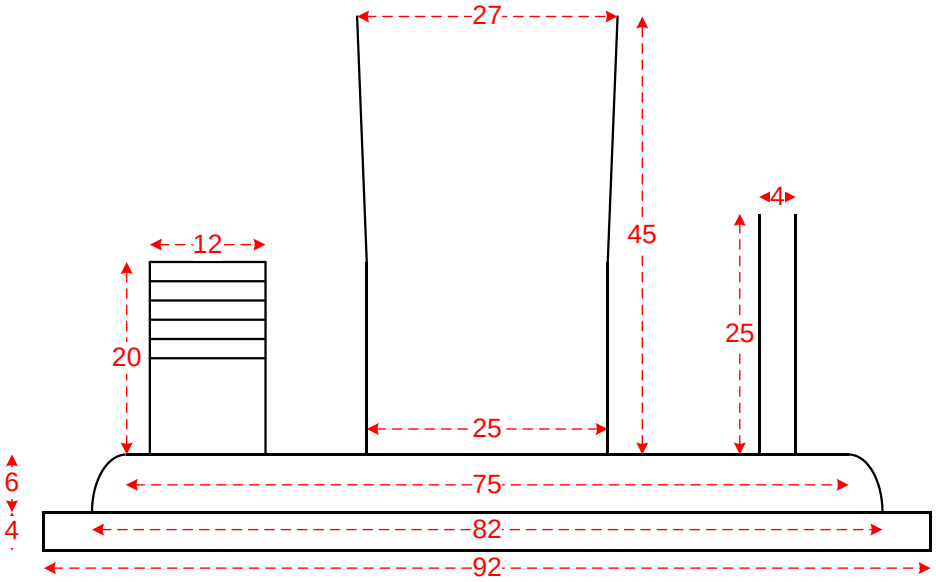


Side View

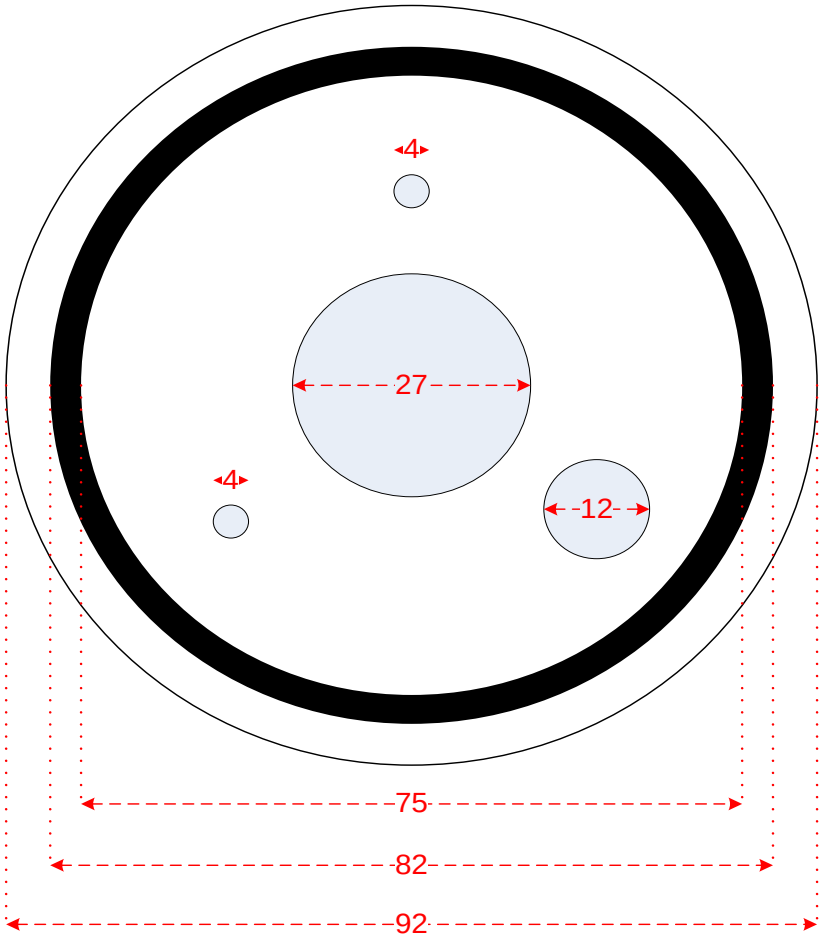


Top View

All dimensions are in millimetres.

Side View

Top View

## A3: Diagram of Moulds Used to Construct the Wire Mesh Electrodes

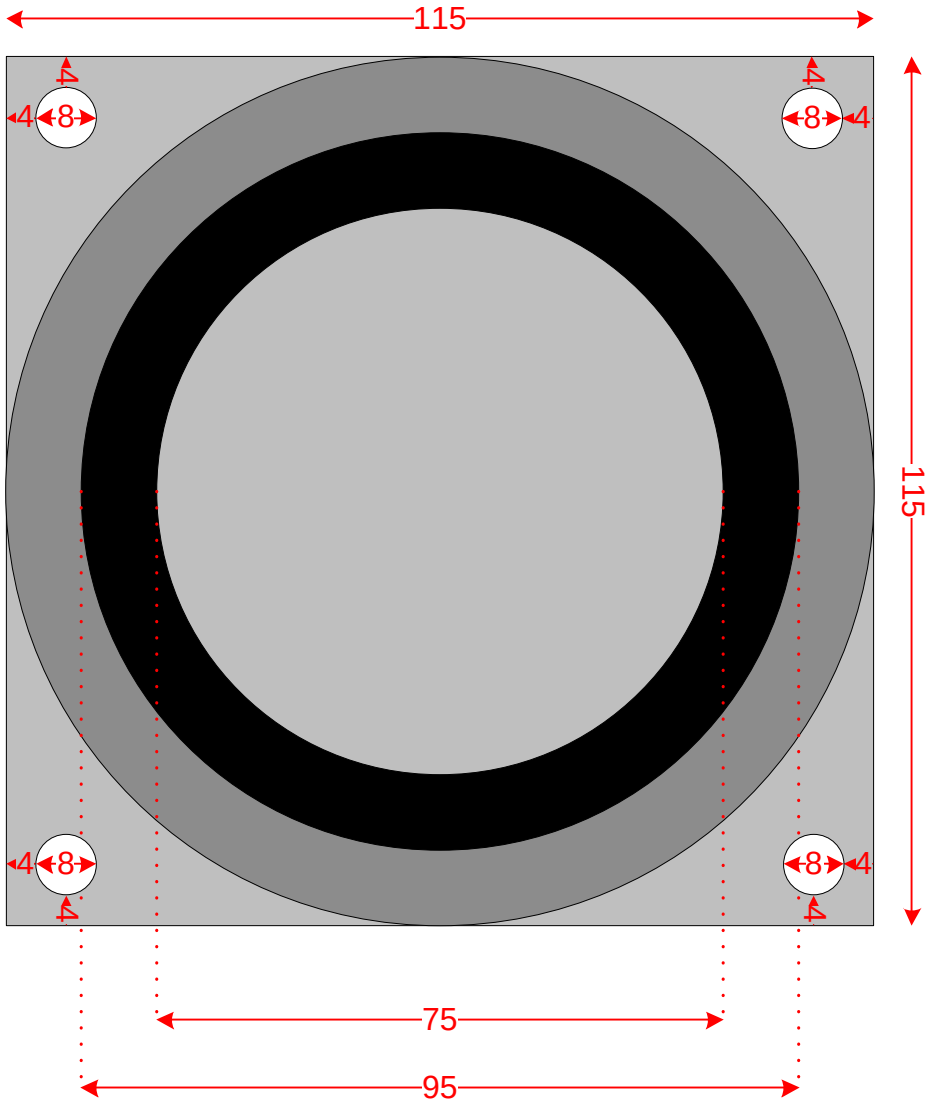


All dimensions are in millimetres. The ring (95 mm ID, 115 mm OD) was adhered onto the square plate (115 mm x 115 mm) using an epoxy adhesive (Araldite, Selleys). Holes (8-mm ∅) were drilled into the four corners of the moulds so that bolts and nuts could be used to apply compression between the two moulds. This diagram also shows an HDPE o-ring (75 mm ID, 95 mm OD) that was placed inside the ring during construction of the wire mesh electrodes.

## A4: Diagram of the Wire Mesh Electrodes

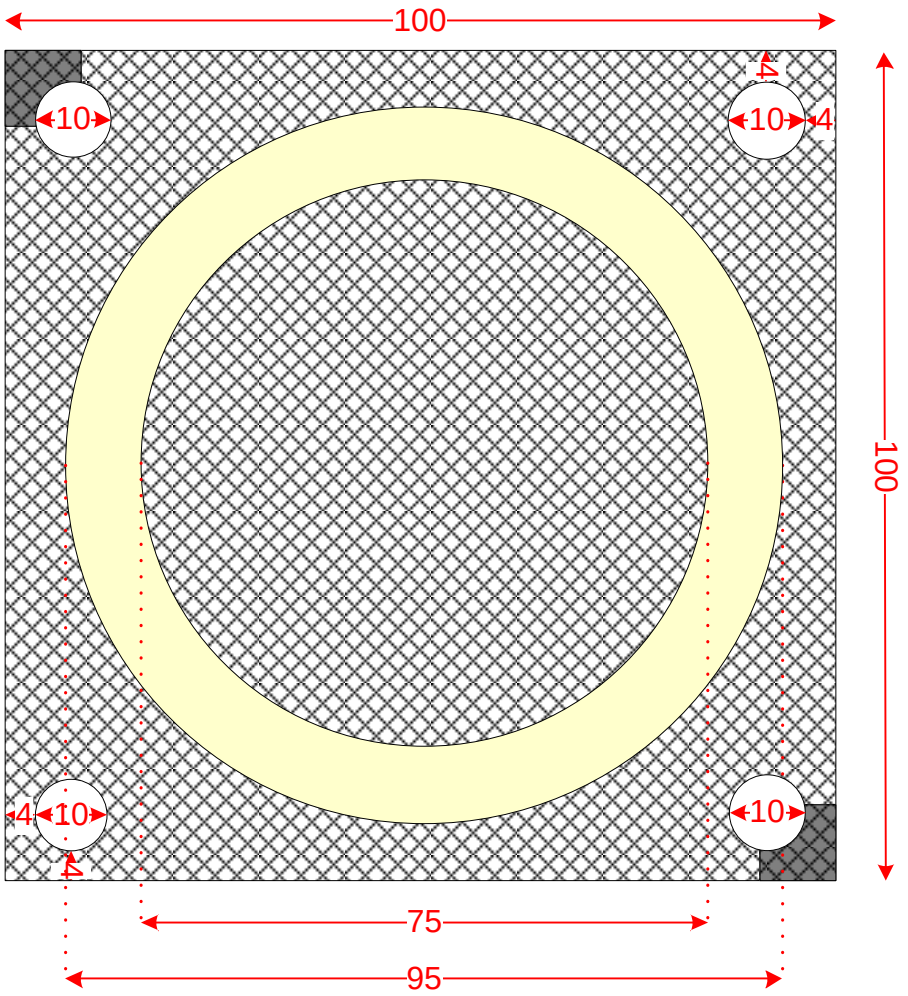


All dimensions are in millimetres. The diagram shows the two opposite corners of the wire mesh that were covered during the coating process and therefore remained uninsulated. This facilitated connection of the electrodes to high-voltage power supplies by soldering Tefzel®-coated stainless steel wire (M22759/16 AWG22, Avial Australia) to one of the uninsulated sections of the wire mesh. The diagram also shows the Polymorph layer, which formed in the shape of the HDPE o-rings (75 mm ID, 95 mm OD) during construction of the wire mesh electrodes.

The diagram does not show that the two opposite sides of the wire mesh electrodes that had insulated corners were cut along the circumference of the Polymorph layer so that the electrodes could fit between the MLC supports.

## A5: Diagram of the Stainless Steel and Viton® MLC Support Plates

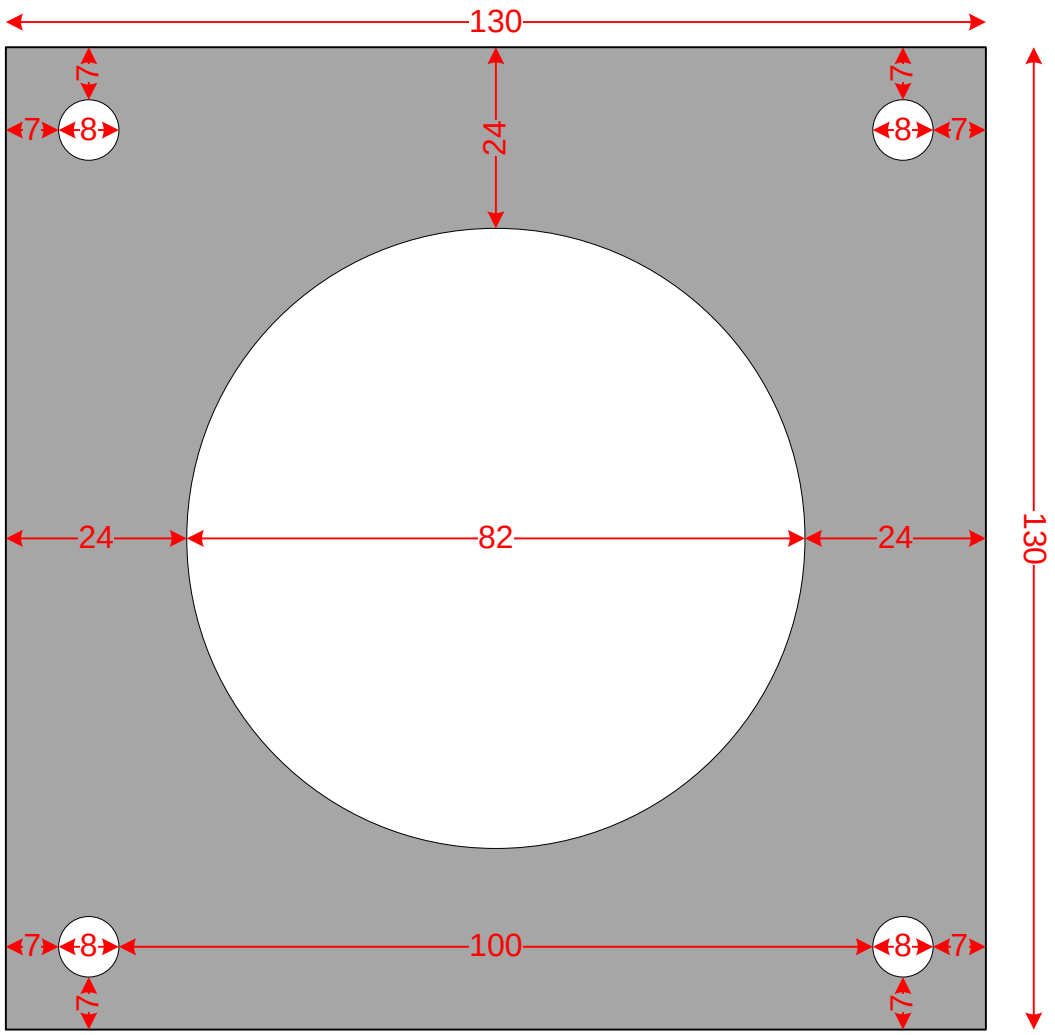


All dimensions are in millimetres. Stainless steel and Viton® support plates were placed below the lower lid and above the upper lid of the MLC. In both cases, the lids were in contact with the Viton® support plates and not the stainless steel plates.

## A6: Photographs of the Procedure for Assembly of the MLC

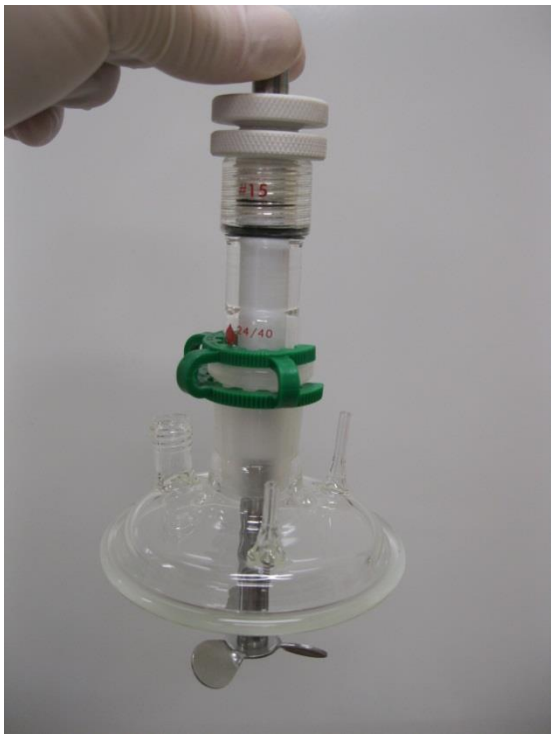

Step 1/8: assembly of lids with stirrer bearings and stirrer shafts

Step 2/8: attach upper stirrer shaft to upper stirrer with universal bearing and rest lower lid on support plates

Step 3/8: placement of glass compartments with o-rings

Step 4/8: placement of wire mesh electrodes with o-rings

Step 5/8: alignment of the MLC using builders wedges

Step 6/8: compression of the support plates

Step 7/8: attach lower stirrer shaft to lower stirrer with universal bearing

Step 8/8: alignment of the of the propeller blades with the glass rod

## A7: Photographs of MLC Experimental Set-up


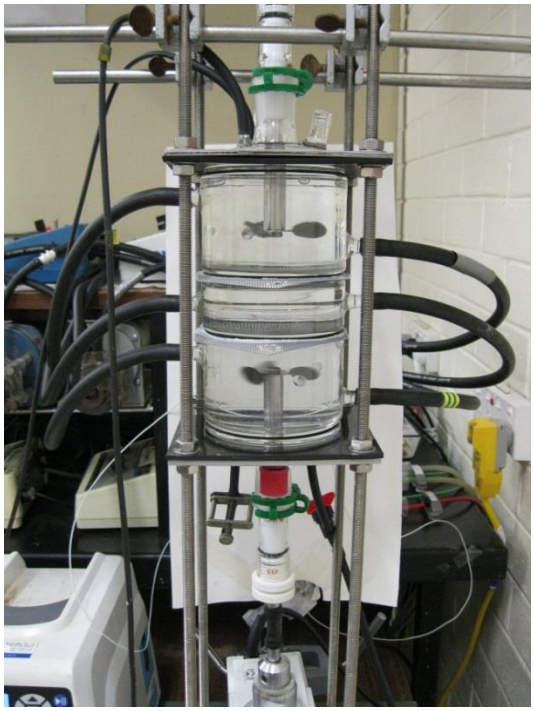

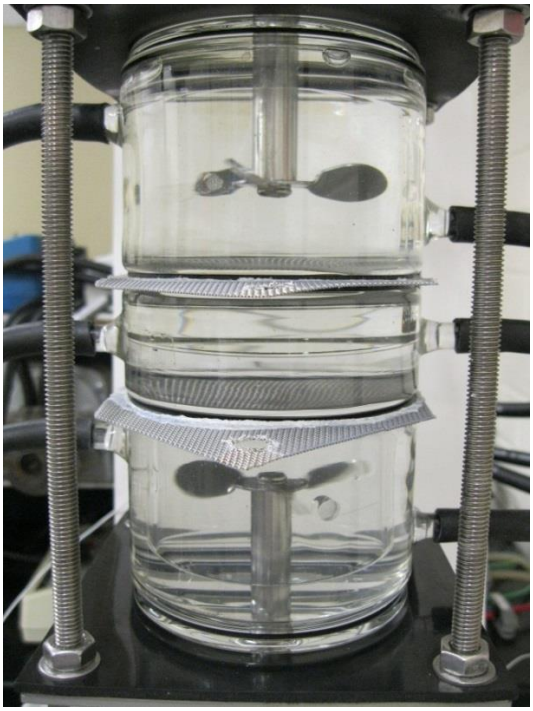

## APPENDIX B: ADDITIONAL INFORMATION FOR DROPLET COLUMN EXPERIMENTS

### B1: Diagram and Photograph of the Droplet Column Body

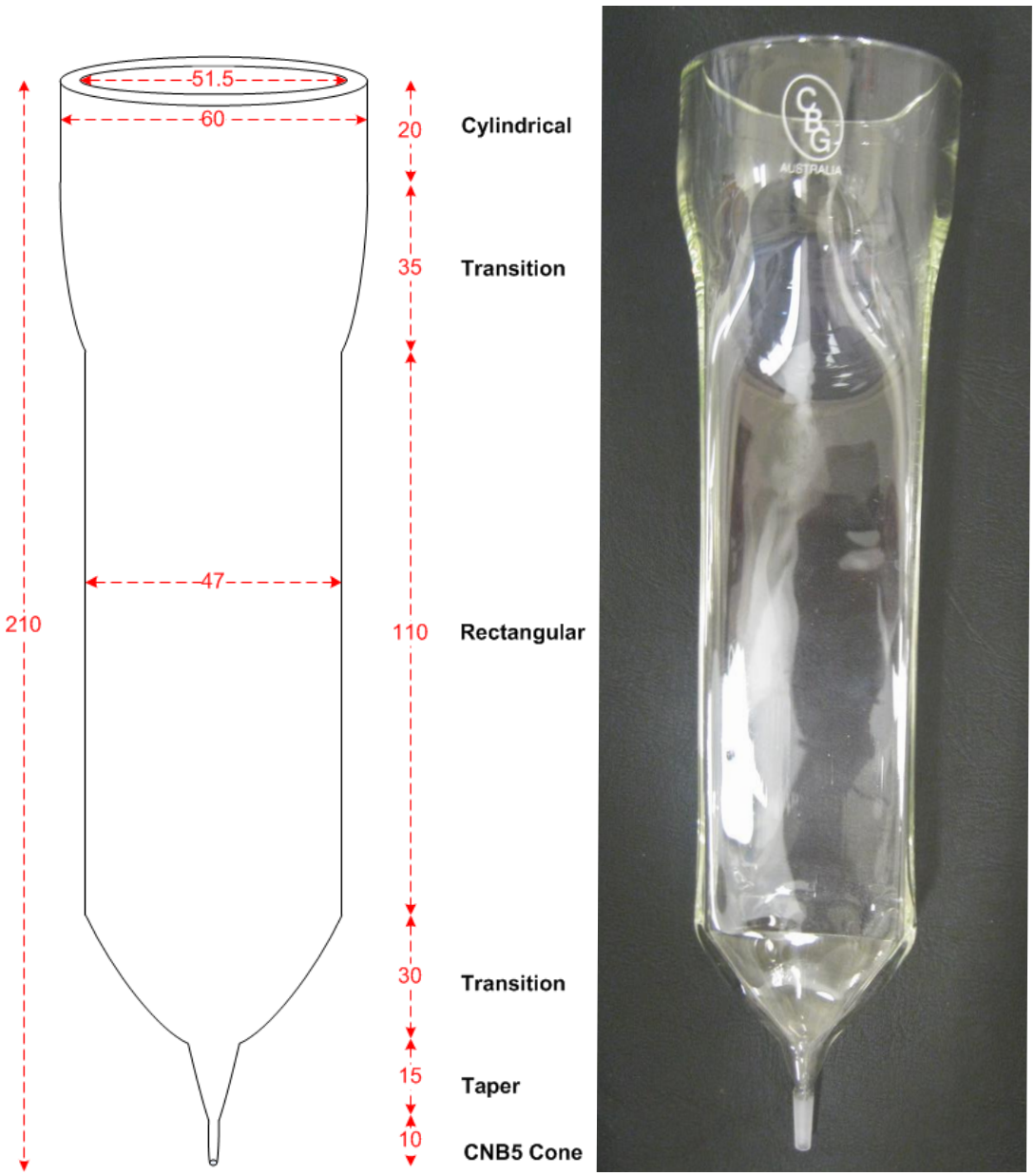


All dimensions are in millimetres.

## B2: Diagram and Photographs of the Parallel-Plate Electrodes

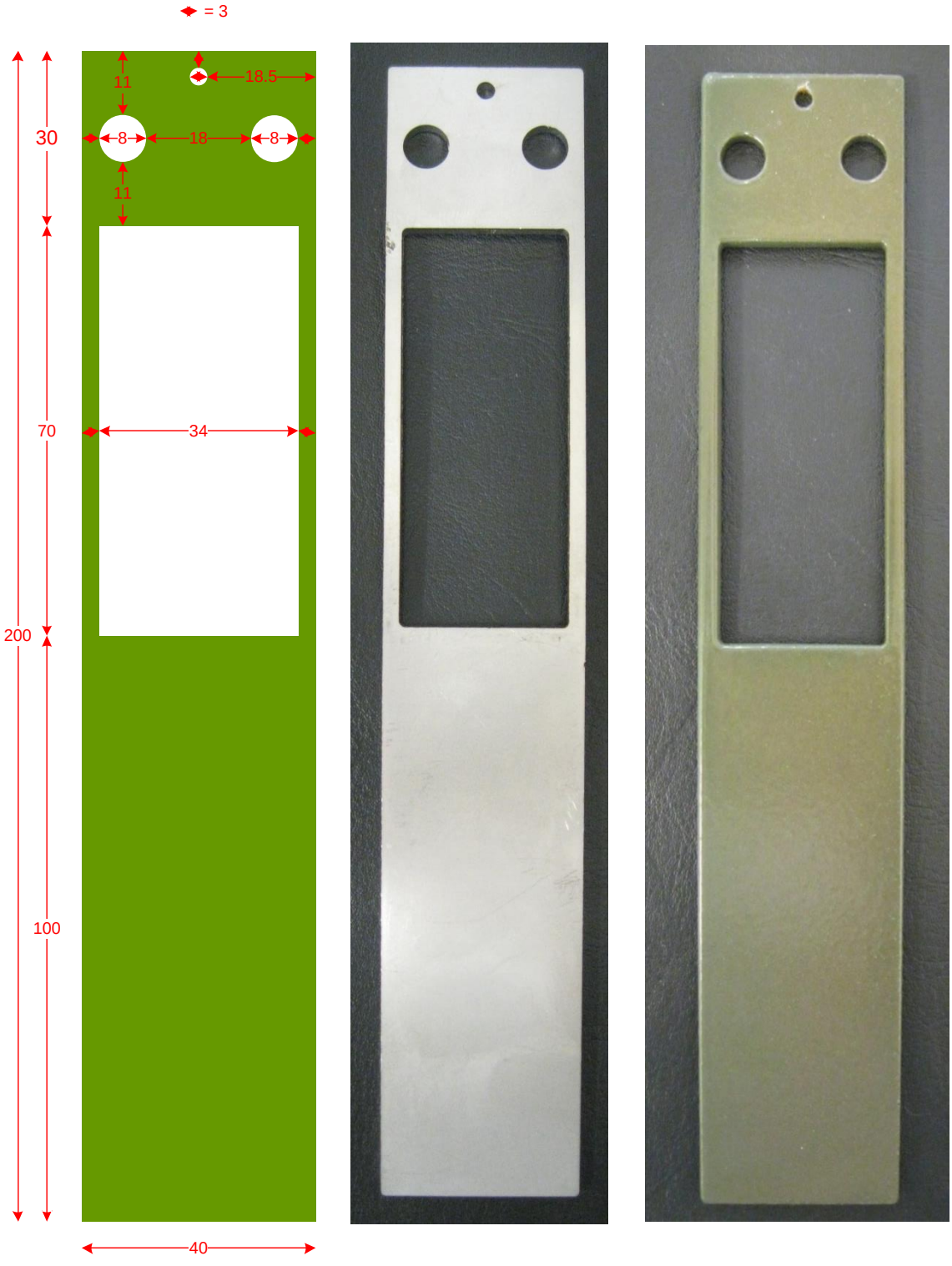


All dimensions are in millimetres. Computerised laser cutting was used to cut these dimensions out of 3-mm thick stainless steel. The photograph in the centre shows an uninsulated electrode. The photograph on the right shows an insulated electrode after coating with ethylene tetrafluoroethylene (ETFE).

## B3: Technique for Measurement of Droplet Sizes

The Oxford Lasers Imaging System (VisiSizer D30V, IMG0021) was used for the measurement of droplet sizes. The following information is taken from the Oxford Lasers Sizing System User Manual (Oxford Lasers Imaging Divison, 2010).

The imaging system uses a technique called Particle/Droplet Image Analysis (PDIA) to measure droplet sizes. This involves illuminating droplets from behind and taking images of the shadows cast by droplets. The background illumination in the absence of any droplets, which is known as the background grey level, is used as a calibration and each pixel within the field of view is assigned a grey level value from 0 (black) to 255 (white), to allow the system to distinguish between the droplet shadows and the background. It is therefore critical that the laser and high-speed camera are positioned such that a uniform background illumination is achieved.

The imaging system can measure the size of droplets that are partly out of focus by analysis of the halo that forms around the shadows of these droplets. If, however, a droplet is more out of focus than the system has been calibrated to measure, the droplet is rejected from the size analysis.

The procedure for calculating the droplet size of non-spherical droplets is shown using the example of the non-spherical droplet shown in the Figure below:

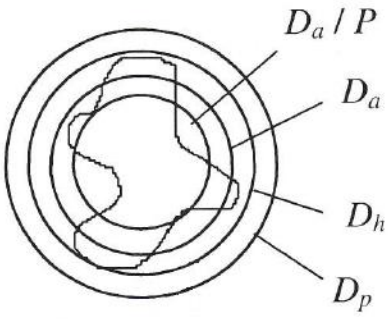


Diagram of droplet size determination for non-spherical droplets (Oxford Lasers 2010)

The Oxford Lasers VisiSize software reports the droplet diameter as $D_a$ when measuring droplet sizes.

Equivalent circular area: $D_a = C\sqrt{\frac{4A}{\pi}}$

where: C is the microns/pixel calibration, and A is the pixel area.

Other methods of measurement of the droplet diameter include:

Equivalent circular perimeter: $D_p = C\left(\frac{P}{\pi}\right)$

Equivalent circular area/perimeter ratio: $\frac{D_a}{D_p} = \sqrt{\frac{4\pi A}{P^2}}$

Heywood diameter: $D_h$ = smallest circle enclosing the particle

where: P is the pixel perimeter.

The diameters of circles corresponding to each of these methods of measurement are shown in the Figure above to allow comparison.

## B4: Technique for Measurement of Droplet Velocity

The Oxford Lasers Imaging System (VisiSizer D30V, IMG0021) was used to measure the velocity of droplets. The following information is taken from the Oxford Lasers Sizing System User Manual (Oxford Lasers Imaging Divison, 2010).

The system measures the magnitude and direction of droplet velocity by comparing a pair of consecutive images (image pairs mode), which is the normal mode of operation for velocimetry. The software matches droplets between the consecutive images, measures the distance that droplets have travelled between images and, given that the time period between images is known, calculates the droplet velocity.

The droplet velocity that is reported consists of a number for the magnitude and an angle for the direction. The VisiSize software reported the direction and angle of droplet velocity using the configuration shown in the Figure below:

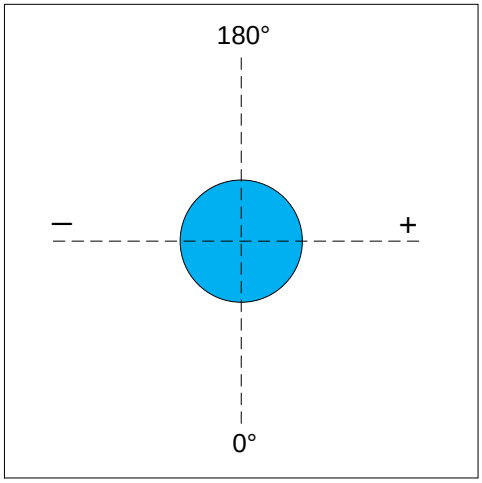

## B5: Photographs of the Droplet Column Supports

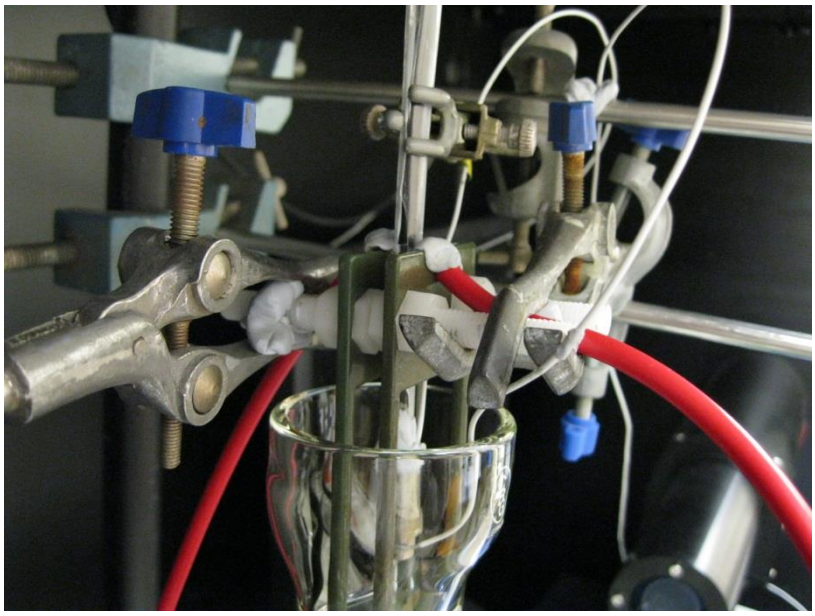

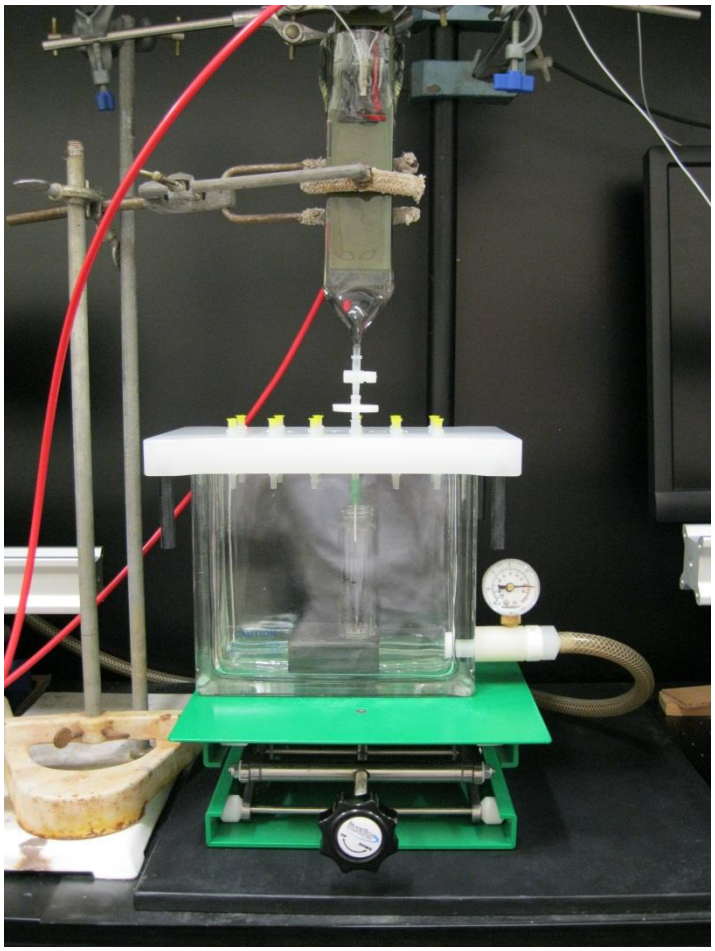

## B6: Photographs of the Droplet Column Experimental Set-up

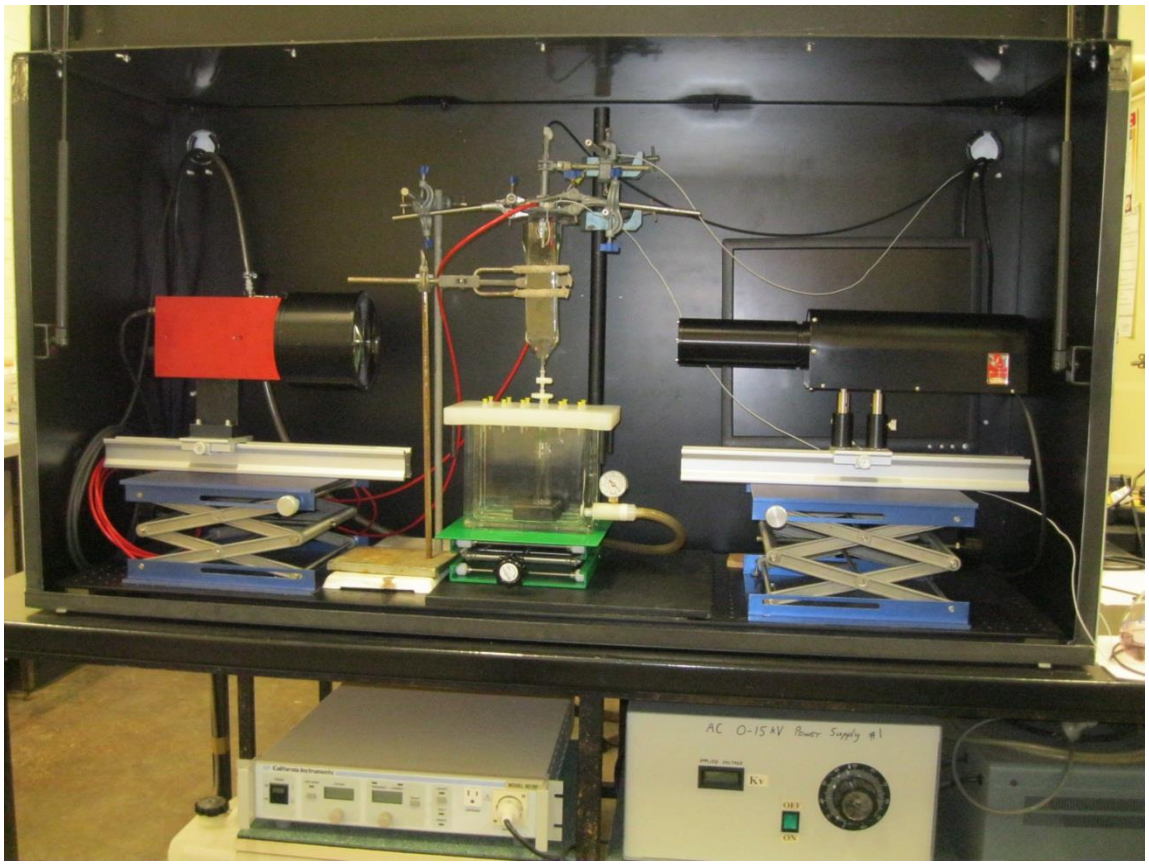


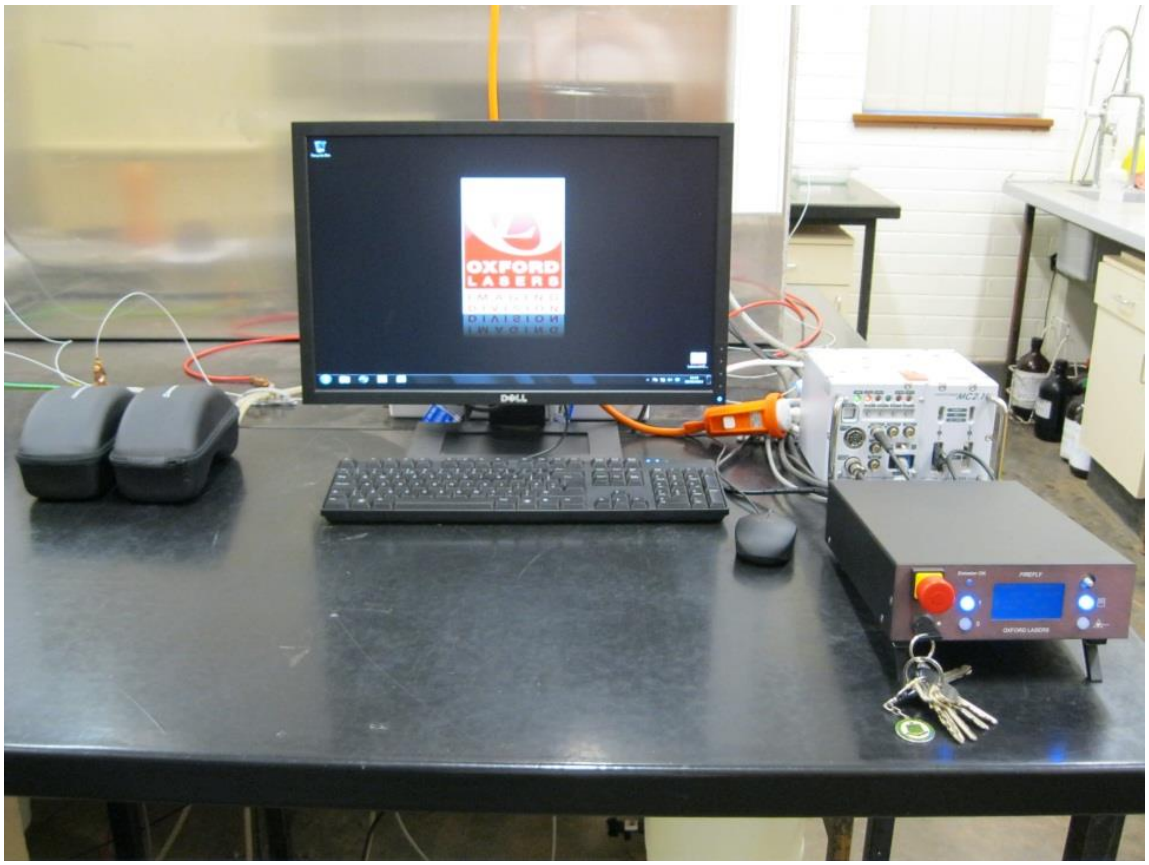
OXFORD
LASERS
DELL

## B7: Example of Droplet Mismatching when Measuring Droplet Velocity

The imaging system measures the direction and magnitude of droplet velocity by matching droplets between two consecutive frames. The software uses the image analysis parameters on the velocity panel, which are set by the user, as its search criteria when attempting to match droplets.

The difference between correct droplet matching and droplet mismatching is shown in the two consecutive frames in the Figure below. The majority of droplets in these frames have been correctly matched. As an example, it is evident that droplet #13 (inside the green ellipses) has travelled from one end to the other end of the blue arrow between frames and therefore, represents an accurate measurement of the droplet velocity. On the other hand, droplets #10 and #28 (inside the red ellipses) are mismatched between the images and therefore, report inaccurate measurement of the droplet velocity. Droplet mismatching generally occurred when two similarly sized droplet were situated close together. Whilst every effort was made to minimise the amount of droplet mismatching by selecting appropriate image analysis parameters, droplet mismatching could not be completely eliminated.

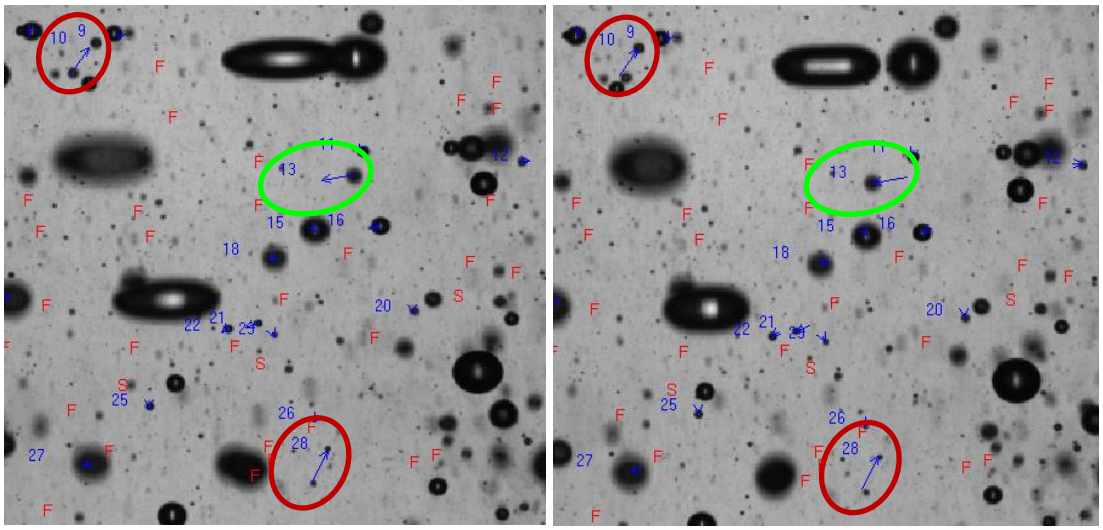

## B8: Example of a VisiSize Analysis Report Generated by the VisiSize Software

| | |
|---|---|
| OXFORD LASERS IMAGING SYSTEMS | |
| VISISIZE ANALYSIS REPORT | |
| VisiSize 6.206 | |
| C:\USERS\VISISIZE\DESKTOP\1_RUN2.TXT | |
| 7/6/2012 14:31 | |
| Velocity mode | |
| Run: 1_Run2(File sequence: Run2000001 - Run2004000) | |
| | |
| Calibration: C:\Program Files\Oxford Lasers\VisiSize\Calibration\MC2LO4x2.clb | |
| Photron MC1/2 Camera | Standard Lens Option 4 |
| | |
| Field Type | AC |
| Applied Voltage | 3.25 kV/cm |
| Applied Frequency | 50Hz |
| Droplet Flowrate | 0.500 mL/min |
| Camera Magnification | 2 |
| | |
| SAMPLE ANALYSIS SUMMARY (diameters in microns) | |
| Averages: | |
| Arithmetic mean | 98.8 |
| Surface mean | 119.8 |
| Volume mean | 152.9 |
| Sauter mean | 249.1 |
| Volume-weighted mean | 536.4 |
| Average velocity | 1 |
| Spread: | |
| Minimum diameter | 43 |
| Maximum diameter | 1357.7 |
| Relative span | 2.65 |
| Deviation | 0.1 |
| Min velocity | 0 |
| Max velocity | 10 |
| Volume percentiles: | |
| 10% | 113.7 |
| 50% | 346.2 |
| 90% | 1031.8 |
| Sphericity | 0.83 |

| DIAMETER (microns) | | DOF FACTOR | EC FACTOR | COUNT | % NUMBER | % AREA | % VOLUME | CUM % VOL | AV. SPEED (m/s) |
|---|---|---|---|---|---|---|---|---|---|
| 43 | 44.1 | 12.83 | 1.01 | 3188 | 0.85 | 0.11 | 0.02 | 0.0191 | 1.04 |
| 44.1 | 45.2 | 12.52 | 1.01 | 556 | 0.15 | 0.02 | 0 | 0.0227 | 0.83 |
| 45.2 | 46.3 | 12.21 | 1.01 | 1345 | 0.36 | 0.05 | 0.01 | 0.0323 | 0.88 |
| 46.3 | 47.5 | 11.92 | 1.01 | 3083 | 0.82 | 0.12 | 0.02 | 0.0556 | 1.15 |
| 47.5 | 48.6 | 11.63 | 1.01 | 1833 | 0.49 | 0.08 | 0.02 | 0.0708 | 1.13 |
| 48.6 | 49.9 | 11.34 | 1.01 | 1548 | 0.41 | 0.07 | 0.01 | 0.0846 | 1.02 |
| 49.9 | 51.1 | 11.07 | 1.01 | 2563 | 0.68 | 0.12 | 0.02 | 0.1094 | 1.09 |
| 51.1 | 52.4 | 10.8 | 1.01 | 8672 | 2.31 | 0.43 | 0.09 | 0.1996 | 1.13 |
| 52.4 | 53.7 | 10.53 | 1.01 | 9540 | 2.54 | 0.5 | 0.11 | 0.3052 | 1.23 |
| 53.7 | 55 | 10.28 | 1.01 | 10465 | 2.78 | 0.57 | 0.13 | 0.4307 | 1.06 |
| 55 | 56.4 | 10.03 | 1.01 | 8599 | 2.29 | 0.5 | 0.11 | 0.542 | 1.05 |
| 56.4 | 57.8 | 9.78 | 1.01 | 12692 | 3.38 | 0.77 | 0.18 | 0.7182 | 1.09 |
| 57.8 | 59.3 | 9.54 | 1.01 | 8026 | 2.14 | 0.51 | 0.12 | 0.8385 | 1.02 |
| 59.3 | 60.7 | 9.31 | 1.01 | 9729 | 2.59 | 0.65 | 0.16 | 0.9942 | 0.95 |
| 60.7 | 62.3 | 9.08 | 1.01 | 10103 | 2.69 | 0.71 | 0.17 | 1.1687 | 1.01 |
| 62.3 | 63.8 | 8.86 | 1.01 | 12063 | 3.21 | 0.89 | 0.22 | 1.3937 | 0.95 |
| 63.8 | 65.4 | 8.65 | 1.01 | 9431 | 2.51 | 0.73 | 0.19 | 1.5833 | 0.95 |
| 65.4 | 67 | 8.44 | 1.01 | 11079 | 2.95 | 0.9 | 0.24 | 1.8229 | 0.87 |
| 67 | 68.7 | 8.23 | 1.02 | 11473 | 3.05 | 0.98 | 0.27 | 2.0896 | 0.86 |
| 68.7 | 70.4 | 8.03 | 1.02 | 10423 | 2.77 | 0.94 | 0.26 | 2.351 | 0.89 |
| 70.4 | 72.2 | 7.83 | 1.02 | 12601 | 3.35 | 1.19 | 0.34 | 2.6917 | 1.01 |
| 72.2 | 74 | 7.64 | 1.02 | 11740 | 3.12 | 1.16 | 0.34 | 3.0323 | 1.15 |
| 74 | 75.8 | 7.46 | 1.02 | 10518 | 2.8 | 1.09 | 0.33 | 3.3606 | 1.18 |
| 75.8 | 77.7 | 7.28 | 1.02 | 10022 | 2.67 | 1.1 | 0.34 | 3.6983 | 1.04 |
| 77.7 | 79.7 | 7.1 | 1.02 | 9442 | 2.51 | 1.08 | 0.34 | 4.0407 | 1.02 |
| 79.7 | 81.7 | 6.93 | 1.02 | 9110 | 2.42 | 1.1 | 0.36 | 4.3962 | 0.95 |

| | | | | | | | | | |
|---|---|---|---|---|---|---|---|---|---|
| 81.7 | 83.7 | 6.76 | 1.02 | 8906 | 2.37 | 1.13 | 0.38 | 4.7713 | 0.99 |
| 83.7 | 85.8 | 6.59 | 1.02 | 10151 | 2.7 | 1.35 | 0.46 | 5.2303 | 0.9 |
| 85.8 | 87.9 | 6.43 | 1.02 | 8413 | 2.24 | 1.18 | 0.41 | 5.6407 | 0.79 |
| 87.9 | 90.1 | 6.27 | 1.02 | 8129 | 2.16 | 1.19 | 0.43 | 6.0671 | 0.82 |
| 90.1 | 92.4 | 6.12 | 1.02 | 6242 | 1.66 | 0.96 | 0.35 | 6.4198 | 0.83 |
| 92.4 | 94.7 | 5.97 | 1.02 | 5684 | 1.51 | 0.92 | 0.35 | 6.7667 | 0.92 |
| 94.7 | 97.1 | 5.83 | 1.02 | 7269 | 1.93 | 1.24 | 0.48 | 7.2436 | 0.9 |
| 97.1 | 99.5 | 5.68 | 1.02 | 6875 | 1.83 | 1.23 | 0.49 | 7.7289 | 0.99 |
| 99.5 | 102 | 5.55 | 1.02 | 5730 | 1.52 | 1.08 | 0.44 | 8.1642 | 1.11 |
| 102 | 104.5 | 5.41 | 1.02 | 5061 | 1.35 | 1 | 0.41 | 8.5785 | 0.87 |
| 104.5 | 107.1 | 5.28 | 1.02 | 5233 | 1.39 | 1.09 | 0.46 | 9.0397 | 0.9 |
| 107.1 | 109.8 | 5.15 | 1.02 | 3816 | 1.02 | 0.83 | 0.36 | 9.4017 | 0.81 |
| 109.8 | 112.6 | 5.02 | 1.03 | 3962 | 1.05 | 0.91 | 0.41 | 9.8074 | 1.17 |
| 112.6 | 115.4 | 4.9 | 1.03 | 4310 | 1.15 | 1.04 | 0.47 | 10.2819 | 1.2 |
| 115.4 | 118.2 | 4.78 | 1.03 | 3746 | 1 | 0.95 | 0.44 | 10.7252 | 1.2 |
| 118.2 | 121.2 | 4.67 | 1.03 | 2593 | 0.69 | 0.69 | 0.33 | 11.0554 | 1.36 |
| 121.2 | 124.2 | 4.55 | 1.03 | 2948 | 0.78 | 0.82 | 0.41 | 11.4611 | 0.95 |
| 124.2 | 127.3 | 4.44 | 1.03 | 2568 | 0.68 | 0.75 | 0.38 | 11.8403 | 0.77 |
| 127.3 | 130.5 | 4.33 | 1.03 | 1807 | 0.48 | 0.56 | 0.29 | 12.128 | 0.78 |
| 130.5 | 133.8 | 4.23 | 1.03 | 1341 | 0.36 | 0.43 | 0.23 | 12.3577 | 1.05 |
| 133.8 | 137.1 | 4.12 | 1.03 | 1284 | 0.34 | 0.44 | 0.24 | 12.5962 | 1.07 |
| 137.1 | 140.5 | 4.02 | 1.03 | 1843 | 0.49 | 0.66 | 0.37 | 12.9639 | 1.23 |
| 140.5 | 144 | 3.93 | 1.03 | 2562 | 0.68 | 0.96 | 0.55 | 13.5152 | 1.06 |
| 144 | 147.6 | 3.83 | 1.03 | 3808 | 1.01 | 1.5 | 0.88 | 14.3935 | 0.93 |
| 147.6 | 151.3 | 3.74 | 1.03 | 2876 | 0.77 | 1.19 | 0.71 | 15.1085 | 1.17 |
| 151.3 | 155.1 | 3.65 | 1.04 | 2627 | 0.7 | 1.14 | 0.7 | 15.811 | 1.06 |
| 155.1 | 159 | 3.56 | 1.04 | 2469 | 0.66 | 1.12 | 0.71 | 16.5186 | 0.94 |
| 159 | 163 | 3.47 | 1.04 | 2591 | 0.69 | 1.25 | 0.81 | 17.3283 | 0.93 |
| 163 | 167 | 3.39 | 1.04 | 2836 | 0.75 | 1.43 | 0.95 | 18.275 | 0.86 |

| | | | | | | | | | |
|---|---|---|---|---|---|---|---|---|---|
| 167 | 171.2 | 3.3 | 1.04 | 2725 | 0.72 | 1.44 | 0.98 | 19.2535 | 0.91 |
| 171.2 | 175.5 | 3.22 | 1.04 | 2178 | 0.58 | 1.21 | 0.84 | 20.0985 | 0.8 |
| 175.5 | 179.9 | 3.14 | 1.04 | 2311 | 0.61 | 1.35 | 0.96 | 21.0635 | 0.95 |
| 179.9 | 184.3 | 3.07 | 1.04 | 2407 | 0.64 | 1.48 | 1.08 | 22.1453 | 1.11 |
| 184.3 | 189 | 2.99 | 1.04 | 1845 | 0.49 | 1.19 | 0.89 | 23.0354 | 1.1 |
| 189 | 193.7 | 2.92 | 1.04 | 1238 | 0.33 | 0.84 | 0.64 | 23.6785 | 1.08 |
| 193.7 | 198.5 | 2.85 | 1.05 | 1245 | 0.33 | 0.89 | 0.7 | 24.379 | 1.22 |
| 198.5 | 203.5 | 2.78 | 1.05 | 1419 | 0.38 | 1.06 | 0.86 | 25.236 | 0.84 |
| 203.5 | 208.6 | 2.71 | 1.05 | 1026 | 0.27 | 0.81 | 0.67 | 25.9014 | 0.74 |
| 208.6 | 213.8 | 2.65 | 1.05 | 1163 | 0.31 | 0.96 | 0.81 | 26.716 | 0.94 |
| 213.8 | 219.1 | 2.58 | 1.05 | 932 | 0.25 | 0.81 | 0.7 | 27.4183 | 0.89 |
| 219.1 | 224.6 | 2.52 | 1.05 | 1131 | 0.3 | 1.03 | 0.92 | 28.3345 | 0.85 |
| 224.6 | 230.2 | 2.46 | 1.05 | 450 | 0.12 | 0.43 | 0.39 | 28.7285 | 0.69 |
| 230.2 | 235.9 | 2.4 | 1.05 | 548 | 0.15 | 0.55 | 0.52 | 29.2458 | 0.75 |
| 235.9 | 241.8 | 2.34 | 1.06 | 760 | 0.2 | 0.81 | 0.77 | 30.0188 | 0.7 |
| 241.8 | 247.9 | 2.28 | 1.06 | 863 | 0.23 | 0.96 | 0.94 | 30.9587 | 0.7 |
| 247.9 | 254.1 | 2.23 | 1.06 | 825 | 0.22 | 0.96 | 0.97 | 31.9307 | 0.63 |
| 254.1 | 260.4 | 2.17 | 1.06 | 974 | 0.26 | 1.19 | 1.23 | 33.1583 | 0.79 |
| 260.4 | 266.9 | 2.12 | 1.06 | 724 | 0.19 | 0.93 | 0.98 | 34.141 | 0.95 |
| 266.9 | 273.6 | 2.07 | 1.06 | 697 | 0.19 | 0.95 | 1.03 | 35.1695 | 0.82 |
| 273.6 | 280.4 | 2.02 | 1.06 | 1024 | 0.27 | 1.46 | 1.62 | 36.7931 | 0.81 |
| 280.4 | 287.4 | 1.97 | 1.07 | 1536 | 0.41 | 2.3 | 2.62 | 39.4131 | 0.9 |
| 287.4 | 294.6 | 1.92 | 1.07 | 1153 | 0.31 | 1.8 | 2.1 | 41.5157 | 0.91 |
| 294.6 | 302 | 1.87 | 1.07 | 810 | 0.22 | 1.33 | 1.6 | 43.111 | 0.96 |
| 302 | 309.5 | 1.83 | 1.07 | 560 | 0.15 | 0.97 | 1.19 | 44.3016 | 1.1 |
| 309.5 | 317.2 | 1.78 | 1.07 | 402 | 0.11 | 0.73 | 0.92 | 45.219 | 0.93 |
| 317.2 | 325.1 | 1.74 | 1.08 | 462 | 0.12 | 0.89 | 1.15 | 46.3652 | 1.11 |
| 325.1 | 333.3 | 1.7 | 1.08 | 455 | 0.12 | 0.91 | 1.2 | 47.5689 | 0.83 |
| 333.3 | 341.6 | 1.66 | 1.08 | 515 | 0.14 | 1.09 | 1.48 | 49.0448 | 0.96 |

| | | | | | | | | | |
|---|---|---|---|---|---|---|---|---|---|
| 341.6 | 350.1 | 1.62 | 1.08 | 582 | 0.15 | 1.29 | 1.79 | 50.834 | 1.12 |
| 350.1 | 358.9 | 1.58 | 1.08 | 449 | 0.12 | 1.05 | 1.49 | 52.3235 | 0.99 |
| 358.9 | 367.8 | 1.54 | 1.09 | 414 | 0.11 | 1.01 | 1.48 | 53.802 | 1.13 |
| 367.8 | 377 | 1.5 | 1.09 | 341 | 0.09 | 0.88 | 1.31 | 55.1141 | 0.99 |
| 377 | 386.4 | 1.46 | 1.09 | 474 | 0.13 | 1.28 | 1.97 | 57.0836 | 1.1 |
| 386.4 | 396.1 | 1.43 | 1.09 | 653 | 0.17 | 1.85 | 2.91 | 59.9952 | 1.13 |
| 396.1 | 406 | 1.39 | 1.1 | 493 | 0.13 | 1.47 | 2.36 | 62.3584 | 0.93 |
| 406 | 416.1 | 1.36 | 1.1 | 230 | 0.06 | 0.72 | 1.18 | 63.5365 | 0.97 |
| 416.1 | 426.5 | 1.33 | 1.1 | 181 | 0.05 | 0.6 | 1.01 | 64.5437 | 1.18 |
| 426.5 | 437.2 | 1.29 | 1.1 | 241 | 0.06 | 0.84 | 1.45 | 65.9962 | 1.23 |
| 437.2 | 448.1 | 1.26 | 1.11 | 309 | 0.08 | 1.12 | 1.99 | 67.987 | 1.18 |
| 448.1 | 459.3 | 1.23 | 1.11 | 202 | 0.05 | 0.77 | 1.4 | 69.3893 | 1.42 |
| 459.3 | 470.8 | 1.2 | 1.11 | 142 | 0.04 | 0.57 | 1.06 | 70.4471 | 1 |
| 470.8 | 482.5 | 1.17 | 1.12 | 86 | 0.02 | 0.36 | 0.7 | 71.1429 | 1.17 |
| 482.5 | 494.6 | 1.14 | 1.12 | 78 | 0.02 | 0.35 | 0.68 | 71.8211 | 1.04 |
| 494.6 | 506.9 | 1.12 | 1.12 | 60 | 0.02 | 0.28 | 0.56 | 72.3823 | 1.15 |
| 506.9 | 519.6 | 1.09 | 1.13 | 103 | 0.03 | 0.5 | 1.04 | 73.4208 | 1.32 |
| 519.6 | 532.6 | 1.06 | 1.13 | 119 | 0.03 | 0.61 | 1.29 | 74.7074 | 1.22 |
| 532.6 | 545.9 | 1.04 | 1.13 | 130 | 0.03 | 0.7 | 1.52 | 76.2224 | 1.14 |
| 545.9 | 559.5 | 1.01 | 1.14 | 94 | 0.03 | 0.53 | 1.19 | 77.4098 | 1.25 |
| 559.5 | 573.5 | 1 | 1.14 | 96 | 0.03 | 0.57 | 1.29 | 78.7043 | 1.16 |
| 573.5 | 587.8 | 1 | 1.14 | 64 | 0.02 | 0.4 | 0.94 | 79.6399 | 1.12 |
| 587.8 | 602.5 | 1 | 1.15 | 89 | 0.02 | 0.59 | 1.41 | 81.0476 | 1.24 |
| 602.5 | 617.5 | 1 | 1.15 | 41 | 0.01 | 0.29 | 0.7 | 81.746 | 1.26 |
| 617.5 | 633 | 1 | 1.16 | 53 | 0.01 | 0.39 | 0.97 | 82.7125 | 1.19 |
| 633 | 648.8 | 1 | 1.16 | 27 | 0.01 | 0.2 | 0.52 | 83.2336 | 1.26 |
| 648.8 | 665 | 1 | 1.16 | 14 | 0 | 0.11 | 0.29 | 83.5276 | 1.02 |
| 665 | 681.6 | 1 | 1.17 | 11 | 0 | 0.09 | 0.24 | 83.7689 | 1.35 |
| 681.6 | 698.6 | 1 | 1.17 | 6 | 0 | 0.05 | 0.14 | 83.9113 | 1.54 |

| | | | | | | | | | |
|---|---|---|---|---|---|---|---|---|---|
| 698.6 | 716.1 | 1 | 1.18 | 8 | 0 | 0.08 | 0.22 | 84.1285 | 1.21 |
| 716.1 | 734 | 1 | 1.18 | 5 | 0 | 0.05 | 0.13 | 84.2618 | 0.86 |
| 734 | 752.3 | 1 | 1.19 | 2 | 0 | 0.02 | 0.07 | 84.3326 | 1.14 |
| 752.3 | 771.1 | 1 | 1.19 | 1 | 0 | 0.01 | 0.04 | 84.373 | 0.79 |
| 771.1 | 790.3 | 1 | 1.2 | 0 | 0 | 0 | 0 | 84.373 | -NAN |
| 790.3 | 810.1 | 1 | 1.21 | 7 | 0 | 0.09 | 0.28 | 84.6535 | 1.48 |
| 810.1 | 830.3 | 1 | 1.21 | 13 | 0 | 0.17 | 0.55 | 85.1986 | 1.78 |
| 830.3 | 851.1 | 1 | 1.22 | 13 | 0 | 0.18 | 0.6 | 85.7954 | 1.61 |
| 851.1 | 872.3 | 1 | 1.22 | 15 | 0 | 0.2 | 0.7 | 86.493 | 1.85 |
| 872.3 | 894.1 | 1 | 1.23 | 5 | 0 | 0.07 | 0.25 | 86.7467 | 0.89 |
| 894.1 | 916.4 | 1 | 1.24 | 5 | 0 | 0.08 | 0.27 | 87.0208 | 0.98 |
| 916.4 | 939.3 | 1 | 1.24 | 6 | 0 | 0.1 | 0.37 | 87.391 | 1.99 |
| 939.3 | 962.8 | 1 | 1.25 | 11 | 0 | 0.19 | 0.72 | 88.111 | 1.87 |
| 962.8 | 986.8 | 1 | 1.26 | 5 | 0 | 0.09 | 0.35 | 88.4645 | 2.12 |
| 986.8 | 1011.5 | 1 | 1.27 | 6 | 0 | 0.12 | 0.47 | 88.9383 | 1.89 |
| 1011.5 | 1036.8 | 1 | 1.27 | 17 | 0 | 0.32 | 1.32 | 90.262 | 2.06 |
| 1036.8 | 1062.7 | 1 | 1.28 | 5 | 0 | 0.1 | 0.44 | 90.7002 | 1.45 |
| 1062.7 | 1089.2 | 1 | 1.29 | 13 | 0 | 0.27 | 1.18 | 91.8768 | 1.99 |
| 1089.2 | 1116.4 | 1 | 1.3 | 5 | 0 | 0.12 | 0.53 | 92.4028 | 2.64 |
| 1116.4 | 1144.3 | 1 | 1.31 | 17 | 0 | 0.4 | 1.81 | 94.212 | 2.09 |
| 1144.3 | 1172.9 | 1 | 1.32 | 11 | 0 | 0.26 | 1.21 | 95.4238 | 1.67 |
| 1172.9 | 1202.2 | 1 | 1.33 | 3 | 0 | 0.07 | 0.32 | 95.7483 | 2.29 |
| 1202.2 | 1232.2 | 1 | 1.34 | 3 | 0 | 0.07 | 0.36 | 96.1046 | 2.04 |
| 1232.2 | 1263 | 1 | 1.35 | 16 | 0 | 0.47 | 2.33 | 98.4344 | 2.03 |
| 1263 | 1294.5 | 1 | 1.36 | 5 | 0 | 0.16 | 0.84 | 99.2719 | 1.68 |
| 1294.5 | 1326.9 | 1 | 1.37 | 3 | 0 | 0.09 | 0.47 | 99.7423 | 2.07 |
| 1326.9 | 1360 | 1 | 1.38 | 1 | 0 | 0.05 | 0.26 | 100 | 5.64 |

## B9: Example of an Individual Particle Data file Generated by the VisiSize Software

| OXFORD LASERS IMAGING SYSTEMS | | | | | |
|---|---|---|---|---|---|
| INDIVIDUAL PARTICLE DATA | | | | | |
| VisiSize 6.206 | | | | | |
| C:\Users\Visisize\Desktop\1_Run2.vsp | | | | | |
| 7/6/2012 14:29 | | | | | |
| Velocity Mode | | | | | |
| | | | | | |
| Frame | Particle ID | Diameter | Velocity | Angle | Shape Factor |
| 1 | 1 | 232.924 | 0.3801 | 0 | 0.725834 |
| 1 | 2 | 174.822 | 0.849929 | 26.565 | 0.744696 |
| 1 | 3 | 427.131 | 1.37047 | -56.3098 | 0.65683 |
| 1 | 4 | 299.266 | 0.537543 | -44.9999 | 0.605796 |
| 1 | 5 | 87.2388 | 0.3801 | 0 | 0.763578 |
| 1 | 6 | 80.5739 | 0.537543 | -44.9999 | 0.743883 |
| 1 | 7 | 236.452 | 0.3801 | 0 | 0.718172 |
| 1 | 8 | 301.497 | 5.07117 | -77.0052 | 0.851503 |
| 1 | 9 | 99.642 | 0.7602 | 0 | 0.734854 |
| 1 | 10 | 46.4516 | 0 | 0 | 0.776136 |
| 1 | 11 | 53.8613 | 0.849929 | 26.565 | 0.865929 |
| 1 | 12 | 79.6939 | 0.3801 | 0 | 0.865237 |
| 1 | 13 | 59.2184 | 0.7602 | 0 | 0.693898 |
| 1 | 14 | 65.2339 | 1.1403 | 0 | 0.881024 |
| 1 | 15 | 107.972 | 0.3801 | 0 | 0.94875 |
| 1 | 16 | 152.465 | 0.3801 | 0 | 0.857479 |
| 1 | 17 | 108.644 | 0.7602 | 0 | 0.906053 |
| 1 | 18 | 158.569 | 2.15017 | -44.9999 | 0.790019 |
| 1 | 19 | 160.69 | 0.7602 | 0 | 0.602253 |
| 1 | 20 | 78.4401 | 1.20198 | -18.4349 | 0.905197 |
| 1 | 21 | 484.005 | 0.849929 | 26.565 | 0.80049 |
| 1 | 22 | 146.161 | 0.849929 | -63.4348 | 0.929698 |
| 1 | 23 | 97.699 | 1.20198 | -18.4349 | 0.827304 |
| 1 | 24 | 79.1645 | 0.3801 | 0 | 0.931089 |
| 1 | 25 | 102.975 | 0.849929 | -26.565 | 0.892316 |
| 1 | 26 | 97.8581 | 1.20198 | -71.5649 | 0.850515 |
| 2 | 1 | 235.864 | 0.3801 | 0 | 0.647219 |
| 2 | 2 | 173.574 | 0.7602 | 0 | 0.696871 |
| 2 | 3 | 128.03 | 0.3801 | 0 | 0.780871 |
| 2 | 4 | 86.9474 | 0.7602 | 0 | 0.852682 |
| 2 | 5 | 94.5909 | 0.537543 | 44.9999 | 0.811533 |
| 2 | 6 | 69.3862 | 0.7602 | 0 | 0.704 |

| | | | | | |
|---|---|---|---|---|---|
| 2 | 7 | 80.583 | 0.3801 | 0 | 0.872123 |
| 2 | 8 | 54.4162 | 0.3801 | 0 | 0.865929 |
| 2 | 9 | 303.286 | 1.07509 | -44.9999 | 0.887889 |
| 2 | 10 | 53.3028 | 0.7602 | 0 | 0.865929 |
| 2 | 11 | 57.1603 | 0.7602 | 0 | 0.740026 |
| 2 | 12 | 74.0135 | 0.3801 | 0 | 0.858812 |
| 2 | 13 | 108.516 | 0 | 0 | 0.930729 |
| 2 | 14 | 150.02 | 0.849929 | 26.565 | 0.786057 |
| 2 | 15 | 108.586 | 0.7602 | 0 | 0.877684 |
| 2 | 16 | 220.77 | 0 | 0 | 0.5935 |
| 2 | 17 | 55.549 | 0.3801 | 0 | 0.833333 |
| 2 | 18 | 81.3011 | 0.7602 | 0 | 0.838177 |
| 2 | 19 | 75.6638 | 0.3801 | 0 | 0.967687 |
| 2 | 20 | 56.6456 | 0.537543 | 44.9999 | 0.88 |
| 2 | 21 | 271.412 | 0.3801 | 0 | 0.906617 |
| 2 | 22 | 484.025 | 2.31206 | 9.4623 | 0.964128 |
| 2 | 23 | 143.223 | 0.7602 | 0 | 0.894091 |
| 2 | 24 | 98.1922 | 1.1403 | 0 | 0.924046 |
| 2 | 25 | 209.331 | 0.7602 | 0 | 0.967657 |
| 2 | 26 | 79.4866 | 0 | 0 | 0.845909 |
| 2 | 27 | 177.652 | 0.3801 | 0 | 0.926874 |
| 3 | 1 | 407.696 | 1.5204 | -89.9998 | 0.660419 |
| 3 | 2 | 240.685 | 0.3801 | -89.9998 | 0.741162 |
| 3 | 3 | 174.353 | 0.3801 | 0 | 0.7707 |
| 3 | 4 | 86.8115 | 0.849929 | 26.565 | 0.783081 |
| 3 | 5 | 95.7457 | 0.7602 | 0 | 0.859621 |
| 3 | 6 | 77.2976 | 0.3801 | 0 | 0.819558 |
| 3 | 7 | 79.3686 | 0.849929 | 63.4348 | 0.679099 |
| 3 | 8 | 55.5476 | 0.849929 | 26.565 | 0.861428 |
| 3 | 9 | 305.238 | 4.24965 | 79.695 | 0.939237 |
| 3 | 10 | 52.6833 | 0.3801 | 0 | 0.85016 |
| 3 | 11 | 67.8803 | 0.849929 | 26.565 | 0.814871 |
| 3 | 12 | 74.4839 | 0.3801 | 0 | 0.872583 |
| 3 | 13 | 108.586 | 0.3801 | 0 | 0.881767 |
| 3 | 14 | 79.831 | 0.3801 | 0 | 0.817698 |
| 3 | 15 | 50.9472 | 0.7602 | 0 | 0.725888 |
| 3 | 16 | 151.029 | 0.7602 | 0 | 0.679911 |
| 3 | 17 | 51.5573 | 0.537543 | 44.9999 | 0.845087 |
| 3 | 18 | 57.7213 | 0.537543 | 44.9999 | 0.674886 |
| 3 | 19 | 107.081 | 0.7602 | 0 | 0.817292 |
| 3 | 20 | 226.465 | 0 | 0 | 0.637176 |
| 3 | 21 | 57.7027 | 0.537543 | 44.9999 | 0.75998 |
| 3 | 22 | 160.785 | 1.37047 | 56.3098 | 0.749769 |
| 3 | 23 | 45.7324 | 0.537543 | 44.9999 | 0.625 |
| 3 | 24 | 82.5066 | 0.7602 | 0 | 0.947675 |

## B10: Example of an Excessive Number of Droplets Preventing Accurate Measurement of Droplet Sizes

The grey-scale photograph in the Figure (a) below shows an example of a droplet dispersion with an excessive number of droplets that cannot be measured accurately using the imaging technique in the present study. It is evident from the two tone image of this photograph, shown in Figure (b), that too many droplets are overlapping and thus, the software cannot accurately distinguish between different droplets.

(a)

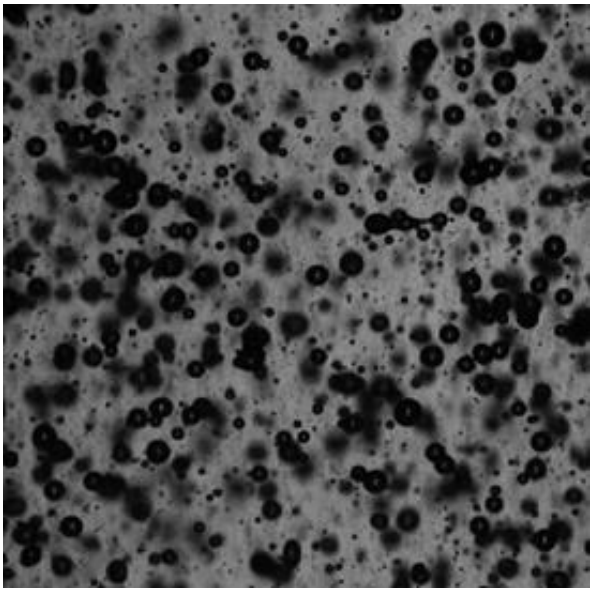

(b)

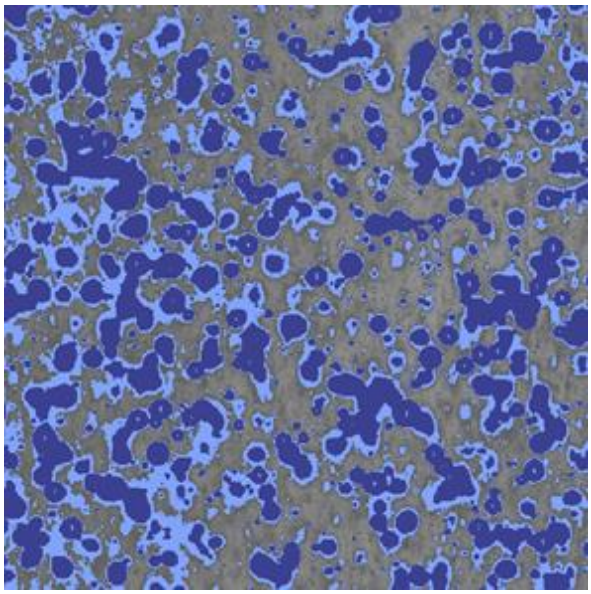

# APPENDIX C: GENERAL LABORATORY PROCEDURES AND CALCULATIONS

## C1: Calibration and Operation of the Aqueous Solution Conductivity Meter

The aqueous solution conductivity meter (Aqua-CPA, TPS) was calibrated and operated using the methods supplied by the manufacturer. The meter was calibrated by firstly plugging the glass-body conductivity sensor (k=10 probe, 122221, TPS) into the sensor socket on the meter, and selecting the Conductivity mode. The sensor was rinsed with distilled water, and blotted dry. When the sensor had dried sufficiently such that the reading had stabilised at or near zero, the Calibrate key was pressed. The sensor was then placed into the appropriate range of standard Conductivity samples and the Calibrate key was pressed after the reading of each sample had stabilised. To measure the conductivity of an aqueous solution, the probe was immersed into the solution and the value of the conductivity was measured after the reading had stabilised.

## C2: Calibration and Operation of the Organic Solution Conductivity Meter

The organic solution conductivity meter (model 1152, Emcee Electronics) was calibrated and operated using the methods supplied by the manufacturer. To calibrate the conductivity meter, the stainless steel probe was attached to the meter and the Measure switch was pressed with the probe out of the sample to ensure that zero conductivity was measured. The Calibrate switch was then pressed with the probe out of the sample to ensure that the reading was equal to 10 times the probe calibration number ±005 (395-405).

To measure the conductivity of an organic solution, the solution was poured into a metal container, and an earthing clip was attached between the meter and the metal container. The probe was immersed into the solution ensuring that the upper holes on the probe were completely immersed in the solution and the Measure switch was pressed. The true conductivity was displayed when the reading had stabilised after 3 s, and this value was recorded as the conductivity.

## C3: Calibration and Operation of the Dielectric Constant Meter

The dielectric constant meter (Alpha TDR-5000, Zadow Electronics) was calibrated for the required range of measurement and operated using the methods supplied by the manufacturer. Calibration involved by connecting the appropriate calibration cable (0.5

ns, 2 ns, or 5 ns) to the meter and adjusting the range on the instrument display to set the range of time constant that could be measured. The calibration cable was then disconnected.

To measure the dielectric constant of a solution, the sensor, which consists of two metal rods, was connected to the meter and immersed completely into the solution. The value of the dielectric constant was read from the digital display on the meter. The sensor was washed thoroughly with methylated spirits and acetone between uses.

## C4: Composition of Aqueous Phase for MLC Experiments

The aqueous phase for experiments with the Modified Lewis Cell (MLC) consisted of an acetic acid/acetate buffer solution with sodium sulphate added to increase the ionic strength. The pH required for 100% extraction of Co(II) with Cyanex® 272 from sulphate media is approximately 6.0 (Cyanex® 272 Extractant, Cytec Brochure). Operating at this pH, however, caused the precipitation of cobalt hydroxide in the aqueous phase owing to localised high concentrations of Co(II) upon injection of a small volume of the concentrated Co(II) solution into the MLC. On the other hand, a pH of 5.5 provided acceptable extraction efficiency and also prevented cobalt hydroxide precipitation, and therefore this was used for all MLC experiments.

$$\mathrm{pH} = \mathrm{pK_a} + \log\frac{[\mathrm{base}]}{[\mathrm{acid}]}$$

$$5.5 = -\log(1.84 \times 10^{-5}) + \log\frac{[\mathrm{base}]}{[\mathrm{acid}]}$$

$$\frac{[\mathrm{base}]}{[\mathrm{acid}]} = 5.8$$

Given that the required base:acid concentration ratio was 5.8, the chosen concentrations of the components of the buffer solution were 0.81 M NaOH, and 0.14 M $CH_3COOH$. The concentration of acetic acid was kept as low as possible to minimise the formation of cobalt(II) acetate, without compromising the capacity of the buffer.

The concentration of NaOH required is 0.81 M. Therefore, the weight of NaOH required in one litre is:

$$\mathrm{n(NaOH)_{required}} = 0.81\ \mathrm{mol}$$

$$\mathrm{m(NaOH)_{required}} = 0.81\ \mathrm{mol} \times 39.998\ \mathrm{g/mol}$$

$$m(NaOH)_{required} = 32.48\ g$$

Taking into account the purity of the reagent (97%),

$$m(NaOH)_{required} = \frac{32.48\ g}{0.97}$$
$$m(NaOH)_{required} = 33.48\ g$$

The concentration of $CH_3COOH$ required is 0.14 M. If there is 0.81 M of NaOH, then the total amount of $CH_3COOH$ required is 0.95 M as the NaOH will be neutralised according to the following equation:

$$CH_3COOH_{(aq)} + NaOH_{(aq)} \rightarrow CH_3COONa_{(aq)} + H_2O_{(aq)}$$

Therefore, the total amount of $CH_3COOH$ required in one litre is:

$$m(CH_3COOH)_{required} = 0.95\ mol/L \times 60.05\ g/mol$$
$$m(CH_3COOH)_{required} = 57.05\ g$$

Taking into account the purity of the reagent (99.7%),

$$m(CH_3COOH)_{required} = \frac{57.05\ g}{0.997}$$
$$m(CH_3COOH)_{required} = 57.22\ g$$

$$V(CH_3COOH)_{required} = \frac{m(CH_3COOH)}{\varrho(CH_3COOH)}$$
$$V(CH_3COOH)_{required} = \frac{57.22\ g}{1.05\ g/mL}$$
$$V(CH_3COOH)_{required} = 54.49\ mL$$

The amount of $Na_2SO_4$ required is 0.2 M. Therefore, the mass of $Na_2SO_4$ required in one litre is:

$$n(Na_2SO_4)_{required} = 0.2\ mol$$
$$m(Na_2SO_4)_{required} = 0.2\ mol \times 142.04\ g/mol$$
$$m(Na_2SO_4)_{required} = 28.41\ g$$

Therefore, one litre of aqueous phase of the specified pH and capacity requires 33.48 g of NaOH, 54.49 mL of $CH_3COOH$ and 28.41 g of $Na_2SO_4$ added to a 1-L volumetric flask and make to the mark with distilled water.

The change in pH during MLC experiments was calculated to ensure that the capacity of this buffer solution is sufficient to maintain a negligible change in the pH. Given that the maximum concentration of cobalt(II) that was transferred into the organic phase in MLC experiments was 60 mg/L, the amount of cobalt that may transfer into the organic phase is as follows:

$$\mathrm{c(Co^{2+})} = 0.06\ \mathrm{g\ L^{-1}}$$

$$\mathrm{c(Co^{2+})} = \frac{0.06\ \mathrm{g\ L^{-1}}}{58.93\ \mathrm{g\ mol^{-1}}}$$

$$\mathrm{c(Co^{2+})} = 1.02 \times 10^{-3}\ \mathrm{mol\ L^{-1}}$$

It was assumed that every cobalt (II) ion reacts with two extractant molecules and thus, releases two hydrogen ions into the aqueous phase, according to the following reaction:

$$Co^{2+}_{(aq)} + 2\mathrm{RH}_{(org)} \rightarrow \mathrm{CoR_{2(org)}} + 2\mathrm{H^{+}_{(aq)}}$$

The corresponding change in concentration of hydrogen ions in the aqueous phase is:

$$\Delta\ \mathrm{c(H^{+})} = 2 \times 1.02 \times 10^{-3}\ \mathrm{mol\ L^{-1}}$$

$$\Delta\ \mathrm{c(H^{+})} = 2.04 \times 10^{-3}\ \mathrm{mol\ L^{-1}}$$

Therefore, the final concentrations of base and acid in the aqueous phase after 100% cobalt extraction would be:

$$\frac{[\mathrm{CH_3COO^{-}}]_{\mathrm{final}}}{[\mathrm{CH_3COOH}]_{\mathrm{final}}} = \frac{0.81 - 2.04 \times 10^{-3}\mathrm{mol\ L^{-1}}}{0.14 + 2.04 \times 10^{-3}\mathrm{mol\ L^{-1}}}$$

$$\frac{[\mathrm{CH_3COO^{-}}]_{\mathrm{final}}}{[\mathrm{CH_3COOH}]_{\mathrm{final}}} = \frac{0.808}{0.142}$$

The final pH would be:

$$\mathrm{pH} = \mathrm{pK_a} + \log\frac{[\mathrm{base}]}{[\mathrm{acid}]}$$

$$\mathrm{pH} = -\log(1.84 \times 10^{-5}) + \log\frac{0.497}{0.143}$$

$$\mathrm{pH} = 5.49$$

Therefore, the change in pH would be minimal and thus, the buffer capacity is suitable.

## C5: Composition of Concentrated Co(II) Solution for MLC Experiments

An aqueous solution containing a high concentration of cobalt (II) ions was prepared so that a small volume of this solution could be injected into the aqueous phase of the MLC to commence an experiment.

The concentrated cobalt solution was prepared by dissolving 97.79 g of cobalt sulphate heptahydrate into 500 mL of distilled water. The calculations are as follows:

$$\mathrm{n}(\mathrm{CoSO_4.7H_2O}) = \frac{97.79\ \mathrm{g}}{281.1\ \mathrm{g\ mol^{-1}}}$$

$$\mathrm{n}(\mathrm{CoSO_4.7H_2O}) = 0.348\ \mathrm{mol}$$

$$\mathrm{n}(\mathrm{Co^{2+}}) = \mathrm{n}(\mathrm{CoSO_4.7H_2O})$$

$$\mathrm{n}(\mathrm{Co^{2+}}) = 0.348\ \mathrm{mol}$$

$$\mathrm{m}(\mathrm{Co^{2+}}) = 0.348\ \mathrm{mol} \times 58.93\ \mathrm{g\ mol^{-1}}$$

$$\mathrm{m}(\mathrm{Co^{2+}}) = 20.50\ \mathrm{g}$$

$$\mathrm{c}(\mathrm{Co^{2+}}) = \frac{20.50\ \mathrm{g}}{0.5\ \mathrm{L}}$$

$$\mathrm{c}(\mathrm{Co^{2+}}) = 41\ \mathrm{g\ L^{-1}}$$

The desired initial concentration in the bulk of the aqueous phase in the MLC is 0.3 g/L. Given that the total volume of the aqueous phase in the MLC is 410 mL, the volume of concentrated cobalt solution that was injected into the MLC was calculated as:

$$\mathrm{c_1V_1} = \mathrm{c_2V_2}$$

$$(41)(\mathrm{V_1}) = (0.3)(0.41)$$

$$\mathrm{V_1} = 3.00 \times 10^{-3}\ \mathrm{L}$$

$$\mathrm{V_1} = 3.00\ \mathrm{mL}$$

For each experiment, 3 mL of concentrated cobalt solution was injected into the MLC using a graduated 5-mL syringe (Terumo). This small volume ensured that the injected solution had a negligible effect on the position of the liquid-liquid interface and the hydrodynamics within the MLC.

The same volume of concentrated methyl violet solution was added to the MLC for the experiments to characterise the MLC so that the position of the interface, and the hydrodynamics within the MLC would be the same.

## C6: Stripping of the Organic Phase

The organic phase that was loaded with Co(II) from mass transfer experiments was stripped so that it could be regenerated and reused for future experiments. Stripping was carried out by firstly transferring approximately 400 mL of loaded organic phase into a volumetric flask (1 L) which contained approximately 400 mL of stripping solution. The phases were shaken vigorously for 5 minutes, and then allowed to disengage. The phases were separated, and aqueous entrainment was removed from the stripped organic phase by heating to 40 °C. The organic phase was allowed to cool to room temperature, and filtered using a PTFE membrane filter with a 0.2-µm pore size (LOT No. 00127500, Advantec®).

Attempts were made to use phase separation paper (1PS, Whatman) to remove aqueous entrainment. It was found, however, that upon contacting the regenerated organic phase with a fresh aqueous phase, a haze formed on the organic side of the interface that became stable in the organic phase. The haze entered the flow cell and significantly interfered with measurements of the concentration. It was concluded that the haze resulted from the organic phase dissolving some of the dimethylsiloxane coating on the phase separation paper, which produces solids in the presence of water and acid.

Filtering was required to remove small white solids that formed in the regenerated organic phase. These were believed to be a by-product from the production of Cyanex® 272 (Bourget, C 2011 pers. Comm., 6 October), and had to be removed to allow accurate measurements of the concentration.

## C7: Composition of Aqueous Phase for Droplet Column Experiments

The aqueous phase for experiments with the droplet column consisted of an acetic acid/acetate buffer solution with cobalt sulphate heptahydrate. Sodium sulphate was also added to increase the ionic strength. A pH of 5.5 was used for the aqueous phase in the droplet column experiments as this was found to provide acceptable extraction efficiency in the MLC experiments in the present study.

$$\mathrm{pH} = \mathrm{pK_a} + \log\frac{[\mathrm{base}]}{[\mathrm{acid}]}$$

$$5.5 = -\log(1.84 \times 10^{-5}) + \log\frac{[\mathrm{base}]}{[\mathrm{acid}]}$$

$$\frac{[\mathrm{base}]}{[\mathrm{acid}]} = 5.8$$

Given that the required base:acid concentration ratio was 5.8, the chosen concentrations of the components of the buffer solution were 0.81 M NaOH, and 0.14 M $CH_3COOH$. The concentration of acetic acid was kept as low as possible to minimise the formation of cobalt(II) acetate, without compromising the capacity of the buffer.

The concentration of NaOH required is 0.81 M. Therefore, the weight of NaOH required in one litre is:

$$\mathrm{n(NaOH)_{required}} = 0.81\ \mathrm{mol}$$

$$\mathrm{m(NaOH)_{required}} = 0.81\ \mathrm{mol} \times 39.998\ \mathrm{g/mol}$$

$$\mathrm{m(NaOH)_{required}} = 32.48\ \mathrm{g}$$

Taking into account the purity of the reagent (97%),

$$\mathrm{m(NaOH)_{required}} = \frac{32.48\ \mathrm{g}}{0.97}$$

$$\mathrm{m(NaOH)_{required}} = 33.48\ \mathrm{g}$$

The concentration of $CH_3COOH$ required is 0.14 M. If there is 0.81 M of NaOH, then the total amount of $CH_3COOH$ required is 0.95 M as the NaOH will be neutralised according to the following equation:

$$\mathrm{CH_3COOH_{(aq)} + NaOH_{(aq)} \rightarrow CH_3COONa_{(aq)} + H_2O_{(aq)}}$$

Therefore, the total amount of $CH_3COOH$ required in one litre is:

$$\mathrm{m(CH_3COOH)_{required}} = 0.95\ \mathrm{mol/L} \times 60.05\ \mathrm{g/mol}$$
$$\mathrm{m(CH_3COOH)_{required}} = 57.05\ \mathrm{g}$$

Taking into account the purity of the reagent (99.7%),

$$\mathrm{m(CH_3COOH)_{required}} = \frac{57.05\ \mathrm{g}}{0.997}$$
$$\mathrm{m(CH_3COOH)_{required}} = 57.22\ \mathrm{g}$$

$$\mathrm{V(CH_3COOH)_{required}} = \frac{\mathrm{m(CH_3COOH)}}{\rho(\mathrm{CH_3COOH})}$$
$$\mathrm{V(CH_3COOH)_{required}} = \frac{57.22\ \mathrm{g}}{1.05\ \mathrm{g/mL}}$$
$$\mathrm{V(CH_3COOH)_{required}} = 54.49\ \mathrm{mL}$$

The concentration of Co(II) required is 300 mg/L (0.3 g/L). Therefore the mass of $CoSO_4.7H_2O$ required in one litre is:

$$m(Co)_{required} = 0.3\ g$$
$$n(Co)_{required} = \frac{0.3\ g}{58.93\ g\ mol^{-1}}$$
$$n(Co)_{required} = 5.09 \times 10^{-3} mol$$

$$n(CoSO_4.7H_2O) = n(Co)$$
$$n(CoSO_4.7H_2O) = 5.09 \times 10^{-3} mol$$
$$m(CoSO_4.7H_2O) = 5.09 \times 10^{-3} mol \times 281.1\ g\ mol^{-1}$$
$$m(CoSO_4.7H_2O) = 1.43\ g$$

The concentration of $Na_2SO_4$ required is 0.2 M. Therefore, the mass of $Na_2SO_4$ required in one litre is:

$$\mathrm{n(Na_2SO_4)_{required}} = 0.2\ \mathrm{mol}$$
$$\mathrm{m(Na_2SO_4)_{required}} = 0.2\ \mathrm{mol} \times 142.04\ \mathrm{g/mol}$$

$$m(Na_2SO_4)_{required} = 28.41\ g$$

Therefore, one litre of aqueous phase of the specified pH and capacity requires 33.48 g of NaOH, 54.49 mL of $CH_3COOH$, 1.43 g of $CoSO_4.7H_2O$, and 28.41 g of $Na_2SO_4$ added to a 1-L volumetric flask and make to the mark with distilled water.

## APPENDIX D: ADDITIONAL DATA FROM DROPLET DISPERSION EXPERIMENTS

### Positive DC Fields

| Field Strength (kV/cm) | 4.00 | 4.12 | 4.25 | 4.37 |
|---|---|---|---|---|
| Arithmetic mean (μm) | 163 | 148 | 133 | 125 |
| Surface mean (μm) | 233 | 209 | 181 | 168 |
| Volume mean (μm) | 312 | 280 | 241 | 224 |
| Sauter mean (μm) | 558 | 503 | 429 | 401 |
| Volume-weighted mean (μm) | 756 | 707 | 647 | 624 |

### Negative DC Fields

| Field Strength (kV/cm) | -4.12 | -4.25 | -4.37 | -4.50 |
|---|---|---|---|---|
| Arithmetic mean (μm) | 179 | 166 | 152 | 148 |
| Surface mean (μm) | 252 | 231 | 212 | 199 |
| Volume mean (μm) | 333 | 310 | 285 | 264 |
| Sauter mean (μm) | 586 | 560 | 515 | 464 |
| Volume-weighted mean (μm) | 826 | 801 | 745 | 696 |

### Positive PDC Fields

| Field Strength (kV/cm) | 5.00 | 5.17 | 5.33 | 5.50 | 5.67 |
|---|---|---|---|---|---|
| Arithmetic mean (μm) | 197 | 202 | 194 | 178 | 178 |
| Surface mean (μm) | 282 | 282 | 271 | 252 | 244 |
| Volume mean (μm) | 387 | 376 | 359 | 337 | 321 |
| Sauter mean (μm) | 734 | 666 | 632 | 601 | 555 |
| Volume-weighted mean (μm) | 1070 | 939 | 889 | 842 | 782 |

| Frequency (Hz) | 20 | 30 | 40 | 50 | 60 |
|---|---|---|---|---|---|
| Arithmetic mean (μm) | 144 | 138 | 113 | 182 | 149 |
| Surface mean (μm) | 216 | 202 | 156 | 276 | 222 |
| Volume mean (μm) | 311 | 285 | 220 | 385 | 323 |
| Sauter mean (μm) | 647 | 568 | 438 | 750 | 683 |
| Volume-weighted mean (μm) | 965 | 843 | 712 | 1016 | 1052 |

**Negative PDC Fields**

| Field Strength (kV/cm) | -8.75 | -9.00 | -9.25 | -9.50 | -9.75 |
|---|---|---|---|---|---|
| Arithmetic mean (μm) | 136 | 156 | 134 | 124 | 122 |
| Surface mean (μm) | 202 | 229 | 190 | 174 | 170 |
| Volume mean (μm) | 305 | 325 | 270 | 247 | 240 |
| Sauter mean (μm) | 695 | 658 | 545 | 500 | 479 |
| Volume-weighted mean (μm) | 1128 | 993 | 890 | 834 | 799 |

| Frequency (Hz) | 20 | 30 | 40 | 50 | 60 |
|---|---|---|---|---|---|
| Arithmetic mean (μm) | 104 | 108 | 110 | 114 | 104 |
| Surface mean (μm) | 140 | 146 | 147 | 161 | 142 |
| Volume mean (μm) | 197 | 204 | 205 | 235 | 208 |
| Sauter mean (μm) | 399 | 400 | 406 | 503 | 449 |
| Volume-weighted mean (μm) | 731 | 695 | 710 | 875 | 863 |

**AC Fields**

| Field Strength (kV/cm) | 2.50 | 2.75 | 3.00 | 3.25 | 3.50 |
|---|---|---|---|---|---|
| Arithmetic mean (μm) | 98 | 98 | 99 | 98 | 102 |
| Surface mean (μm) | 123 | 121 | 122 | 120 | 124 |
| Volume mean (μm) | 180 | 169 | 166 | 154 | 156 |
| Sauter mean (μm) | 386 | 329 | 309 | 255 | 246 |
| Volume-weighted mean (μm) | 1136 | 885 | 773 | 552 | 476 |

| Frequency (Hz) | 20 | 30 | 40 | 50 | 60 |
|---|---|---|---|---|---|
| Arithmetic mean (μm) | 111 | 108 | 108 | 104 | 100 |
| Surface mean (μm) | 138 | 134 | 131 | 125 | 120 |
| Volume mean (μm) | 175 | 169 | 163 | 156 | 152 |
| Sauter mean (μm) | 278 | 271 | 254 | 243 | 243 |
| Volume-weighted mean (μm) | 437 | 447 | 439 | 457 | 531 |